FUNDAMENTAL STUDIES ON THE MECHANICAL CHARACTERISTICS OF SOFT ROCKS AND THEIR APPLICATION TO GEOTECHNICAL ENGINEERING

By

Der-Her Lee

Department of Transportation Engineering

Kyoto University

Kyoto, Japan

August, 1982

FUNDAMENTAL STUDIES
ON THE
MECHANICAL CHARACTERISTICS OF SOFT ROCKS
AND
THEIR APPLICATION TO GEOTECHNICAL ENGINEERING

By

Der-Her Lee

Department of Transportation Engineering

Kyoto University

Kyoto, Japan

August, 1982

SUMMARY

The conventional triaxial shear test in laboratory can only provide a pair of peak and residual strengths from a rock specimen. Therefore, the exploration of mechanical properties of rock by the conventional method becomes inadequate and even inconvenient when the amount of rock specimen is so limited due to the geological conditions, etc.. To improve the conventional method and initiate a more convenient testing procedure have formed the main purpose of this research.

A multiple stage triaxial test (MST) method for soft rock is developed. With this method, the mechanical properties of soft rock, especially the peak strength envelope and residual strength envelope can now be obtained from using only one or two specimens. A more advanced MST method incorporated with the monitoring of lateral strain of the specimen is also recommended.

The changes of internal structure within a soft rock specimen are influential to its strength. However, it is inherently difficult to measure or observe these changes directly. The measurement of permeability of a specimen during shearing process is elaborately employed to reflect the internal structure change of a soft rock specimen. The characteristics of micro-crack and crack growth have also been taken into account.

Two engineering applications stemmed out from these new MST method and the results of tests (particularly, the basic properties of soft rock) are envisaged. The influence of structure rocking induced by natural forces (such as from wind, wave or current) on rock mass beneath the foundation of structure is investigated first. Based upon the change in permeability of the specimen in simulation test, the damage created in rock mass can be indirectly determined, thereby providing useful information to the design of tall building.

The second case is to simulate the behavior of rock mass around an opening by using MST method and other experimental methods developed in laboratory, whilst excavating an opening. The results of simulations are of beneficial to support design, it also suggests that excavation speed bears significant effect on the deformation of rock mass around an opening.

ACKNOWLEDGEMENTS

The author expresses his heartfelt gratitude to Professor Koichi Akai of the Department of Transportation Engineering, Kyoto University, for his invaluable guidance and continuous encouragement throughout the course of this research. Also thanks are due to Assistant Professor Yuzo Ohnishi of the Department of Transportation Engineering, Kyoto University, for his helpful suggestions and criticisms.

Grateful acknowledgements are extended to Dr. Chikaosa Tanimoto, Lecturer of Kyoto University, for the profitable discussion on tunneling mechanics, and to Dr. John R. C. Hsu of Department of Civil Engineering, University of Western Australia, formerly a Guest Scholar of Kyoto University during 1980, for his patient advice in English writing.

Thanks are also given to Mr. Takao Yano, for his help in drawing the figures; to Messrs. M. Kawanishi and M. Soya, graduate students of Kyoto University, for typing the manuscript.

Finally, the author should acknowledge the help from many technical staffs and students in the Foundation Engineering Laboratory, Kyoto University, and from the Iwatani Naoji Foundation, for the financial support at the final period of this study.

Der-Her Lee

LIST OF SYMBOLS

a : radius of opening

B : pore pressure coefficient

C, C_i : stiffness of loading machine

C_s : stiffness of rock specimen

c : cohesion force

D_i : deformation

E : energy

e : void ratio

E_{crack} : irrecoverable energy expended for propagating cracks

$E_{friction}$: irrecoverable energy expended for resisting the friction between particles or liquid phase

E_i : irrecoverable energy

E_r : recoverable energy

E_t : total external energy

E_{tp} : total external energy at the peak strength point

G : elastic shear modulus

G_s : specific gravity

L_i : load

m : length of the spring representing loading machine (Chapter 2 and Appendix A)

m_f : compressibility of fluid phase of specimen

m_i : deformation of machine

m_v : compressibility of skeleton of specimen

N_ϕ : flow value ($= \frac{1+\sin\phi}{1-\sin\phi}$)

n : porosity

P : external load

P : peak state, peak strength point

p : peak strength point

p : mean stress ($=1/3x(\sigma_1+2\sigma_3)$)

p' : mean effective stress ($=1/3x(\sigma_1'+2\sigma_3')$)

p_e : excavation force

p_h : horizontal stress of rock mass

p_i : rock pressure acting on support

$p_{i,min}$: the minimum of p_i

p_o : primary stress of rock mass before excavation

p_v : vertical stress of rock mass

q : deviatoric stress ($=\sigma_1-\sigma_3$)

q_p, q_{peak} : deviatoric stress at peak state

$q_{residual}$: deviatoric stress at residual state

q_r : the ultimate cyclic loading

q_r : deviatoric stress at residual state

R_i, R : resistance of rock specimen

R : residual state, residual strength point

r : distance measured from the center of opening

S_r : degree of saturation

s : length of rock specimen

s_i : deformation of rock specimen

u : pore water pressure

V : potential

v : permeability (cm^3/min)

V_p : P-wave velocity

V_s : S-wave velocity

v_s : volumetric change of rock specimen

w : moisture content

α : inclination angle of discontinuity of rock specimen

α : coefficient of strength envelope (Chapter 3)

β : coefficient of strength envelope

Δu_t : true increment of pore pressure

γ_d : dry density

γ_t : wet density

ε : strain

ε_1 : axial strain

ε_3 : lateral strain

$\dot{\varepsilon}_1$: rate of shearing (axial direction)

$\dot{\varepsilon}_3$: rate of shearing (lateral direction)

ε_p : axial strain at the peak strength point

ε_p : axial plastic strain (Chapter 6)

ε_v : volumetric strain ($=\varepsilon_1+2\varepsilon_3$)

θ : angle

ν : Poisson ratio

σ : stress

σ' : effective normal stress

σ_1 : axial stress

σ_1' : effective axial stress

σ_3 : confining pressure, lateral stress

σ_3' : effective lateral stress

σ_{1p} : σ_1 in peak state

$\sigma_{1p,1}$: σ_1 in peak state (case 1)

$\sigma_{1p,2}$: σ_1 in peak state (case 2)

σ_{1r} : σ_1 in residual state

$\sigma_{3p,1}$: σ_3 in peak state (case 1)

$\sigma_{3p,2}$: σ_3 in peak state (case 2)

$\sigma_{3,min,1}$: first minimum value of σ_3

$\sigma_{3,min,2}$: second minimum value of σ_3

σ_m : isotropic pressure

σ_r : normal stress in radial direction (Chapter 6)

σ_θ : normal stress in circumferential direction

σ_z : normal stress in axial direction

σ_{rp} : σ_r in peak state

$\sigma_{\theta p}$: σ_θ in peak state

σ_{rr} : σ_r in residual state

$\sigma_{\theta r}$: σ_θ in residual state

τ : shear stress

τ_{xy} : shear stress

τ_{rz} : shear stress

τ_{zr} : shear stress

ϕ : diameter

ϕ : angle of internal friction

∇^2 : Laplacian

LIST OF FIGURES

LIST OF TABLE

LIST OF PHOTOGRAPHS

TABLE OF CONTENTS

Chapter 1 INTRODUCTION

1-1 General Description

Following the rapid expansion of human activities in all socioeconomic fronts, the requirement of even larger constructions of structures becomes more apparent, with application to traffic, energy and housings. But, the bigger in scale of these constructions, the more complicated problems to rock mass will be met in constructing them, and the more serious damage may occur if they failed. Therefore, how to promote the safety of larger structures and to observe various technique level while construction have become a practical and yet urgent topic.

Along this line, it is essential, as a first step, to investigate throughly the fundamental mechanical properties of rock mass, especially those of soft rocks, which are fragile and porous and often become weakened by water.

In laboratory work, triaxial shear test has been the most popular method to explore the mechanical properties of rock. Many works have been developed to this, for example, Von Karman (1911)[1], Böker (1915)[2], Jaeger and Cook (1969)[3] and Hallbauer, et al. (1973)[4].

Because most rock specimens have a strength much greater than clay, hence, a loading system with sufficiently strong stiffness is required to accomplish a triaxial shear test. A complete relationship between axial stress and axial strain, especially the part beyond peak strength point, can then be obtained.

Unfortunately, the traditional triaxial shear test method can render only a pair of strengths (peak and residual strength) from a rock specimen. In order to describe in full the strength envelope of a rock, which is often de-

manded in rock engineering, many rock specimens are necessary. To reduce the number of rock specimens and testing time, as well as to lessen the influence of material variation among different specimens, a convenient test method called as Multiple Stage Triaxial shear test for soft rock (MST) is developed to substitute the conventional triaxial shear test method. Using this method, only one or two rock specimens are needed to explore the full strength envelopes of a rock mass.

Besides the resultant strength envelopes obtained from shear test, the internal structure change of a specimen in accompanying with shear test is also of vital importance to understand the characteristics of rock. Because of the difficulty in measuring directly the internal structure change, the permeability of a rock specimen, which is affected by the number of pores and cracks, is then monitored to reflect this internal change.

The knowledge gained from testing soft rocks and testing technologies obtained from laboratory experiments will be applied to geotechnical engineering, such as the design of structure foundation and the support of tunnel.

1-2 Scope of Study

The purpose of this study is to investigate the fundamental mechanical properties of soft rock specimen in laboratory and to initiate useful new testing methods which can replace traditional testing methods and increase accuracy in techniques of monitoring rock behaviors.

Based upon the experimental results obtained from various preliminary and new test runs in laboratory, the applicability of these to geotechnical engineering will also be examined.

In Chapter 2, experimental apparatus and rock specimens will be described in details, these including triaxial shear test cells, loading system, data measurement devices and treatment.

As a complete stress-strain curve of rock specimen provides information of the most fundamental importance to study rock mechanics, therefore, a loading machine with a stiffness higher enough than the highest stiffness of all rock specimens should be used in this study. To process the enormous amount of data obtained, a micro computer system is to be utlized.

In addition, physical properties of the three soft rock specimens used in this study are discussed, together with their sampling method.

Two series of fundamental tests on rock specimens are reported in Chapter 3. The first is triaxial shear test series, which is performed under various confining pressures, to explore stress, pore water pressure and volume change of rock specimen during shearing. The other examines the behaviors of rock specimen subjected to a cyclic loading, with attention to the energies dissipated in each cycle of test.

A multiple stage triaxial test method for saturated soft rock, tentatively call it as MST method, is developed and described later in Chapter 4. This method is derived on the basis of the MST for hard rock originally proposed by Kovari and Tisa (1975)[5] . Since the strength of a saturated soft rock is critically affected by the excess pore water pressure generated in shearing process, hence, how to handle skillfully the problem of excess pore water pressure becomes the key issue in developing the MST method for saturated soft rock.

In order to improve the accuracy of the MST method, the lateral strain of a rock specimen, which is one of the sensitive responses of crack growth within specimen, should then be monitored carefully.

Furthermore, after developing the MST method for saturated soft rock, this methed will be applied to investigate the mechanical behaviors of sandy silt rock with an artificial discontinuity. In this series of tests the influences of confining pressure and angle of discontinuity on the strengths of

rock specimen will be studied.

In Chapter 5, to confirm the characteristic change of rock specimen from microscopic view during a shearing test, a series of permeability tests on soft rock will be carried out. Because the permeability of a rock specimen is strongly related to the number of pore and crack within it, then, the measurement of variation of permeability during shearing process will indirectly conjectured the internal structure change created in the specimen. A simple triaxial test cell for rock is used to serve the purpose.

In Chapter 6, the rock characteristics derived from previous experiments, including various new testing techniques, will be applied to practical geotechnique engineering. Two applications will be discussed. The first case is to study the reaction of the rock mass located under a structure foundation and subjected to a low frequency structure rocking. The rocking is induced by wind or other nature forces, such as wave force or current force.

In order to simulate the structural rocking, the rock mass beneath a structure foundation is considered to be loaded by a loading-unloading cyclic test. Two cyclic loading tests with different amplitudes are carried out to simulate different degrees of rocking. In addition, by comparing the variations in permeability and elastic shear modulus of rock specimens during tests, information about foundation design can be collected.

The second application is to model the behavior of rock mass around an opening using laboratory test methods. The influence of excavation speed on support design will be investigated. Because the suitable stiffness of support and the timing to set up the support can be decided by employing a p_i-u_w curve, where, p_i is the rock pressure acts on the support and u_w is the deformation of opening wall, p_i -u_w curve would in turns to be affected by excavation speed. Therefore, the relationship between excavation speed (simulated by shearing speed of triaxial test) and the shape of p_i-u_w curve

(equivalent to the σ_3-ε_3 curve of rock specimen) should also be determined.

In the current study, development is also focused on how to apply the multiple stage triaxial shear test method for saturated soft rock using a simpler yet precise procedure to explore the strength envelopes.

References for Chapter 1

(1) Karman, Th. V., "Festigkeitsversuche unter Allseitigem Druck", Verein Deutscher Ingenieur, Berlin, No. 42, 1911.

(2) Böker, R., "Die Mechanik der bleibenden Formänderung in kristallinisch aufgebauten Körpern", Mitteilungen über Forschungsarbeiten auf dem Gebiete des Ingenieurwesens, Vols. 175 and 176, 1915.

(3) Jaeger, J. C. and N. G. W. Cook,"Fundamentals of Rock Mechanics", Methuen and Co., Ltd., London, 1969.

(4) Hallbauer, D. K., H. Wagner and N. G. W. Cook,"Some Observations Concerning the Microscopic and Mechanical Behaviour of Quartzite Specimens in Stiff, Triaxial Compression Tests", Int. J. Rock Mech. Min. Sci. & Geomech. Abstr., Vol. 10, pp. 713-726, 1973.

(5) Kovari, K. and A. Tisa, "Multiple Failure State and Strain Controlled Triaxial Tests", Rock Mechanics, 7, pp. 17-33, 1975.

Chapter 2 TESTING APPARATUS AND SPECIMEN DESCRIPTION

Experimental program can only be carried out effectively with proper instruments and working procedures. Relevant account on testing apparatus, i.e., loading system, triaxial shear test cell and the devices for measuring and treating data will be made, besides the description of rock specimens and its sampling methods.

2-1 Loading Facility

Strain softening raises in the post peak strength during a triaxial shear test is an important mechanical property of rock. This implies that beyond the point of peak strength, rock specimen will gradually lose its strength untill a residual state is reached. As this phenomenon had never been obtained by using conventional (flexible) testing machines, strain-softening was considered as an unstable state of rock specimen, where the term 'flexible' reflects that the stiffness of a testing machine is smaller than that of the rock specimen.

A complete curve of stress-strain relationship of rock specimen is an essential and important prerequisite in all investigations related to the field of rock mechanics. Therefore, it is not sufficient to employ a coventional testing machine for exploring the entire range of rock behaviors, particularly in the range of post-peak strength.

From the investigations into the relative stiffness between loading facility and concrete specimen carried out by Turner and Barnard (1962)[1] and Hinde (1964)[2], it is obvious that a complete stress-strain relationship of concrete specimen, for region before and beyond the peak strength point, can

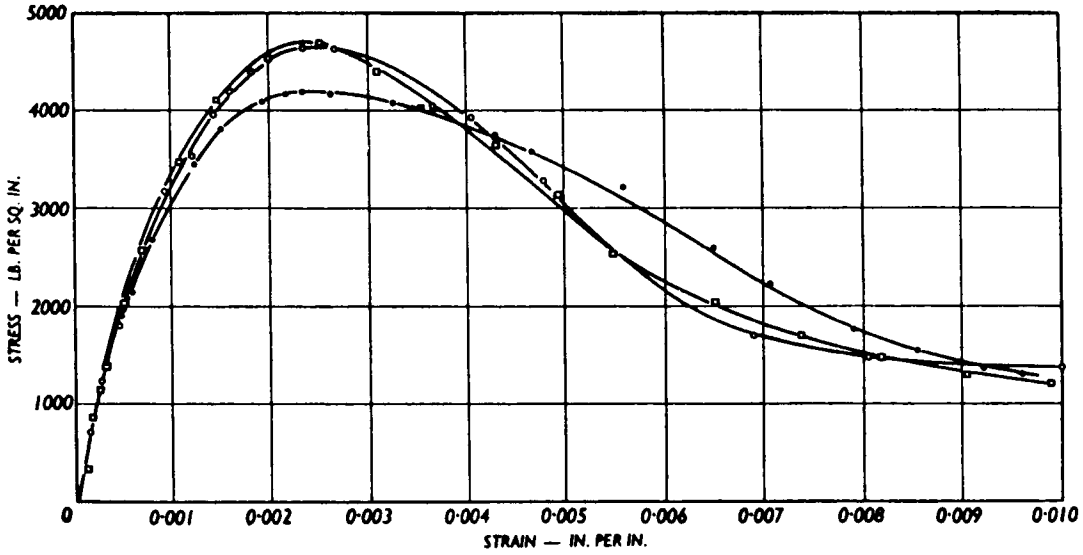

Fig. 2-1 Stress/strain curves for concrete obtained using stiff constant strain rate testing machine (Ref. 2-1).

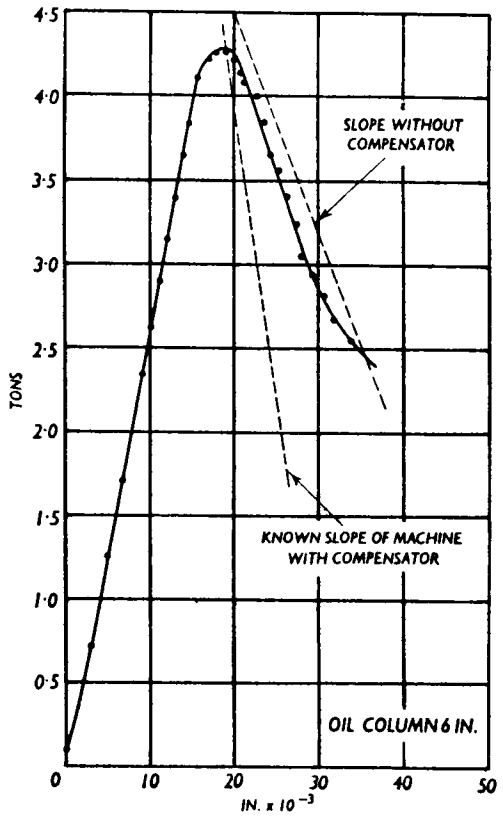

Fig. 2-2 Strut test using compensator (Ref.2-2)

be monitored by a testing machine with relatively higher stiffness (see Fig. 2-1 and Fig. 2-2).

On the other hand, Cook (1965)[3], Bieniawski (1969)[4], Bieniawski, Denkhans and Vogler (1969)[5], Rummel and Fairhurst (1970)[6] studied the stiffness of testing machine with rock specimen. Among them, Bieniawski, et al. (1969)[5] successfully proposed a model consisted of a spring (representing the testing machine) in series with rock specimen, to explain why a stiffer loading system can monitor the post failure portion of resistance-deformation curve of a rock specimen (see Fig. 2-3).

Employing the same model, Lee (1979)[7] could simulate the resistance - deformation curves of a rock specimen obtained separately by flexible and stiff loading system. Some conclusions were proposed in that paper and are represented again in Appendix A of this thesis.

Because three rock specimens were used in this study, being sandy silt rock, Nikko tuff and Funyu tuff with shear modulus (gained from uniaxial test) at 1.2×10^3, 3×10^4 and 4.1×10^4 kgf/cm^2 ,respectively, a loading facility with stiffness greater than the highest of these three specimens is needed to obtain a complete stress-strain curve of these specimens. Moreover, stiff loading machine can be divided into two groups. One is servo-controlled system or so-called closed loop machine, the other is structurally stiff machine which has a strong enough loading frame. In this study, a servo-controlled loading machine made by American MTS Systems Co. was employed (see Photos. 2-1, 2-2), which incorporates hydraulic power system, control package and loading frame. The loading frame, with stiffness about 1.6×10^6 kgf/cm^2, was much stronger than the required maximum stiffness judging from the specimens to be used in this investigation. The maximum allowable loading capacity was 25 tons.

This loading system can be used to perform a wide range of tests, such as strain rate control test, stress rate control test, fatigue test, cyclic load-

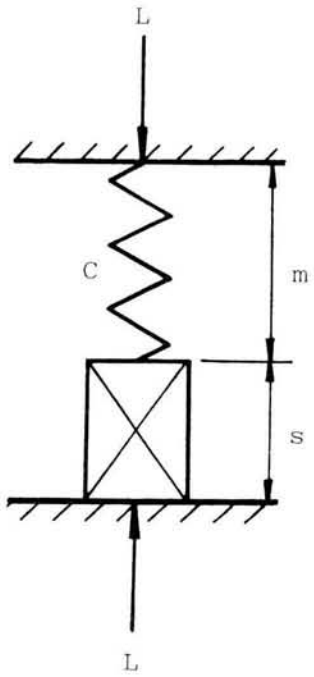

Fig. 2-3 The model of loading machine and rock specimen proposed by Bieniawski, et al. (Ref. 2-5).

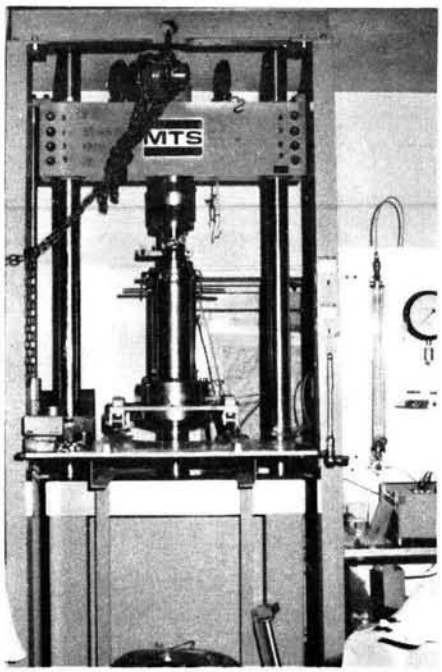

Photo. 2-1 Photo of loading apparatus

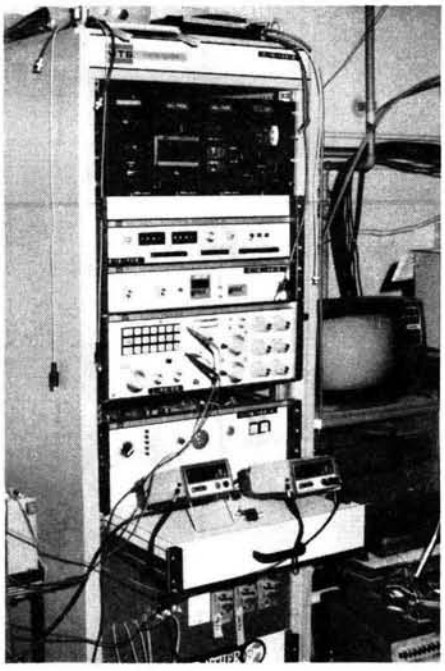

Photo. 2-2 Control system of loading machine

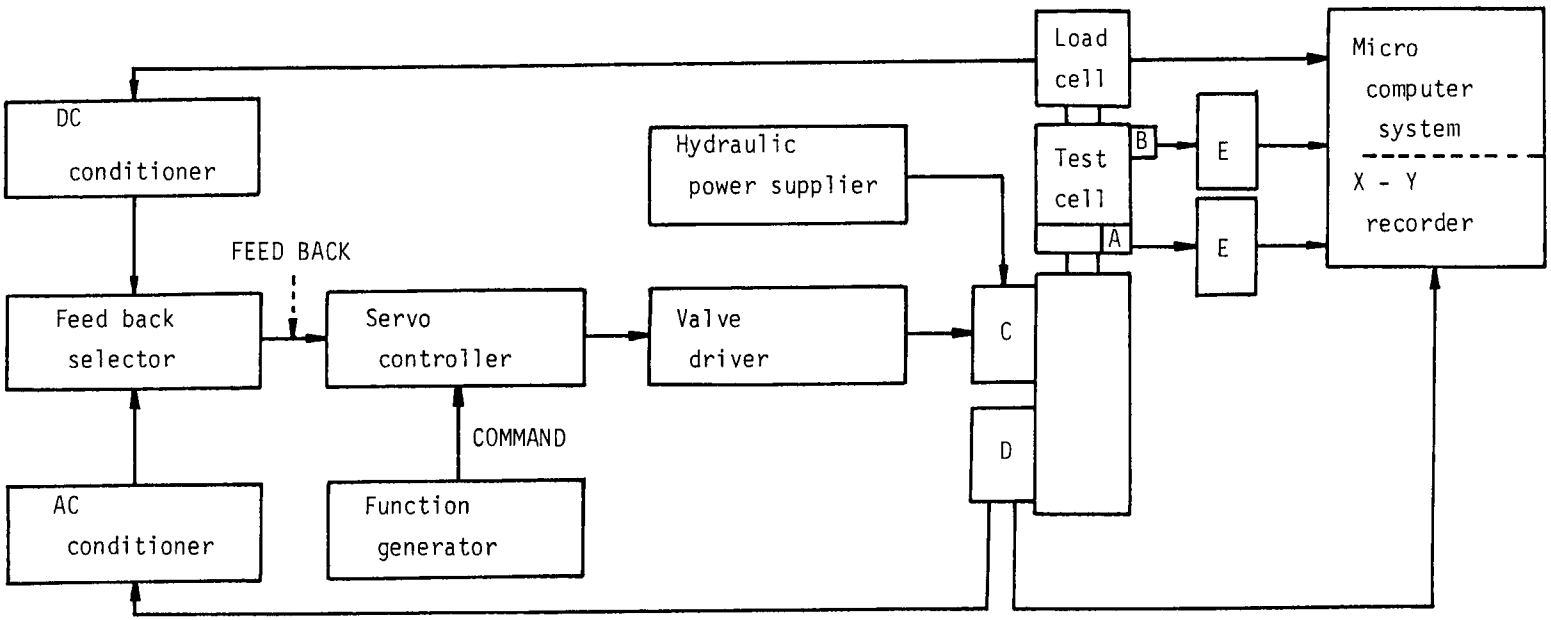

A : Electrical pore water pressure transducer
B : Electrical confining pressure transducer
C : Servo valve
D : L.V.D.T.
E : Amplifier

Fig. 2-4 The electric net work of MTS loading system

ing test and relaxation and creep tests, among other. The test condition can conveniently be changed, by simply resetting the condition setting knob of the control package to a suitable position. The control package consisted four parts, controller, function generator, control panel and counter panel.

A simplified electric net work of the MTS loading system is depicted in Fig. 2-4.

2-2 Triaxial Shear Cell

Two triaxial shear cells made of cylindrical steel tube (with profiles shown in Figs. 2-5 and 2-6), which could sustain cell pressure up to 100 and 200 kgf/cm^2 were used in this study. Since the stronger cell at 200 kgf/cm^2 was introduced into our laboratory later than the 100 kgf/cm^2 one, therefore, most of the tests on sandy silt rock and Nikko rock were performed in the 100 kgf/cm^2 cell, whilst Funyu rock was tested with the 200 kgf/cm^2 one.

Moreover, as a drainage hole was prepared in the loading rod of the 200 kgf/cm^2 cell, it was also possible to implement the series of permeability test on Funyu rock (to be discussed in chapter 5).

A special channel was equipped to pass out the information measured by lateral strain gauge stuck directly onto the lateral surface of a specimen. In addition, the 200 kgf/cm^2 cell had three other channels to output the lateral extension of specimen which was monitored by three cantilever style strain gauges (review Fig. 2-6).

2-3 Data Processing

Besides the measurement of data during the testing, data processing after it was laborious. To minimize the time spent for these calculations or to im-

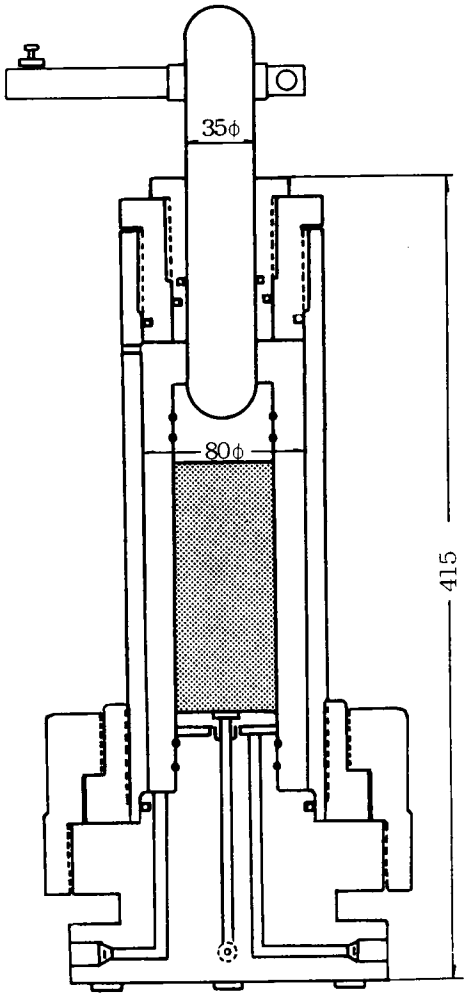

Fig. 2-5 Triaxial shear cell with tolerable cell pressure 100 kgf/cm^2

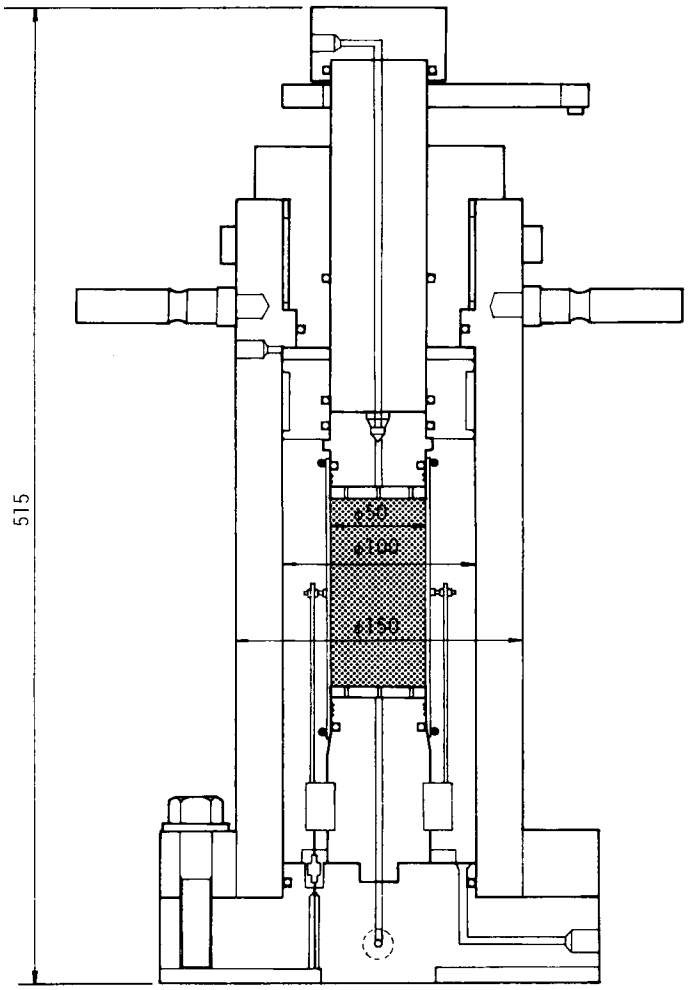

Fig. 2-6 Triaxial shear cell with tolerable cell pressure 200 kgf/cm^2

prove the accuracy of data measurement, a microcomputer system was employed. This system consisted of a microcomputer and other complementary components, as schematically illustrated in Fig. 2-7.

Each component of this microcomputer system was designated to perform a specific function. The process of data obtained is as follows.

The experimental data was firstly picked up by various sensors, such as load cell, strain gauge, displacement gauge (LVDT) and pore pressure meter, etc.. The analog signals (sent out from sensors) were converted into digital signals through an A/D converter, for the ready acceptance by the microcomputer. The time intervals for sampling experimental data were controlled by a written program as a part of built-in package.

Data were then stored in the complementary memory part called mini disk of the microcomputer. Mini disk, acted just like the disk used in the file-system of a large computer, was adopted to store not only the program which schedules the data sampling but also data storage.

A cathode rays tube display (CRT) was used to write in (input) and delete program or to examine the data recorded in the minidisk. On the other hand, controlling program and data calculation program could be listed out with a lineprinter. Data processed by the calculation program were then written out (output) also by the lineprinter.

When necessary, resultant data could be directly plotted using a X-Y plotter.

2-4 Description and Preparation of Specimens

Three kinds of soft rock were used in this investigation, each with a specific uniaxial shearing strength. Among these, the weakest was sandy silt rock, whilst two others sedimentary tuff - Nikko and Funyu rock, had higher

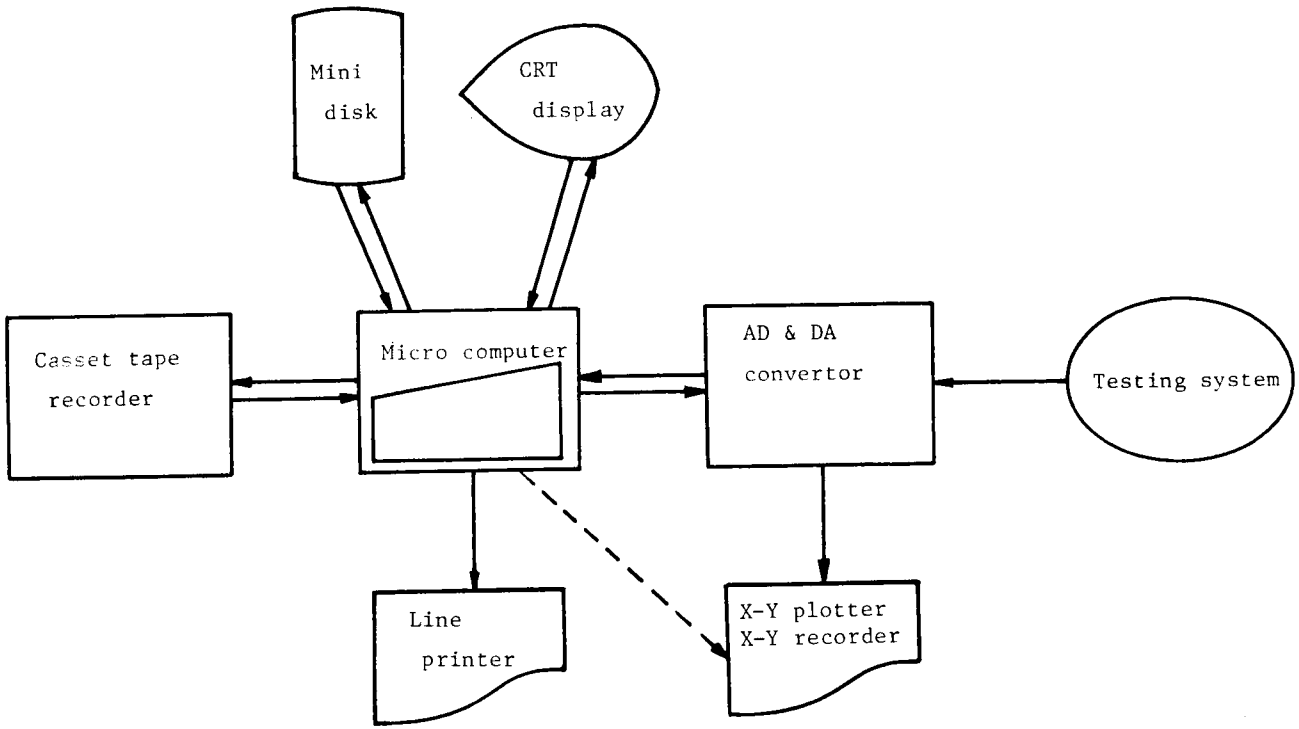

Fig.2-7 The microcomputer system used in this research

uniaxial strength.

Upon examining the physical properties of these rocks as presented in Table 2-1, it is clear that these three soft rocks had like properties of high porosity and significant water content. Due to the common properties of high porosity and water content, saturated soft rocks are ready to induce constructional trouble in situ. Therefore, the study into mechnical properties of saturated soft rock is of vital importance in the field of geotechnical engineering.

Specimens were firstly cored from a block of rock in same direction with a ϕ-5 cm core cutter, as shown in Photo. 2-3. They were then carefully trimmed up to 10 cm in length with a diamond-bladed saw (Photo. 2-4). Successively, these specimens were fully saturated with distilled water by a suction pump for at least 7 days, and kept in water until the time for testing.

However, in special test series, such as the investigation into the mechanical behaviors of sandy silt rock with an artificial discontinuity (to be mentioned in Chapter 4), a rock specimen must further be sawed into two parts with an oblique angle to radius direction of the specimen. On the other hand, in permeability test series (discussed in Chapter 5) the lateral surface of specimen must be pasted by a waterproof layer about 0.5 mm in thickness before it was set into the triaxial cell.

Treatment of specimen will be described in details in each test series in relevant chapters.

Table 2-1 Physical Properties of Sandy Silt Rock & Tuffs

Rocks	Sandy Silt Rock	Nikko Tuff	Funyu Tuff
Dry Density γ_d(g/cm^3)	1.14	1.914	1.873
Wet Density γ_t(g/cm^3)	1.68	2.234	2.157
Void Ratio e	1.19	0.548	0.406
Porosity n(%)	54.4	35.4	28.9
Water Content w(%)	48.0	16.7	15.3
Specific Gravity G_s	2.485	2.805	2.649
Degree of Saturation S_r(%)	100.0	-	97.0
P-Wave Velocity V_p(km/sec)	1.70	-	-
S-Wave Velocity V_s(km/sec)	0.51	-	-
Poisson Ratio ν	0.35		

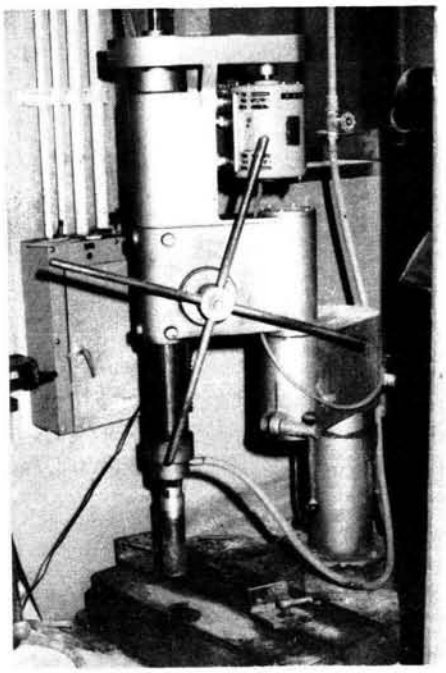

Photo. 2-3 Photo of core cutter

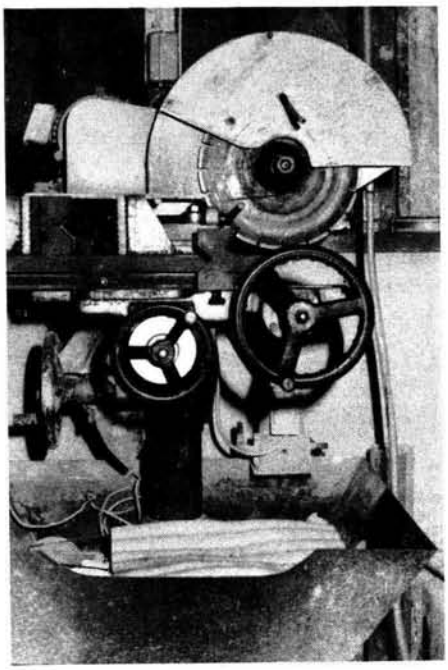

Photo. 2-4 Photo of diamond saw

References for Chapter 2

(1) Turner, P. W. and P. R. Barnard, "Stiff Constant Strain Rate Testing Machine", The Engineer, July 27, pp. 146-148, 1962.

(2) Hinde, P. B., "Testing Machine Stiffness Problem", The Engineer, pp. 1124-1127, 1964.

(3) Cook, N. G. W., "The Failure of Rock", Int. J. Rock Mech. Min. Sci., Vol. 2, pp. 389-403, 1965.

(4) Bieniawski, Z. T., "Deformational Behaviour of Fractural Rock under Multiaxial Compression", Structure, Solid Mech. and Eng. Design, Proceedings Conference on Civil Eng. Materials, Southampton, pp. 589-598, 1969.

(5) Bieniawski, Z. T., H. G. Denkhans and U. W. Vogler, "Failure of Fractured Rock", Int. J. Rock Mech. Min. Sci., Vol. 6, pp. 323-341, 1969.

(6) Rummel, F. and C. Fairhurst, "Determination of the Post-Failure Behaviour of Brittle Rock Using a Servo-Controlled Testing Machine", Rock Mechanics, 2, pp. 189-204, 1970.

(7) Lee, D. H., "The Strength Characteristics of Sandy Silt Rock Obtained from Multiple-Stage Triaxial Test Method", Master Thesis, Kyoto University, 1979.

Chapter 3 LABORATORY INVESTIGATION OF SOFT ROCK SPECIMEN

3-1 Background

To investigate the mechanical behaviors of soft rock specimen subjected to various kinds of external force in laboratory, triaxial shear test has been one of the most popular and convenient methods. The traditional triaxial shear test of rock was first developed by [redacted]n Karman in 1911[1], and modified with improvements by Böker in 1915[2]. However, when the conventional testing machine is used to perform triaxial shear test, it becomes very difficult to control the fracture of rock specimen beyond its peak strength point, especially under low confining pressure. Therefore, a stiffer loading system, mentional in section 2-1, was then employed.

Pioneer work on the time-dependent or rate-dependent behavior of hard specimen, such as concrete or rock was investigated by Rüsch (1960)[3]. It was obvious that the elastic modulus, peak strength and the drop of strength after the peak strength of concrete specimen were largely affected by the strain rate applied. It showed that a rapid strain rate used in triaxial shear test would derive a complete stress-strain curve with a bigger elastic modulus, peak strength and a steeper drop of strength beyond the peak strength point (see Fig. 3-1-1). Bieniawski (1970)[4] first researched into the influence of changing the strain rate in the strain softening process on the behavior of a fine-grained sand stone (Fig. 3-1-2). On the other hand, Sangha and Dhir (1972)[5] investigated the relationship between strain rate and the rupture mode of Laurencekirk sandstone. Having the strain rate decreased stepwise from 2.5×10^{-3} /sec to 2.5×10^{-6} /sec, the broken surfaces were found to be less planar, but more curved and irregular or conical in appearance.

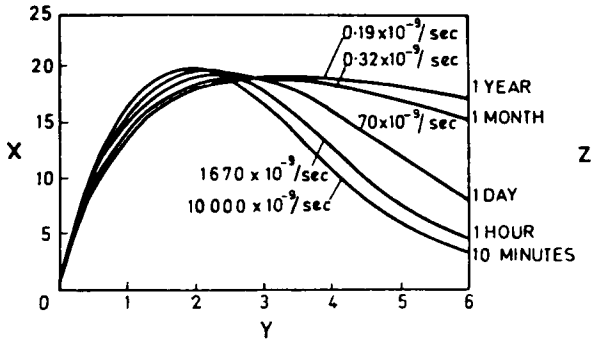

Fig. 3-1-1 Stress-strain relationships for concrete for various constant strain rates (Ref. 3-2)

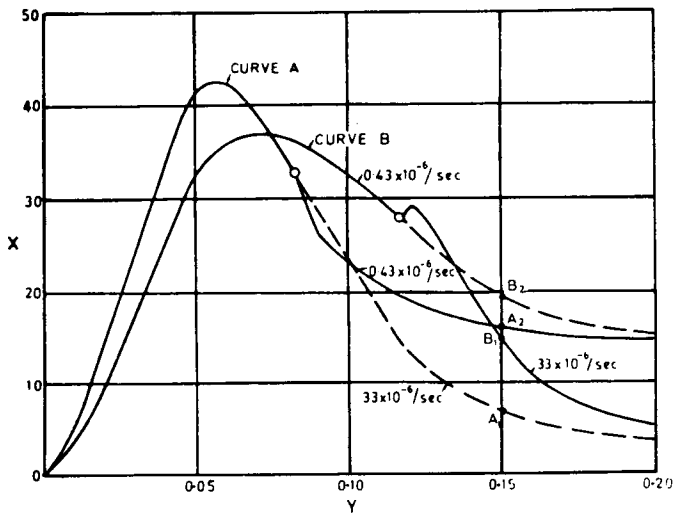

Fig. 3-1-2 Effect of changing strain rate on the behavior of fractured rock X = load (kN); Y = deformation (mm) (Ref. 3-3)

Peng (1973)[6] used a servocontrolled hydraulic testing machine to investigate the relaxation and creep behaviors of Berea sandstone, Tennessee marble and Arkose sandstone. In 1976, Akai and his coworkers[7] successfully predicted the creep deformation of weathered granite with a rheological model. Although the time-dependent behavior of soft rocks was not examined in this study, in the latter, a quasi-creep test, i.e. a constant upper stress cyclic loading test (see Fig. 3-1-3) had been carried out. This will be discussed in details in sections 3-3 and chapter 5.

On the other hand, as micro-cracks progressing often initiates the failure of rock-like materials, the crack growth has directly been related to the irrecoverable energy during shearing process. Okada and his followers (1976, 1979)[8),9] inspected the expended energy of concrete specimen during cyclic loading tests. From the change in expended energy, the fracture process of concrete was monitored. Spooner and Dougill (1975)[10], Spooner, Pomeroy and Dougill (1976)[11], also investigated the damage and energy dissipation in concrete specimen in simple cyclic loading approach (see Fig. 3-1-4).

In addition to this cyclic loading method, Spooner, et al. (1976)[11] also used the acoustic emission to reinforce their estimation of the damage of concrete specimen. Recently, Yashima (1981)[12] used the same method to study the damage of Funyu rock (tuff), and obtained excellent results.

Because the energy dissipation during shearing process or cyclic loading is substantively impotant to the change of microstructure of specimen, with the latter even induces the failure of rock-like materials, earlier investigations into the crack growth and the failure of rock-like material had achieved valuable contributions. Along the line, Griffith (1921, 1924) [13), 14)] developed a fracture theory of brittle material with an existing crack. Brace and Bombolakis (1963)[15] studied the crack growth and the interaction of cracks in photoelastic material and glass. And then in 1965, Walsh[16), 17), 18)] con-

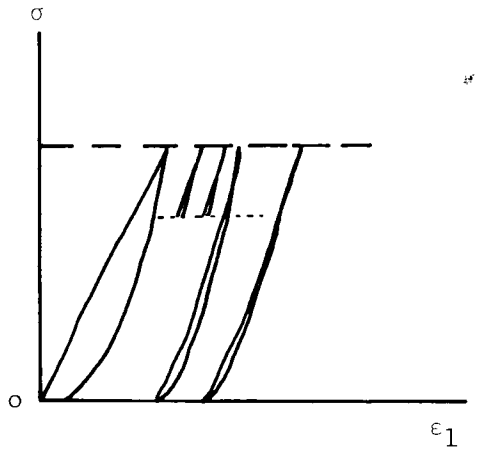

Fig. 3-1-3 Constant upper stress cyclic loading test

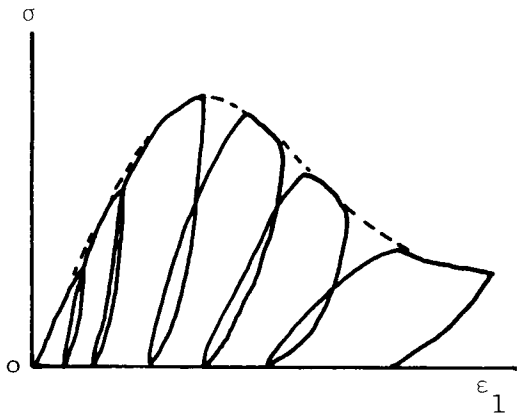

Fig. 3-1-4 Simple cyclic loading test

ducted a series of investigation into the influence of cracks on the uniaxial elastic compression, Poisson's ratio and compressibility of rock.

Meanwhile, Brace, Paulding and Scholz (1966)[19], Scholz and Kranz (1974)[20], Zoback and Byerlee (1975)[21] and Holcomb (1978)[22] explored the relationship between crack growth and dilatancy of rocks.

However, Akai, Ohnishi and Lee (1981)[23] also attempted to explore the change of microstructure of rock during triaxial shear test. An indirect monitoring method was developed for this purpose. It was applying the variation of permeability of soft rock to estimate the internal change of rock while shearing process was being underway.

3-2 Characteristics of Soft Rock in Triaxial Compression Shear Tests

The triaxial compression shear test had been proved as the most useful test in studying the mechanical properties of rock-like materials over a wide range of stress and strain. This method had been applied in this study under various testing conditions.

Three kinds of rock were used in this investigation, sandy silt rock, Nikko rock and Funyu rock. Their physical properties were summarized in Table 2-1. The loading system, also mentioned previously in chapter 2, was a stiff one.

3-2-1 Experimental Results

Firstly, several specimens of sandy silt rock, 5 cm in diameter and 10 cm high, were used to carry out the consolidated-undrained triaxial compression shear test under confining pressures from 6 to 50 kgf/cm^2 in a triaxial cell, which could sustain a maximum tolerable pressure up to 100 kgf/cm^2. Back pressure at 3 kgf/cm^2 was adopted in each test to prevent the pore water

pressure from becoming negative (suction) during the shearing process. Tests were carried out under constant strain rate control at 0.12%/min.

The relationship between the axial strain ε_1 of each specimen and deviatoric stress q (= σ_1-σ_3) is shown in Fig. 3-2-1(a), and that with the excess pore water pressure created in it is depicted in Fig. 3-2-1(b). Because the drop in strength after a peak strength in q-ε_1 curves becomes smaller under higher confining pressures (see Fig. 3-2-1(a)), it is evident that these sandy silt rock specimens had behaved from as a brittle material at lower confining pressure (6 kgf/cm^2) and gradually into a ductile one at about σ_3=40 kgf/cm^2.

The elastic modulus of each specimen can be determined from the slope of the initial linear part of each q-ε_1 curve. These slopes present an inclination that higher confining pressures would induce a q-ε_1 curve with steeper slope indicating a more homogeneous and stiff specimen, though the distinction among these slopes is not very clear.

Upon inspecting the relation of u-ε_1 (Fig. 3-2-1(b)), an interesting fact is that all curves, except where σ_3 is greater than 30 kgf/cm^2, had a peak point of excess pore water pressure appeared well before the peak strength point in its corresponding q-ε_1 curve shown in Fig. 3-2-1(a). This special property would be utilized as one of the hint of unloading in MST method which would be discussed in the next chapter.

When the confining pressure was high enough ($\geqq$30 kgf/cm^2), the point of peak excess pore water pressure would become less apparent and the dropping of u after the peak point would also be substituted by a monotoneous increasing curve. It is obvious that during these shearing processes, neither suction nor volumetric dilatation had been generated in the specimen after peak strength.

Combining Figs. 3-2-1(a) and (b), and letting $q=\sigma_1-\sigma_3$, $p'=\frac{1}{3}(\sigma_1+2\sigma_3)-u$, the effective stress paths of these specimens are shown in Fig. 3-2-2.

Because the B-value (pore pressure coefficient) of sandy silt rock was

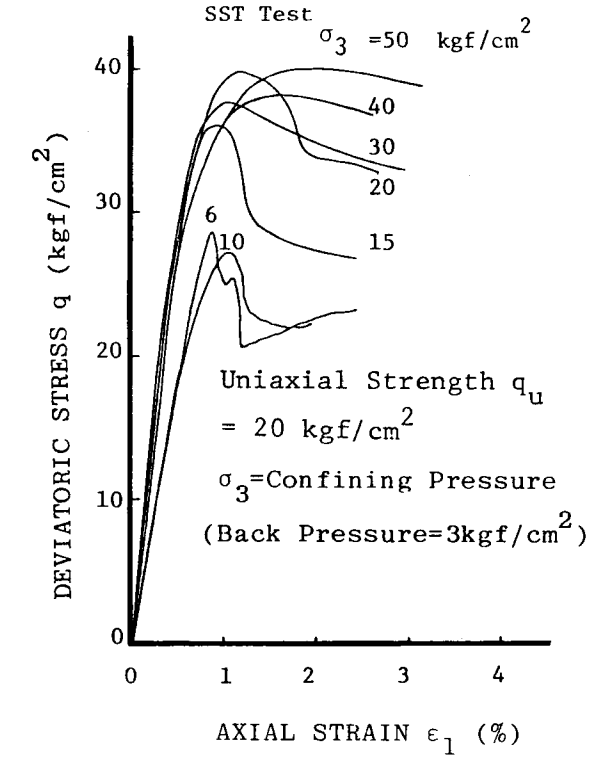

Fig. 3-2-1(a) q-ε_1 curves of sandy silt rock (SST)

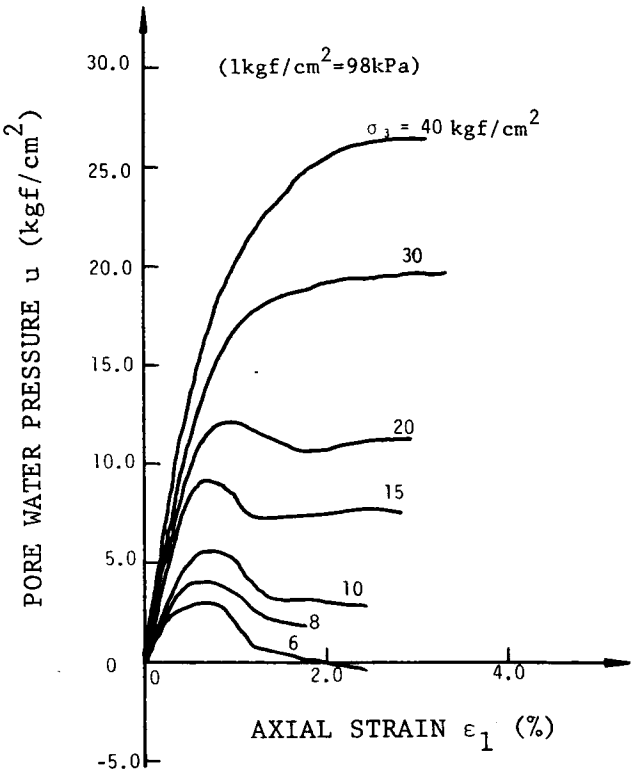

Fig. 3-2-1(b) u-ε_1 curves of sandy silt rock (SST)

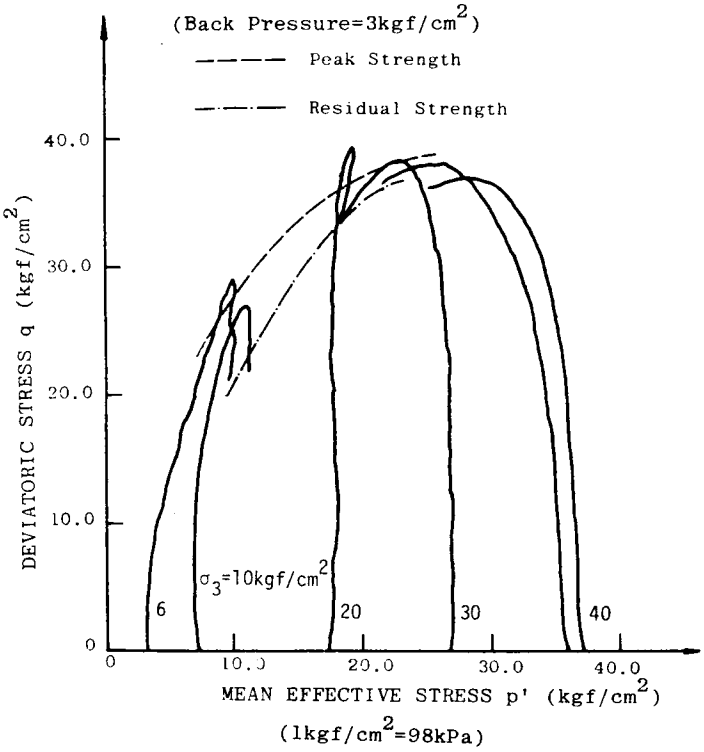

Fig. 3-2-2 Effective stress paths of SST

0.95, in the close proximity of unity, hence, following the discussion made on the dilatancy and the inclination of effective stress path as proposed by Akai, et al. (1979)[24], the possibility of whether these specimens would dilate or not during shearing process can be detected.

However, upon observing the effective stress paths of σ_3 = 6, 10 kgf/cm^2, it shows that they tend to bend to the direction of increasing p'. This means that in shearing process, these two specimens would certainly dilate especially in the later half of the test. Meanwhile, the skeleton of these specimens at σ_3= 30 and 40 kgf/cm^2 were compressed through the shear test, because their effective stress paths curved into the direction of decreasing p'.

Upon collecting the peak and residual strength points of these effective stress paths obtained from different specimens under different confining pressures, a pair of strength envelopes of peak and residual strength, could

be arrived. From Fig. 3-2-3, the higher the p' is, the lesser the difference between these two envelopes will be.

Following the arranging method suggested by Hobbs (1966)[25], the two curved strength envelopes in Fig. 3-2-3 could be replotted into straight line on log q - log p' plane (see Fig. 3-2-4). Each of these two straight lines could be represented by an equation such as :

$$q = \alpha \cdot (p')^{\beta} \qquad (3\text{-}2\text{-}1)$$

where coefficients α=10.0, β=0.44 for peak strength envelope, and

α=4.35, β=0.70 for residual strength envelope.

Coefficients α and β can be considered as being similar to c and $\tan\phi$ values used in Mohr-Coulomb's criteria ($\tau = c + \sigma_n \cdot \tan\phi$), respresenting the cohesive and frictional strength parameters, respectively, of a rock specimen.

It has been submitted that Funyu rock is a very sound rock (uniaxial strength about 120 kgf/cm^2, much bigger than that of sandy silt rock of 20 kgf/cm^2). In order to derive useful information of this rock it was necessary to change the triaxial cell to cover all the properties (brittle and ductile) of this rock.

A high tolerable pressure cell which could be used up to σ_3=200 kgf/cm^2 shown in Fig. 2-6, was employed in testing the Funyu rock. The experimental results of this series are presented in Figs. 3-2-5(a) and (b), displaying the relationship between deviatoric stress q and axial strain ε_1 and that of the corresponding excess pore water pressure u and ε_1 curves[12].

The u-ε_1 curves in Fig. 3-2-5(b) indicate similar tendency to those in Fig. 3-2-1(b), showing monotonous increasing during the post-failure process when $\sigma_3 \geqq 120$ kgf/cm^2 . The corresponding effective stress path shown in Fig. 3-2-6 turns down toward the direction of decreasing p', i.e., the skeleton of

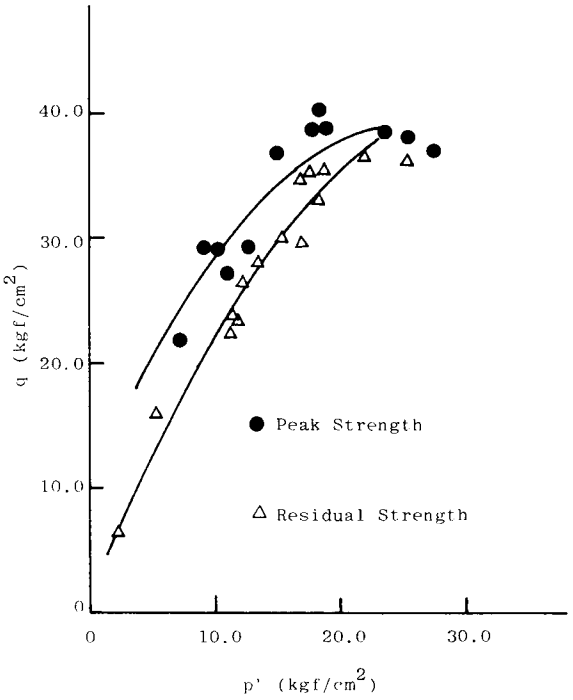

Fig. 3-2-3 Strength envelopes of sandy silt rock

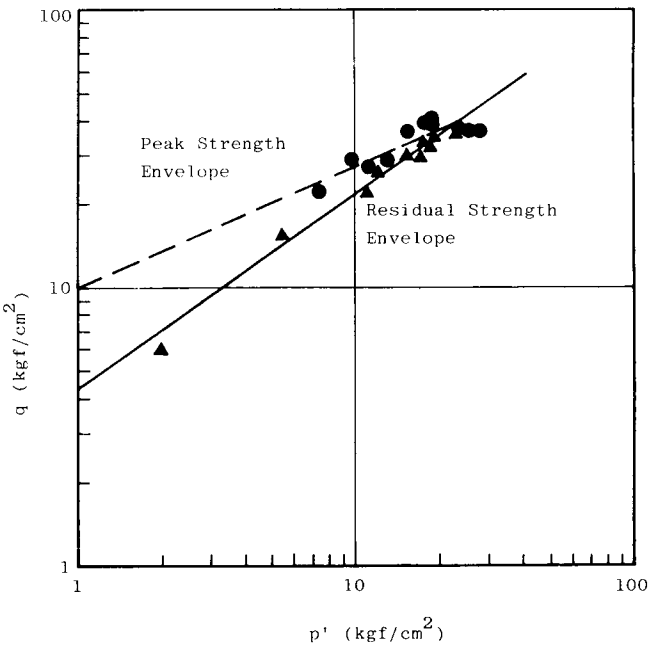

Fig. 3-2-4 Strength envelopes of sandy silt rock (in log-log scale)

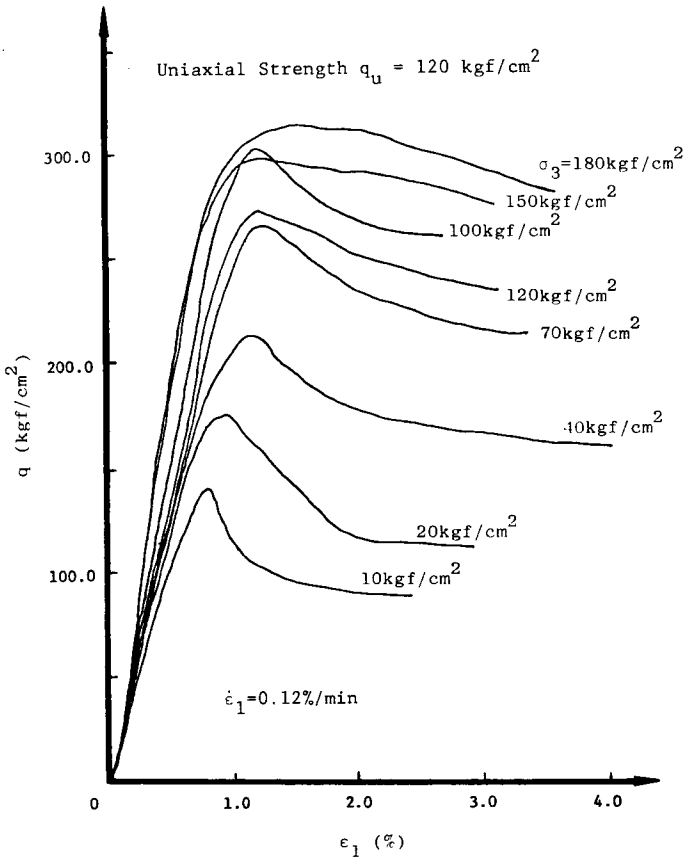

Fig. 3-2-5(a) q-ε_1 relationships of Funyu rock (Ref. 3-12)

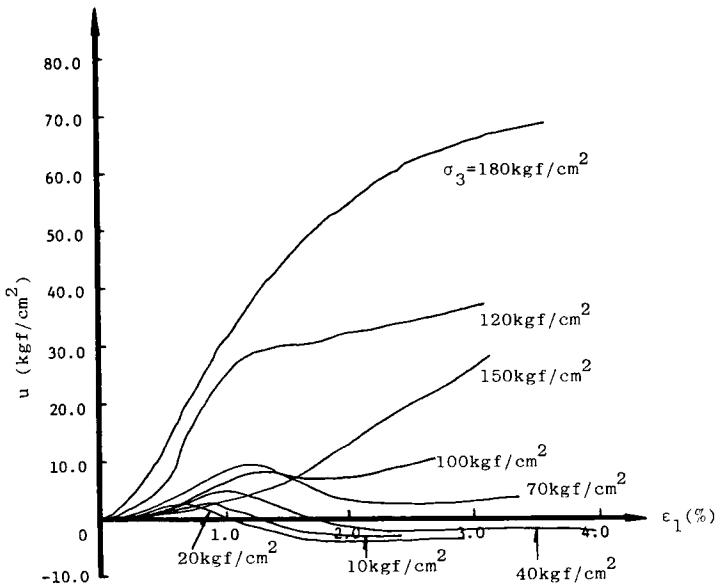

Fig. 3-2-5(b) u-ε_1 curves of Funyu rock (Ref. 3-12)

specimen should gradually contract and become denser than that at peak strength point.

On the other hand, since the B-value of Funyu rock is 0.5 - 0.8, the excess pore water pressure generated in each specimen during a pre-failure shearing process was relatively lower than the increase of mean principal stress. Consequently, the influence of the excess pore water pressure on the effective stress paths became so weak that all the pre-failure parts along these paths (in Fig. 3-2-6) had the same inclination about 3. In other words, these paths were approximately near to the total stress paths.

Expressing the peak and residual strength points of these effective stress paths into a log q - log p' plane, (see Fig. 3-2-7), the peak and residual strength envelope of Funyu rock rendered:

$$q/p'_0 = \alpha \cdot (p'/p'_0)^{\beta} \qquad (3\text{-}2\text{-}2)$$

where p'_0 = 10 kgf/cm^2, and α=5.69, β=0.52 for peak strength envelope,

α=3.00, β=0.71 for residual strength envelope.

It is obvious that, when p'=250 kgf/cm^2, the difference in peak and residual strengths should vanish.

Nikko rock specimens were also tested. It was a kind of green sedimentary tuff containing some quartz particles about 0.2 mm in diameter. The B-value of Nikko rock was 0.65-0.7.

The triaxial cell used in this series was the one whose maximum tolerable pressure was 100 kgf/cm^2. It was the same cell which had been used in the tests of sandy silt rock. The highest confining pressure adopted in this series was 60 kgf/cm^2. Back pressure of 5 kgf/cm^2 was applied in each test.

To monitor the ε_v (= ε_1+2 ε_3) change of the specimen during shearing process (although these shear tests were performed under undrained condition),

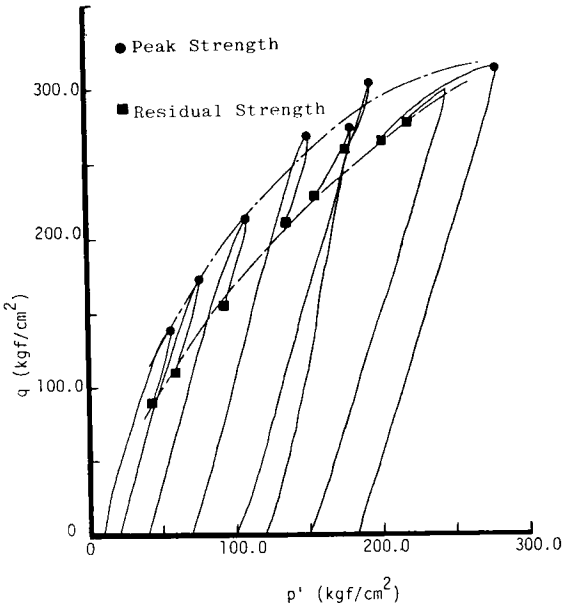

Fig. 3-2-6 Effective stress paths of Funyu rock (SST) (Ref. 3-12)

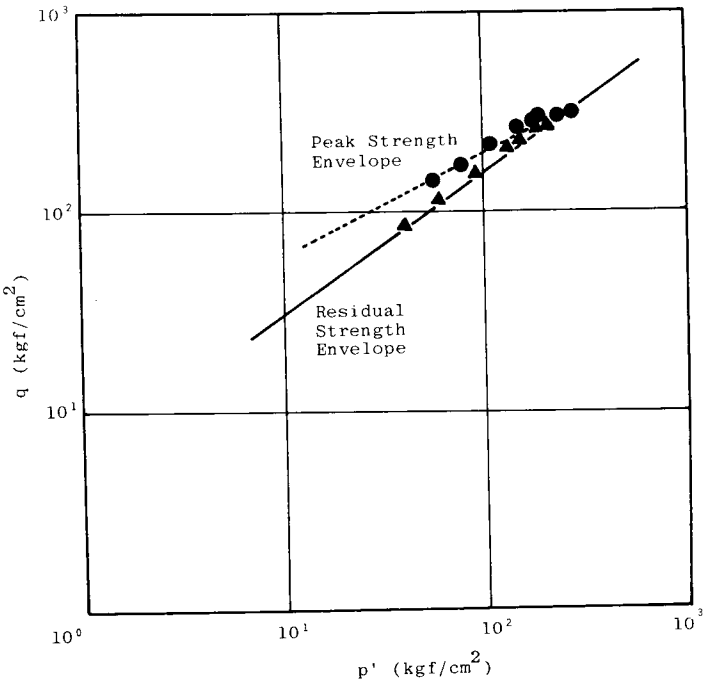

Fig. 3-2-7 Strength envelopes of Funyu rock (in log-log scale) (Ref. 3-12)

a strain gauge was used to measure the lateral strain change of it. As it was unexpected that the strain gauge might fail during the shearing process, a kind of plastic strain gauge was selected, which had 60 mm in length and could provide extension up to 10 %.

But, in securing the strain gauge on to the surface of rock specimen, several difficulties were encountered. Since the specimen was saturated with water, it was difficult to paste the gauge directly on to it. And, comparing with the circumference of the specimen (15.7 cm), the length of strain gauge was not long enough for monitoring the overall lateral strain change around a specimen.

In order to overcome these difficulties, a thin narrow strip of aluminum foil was used. The tension stiffness of the foil was stronger than the strain gauge, yet did not restrict the deformation of specimen. Rolling the strip over the central part of the lateral surface of a specimen, with ends firmly secured with a strong adhesive agent. Finally, strain gauge was pasted on the strip with the same adhesive agent (see Fig. 3-2-8(a)). In setting the specimen, the lead wire which transmitted the resistance change of the strain gauge must be drawn out through the membrane covering the specimen. To prevent water leakage through the hole digged for the passage of lead wire, the hole was stuffed with coating tape, coating paste and rubber adhesive agent. A specimen after complete preparation is shown in Fig. 3-2-8(b).

Mechanic results of the Nikko rock were derived after a series of triaxial compression shear test. Fig. 3-2-9(a) shows the q-ε_1 relationships, while the excess pore water pressures against axial strains are despicted in Fig. 3-2-9(b). All tests were conducted under axial strain control with a rate of 0.12 %/min.

According to Fig. 3-2-9(a), all tested specimens had behaved as strain-softening material beyond the peak strength. Similarly to the behavior of the

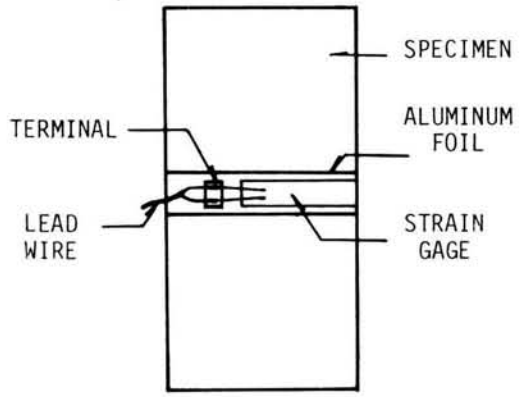

Fig. 3-2-8(a) The setting manner of lateral strain gauge

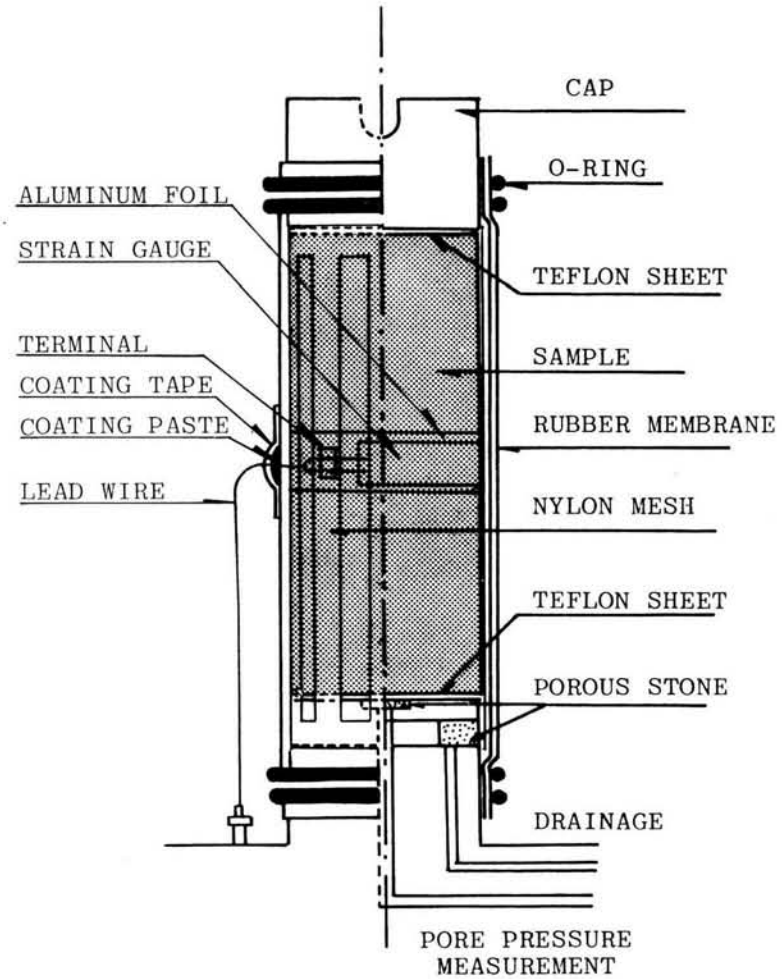

Fig. 3-2-8(b) The detail of a specimen after complete preparation for test

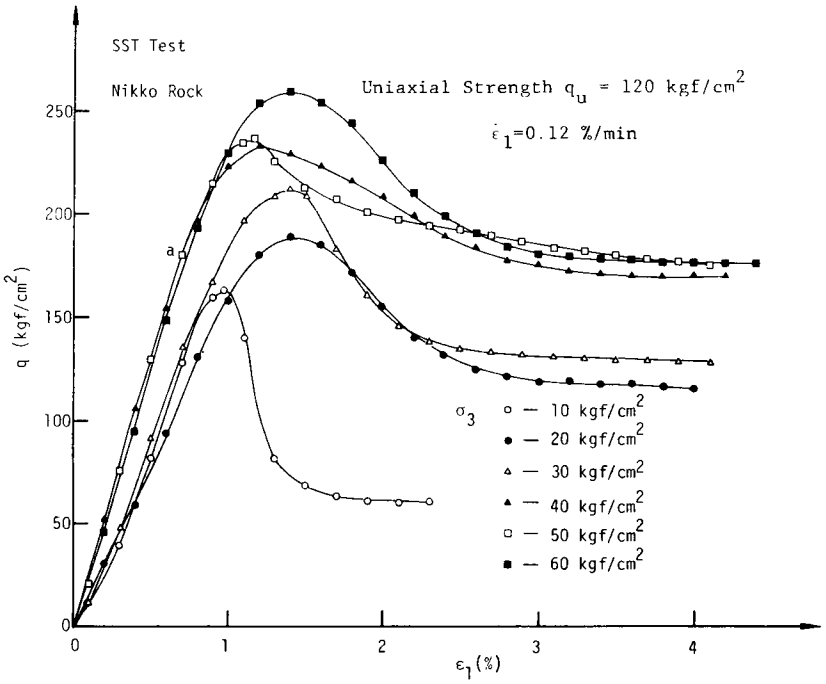

Fig. 3-2-9(a) q-ε_1 relationships of Nikko rock (SST)

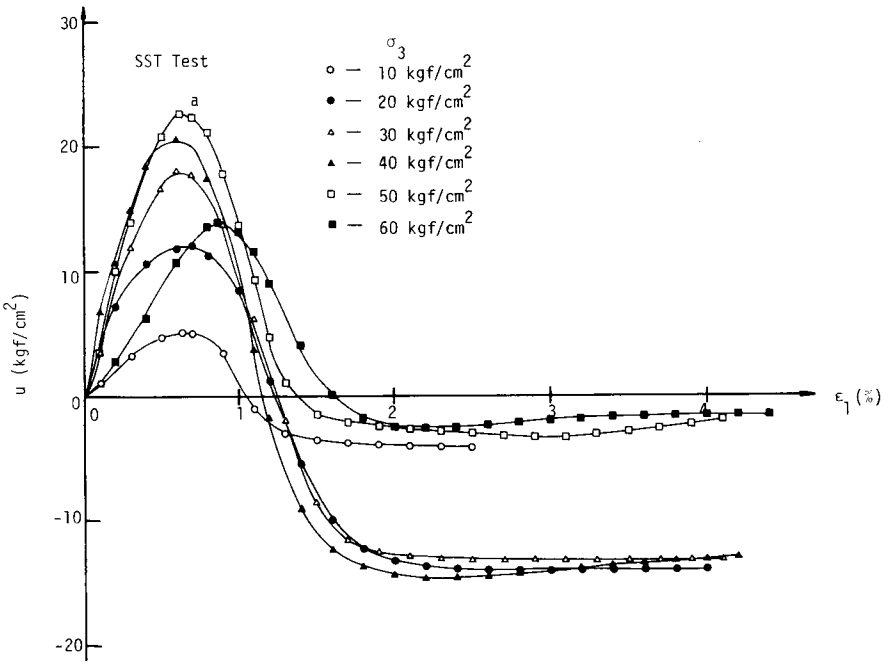

Fig. 3-2-9(b) u-ε_1 curves of Nikko rock (SST)

sandy silt rock and Funyu rock (tuff), the peak strength, elastic modulus of the initial part of shearing of Nikko rock increased with raising confining pressure. However, the strength recedence beyond the peak strength point became less in the range of higher confining pressures.

A common feature exists in Fig. 3-2-9(a), that is the peak strength points appeared within the range of ε_1 from 1.0 to 1.4 %. On the contrary, the peak u points were distributing within ε_1 = 0.6 to 0.9 % (see Fig. 3-2-9(b)).

The relationships between the volumetric strain change ε_v (calculated by $(\varepsilon_1 + 2\varepsilon_3)$) and axial strain ε_1 in Fig. 3-2-9(c) indicate that all peak strain points of volumetric change curves can be located in ε_1 from 0.6 to 0.9 %. And, the relation curves of q-ε_v are depicted in Fig. 3-2-9(d). Hence, from the microscopic views, it can be confirmed that the change of excess pore water pressure is an equivalent phenomenon to the volumetric strain change. Especially, this is evident before the shear failure band had been completely formed in rock specimen. The microstructure change of rock specimen will be discussed in details in Chapter 5.

Finally, the effective stress paths, peak strength and residual strength envelope of Nikko rock are depicted in Fig. 3-2-10. Since the B-value of Nikko rock (0.65-0.9) was somewhat larger than that of Funyu rock (0.5-0.8), the influence of excess pore water pressure on effective stress path would be more apparent. Therefore, the slope of effective stress paths of Nikko rock specimens would be different from 3. This could be found in the effective stress paths of Funyu rock shown in Fig. 3-2-6 previously.

Moreover, the peak strength envelope and residual strength envelope for the Nikko rock tested assumes the following relation in logarithmic scales as,

$$q/p'_0 = \alpha \cdot (p'/p'_0)^{\beta} \qquad (3\text{-}2\text{-}3)$$

where, p'_0 = 10 kgf/cm^2

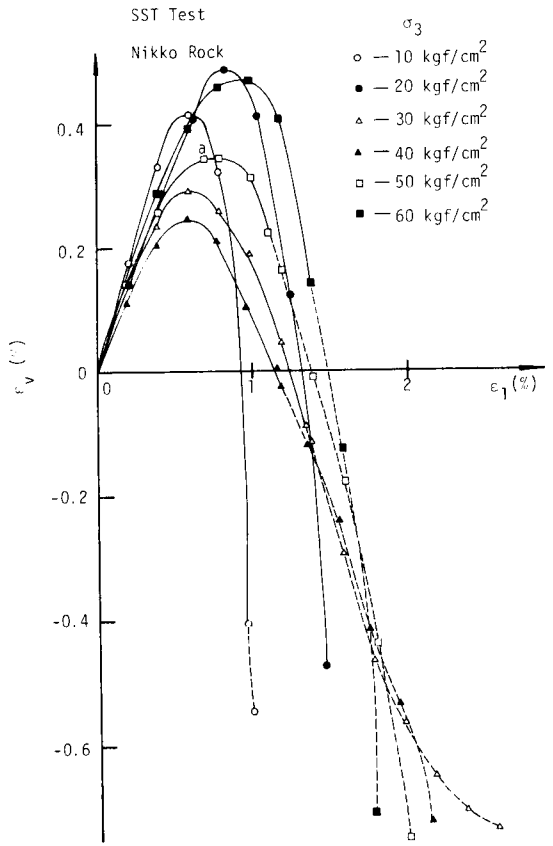

Fig. 3-2-9(c) ε_v-ε_1 curves of Nikko rock

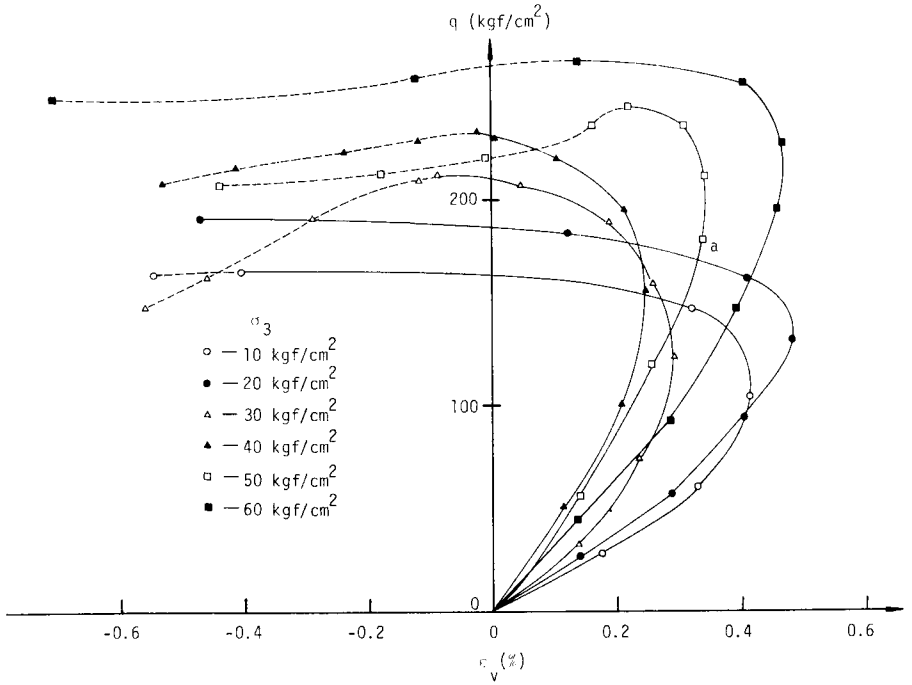

Fig. 3-2-9(d) q-ε_v relationships of Nikko rock

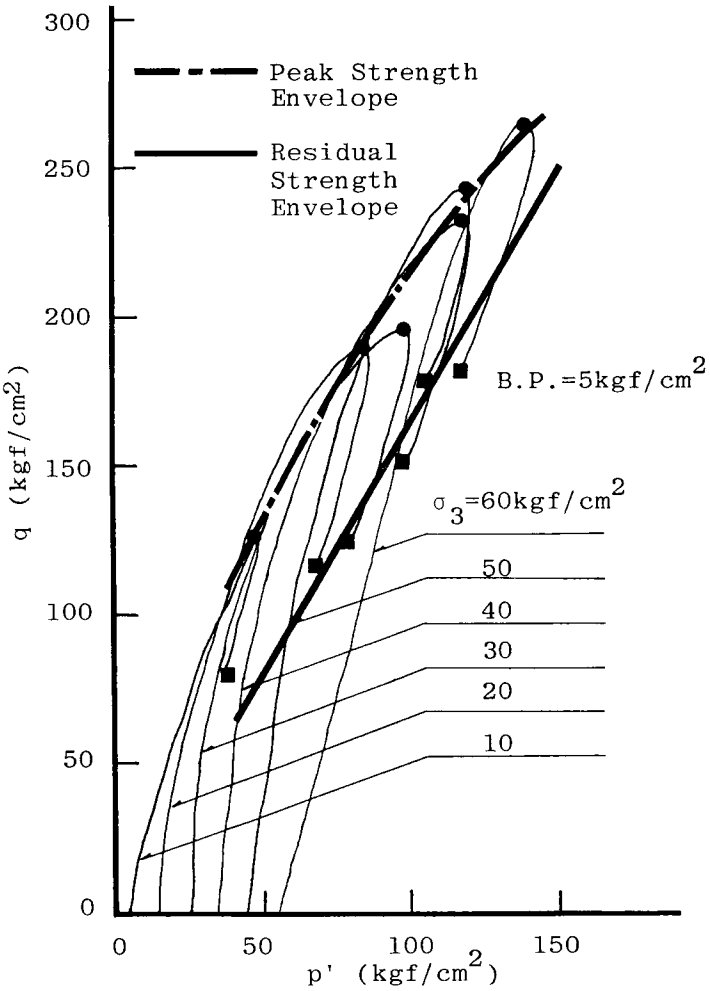

Fig. 3-2-10 The effective stress paths, strength envelopes of Nikko rock

and α = 6.20, β = 0.54 for peak strength envelope

α = 2.68, β =0.77 for residual strength envelope (see Fig. 3-2-11).

3-2-2 Conclusions

Upon the completion of a series of triaxial compression shear tests on sandy silt rock, Funyu rock and Nikko rock, the behavior of soft rocks may be generalized as follows:

(1) From Figs. 3-2-1(a) and (b), Figs. 3-2-5(a) and (b) and in addition to Figs. 3-2-9(a), (b), it is clear that under appropriate confining pressure, the culmination of excess pore water pressure always appeared well before the peak strength point. The same phenomenon can also be observed from $\varepsilon_v(=\varepsilon_1+2\varepsilon_3)$ $-\varepsilon_1$ curves in Fig. 3-2-9(c).

Moreover, these $q-\varepsilon_1$ curves had linear relationship before reaching a peak excess pore water pressure point. Hence, it is reasonable to refer to the portion of shearing process before peak u point as "elastic region". Further classification of shearing process of soft rocks will be discussed in Chapter 5, revealling different result from that of quartizite proposed by Bieniawski (1969)[26] (see Fig. 3-2-12).

(2) The failure pattern of specimen after shearing failure was deeply affected by confining pressure and can be primarily divided into three types (see Photo. 3-2-1). In low confining pressure triaxial test (or uniaxial shear test), the failure planes of specimen always resembled the type (a) in Photo. 3-2-1. It was formed by a tensile fracture passed through the top and bottom edge of the specimen.

However, if higher confining pressure was used in triaxial shear test, the specimen was deformed into a "barrel" type. No obvious rupture pattern could be found in the lateral surface of the specimen (see Photo. 3-2-1(c)).

When triaxial shear test was carried out under an intermediate confining

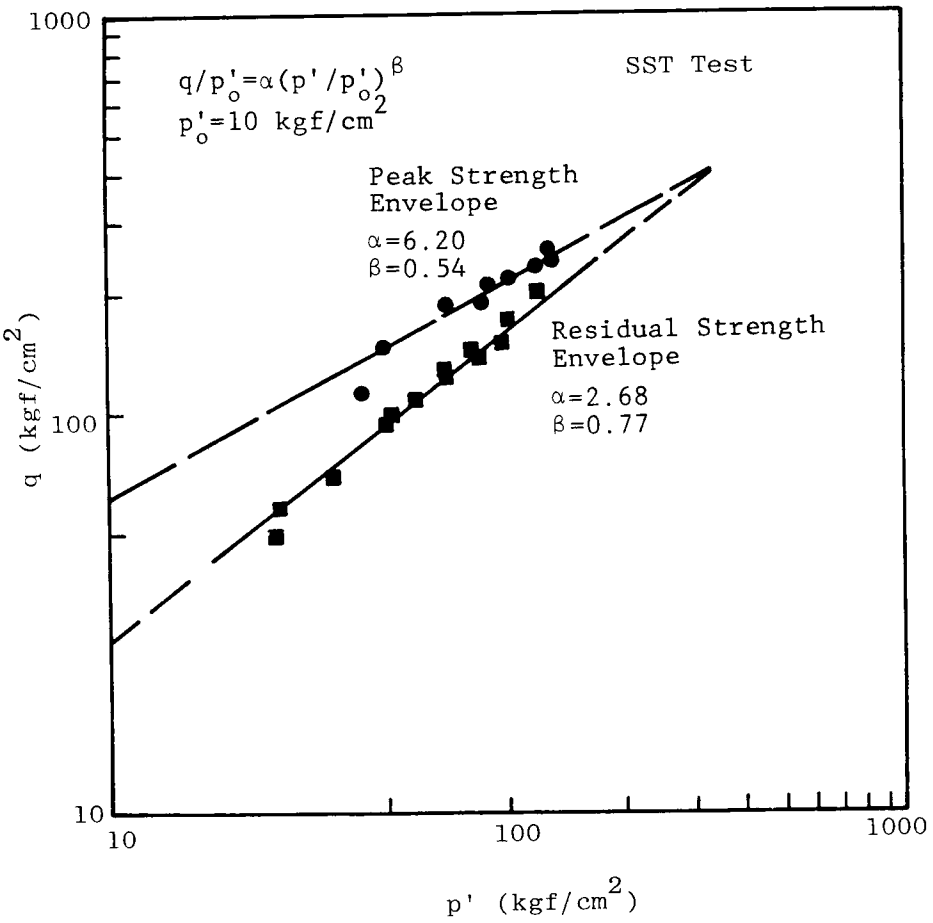

Fig. 3-2-11 Strength envelopes of Nikko rock (in logarithmic scales)

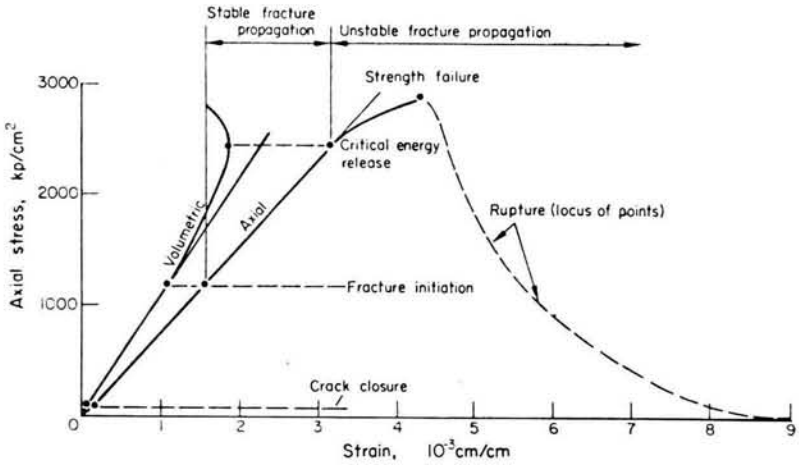

Fig. 3-2-12 **Brittle fracture processes in rock—for quartzite in gradually increased compression.** (Ref. 3-25)

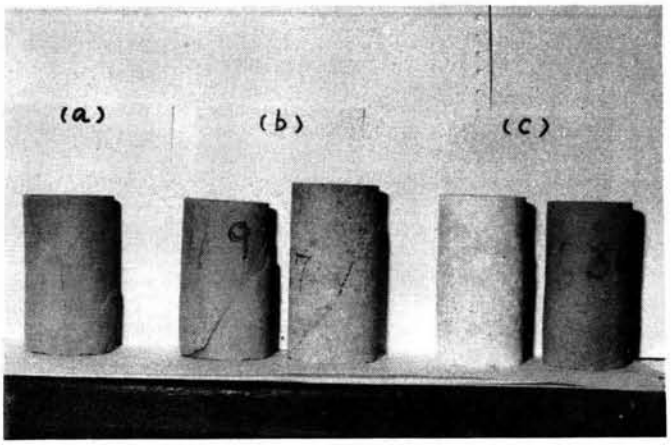

Photo. 3-2-1 The failure pattern of rock specimen

pressure, the failure pattern of specimen was identical to that shown in Photo. 3-2-1(b). A single inclinating shear plane could be clearly seen.

(3) Under low confining pressure, the peak strength was quite different from the residual strength (see Fig. 3-2-4, Fig. 3-2-7 and Fig. 3-2-11). The peak strength envelope intersected with the residual strength envelope at p'= 25 kgf/cm^2 in the case of sandy silt rock, at 250 kgf/cm^2 for Funyu rock and about 350 kgf/cm^2 for Nikko rock.

The stress state of the intersection of peak and residual envelopes was termed as "pre-hereditary stress" by Adachi (1979)[27]. A confining pressure higher than this pre-hereditary stress is called high confining pressure. A specimen behaved as a strain hardening material under high confining pressure in all tests, thus, resulting no difference between the peak strength and the residual strength, just like the normally consolidated clay does.

(4) All series of triaxial shear test were performed under undrained condition. However, during the undrained shearing process, the increment of pore water pressure Δu and the change of total isotropic pressure $\Delta\sigma_m$ could be related as:

$$\Delta u = B \cdot \Delta\sigma_m \quad (3\text{-}2\text{-}4)$$

where B is the pore pressure coefficient.

The value of B can be determined by

$$B = \frac{1}{1 + n \cdot \frac{m_f}{m_v}} \quad (3\text{-}2\text{-}5)$$

where n is the porosity of rock specimen, while m_f and m_v are the compressibility of the fluid phase and the skeleton of rock, respectively[28].

m_f is a constant about 4.9×10^{-5}/kgf/cm^2 (15°C). But, m_v is significantly dependent on the kind of the matrix of specimen. For example, to the normally consolidated clay, m_v = $6{,}000\times10^{-5}$ /kgf/cm^2 was obtained by Skempton (1961)[29],

thus B≒1.

Skempton did not talk about the m_v value of such materials as Funyu rock or Nikko rock. Because Funyu rock is a well defined soft rock, it is therefore reasonable to estimate that m_v of Funyu rock is slightly larger than that of concrete. According to Skempton (1961)[29], m_v value of concrete is 2×10^{-5} / kgf/cm^2. From Table 2-1, n = 28.9 % is obtained for Funyu rock, and taking $m_v = 3\times10^{-5}$ /kgf/cm^2, thus rendering the B value as:

$$B \doteqdot 0.68$$

The B value is about the mid-value of 0.5 and 0.8, both being measured in practical testings.

(5) The relationship between the direction of stress path and the dilatancy of rock specimen will now be arrived.

As all tests were performed under constant confining pressure, $\Delta\sigma_3 = 0$, therefore, $\Delta q = \Delta\sigma_1 - \Delta\sigma_3 = \Delta\sigma_1$, $\Delta p = \Delta\sigma_m = \frac{1}{3}(\Delta\sigma_1 + 2\Delta\sigma_3) = \frac{1}{3}\Delta\sigma_1$ and $\Delta p' = \frac{1}{3}\Delta\sigma_1 - \Delta u$.[28] The total stress path had an inclination of $\Delta q/\Delta p = 3$. But, the slope of effective stress path is calculated by $\Delta q/\Delta p' = \Delta\sigma_1/(\frac{1}{3}\Delta\sigma_1 - \Delta u)$. If there were not any tendency to change the skeleton of specimen during shearing process, then, neither suction nor excess compression would be created inside the specimen. Therefore, any increase in the average of external force (Δp) must be supported by the pore water. Assuming B=1, then $\Delta u = B\cdot\Delta\sigma_m = B\cdot\Delta p = 1\cdot\frac{\Delta\sigma_1}{3} = \frac{\Delta\sigma_1}{3}$, the slope of effective stress path $\Delta q/\Delta p'$ would approach infinitive ($\Delta q/\Delta p' = \Delta\sigma_1/(\frac{1}{3}\Delta\sigma_1 - \Delta u) = \Delta\sigma_1/(\frac{1}{3}\Delta\sigma_1 - \frac{1}{3}\Delta\sigma_1) = \Delta\sigma_1/0 = \infty$).

If the specimen tends to dilate, suction will naturally be created in the pore of skeleton, thus reducing the pore water pressure to a level lower than it would take up alone without suction, i.e., $\Delta u = B\cdot\Delta p = \frac{1}{3}\Delta\sigma_1$. In other words, the true increment of pore water pressure becomes $\Delta u_t < \Delta u = \frac{1}{3}\Delta\sigma_1$, and $\frac{1}{3}\Delta\sigma_1 - \Delta u_t > 0$.

Accordingly, if dilatancy is being created in specimen, the slope of effective stress path is $\Delta q/\Delta p' = \Delta\sigma_1/ (\frac{1}{3} \Delta\sigma_1-\Delta u_t) > 0$, indicating a positive inclination in the q-p' plane.

However, if the specimen skeleton was compressed, then, the pore water would be subjected to a pressure higher than it would have taken alone ($\frac{1}{3}\Delta\sigma_1$). Therefore, $\Delta u_t > \frac{1}{3}\Delta\sigma_1$, $\Delta q/\Delta p' = \Delta\sigma_1/(\frac{1}{3}\Delta\sigma_1-\Delta u_t) < 0$, the effective stress path will direct toward the bottom left of the q-p' plane, when negative-dilatancy (compression) is generated in a specimen.

The relation of the inclination of effective stress paths and the skeleton change of rock specimen with B=1 can be conclusively depicted in Fig. 3-2-13.

Practical application has found that rock-like materials often have a B-value less than 1. Then, a question exists that whether a new method, based on the inclination of effective stress path, can be used to distinct the specimen when B<1 is being dilatant or not.

Applying an increment Δp to a saturated rock-like specimen and without disturbing its skeleton, a differential amount of pore water pressure $\Delta u=B\cdot\Delta p$ can be obtained. Thus, an effective stress path, which presents a shearing process with no tendency of changing the skeleton of specimen, can be expressed as a straight line with a positive gradient $\Delta q/ \Delta p' = \Delta\sigma_1/(\Delta p-\Delta u) = \Delta\sigma_1/ (\frac{1}{3}\Delta\sigma_1-\frac{B}{3}\Delta\sigma_1) = 1/(\frac{1}{3}(1-B)) = 3/(1-B)$ (see Fig. 3-2-14).

Any effective stress path directs to the right hand side of the straight line indicates that the specimen is dilatant in shearing. On the other hand, the path which turns to the left of this line says that the skeleton of the specimen is compressed.

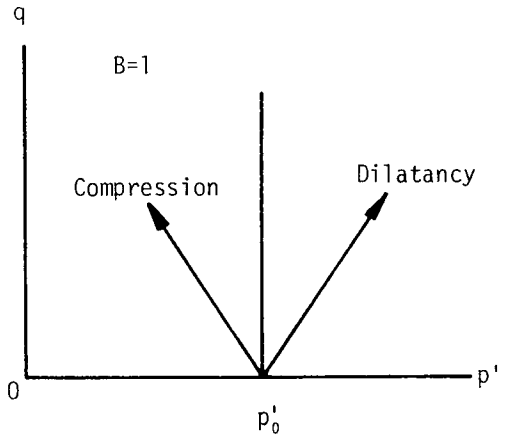

Fig. 3-2-13 The relationship between the direction of effective stress path and the dilatancy of rock specimen (B=1)

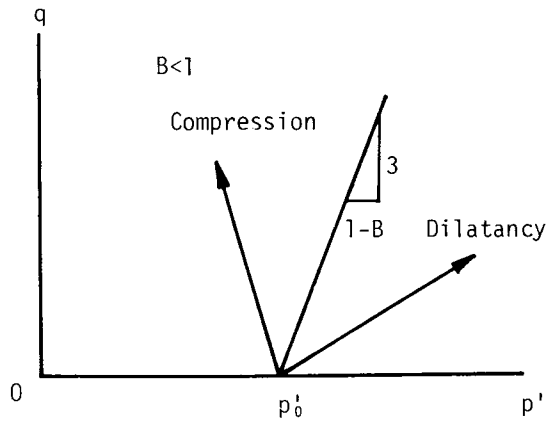

Fig. 3-2-14 On the basis of the direction of effective stress path to determine whether the specimen is dilatant or not (B<1)

3-3 Mechanical Behaviors of Soft Rock in Cyclic Loading

3-3-1 Introduction

The examination of the failure of rock-like materials can be performed from either microscopic or macroscopic point of view.

On the basis of microscopic view, stress concentration around micro-crack or fault in a specimen is the main factor which directly causing failure. Of course, the localized tensile stress and strain, induced by the axial loading, have often contributed to the occurrence of failure. Griffith failure theory[14], a crack progression theory in isotropic brittle material, is a representative theory of the microscopic field.

However, because of the further extending of a progressed crack needs quite a large amount of energy[15], a compression failure of rock or concrete specimen is not likely to be promoted alone by the progression of a single crack. From experimental evidence available, it has been found that the failure is always produced by the penetration of many progressed cracks. It is obvious that although the Griffith theory can explain the onset of the failure of a rock-like material very well, it is inadequate for monitoring the process of compression failure.

Consequently, in order to understand the pertinent behavior of the failure process, technique derived from the macroscopic concepts is naturally employed.

Sponer & Dougill (1975)[10], and Okada, Koyanagi & Rokugo (1976, 1979)[8),9] have investigated the fracture process of a concrete specimen in compression, by using the concept of energy - the total energy of specimen. They proposed that the external energy supplied to concrete specimen during the process of shearing failure is intrinsically transformed into two parts, recoverable

strain energy E_r and irrecoverable strain energy E_i. The former is continously stored in specimen during the shearing process, whilst the latter could further be divided into two parts, E_{crack} and $E_{friction}$. The E_{crack} is the energy used to progress the crack growth and $E_{friction}$ is expended against the viscous friction within the liquid phase and the friction between the particles of specimen.

By carefully measuring these three kinds of energy during shearing process, the behavior of compression failure of a concrete specimen can quantitatively be comprehended.

Recently, Yashima (1981)[12] smoothly expands this technique into the field of the failure of saturated soft rock (Funyu rock), with excellent results.

3-3-2 Definition of Energy and Results

To distinct the energies which would be stored or dissipated during the process of compression failure, the use of a σ-ε_1 relationship of "cyclic loading test" is the most appropriate.

Generally, two different cyclic loading tests are adopted in the laboratory works. The first is formed by several loading-unloading cycles within the shearing process as illustrated in Fig. 3-3-1 and Fig. 3-1-4, and tentatively referred as simple cyclic loading test. The other is called as constant upper stress cyclic loading test, depicted in Fig. 3-3-2 and Fig. 3-1-3. In the latter test, unloading process in each cycle is carried out when the stress of specimen reaches a previously determined level, and it can also be regarded as a dynamic creep test.

Before explaining the physical meaning contained in Figs. 3-3-1 and 3-3-2, it is necessary to define the E_r and E_i in a single loading-unloading cycle, for example, the OPR cycle as illustrated in Fig. 3-3-3. The curve OP indicates the loading process, whilst PR representing the unloading process. The

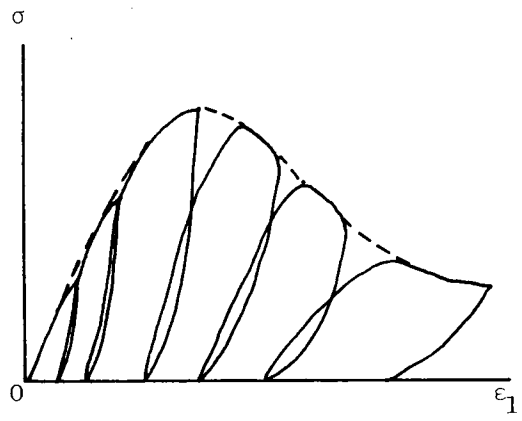

Fig. 3-3-1 Simple cyclic loading test

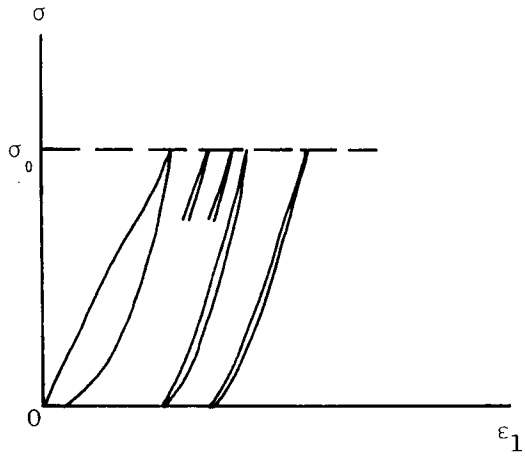

Fig. 3-3-2 Constant upper stress cyclic loading test

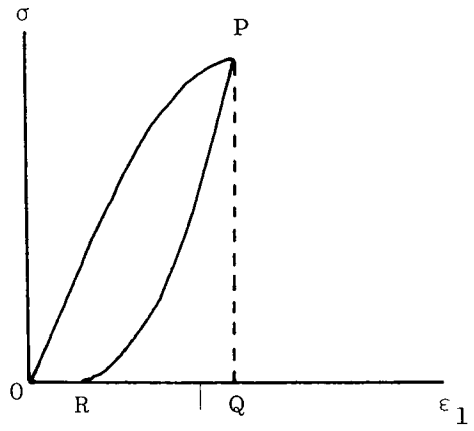

Fig. 3-3-3 A single cycle of cyclic loading test used for defining the recoverable and irrecoverable energies.

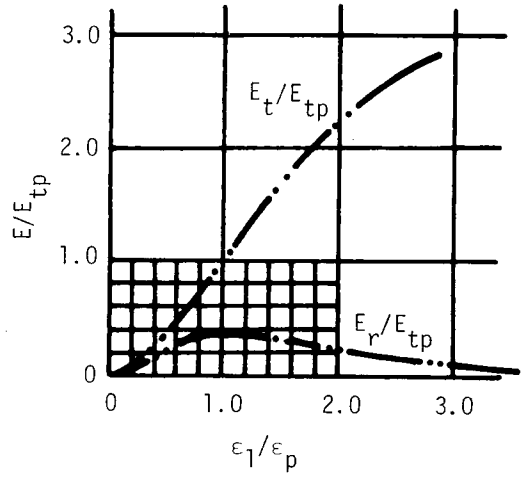

Fig. 3-3-4 E/E_{tp}-$\varepsilon_1/\varepsilon_p$ relation curves of concrete (Ref. 3-7)

total external work E_t, provided to the specimen for the shear strain reaching at point P, can be calculated by the area under the loading curve OP, i.e., the area of OPQ. On the other hand, the area PQR under unloading curve PR characterizes the recoverable energy (E_r) of this cycle. Finally, the difference between the total external work E_t and the recoverable energy E_r is tentatively defined as the irrecoverable energy (E_i). This can be schematically indicated by the area of OPR.

Assuming that the σ-ε_1 envelope of a simple cyclic loading test, the broken line in Fig. 3-3-1, is so similar to that of an original triaxial shear test. Therefore, the total external energy input E_t, which originally must be calculated from the σ-ε_1 curve of an original triaxial test, can alternatively be obtained from the envelope of a simple cyclic test.

Dividing all energies by E_{tp} (the total energy at the peak strength point P) and all strains by ε_p (the axial strain at the peak strength point), a relationship of normalized energy and axial strain can be deduced to a specimen. As an example, the result obtained from a concrete specimen is presented in Fig. 3-3-4[8]. According to the inclination of E_r/E_{tp} in this figure, it is

clear that the maximum recoverable strain energy appears at the peak strength point which corresponds to some 40 % of the total external work.

After this peak, E_r gradually decreases even with the increasing of shearing strain. The value of E_r/E_{tp} becomes negligible when the residual state is reached. Therefore, on the basis of the concept of energy, it follows that the peak strength has a special significance. Clearly, if a specimen can not further store any other increment of recoverable strain energy, then, the stress state of this specimen will arrive at its maximum level, that is to say, its peak strength.

This phenomenon can also be observed from the result obtained by Yashima[12], from soft rock specimen (see Figs. 3-3-5(a) and 3-3-5(b)). These two figures also indicate that E_r/E_{tp} usually varies with the confining pressures.

Moreover, from the relationship of constant upper stress cyclic loading test, energy which is spent or stored in each cycle may be measured in the way similar to that mentioned in Fig. 3-3-3.

Upon comparing the irrecoverable strain energy in each cycle, the change within the specimen under test can indirectly be detected. Fig. 3-3-6 depicts the relationship of E_i versus the number of cycles to a concrete specimen proposed by Okada and his coworkers (1976)[8]. It shows that the irrecoverable strain energy which is expended for propagating cracks (E_{crack}) and resisting the friction between particles or liquid phase ($E_{friction}$) has an extremely large value at the first cycle. But, it decreases rapidly and becomes relatively small at the second cycle and gradually converges to a constant value, $E_{friction}$.

From the view of mechanical behavior, the difference between the first cycle and other cycles is that most of the crack propagation takes place during the first cycle, not during the later cycles.

It is then obvious that the converged E_i, represented by broken line in

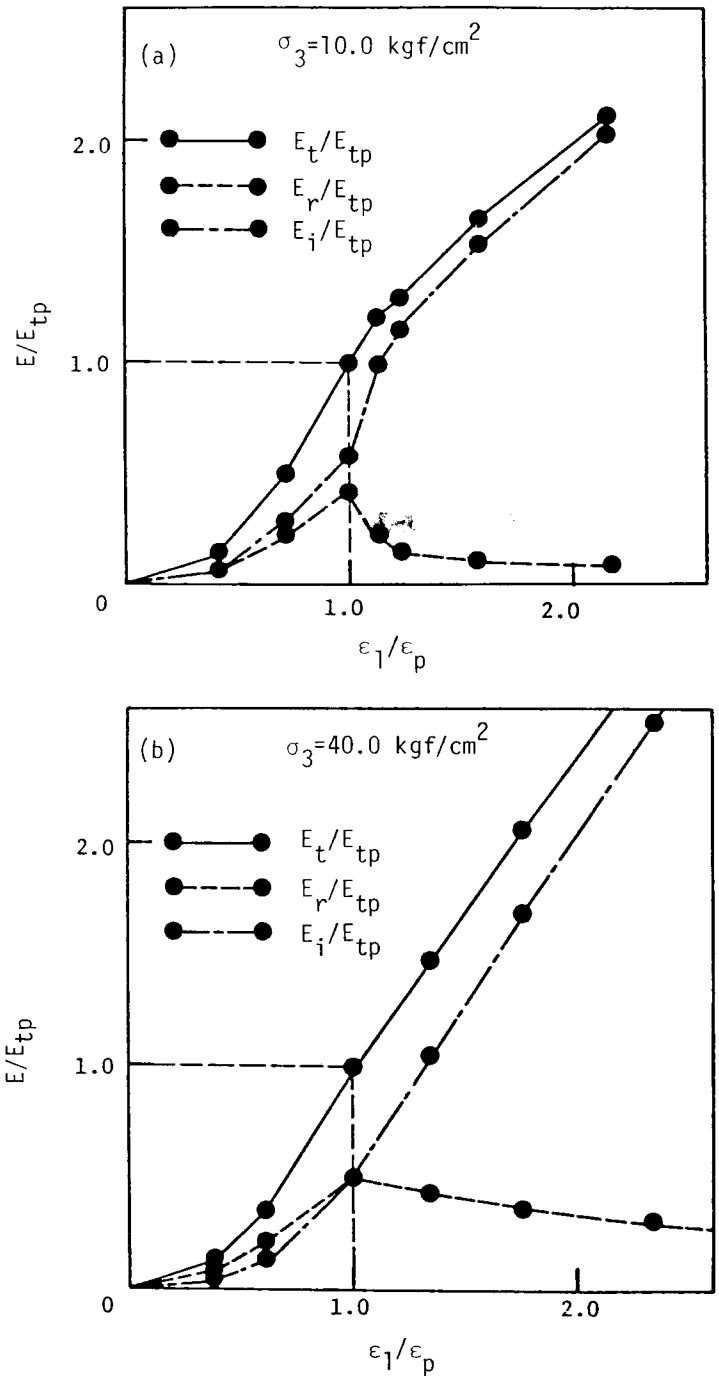

Fig. 3-3-5 E/E_{tp} - $\varepsilon_1/\varepsilon_p$ curves of Funyu rock (a) σ_3=10 kgf/cm^2; (b) σ_3=40 kgf/cm^2 (Ref. 3-12)

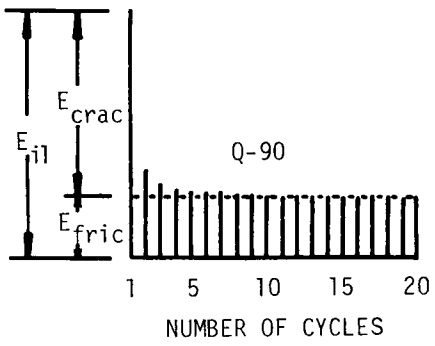

Fig. 3-3-6 E_i-number of cycles relationship of concrete specimen (Ref. 3-8)

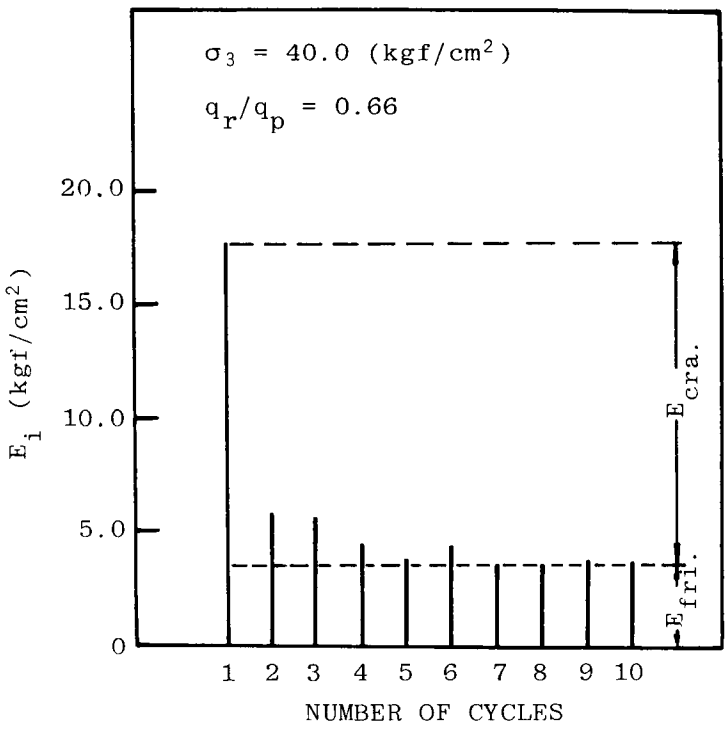

Fig. 3-3-7 E_i-number of cycles relationship of Funyu rock (Ref. 3-12)

Fig. 3-3-6, indicates only the friction resisting energy ($E_{friction}$). Hence, E_{crack} in the first cycle would be evaluated by ($E_i - E_{friction}$). Consequently, the irrecoverable energy in the first cycle can correctly be separated into E_{crack} and $E_{friction}$. From Fig. 3-3-6, it is seen that the energy used to progress cracks in the concrete specimen amounts approximately to three-quarters of the E_i in the first cycle.

In a similar manner, the E_i - Number of cycles relation of a soft rock (Funyu rock) is depicted in Fig. 3-3-7[12]. Under a confining pressure of 40 kgf/cm^2, energy used in crack growth in this soft rock specimen was about 78% of the total irrecoverable energy. From Fig. 3-3-5(b), the measured value of E_i/E_t just before reaching the peak strength point was about 0.5. Therefore, approximately 39 % (78 % x 0.5) of the total external work were transformed to the crack-propagation in the first loading cycle of the soft rock specimen.

On the other hand, if increase in the time of consolidation before shearing process in the constant upper stress cyclic loading test, what kind of change about irrecoverable strain energy will happen?

A cyclic loading test was carried out with a constant strain rate of 0.04 %/min. Before performing the 6th cycle, 6 hours consolidation process was undergone. The relationship of σ-ε_1 thus obtained is shown in Fig. 3-3-8(a), whilst Fig. 3-3-8(b) describes the change of irrecoverable energy corresponded to the former.

According to Fig. 3-3-8(b), E_i had almost converged to a constant value in the 4th or 5th cycle. But, after being consolidated for 6 hours, a higher value of E_i was observed at the 6th cycle. It was likely that the increment of E_i in the 6th cycle was not used for new crack growth, but was transferred to $E_{friction}$. Therefore, it is apparent that the extension of consolidation process can slightly improve the viscous friction in the liquid phase or the sliding friction resistance between particles of specimen.

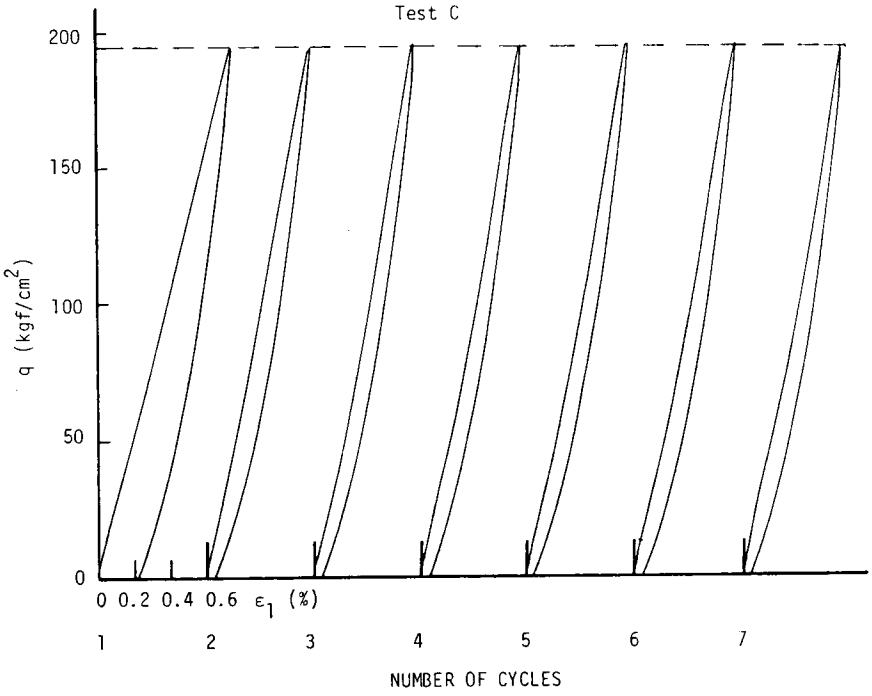

Fig. 3-3-8(a) The q-ε_1 curves of a constant upper stress cyclic loading test with $\dot{\varepsilon}_1$=0.04 %/min (Test C)

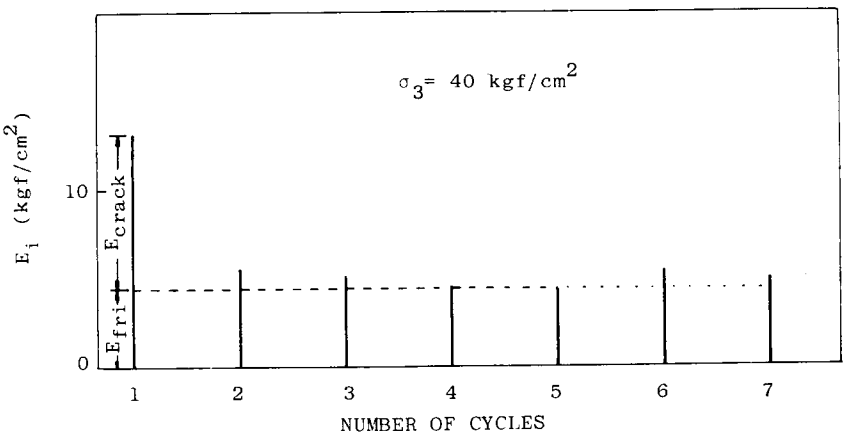

Fig. 3-3-8(b) The irrecoverable energy (E_i) expended in each cycle; E_i can further be divided into two parts- $E_{friction}$ and E_{crack}

References for Chapter 3

(1) Karman , Th. V., "Festigkeitsversuche unter Allseitigem Druck", Verein Deutscher Ingenieur, Berlin, No. 42, 1911.

(2) Böker, R., "Die Mechanik der bleibenden Formänderung in kristallinisch aufgebauten Körpern", Mitteilungen über Forschungasarbeiten auf dem Gebiete des Ingenieurwesens, Vols. 175 and 176, 1915.

(3) Rüsch, H., "Researches Towards General Flexural Theory for Structural Concrete", American Concrete Institute Proceedings 57, pp. 1-28, 1960.

(4) Bieniawski, Z. T., "Time-Dependent Behaviour of Fracture Rock". Rock Mechanics, 2, pp. 123-137, 1970.

(5) Sangha, C. M. and R. K. Dhir, "Influence of Time on the Strength, Deformation and Fracture Properties of a Lower Devoniar Sandstone", Int. J. Rock Mech. Min. Sci., Vol. 9, pp. 343-354, 1972.

(6) Peng, S. S., "Time-Dependent Aspects of Rock Behavior as Measured by a Servocontrolled Hydraulic Testing Machine", Int. J. Rock Mech. Min. Sci. & Geomech. Abstr., Vol. 10, pp. 235-246, 1973.

(7) Akai, K., T. Adachi, K. Yamamoto and Y. Ohnishi, "Creep Deformation Characteristics of Weathered Granite", Memoirs of the Faculty of Engineering, Kyoto University, Vol. XXXIX, Part 1, pp. 183-200, 1977.

(8) Okada, K., W. Koyanagi and K. Rokugo, "Energy Approach on the Fracture Process of Concrete in Compression Related to its Water Content", Proceedings of the Japan Society of Civil Engineers, No. 248, pp. 129-136, 1976.

(9) Okada, K., W. Koyanagi and K. Rokugo, "Energy Approach on the Fracture Process of Concrete in Flexure", Proceeding of JSCE No. 285, pp. 109-119, 1979.

(10) Spooner, D. C. and J. W. Dougill, "A Quantitative Assessment of Damage

Sustained in Concrete during Compressive Loading", Magazine of Concrete Research, Vol. 27, No. 92, pp. 151-160, 1975.

(11) Spooner, D. C., C. D. Pomeroy and J. W. Dougill, "Damage and Energy Dissipation in Cement Pastes in Compression", Magazine of Concrete Research, Vol. 28, No. 94, pp.21-29, 1976.

(12) Yashima, A., "Experimental Study in the Mechanical Properties of Sedimentary Soft Rock", Master Thesis, Kyoto University, 1981.

(13) Griffith, A. A., "The Phenomenon of Rupture and Flow in Solids", Phil. Trans. Roy. Soc. London, A., 221, pp. 163-197, 1921.

(14) Griffith, A. A., "Theory of Rupture", Intern. Congr. Appl. Mech. 1st., Delft, edited by J. Waltman, Jr., pp. 55-63, 1924.

(15) Brace, W. F. and E. G. Bombolakis, "A Note on Brittle Crack Growth in Compression", Journal of Geophysical Research, Vol. 68, No. 12, pp. 3709-3713, 1963.

(16) Walsh, J. B., "The Effect of Cracks on the Uniaxial Elastic Compression of Rocks", Journal of Geophysical Research, Vol. 70, No.2, pp. 399-411, 1965.

(17) Walsh, J. B., "The Effect of Cracks in Rocks on Poisson's Ratio", Journal of Geophysical Research, Vol. 70, No. 20, pp. 5249-5257, 1965.

(18) Walsh, J. B., "The Effect of Cracks on the Compressibility of Rock", Journal of Geophysical Research, Vol. 70, No. 2, pp. 381-389, 1965.

(19) Brace, W. F., B. W. Paulding, Jr. and C. Scholz, "Dilatancy in the Fracture of Crystalline Rocks", Journal of Geophysical Research, Vol. 71, No. 16, pp. 3939-3953, 1966.

(20) Scholz, C. H. and Kranz, R., "Notes on Dilatancy Recovery", Journal of Geophysical Research, Vol. 79, No. 14, pp. 2132-2135, 1974.

(21) Zoback, M. D. and J. D. Byerlee, "The Effect of Cyclic Differential Stress on Dilatancy in Westerly Granite under Uniaxial and Triaxial

Conditions", Journal of Geophysical Research, Vol. 80, No.11, pp. 1526-1530, 1975.

(22) Holcomb, D. J., "A Quantitative Model of Dilatancy in Dry Rock and its Application to Westerly Granite", Journal of Geophysical Research, Vol. 83, No. B10, pp. 4941-4950, 1978.

(23) Akai, K., Y. Ohnishi and D. H. Lee, "The Permeability of Sedimentary Soft Rock in Triaxial Shear Test", 16th JSSMFE Ann. Meeting, pp. 1345-1348, 1981.

(24) Akai, K., Y. Ohnishi and D. H. Lee, "The Mechanical Behavior of Sandy Silt Rock in Multiple Stage Triaxial Test", 34th JSCE Ann. Meeting, pp. 331-332, 1979.

(25) Hobbs, D. W., "A Study of the Behavior of Broken Rock under Triaxial Compression, and its Application to Mine Road Ways", Int. J. Rock Mech. Min. Sci., Vol. 3, pp. 11-14, 1966.

(26) Bieniawski, Z. T., H. G. Denkhaus and U. W. Vogler, "Failure of Fractured Rock", Int. J. Rock Mech. Min. Sci., Vol. 6, pp. 323-341, 1969.

(27) Adachi, T., "A Study of the Mechanical Behavior of Sedimentary Soft Rock" Doctoral Thesis, Kyoto University, 1979.

(28) Akai, K., "Advanced Soil Mechanics", Morikita Publication Co. Ltd., pp. 25-53, 1974 (In Japanese).

(29) Skempton, A. W., "Effective Stress in Soils, Concrete and Rocks", Pore Pressure and Suction in Soils, 38, Butterworths, 1961.

Chapter 4 LABORATORY INVESTIGATION OF MST METHOD FOR SATURATED SOFT ROCK

4-1 Introduction

The triaxial test has usually been employed to characterize the mechanical properties of rock-like materials in a laboratory. This conventional method, called the single-stage triaxial test (SST) provides only a pair of peak and residual strengths from a single specimen (see Fig. 4-1-1(a)). Therefore, it is very inconvenient in achieving the whole spectrum of mechanical characteristics of rock specimens whose amount is so limited due to the geological conditions, etc..

Kovari and Tisa (1975)[1)] have proposed a plausible and economical triaxial shearing test method, designated as the Multiple Failure State Triaxial Test or Multiple Stage Triaxial Test (MST) method.

The stress path of this method is represented in Fig. 4-1-1(b). It is seen from the diagram that a specimen is axially loaded under an initial confining pressure $\bar{\sigma}_3$ in triaxial cell, a peak strength $s_1(\bar{\sigma}_3,\sigma_p)$ can be reached. Subsequently increasing the confining pressure, the second stage of shearing test is then proceeded and yielding peak strength point s_2. Repeating the same operation, it yields s_3 , s_4 and so on until obtaining enough peak strength points or having fracture failure within the specimen. Therefore, the peak strength envelope of this rock can be determined from these points (s_1, s_2, s_3 ,....). In the same manner, a series of residual strengths under different confining pressures and a residual strength envelope can also be obtained.

Therefore, this method is capable of deducing more sets of strength parameters from a single specimen and comprehending the full range of strength envelopes by using a few specimens.

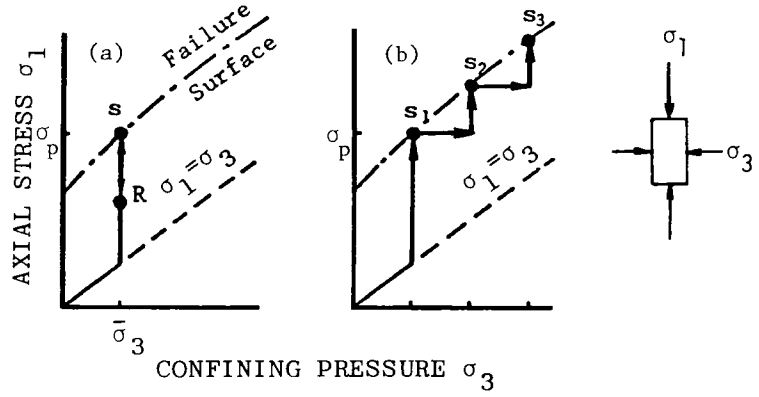

Fig. 4-1-1 Loading procedure in the triaxial test (a) conventional test; (b) multiple failure state test (Ref. 4-1)

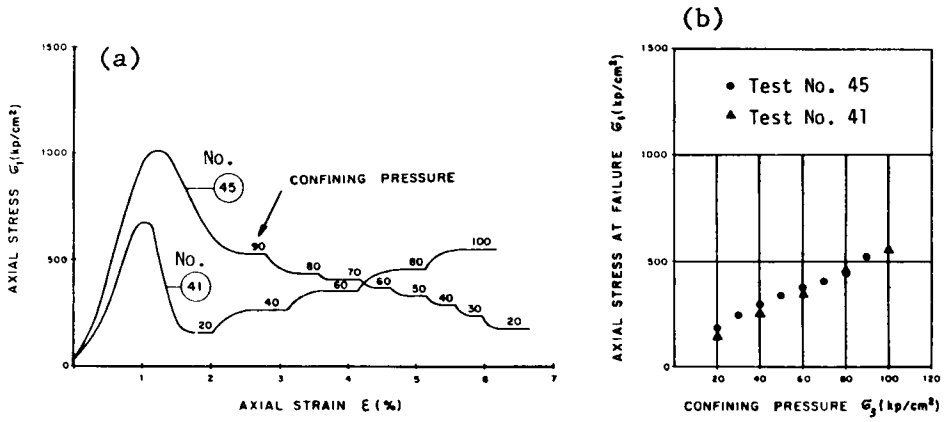

Fig. 4-1-2 Triaxial tests with many limiting states of residual strength. On the left- stress-strain diagrams; on the right- stress points on the yield surface. Marble (Carrara) (Ref. 4-1)

A result of this MST method (Kovari and Tisa (1975))[1] is given in Fig. 4-1-2. It was found, from two marble specimens with different loading processes, that the same residual strength yielded when confining pressures were identical and producing also similar failure envelopes (Fig. 4-1-2(b)). Hence, it has been proved that their MST method is a suitable substitute for the conventional SST when a dry and hard rock specimen such as marble and sandstone is used. However, their test procedure may not be adequate for a saturated porous soft rock.

A new triaxial test method was developed to determine the mechanical behaviors of saturated soft rocks under various confining pressures. The new one is tentatively called as MST for soft rock in order to differentiate from the SST and the MST for hard dry rocks. In this method, a set of peak and residual strengths are obtained after each consolidation-loading-unloading cycle. Loading is normally done by the axial strain rate control.

When the specimen is subjected to lower confining pressure, there exist some difficulties in loading-unloading control of the MST for finding peak strength, especially with a brittle specimen. As the gradient change near the peak strength of the axial stress-axial strain curve is insignificant, a correct prediction of the peak strength point is usually very difficult and misjudgement causes an abrupt failure of the test specimen.

To improve the accuracy of peak-strength MST under lower confining pressure, a new test procedure has been added. This involves the measurement of lateral strain while the test specimen is in axial compression. This is beneficial as the lateral strain can sensitively reflect the volume change due to the development of microcracks within the specimen. Including the monitoring of the axial stress-lateral strain curve, the correct position of peak strength can more accurately be predicted.

In addition, a peak strength MST method with lateral strain rate control

has also been studied. The mechanical behaviors of the specimen, obtained from the results under lateral strain rate control, are compared with those under axial strain rate control.

4-2 Development of MST Method for Saturated Soft Rock

4-2-1 Rock Specimen

In the study, two kinds of rock specimen were used, namely sandy silt rock and tuff (Nikko rock). From the physical properties listed in Table 2-1, one can readily presume that all of these two specimens were very porous and comparatively isotropic and homogeneous.

Cylindrical specimens were prepared in the same direction from rock block and carefully trimmed up to 5 cm in diameter and 10 cm in height, with core cutter and diamond-bladed saw. They were then fully saturated with water by a suction pump for at least 7 days, and kept in water till the time for testing.

4-2-2 Test Procedure

An attempt was made firstly by combining the Kovaris' MST method with unloading operation just prior to the appearance of a peak strength point in each test stage. The reason in adopting unloading was that in Kovaris' MST method, the confining pressure must be changed accordingly when a peak strength point is attained. Practically, it is very difficult to change the confining pressure smoothly during the short interval of time, realizing (from monitoring the σ_1-ε_1 curve) that the peak strength point is very close.

Moreover, in triaxial shearing test, especially under lower confining pressure, the possibility of a sudden fracture failure was very high, when the stress state of specimen genuinely reached a peak strength point. As soon as a

fracture failure was generated, the specimen would drop into strain-softening state and could not be used to obtain the peak strength of other stages any more. In other words, peak strengths could only be yielded when the specimen remained intact. Therefore, due to the hesitation of changing a confining pressure or miss-timing, it often results in over shearing the specimen. In order to extend the time available for changing confining pressure, the unloading of axial load may be adequate and convenient for MST. This procedure is similar to the ones proposed by Chang and Jumper (1978)[2], Kim and Ko (1979)[3] and Chang and Bondurant (1979)[4], at their MST test of oil shale and Raton shale, etc. whose results have been shown to be very reasonable. The stress paths of this loading-unloading MST, tentatively called MST:1, is given in Fig. 4-2-1.

In order to investigate the applicability of MST:1, fully saturated sandy silt rock specimens (Table 2-1) were prepared. A cylindrical specimen was set in a triaxial cell and loaded with initial confining pressure at 10 kgf/cm^2 and a back pressure 3 kgf/cm^2 to proceed consolidation. MST:1 was then carried out in undrained condition with an axial strain rate of 0.12%/min and following

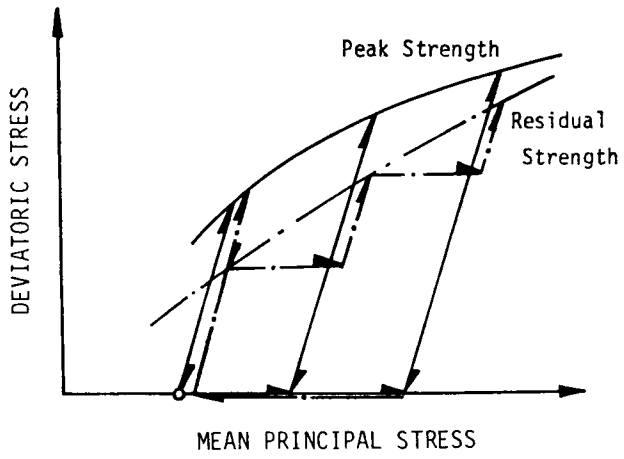

Fig.4-2-1 Stress paths of MST:1

the stress paths depicted in Fig. 4-2-1. The result shown in Fig. 4-2-2 is the deviatoric stress - axial strain relationship. In spite of the changes of confining pressure at each stage, there exist virtually no significant differences among the peak and residual strengths. (In this figure, P10 means that the confining pressure is 10 kgf/cm^2 in the peak-strength test series, R designates "residual".)

It was found later, that the change of pore water pressure in the specimen during test could witness the inadequacy of this MST:1 method. In Fig. 4-2-3, except at P10 stage, whenever the confining pressure was changed from one stage to another, pore water pressure in the specimen was increased at a rate seemingly being proportional to the increment of confining pressure. According to this phenomenon, it was likely that after the shear test of first P10 stage, the existing pores in specimen, which were filled with water, might be compressed. And, a part of the pore water might be separated from the pore and out of the skeleton of the specimen. Hence, the degree of saturation S_r of this specimen would be changed and probably over 100%. Under this condition, whenever the confining pressure was raised by an increment after the first stage, the entire increment would be supported by pore water rather by the skeletal material of the specimen.

A similar phenomenon may be observed in the process of unconsolidated-undrained triaxial test of saturated soils. Conclusively speaking, the MST:1 method is not adequate for deriving strength envelopes of porous saturated soft rock.

It was found out that during the MST of saturated soft rocks, drainage of excess pore water in the specimen must be done before the starting of shearing at every stage, i.e., consolidation process should be introduced. Consequently, we induced a guide line of the multiple stage triaxial test for saturated soft rock; it consisted of three items as follows:

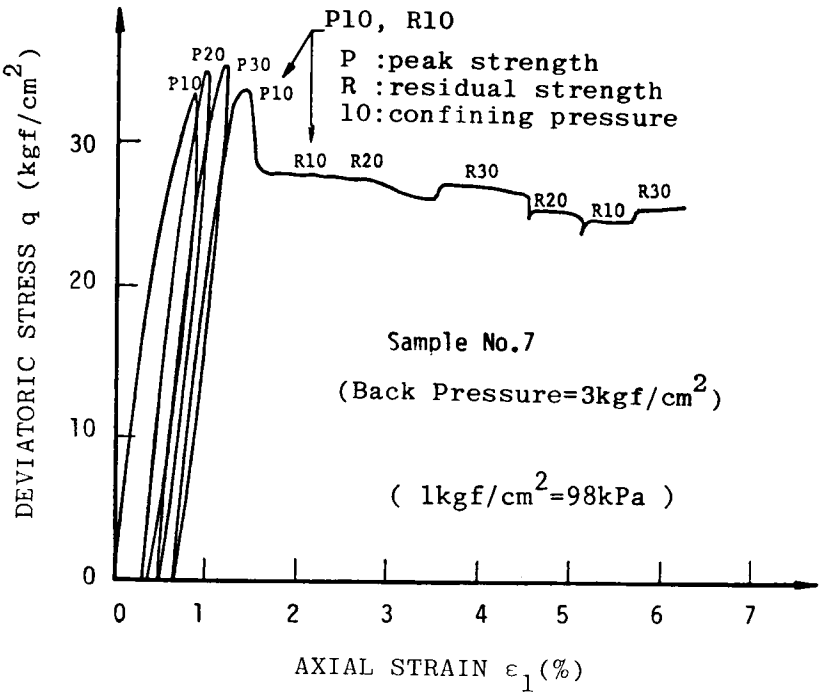

Fig.4-2-2 $q-\varepsilon_1$ curve derived by MST:1

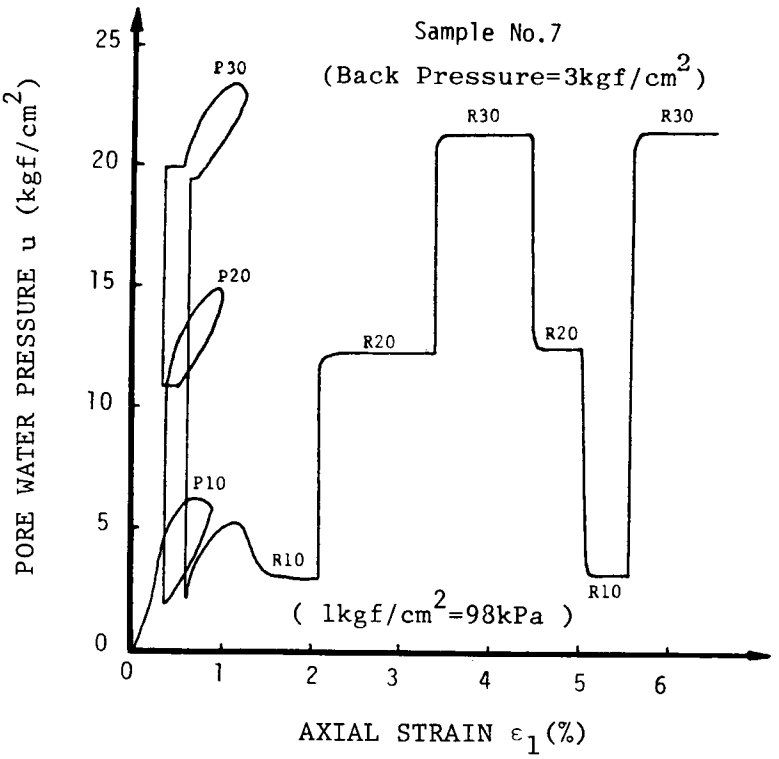

Fig.4-2-3 Pore water pressure created in sample No.7

(1) In each stage, consolidation process had to be done before the shearing (compression) of a specimen was carried out.

(2) To prevent an unexpected abrupt failure, unloading of the axial load must be done as soon as possible when the stress of the specimen was near to the peak. And, in order to standardize the operation procedure, unloading and consolidation was also required in those stages to obtain the residual strengths.

(3) It was recommended that confining pressure should be changed from a lower value to a higher one in a series of MST.

However, the second item mentioned above is not so clear when the actual MST is conducted in a laboratory. Here, we adopted several practical approximations. When the confining pressure is relatively high, the specimen shows a strain hardening type stress-strain relationship, a curve without a pronounced peak strength point. A tentative measure to determine the peak strength had been set. This consisted of monitoring the axial stress-axial strain curve and determining a point where slope was very small or where its axial strain was some amount (say 2%) greater than that at the starting of shearing in each stage.

When the confining pressure is lower, it is not so easy to decide the exact timing of unloading. As a result, hesitation would induce an over-shearing of specimen and a premature failure. On the contrary, if the unloading was undertaken too early from its due peak strength, an incorrect and much lower peak strength would be deduced.

To avoid these deficiencies and ambiguity, some improving work should be considered. Besides the use of stiff loading machine to control the rate of crack growth in the specimen and prevent an abrupt failure, alternatives to promote the accuracy of predicting the peak strength should be one of the most

effective approaches. It was noted that to increase the accuracy of prediction, other two complementary monitors were also necessary. One was the monitoring of pore water pressure-axial strain curve of the specimen. As under lower confining pressure, the pore water pressure of a saturated soft rock reaches an extreme well before that of the strength. This is a special property of saturated soft rock as mentioned previously in section 3-2, providing a valuable hint of the unloading in MST method. The other was to pick up the lateral strain of specimen while the shear test was being undertaken. This will be explained in detail in Sec. 4-2-3.

4-2-3 Consolidation-Loading-Unloading MST

Based upon the three operation controls described previously, two other MST methods were introduced. Their stress path of operation are illustrated in Figs. 4-2-4(a) and (b), with both showing peak strength MST and residual strength MST series. The MST:2 method allowed, after yielding a series of peak strengths, the confining pressure to be lowered to a certain level and then

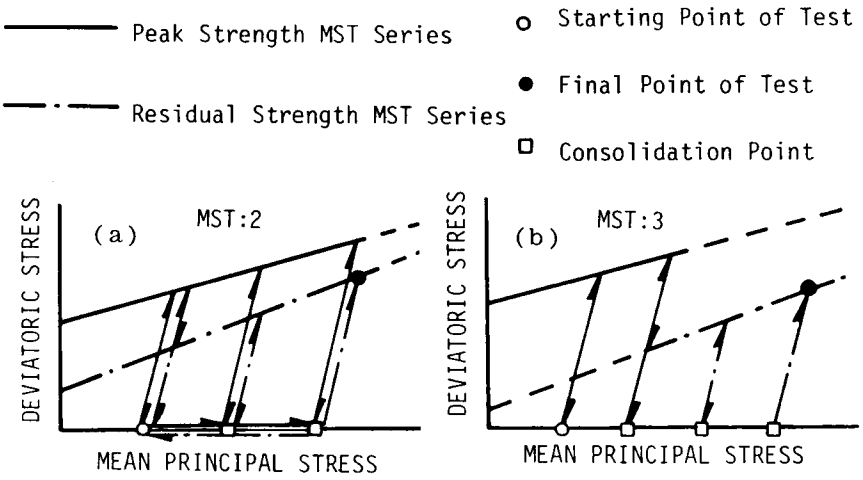

Fig. 4-2-4 Stress paths of MST:2 and MST:3

the series of residual strength MST be carried out. In each stage consolidation must be performed. A main feature of the MST:3 method shown that a series of residual strength MST test under higher confining pressure was following after several stages of peak-strength test. Naturally the confining pressures used in the tests were higher at the latter stages.

To evaluate these two MST methods, sandy silt rock had been used. Following the stress path of MST:2, curves of q (deviatoric stress) - ε_1 (axial strain) and u (pore water pressure) - ε_1 (axial strain) relationships were obtained. An example of results is given in Figs. 4-2-5(a) and 4-2-6(a). Results of the MST:3 is exemplified in Figs. 4-2-5(b) and 4-2-6(b). In Figs. 4-2-5(a) and (b), it is clear that under different confining pressures a variety of reasonable strengths was resulted. And, upon viewing the pore water pressure curves shown in Figs. 4-2-6(a) and (b), it is readily understood that after consolidation in each stage, the increment of confining pressure was not supported by pore water but exactly by the skeleton of the specimen.

The validity and accuracy of these MST:2 and MST:3 methods should desirably be assessed by comparing the results with that obtained from the conventional triaxial test method (SST). For this purpose, a series of SST test of sandy silt rock had been performed. Examples of results had been demonstrated in Figs. 3-2-1(a) and (b).

Upon comparing Fig. 3-2-1(a) with Figs. 4-2-5(a) and (b), it can be found that strengths yielded in the MST:2 and MST:3 methods were very similar to those obtained from SST method. It also indicates, from Fig. 3-2-1(b) and Figs. 4-2-6(a) and (b), that incorporating the procedure of consolidation in each stage of MST test, the reaction of pore water pressure (particularly their peak states) was identical to those appeared in SST test.

Furthermore, the effective stress paths of SST test and MST test were compared. They are given in Figs. 3-2-2 and 4-2-7, respectively, with the lat-

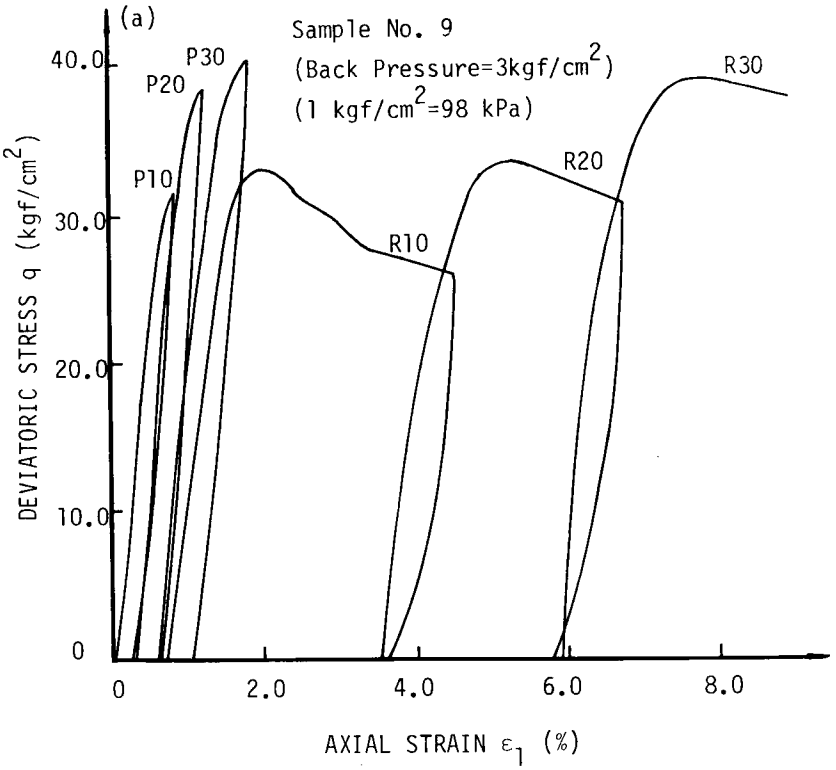

Fig.4-2-5(a) Example of MST:2 ($q-\varepsilon_1$)

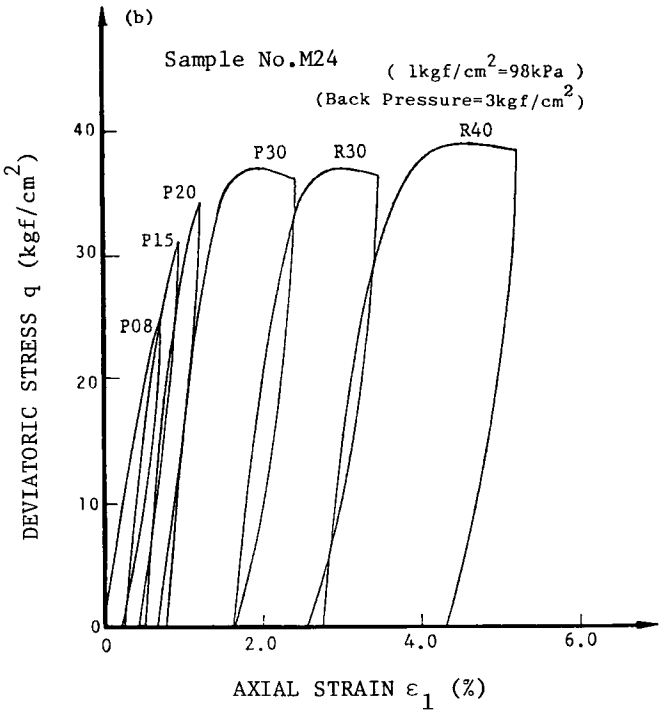

Fig.4-2-5(b) Example of MST:3 ($q-\varepsilon_1$)

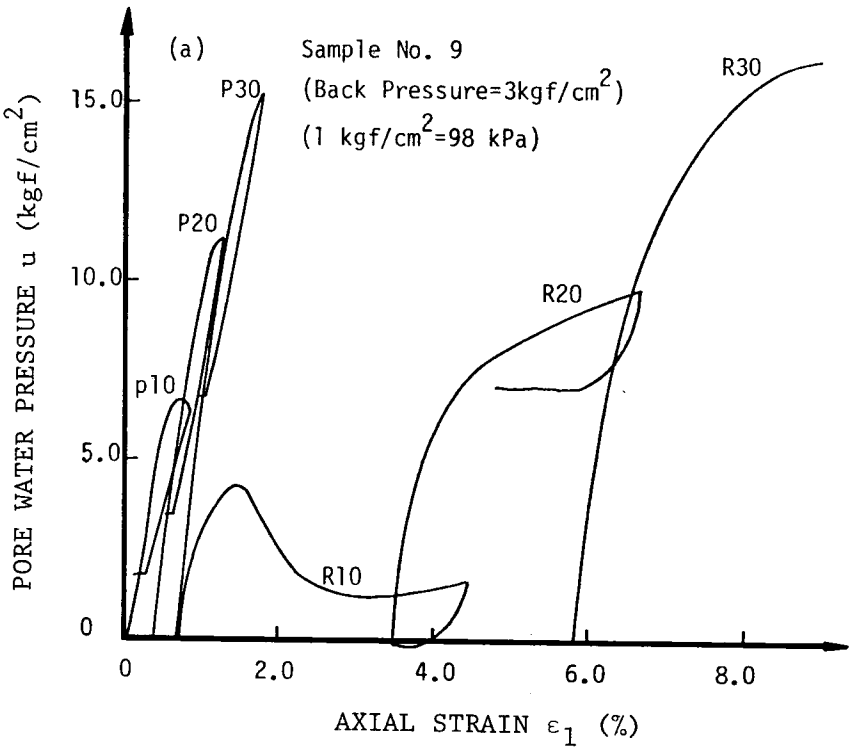

Fig.4-2-6(a) Example of MST:2 (u-ε_1)

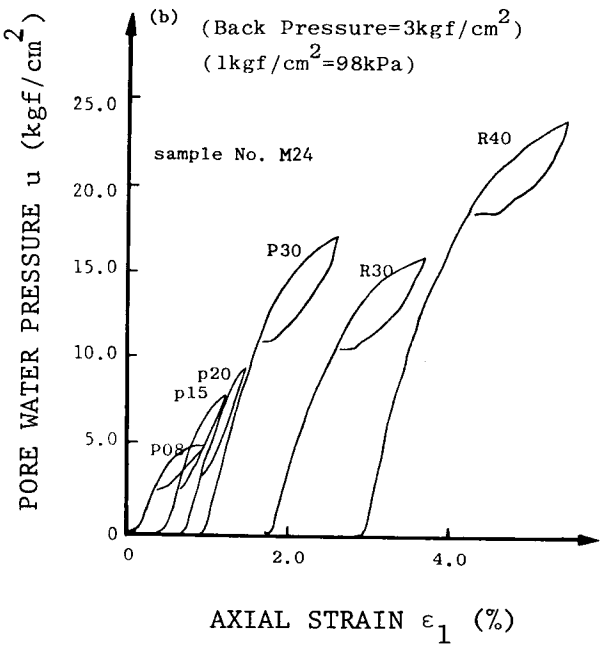

Fig.4-2-6(b) Example of MST:3 (u-ε_1)

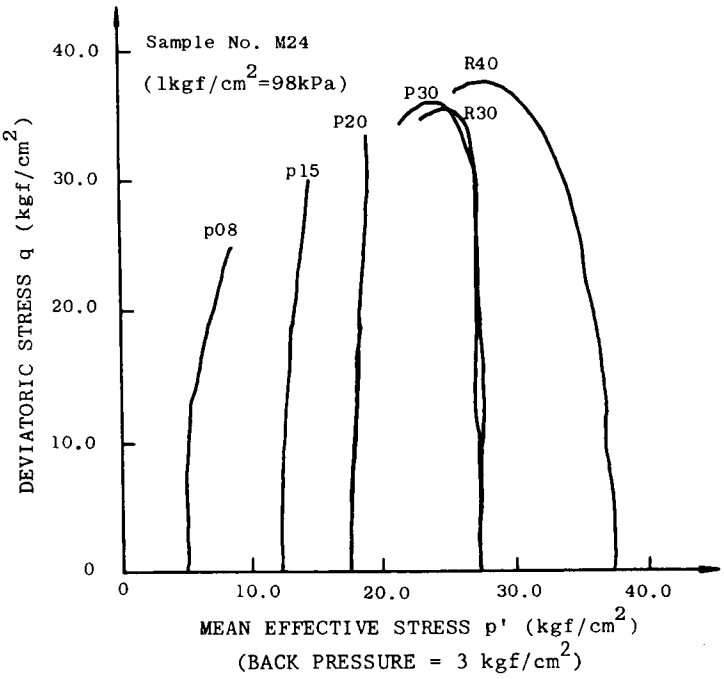

Fig. 4-2-7 Effective stress paths of MST (sandy silt rock)

ter presenting results from using the MST:3 test. From the inclination of effective stress paths, the dilation or compression property of specimen under shearing can be detected. As the paths in Fig. 4-2-7 resemble those in Fig. 3-2-2, it implies that by using only one specimen in these MST methods a whole spectrum of information can be derived, while this requires a number of specimens by SST method. Yet, some minor differences existed between the slope changes in the effective stress paths which were derived in SST and MST test, though corresponding to each other. It was probably that specimen No. M24 in MST test had been sheared in the former stages, and hence became 'denser'.

Fortunately, confining pressures applied in the MST method were lower in the former stage and becoming gradually higher in the latter stages. Therefore, the higher confining pressure employed in latter stage should counterbalance the effect of provious shearing process, an effect accumulated from former stages.

A series of MST tests and SST test on sandy silt rock were conducted. Their peak strength envelopes and residual strength envelopes are represented in Figs. 4-2-8 and 4-2-9, respectively. The middle parts of the peak strength envelope of SST test were somewhat higher than that from MST test (see Fig. 4-2-8). The difference may be generated by the incorrect timing of unloading operation. While, in Fig. 4-2-9 the two residual strength envelopes of SST test and MST test agreed with each other very well, indicating that unloading operation in residual strength MST had almost no effect on the determination of residual strength envelope. This means that residual strength is a more stable property of rock.

From the results (Fig. 4-2-4 to Fig. 4-2-9) and discussions mentioned above, it is sufficient to imply that the MST:2 and MST:3 methods, involving peak strength MST series and residual strength MST series, are appropriate methods to determine the whole spectrum of information of sandy silt rock by using only one specimen, while this requires a number of specimens by SST method.

It is necessary to investigate whether the two MST methods are versatile to other kinds of porous soft rock. Green sedimentary tuff (Nikko rock) was then used (physical properties summarized in Table 2-1). A series of tests had been carried out. Then, resultant examples are presented in Figs. 4-2-10 and 4-2-11, illustrating different but reasonable strengths could be deduced under different confining pressures. The peak and residual strength envelopes of the tuff, obtained from these MST methods, are compared with that from traditional SST (in Figs. 4-2-12 and 4-2-13). Excellent agreement can be observed.

Conclusively speaking, the MST:2, MST:3 methods previously described in Fig. 4-2-4 are two of the substantial substitutes for the conventional triaxial shear test method (SST), when strength envelope or some other mechanical properties of saturated soft rock are required.

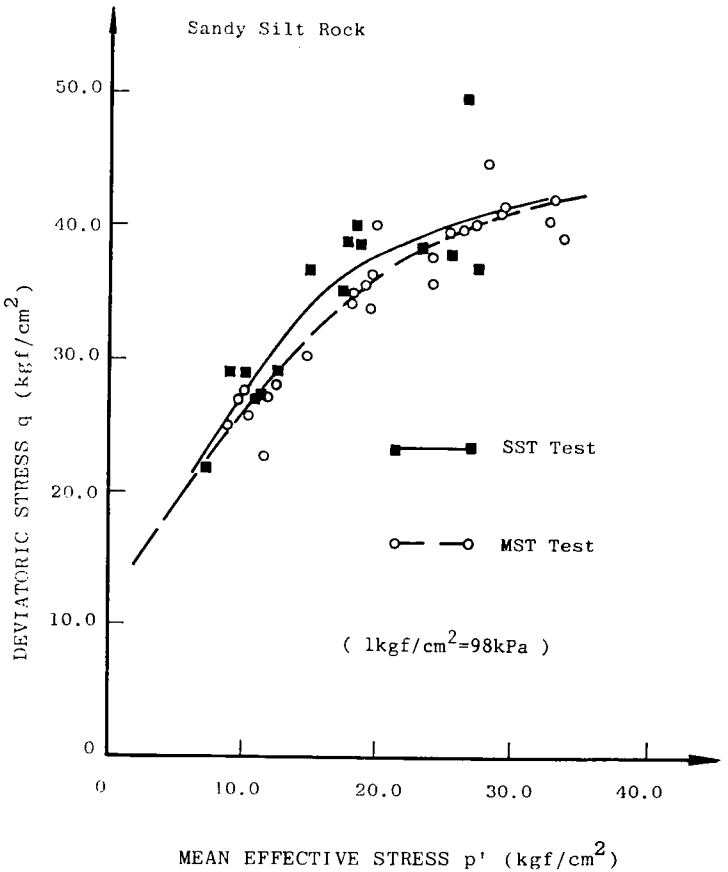

Fig. 4-2-8 Peak strength envelopes of sandy silt rock

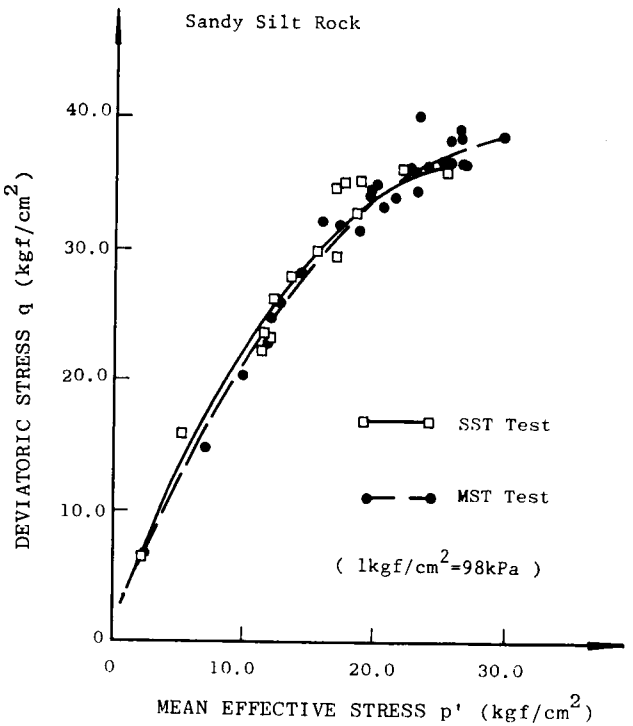

Fig. 4-2-9 Residual strength envelopes of sandy silt rock

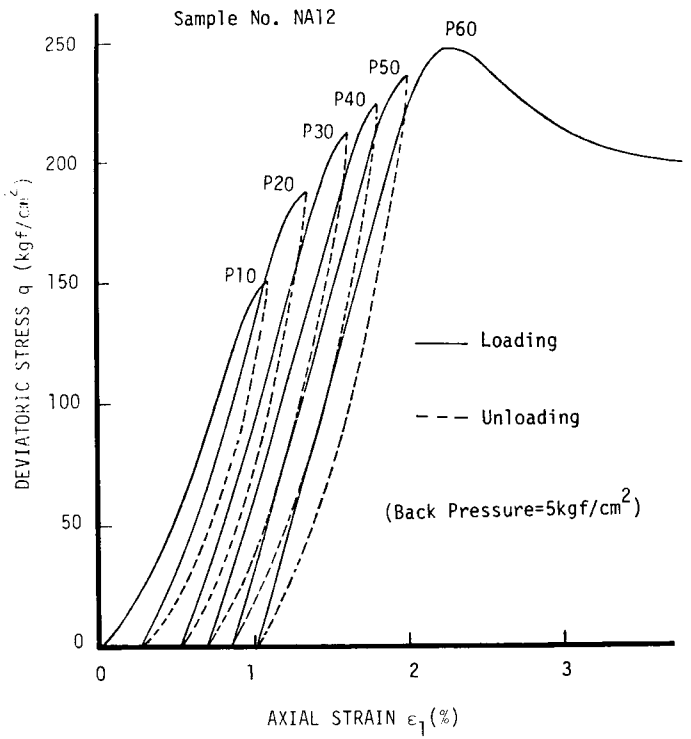

Fig. 4-2-10 Example of MST:2 with Nikko rock (q-ε_1)

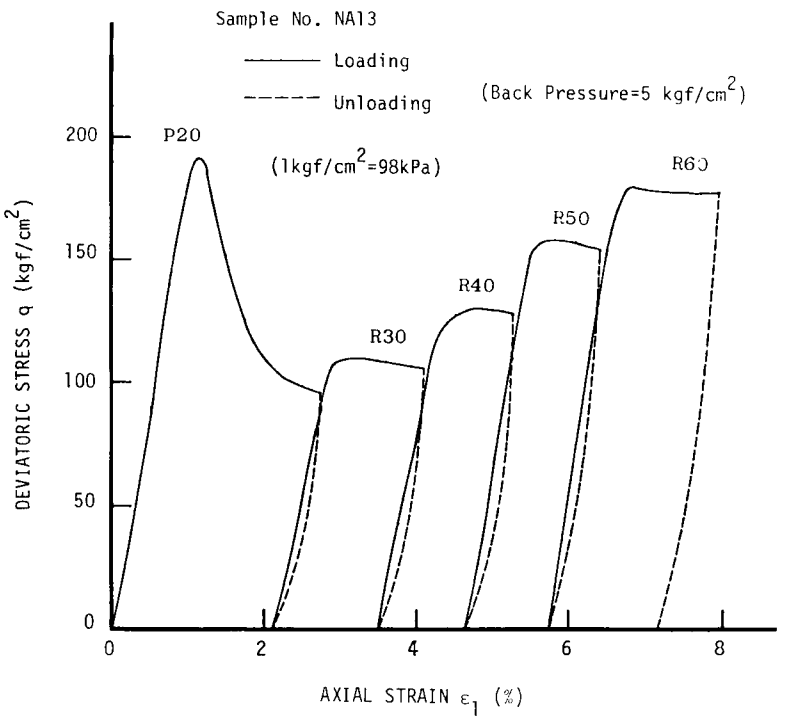

Fig. 4-2-11 Example of MST:3 with Nikko rock (q-ε_1)

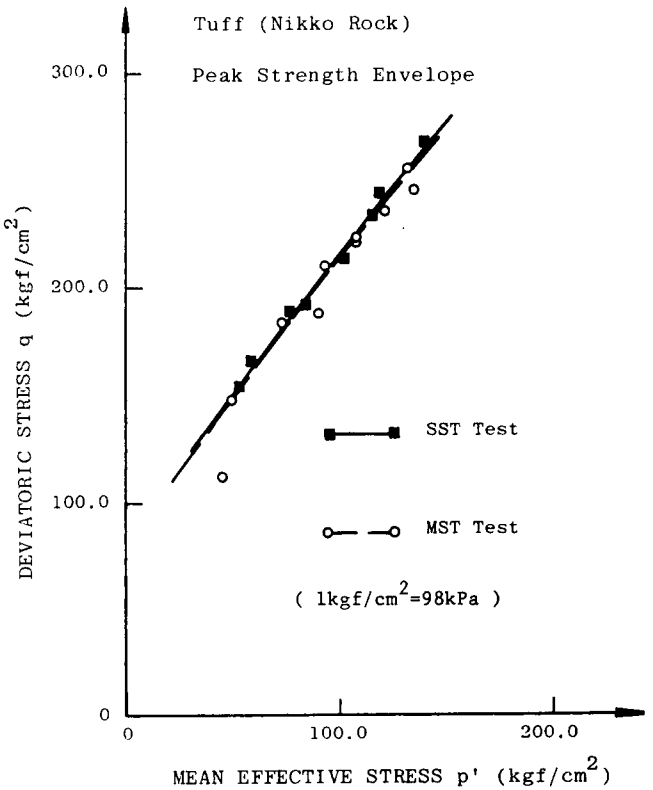

Fig. 4-2-12 Peak strength envelopes of Nikko rock

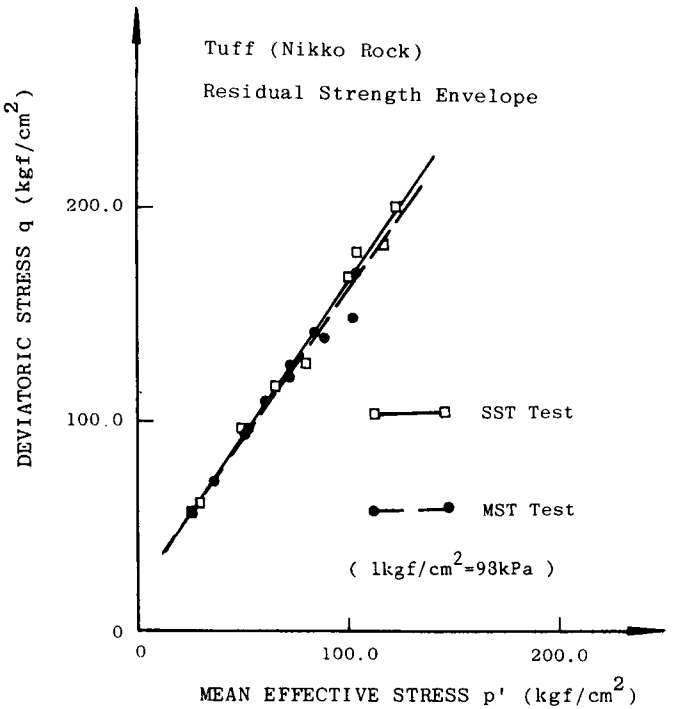

Fig. 4-2-13 Residual strength envelopes of Nikko rock

4-3 Improved MST for Predicting Peak Strength

To eliminate error in unloading operation and to improve the accuracy of peak strength MST under lower confining pressure, alternatives are necessary for detecting the appearance of the peak strength point. Therefore, besides the close monitoring of the axial stress - axial strain curve, the author has adopted a new test procedure which including the measurement of lateral strain of specimen when the MST test is being underway. It has been observed that, during a shearing process, microcrack growth parallel to the direction of axial stress, will take place around existing pores and cracks in the specimen, as a result from increasing the axial stress. Crack width will simultaneously spread in the direction normal to the axial stress, thus inducing lateral shear strain. Therefore, by measuring the change of lateral strain, it is possible to infer indirectly the reaction of crack growth in the specimen. Shall the crack yields a big fracture, significant change of lateral strain will occur.

In this study, a kind of plastic strain gauge which had 60 mm in length was employed (section 3-2) to correctly monitor the lateral strain change of the specimen until the extensile strain of the gauge was 10%. The strain gauge was secured indirectly on the lateral surface of the specimen as shown in Figs. 3-2-8(a) and (b), with the procedure of setting the specimen detailed also in section 3-2.

4-3-1 Lateral Strain

A tuff (Nikko rock) specimen (Table 2-1) was compressed by a SST method under low confining pressure (10 kgf/cm^2), back pressure 5 kgf/cm^2 and axial strain rate control (0.12%/min). Comparisons were made between the reaction of lateral strain with axial strain during the test. An example of the axial load

P - axial strain ε_1 curve and the axial load P - lateral strain ε_3 curve are illustrated in Fig. 4-3-1. It is clear, from Fig. 4-3-1(a), that when the peak strength point is passed, fracture failure appears abruptly in the specimen, load can not be sustained any more. And, the specimen may not be reused to yield peak strengths any more.

Upon viewing the pre-peak strength portion of the curve in Fig. 4-3-1(a), it is found that no apparent change of the gradient to the axial stress - axial strain curve was recorded, even when a point is near at hand to the peak strength point P_p. On the contrary, shown in Fig. 4-3-1(b), the lateral strain is very small at the beginning of test. But, the nearer the stress state from the peak strength point, the more remarkable the gradient change wolud occur. Therefore, once the monitoring of p - ε_3 curve be introduced into the peak strength MST test, the location of peak strength can more correctly be predicted and the unloading operation be carried out with more confidence.

A MST test, used specimen No. NA12, with axial strain rate control and by monitoring q - ε_3 curve had been carried out. Its q - ε_3 relationship is given in Fig. 4-3-2(a) and q - ε_1 curve in Fig. 4-2-10, and again in Fig. 4-3-2(b). It is obviously concluded from these two figures that, at the first and second stages of this MST test, the use of q-ε_3 curve could predict the appearance of peak strength more precisely than that using q - ε_1 curve in Fig. 4-3-2(b). However, this special feature is not apparent when the confining pressure is relatively high. Fortunately, under higher confining pressure, a rock specimen will become much ductile, thus, minimizing the occurrence of any abrupt failure.

It can be said that, in order to promote the accuracy of peak-strength MST method with axial strain control, test procedure incorporated with a simultaneous monitoring of q - ε_3 relationship during test seems the best and easiest approach.

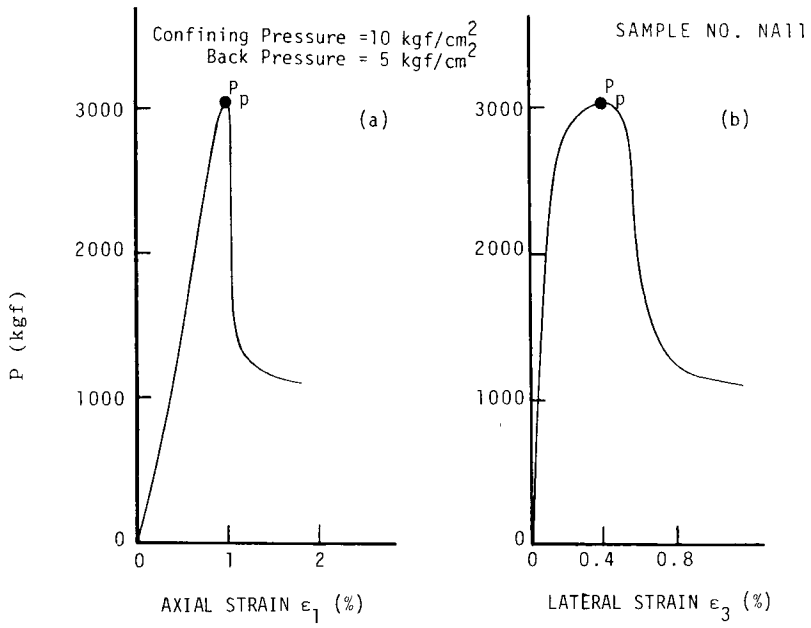

Fig. 4-3-1 P-ε_1 and P-ε_3 relationships of Nikko rock under axial strain rate control ($\dot{\varepsilon}_1$=0.12%/min)

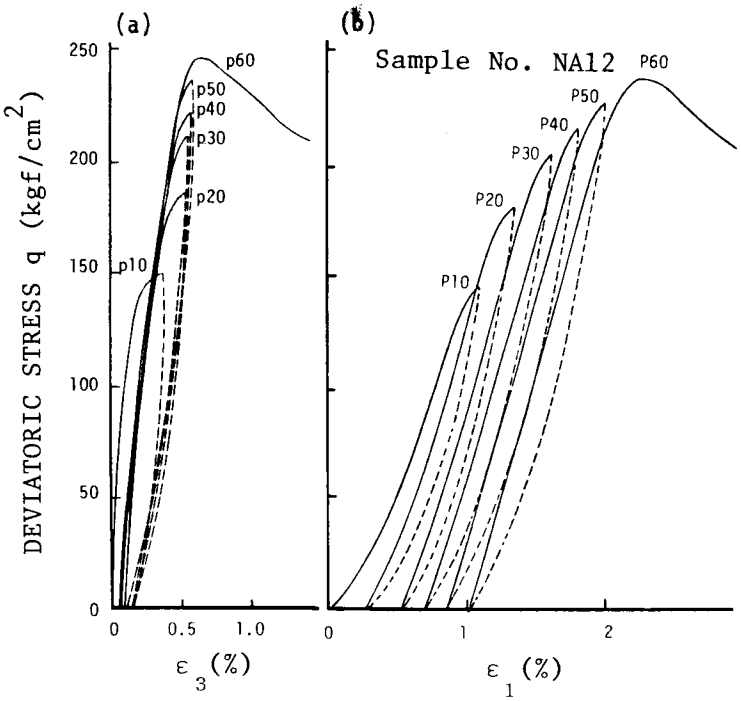

Fig. 4-3-2 Example of axial strain rate control MST ($\dot{\varepsilon}_1$=0.12%/min)

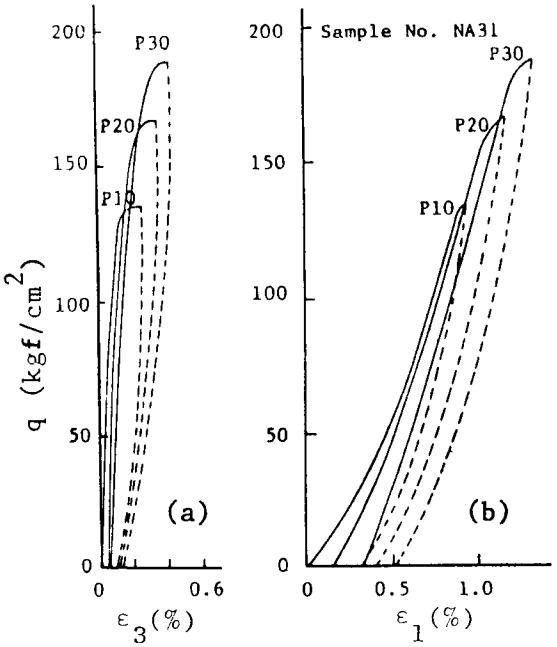

Fig.4-3-3 Example of lateral strain rate control MST ($\dot{\varepsilon}_3$=0.06%/min)

4-3-2 MST with Lateral Strain Control

According to the results of $q - \varepsilon_3$ relationships of SST and MST with axial strain rate control illustrated in Figs. 4-3-1(b) and 4-3-2(a), the possibility of lateral strain rate control in MST is foreseen. Hudson, Brown and Fairhurst (1971)[5] had proposed a method by using lateral displacement as feedback to control the failure of some rocks which had failed explosively in axial displacement control test. Hence, we decided to use this approach as a basic method to perfrom the lateral strain control triaxial test of soft rock. The results of the lateral strain rate (0.06 %/min) MST are shown in Figs. 4-3-3(a) and (b) as $q - \varepsilon_3$ and $q - \varepsilon_1$ relationships, respectively. Comparing these two figures with each other, it is needless to say, the obliquity changes of $q-\varepsilon_3$ curve near the peak strength point in each stage are more vivid and stable than those of the $q - \varepsilon_1$ curve. This phenomenon, especially

in low confining pressure stage, is remakable.

Furthermore, in this lateral strain control test, because crack growth in specimen could be indirectly governed within a stable rate, the occurrence of abrupt fracture might also be under control. Basing on monitoring the q-ε_3 curve of lateral strain rate control MST, we can get enough courage to perform the shear process till a point which quite near to the peak. In other words, unloading operation of the axial load can be done at the position as near the peak strength point as possible.

On the other hand, it should be noticed in this new method that at the beginning of shearing in each stage, quite a lot of force is required to load on the specimen during a short time interval and let the specimen produce enough lateral strain to satisfy the order signal which transmitted from the servocontrolled system. Therefore, sometimes, there exist some troubles to pursue the q - ε_3 relationship at the initial of the test. More detailed fundamental study is necessary to get rid of this difficulty. In spite of having this defect, the lateral strain rate control MST method may be expected as one of the improved test methods to promote the accuracy of peak strength MST.

4-4 Mechanical Behavior of Sandy Silt Rock with an Artificial Discontinuity

4-4-1 Introduction

In order to satisfy the ever increasing human activities, the quantity required from primary energies is tremendous. Besides the productions of petroleum and coal, nuclear energy also newly enters as a highly potential source.

To secure a bulk storage, huge opening excavated underground has become revolutionarily popular in storing petroleum, instead of the conventional

steel tank. However, to prevent petroleum leaking out from the large underground opening along cracks or faults of rock mass, it is necessary to explore the behavior of these discontinuities of rock mass when the stress state is changed.

On the other hand, in order to establish a sufficiently safe big structure such as nuclear power plant or skyscraper, the influence on supporting ability of rock mass from the existing crack and discontinuity must be seriously taken into account.

To simulate a crack or fault in a rock mass, especially in the soft rock mass, a series of triaxial tests using soft rock specimens with artificial discontinuity had been performed.

Sandy silt rock was selected to this series of test. Each specimen was carved with an artificial discontinuity obliquely at an angle α against the horizontal plane. These specimens were tested by the MST method discussed previously in section 4-2.

Two kinds of MST were employed. One was to explore the "peak strengths" of the specimen under different confining pressures. The second was to shear the specimen so as to form another shear failure plane under a lower confining pressure, then, changing the confining pressure sequentially from lower to higher to find residual strengths in others stages. Consequently, the influence of discontinuity on the peak strengths or residual strengths can be detected from the test results.

4-4-2 Specimen and Testing Procedure

Sandy silt rock specimens with ϕ 5 cm x H 10 cm (diameter and height) and an artificial cut having an inclination angle α against the horizontal (see Fig. 4-4-1) were prepared for tests, where the ranges of α were 0^0 , 15^0 , 30^0, 45^0, 55^0, 60^0, 75^0 and 90^0. Each specimen was saturated in water for at least

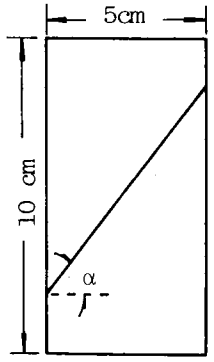

Fig. 4-4-1 Rock specimen with an artificial joint shown schematically

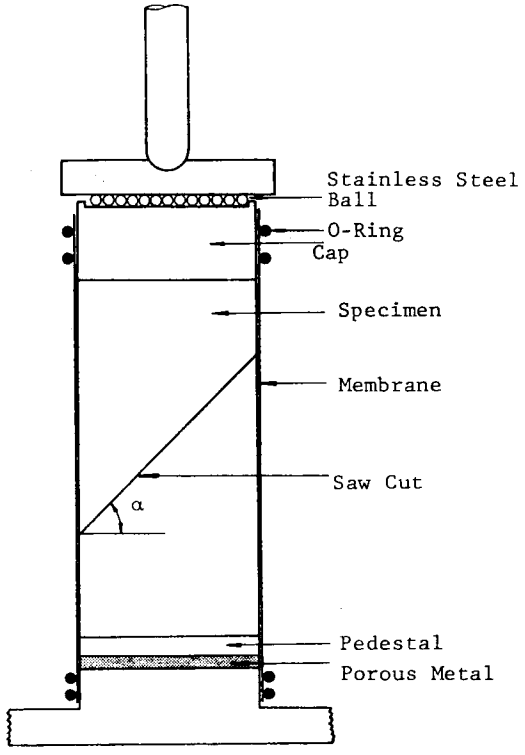

Fig. 4-4-2 The setting of a rock specimen with an artificial discontinuity

7 days.

The setting procedure for these specimens with artificial discontinuity was almost the same as that used for intact specimen (mentioned in section 3-2), except using an improved apparatus to prevent the two intact pieces from relative rotation during shearing test. The setting of specimen is schematically illustrated in Fig. 4-4-2. Stainless steel balls paved on the top of cap, allowed the applied external force uniformly distributed down to the specimen.

The total stress paths of test are shown in Figs. 4-4-3(a) and (b), in which the first diagram indicates the testing procedure to the first series. According to the stress path, after finishing the prescribed setting process, the specimen was subjected to a lower confining pressure and a back pressure of 3 kgf/cm^2 to commence the consolidation process. Shearing process with axial strain rate at 0.12%/min was then carried out continuously. Before the stress state of the specimen reached near the peak strength, the axial stress was released and returned to the same level of previous confining pressure.

Test was further carried out with a predetermined higher confining pressure. The same procedure was repeated several times, with the confining pressure sequentially from lower to higher value in the order of 3, 6, 10, 15, 20, 30, 40 and 50 kgf/cm^2. Thus, a series of peak strengths of the sandy silt rock with a discontinuity can be derived.

Moreover, according to the stress path depicted in Fig. 4-4-3(b) and following the experimental procedure mentioned in the first series, several residual strengths were recorded from a specimen under different confining pressures. This series of test is tentatively called "the second series test".

4-4-3 Experimental Results

(a) The peak strengths of sandy silt rock specimen with a discontinuity

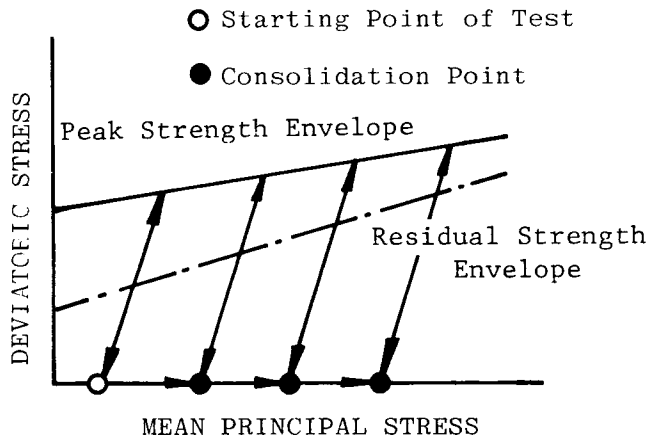

(a)

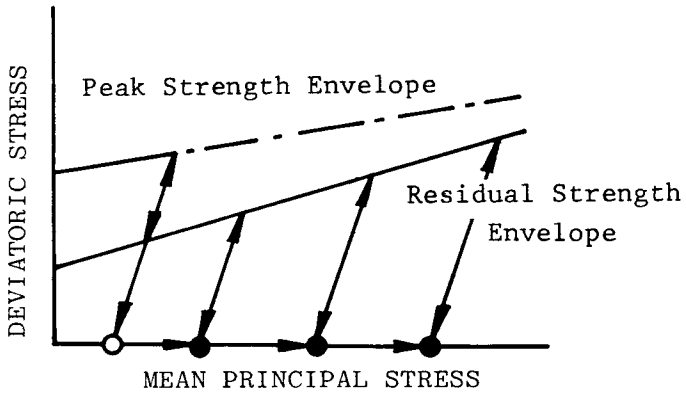

(b)

Fig.4-4-3 Total stress paths of the test of sandy silt rock with an artificial discontinuity
(a) first series of test
(b) second series of test

After a series of peak strength MST test (first series) had been performed, the deviatoric stress (q) - axial strain (ε_1) relationships for the same sandy silt rock but having different discontinuity angle α were obtained. The results of sample A00 ($\alpha=0^0$), B60 ($\alpha=60^0$) and A90 ($\alpha=90^0$) are presented in Fig. 4-4-4, Fig. 4-4-5 and Fig. 4-4-6, respectively.

Upon comparing Fig. 4-4-4 with Fig. 4-4-6, these two specimens behaved identically while shearing under the same confining pressure, although having different α (0^0 and 90^0, respectively). But, sample B60 presented quite differently when compared with A00 or A90. Of particular importance, in the case when confining pressure was not higher than 20 kgf/cm^2, their q-ε_1 curve had a peak point and following up with a residual state. This phenomenon means that, in these states, friction resistance existed between the two intact pieces increased with the increasing of axial strain until the peak appeared. Once beyond the peak strength, relative sliding along the discontinuity would take place immediately. Therefore, the friction resistance changed from a static one to dynamic (a frictional strength of residual state). However, if the confining pressure was higher than 30 kgf/cm^2, the phenomenon of strength dropping did not appear any more. It means that the relative sliding between the two intact pieces vanished in these stages.

Furthermore, lumping the Mohr's envelopes for all specimens which posses different discontinuity angle α to form Fig. 4-4-7. It suggests that any specimen having an angle α near to either 90^0 or 0^0, would have its strength envelope located in a higher position in the graph when compared with others. This means that the specimen possessed stronger peak strengths (in different confining pressures) than other specimens. On the contrary, specimen having α angle equal to 60^0 rendered the lowest peak strength envelope. These facts presented above reveal the likely influence on peak strength from the angle of discontinuity under lower confining pressure. However, when the confining

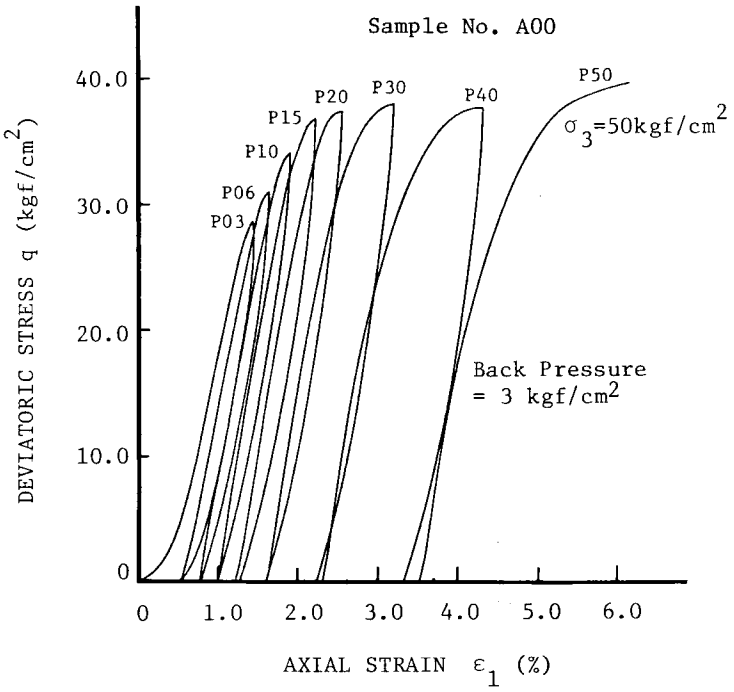

Fig.4-4-4 $q-\varepsilon_1$ curves of a sandy silt rock specimen with $\alpha=0^0$ (first series of test)

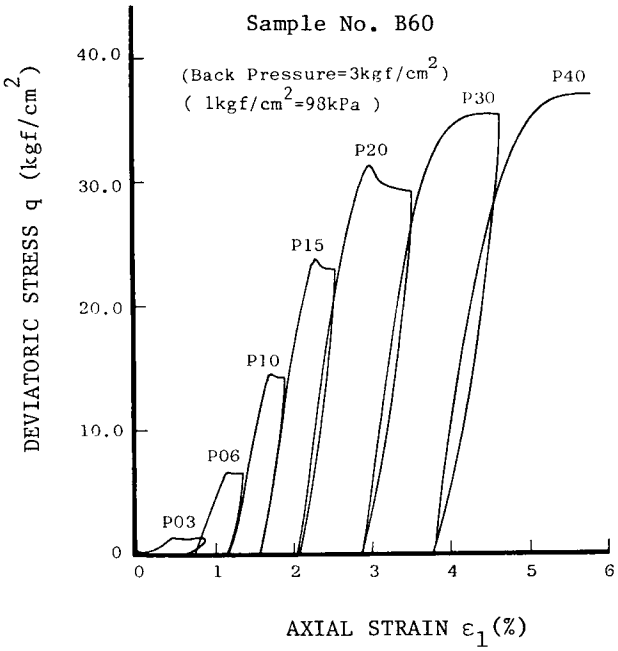

Fig.4-4-5 $q-\varepsilon_1$ relationships of sandy silt rock specimen with $\alpha=60^0$ (first series of test)

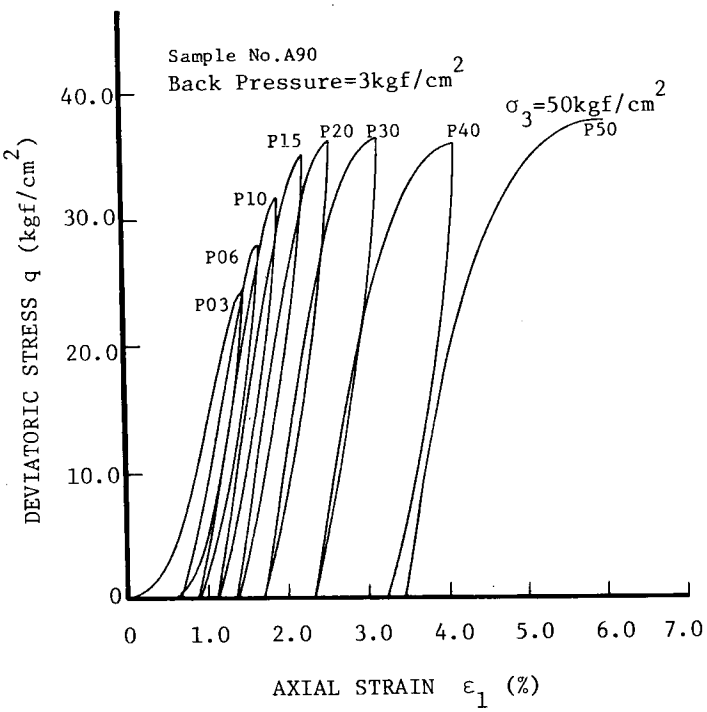

Fig.4-4-6 $q-\varepsilon_1$ curves of sandy silt rock specimen with $\alpha=90^0$(first series of test)

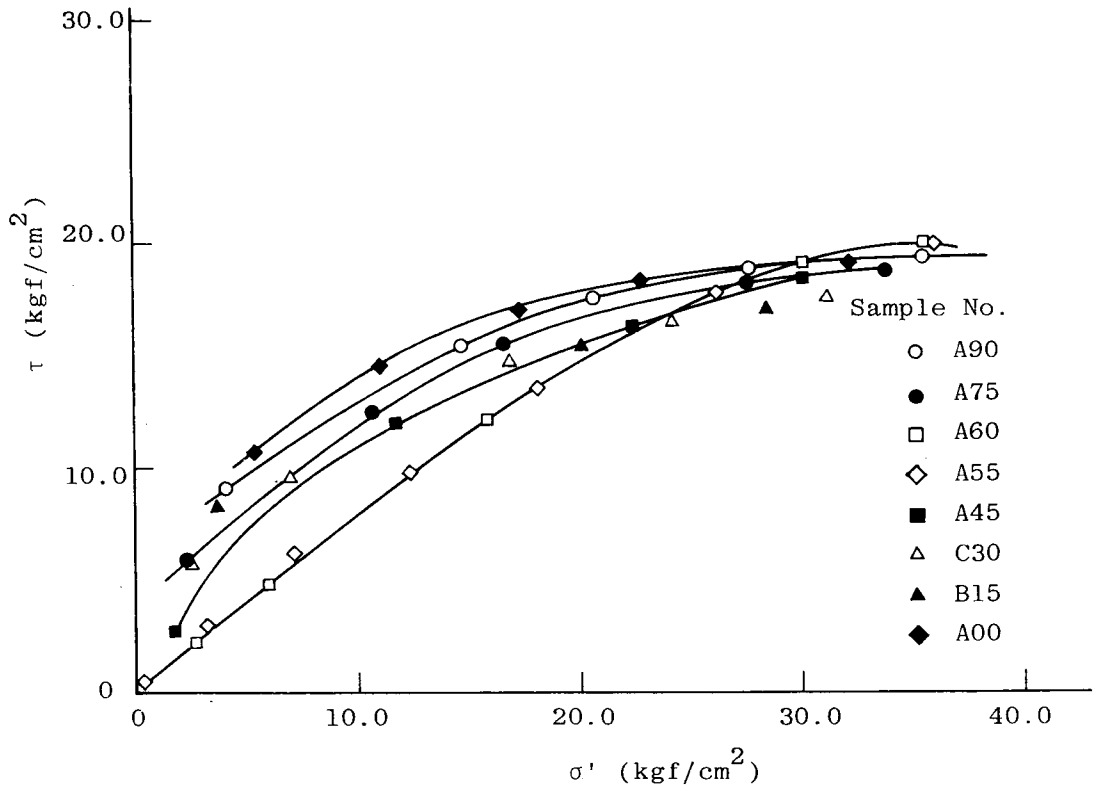

Fig.4-4-7 Peak strength envelopes in $\tau-\sigma'$ plane

pressure was higher enough, these envelopes almost crowded together, indicating that the shear strength was independent of the angle of discontinuity, α .

To compare the results obtained for the intact specimen with that for artificially cut specimen, the strength envelope of the intact specimen in q-p' plane (referred to the section 4-2) is reproduced in Fig. 4-4-8 for cross-reference. Similar to Fig. 4-4-7, the Fig. 4-4-8 indicates that the envelopes for specimens with $\alpha=0^0$ and 90^0 were very nearer to that of the intact one, and, under lower confining pressures, the strength of the former was even higher than that of the latter. Therefore, it can be reasonably assert that if the inclination α of a discontinuity is nearer to 0^0 or 90^0, the discontinuity has no effect on the peak strength. Furthermore, the relationships between deviatoric strength q and the angle of discontinuity α as a function of different confining pressures are shown in Fig. 4-4-9, bearing the influence of discontinuity on the peak strength of sandy silt rock.

It is obvious that the specimen with $\alpha=60^0$, always produced the lowest peak strengths and that with $\alpha=0^0$ and 90^0 rendered higher peak strengths. A similar result had also been obtained by Jaeger and Cook (1979)[6] , with a fractured rock model and linear Mohr-Coulomb's failure criterion. It is equally clear that the difference in peak strength between the specimen with $\alpha=0^0$ or 90^0 and others were remarkable in lower confining pressures, but gradually became indistinguishable when confining pressure increased. In the case of sandy silt rock, the difference completely vanished when confining pressure over 50 kgf/cm^2.

(b) The residual strengths of sandy silt rock specimen with a discontinuity

Referring to the total stress path shown in Fig. 4-4-3(b) and the test procedures mentioned in section 4-4-2, a series of experiments to study the

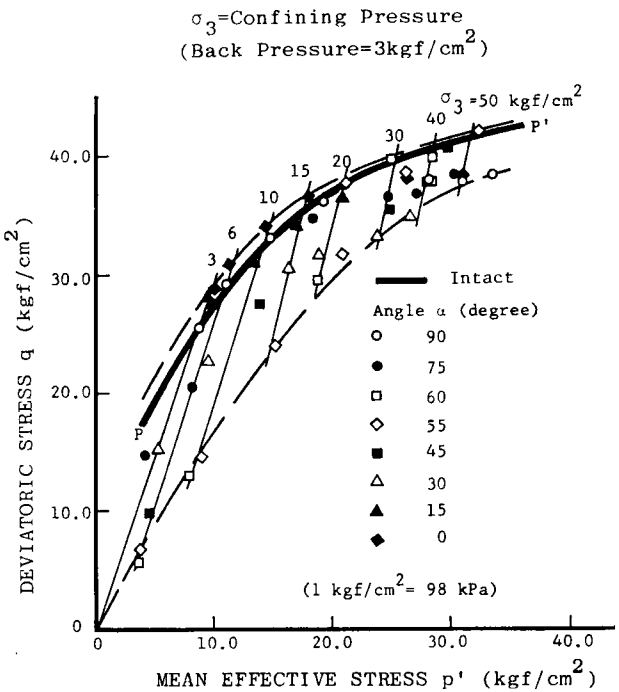

Fig. 4-4-8 Peak strength envelopes of sandy silt rock in q-p' plane

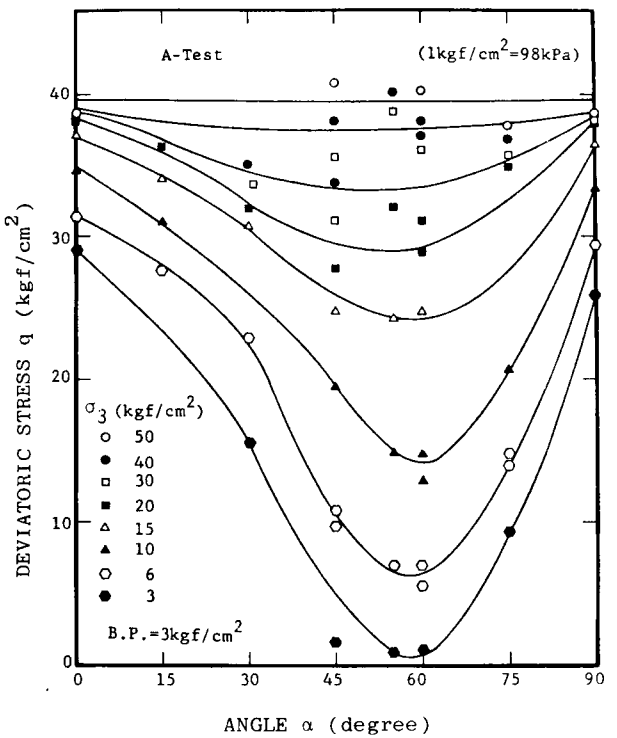

Fig. 4-4-9 The variation of q_{peak} with α

influence of a discontinuity on the residual strengths of sandy silt rock had been carried out. The experimental results were similar to that obtained for the peak strengths in section 4-4-3(a), in relation to the deviatoric stress (q) - axial strain (ε_1) relationship of the specimens.

Figures 4-4-10, 11 and 12 present the test results of samples B00 ($\alpha=0^0$), D30 ($\alpha=30^0$) and B90 ($\alpha=90^0$), respectively. The first and third figures (10 and 12) show that after a new shearing failure plane had been formed under σ_3 = 6 kgf/cm^2 in these specimens ($\alpha=0^0$ and 90^0), they behaved very similar when subjected to same confining pressure. However, from Fig. 4-4-11, specimen D30 yielded somewhat different result compared with those of B00 and B90.

Unfortunately, because specimens with α = 45^0, 55^0 and 60^0 could not be sheared to form a new shearing failure plane under σ_3 = 6 kgf/cm^2, the residual strength of these specimens will be tentatively considered as the dynamic friction resistance when the relative sliding of the two intact pieces of specimen had been happening. An example was shown in Fig. 4-4-5.

Again, tracing the Mohr's envelopes of residual strength, which were observed from several specimens with different angle α, gained the Fig. 4-4-13. It shows that specimen having α near 0^0 or 90^0 had higher value of residual strength. However, the range of difference between the highest and the lowest envelopes was not so apparent as the peak strength envelopes had (see Fig. 4-4-7). This means that the effect of an artificial discontinuity within specimen at its residual strength was not more influential than it was at peak strength. This phenomenon can also be found when comparing the q-p' relationship of residual strength shown in Fig. 4-4-14 to that in Fig. 4-4-8.

The results of residual strength presented in this section are rearranged and plotted on the q-α plane, Fig. 4-4-15. The influence of various α on residual strengths are intrinsically very similar to that on peak strengths depicted previously in Fig. 4-4-9.

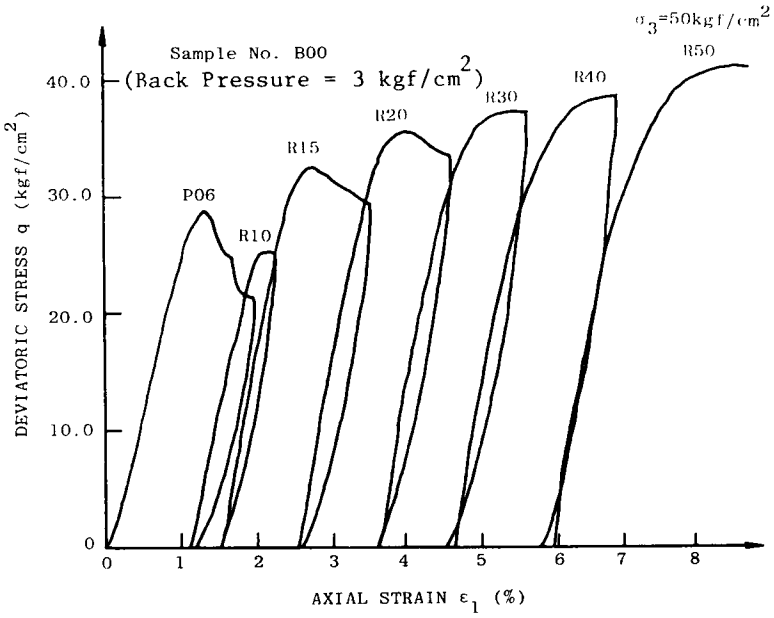

Fig.4-4-10 q-ε_1 curves of sandy silt rock specimen with $\alpha=0^0$(second series of test)

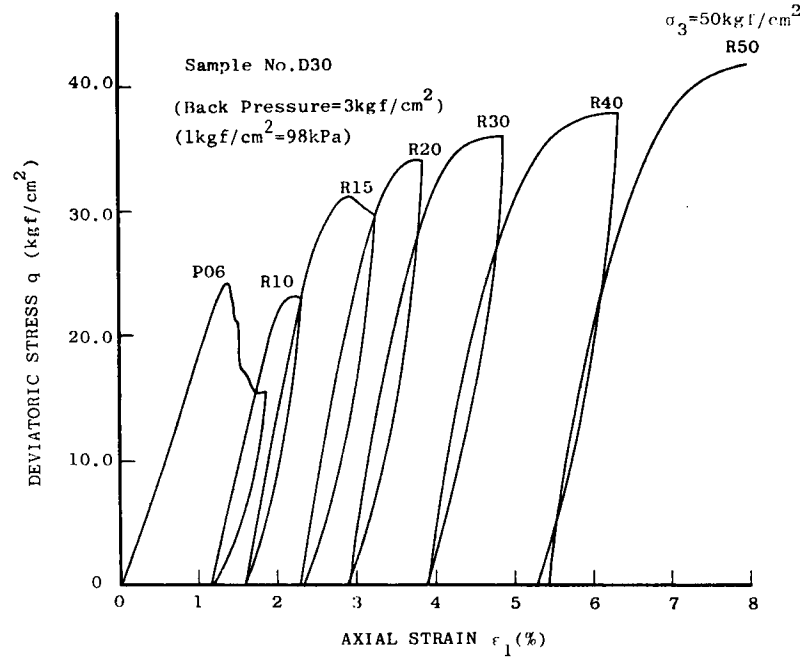

Fig.4-4-11 q-ε_1 curves of $\alpha=30^0$(second series)

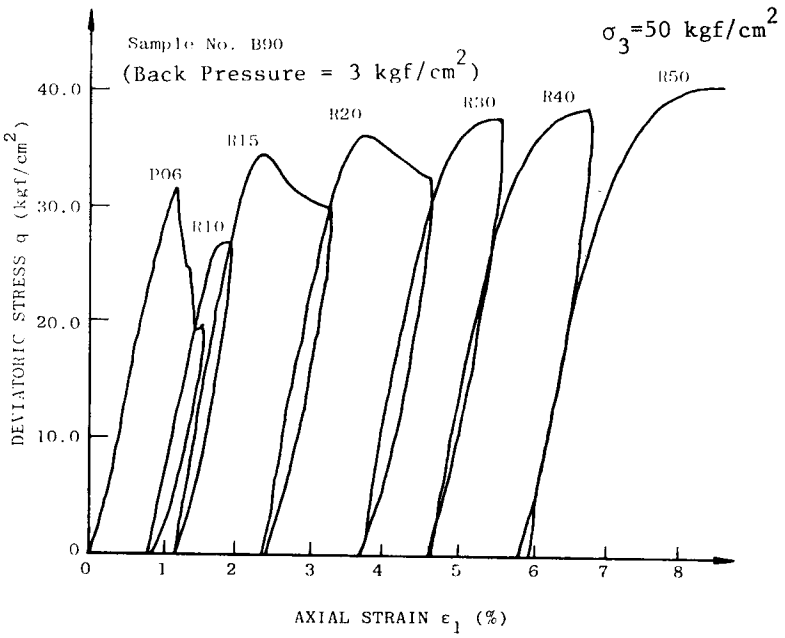

Fig.4-4-12 q-ε_1 relationships of $\alpha=90^0$(second series)

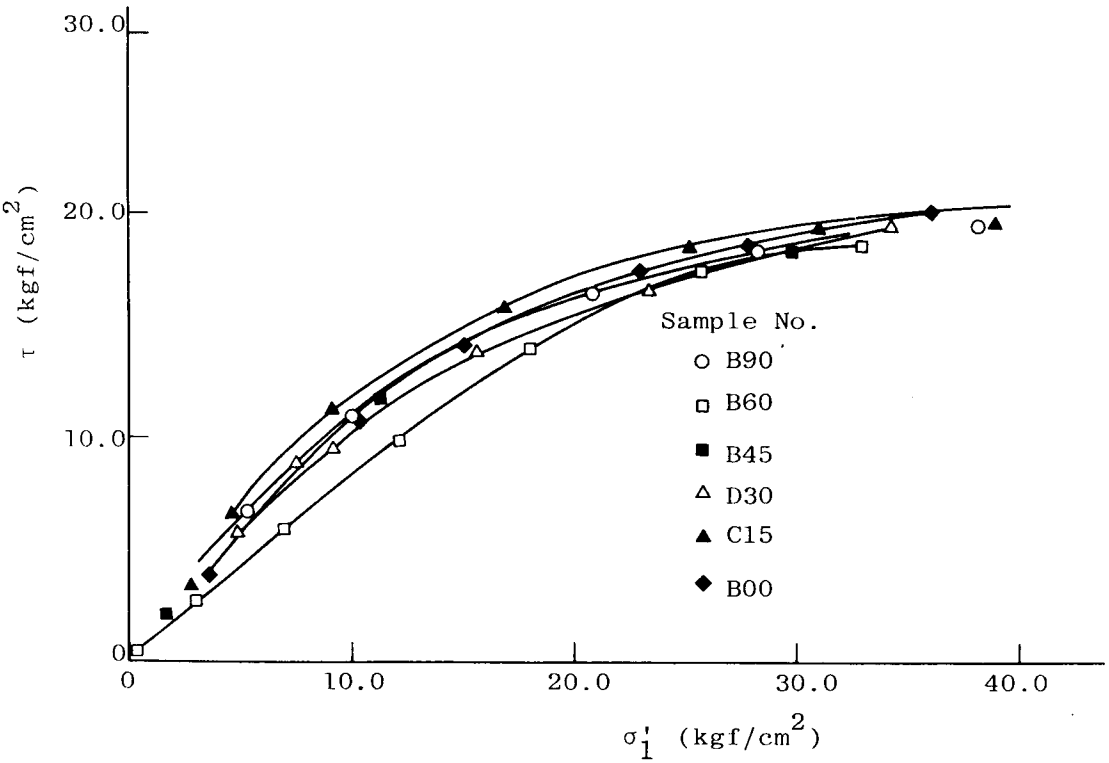

Fig.4-4-13 Residual strength envelopes in τ-σ' plane

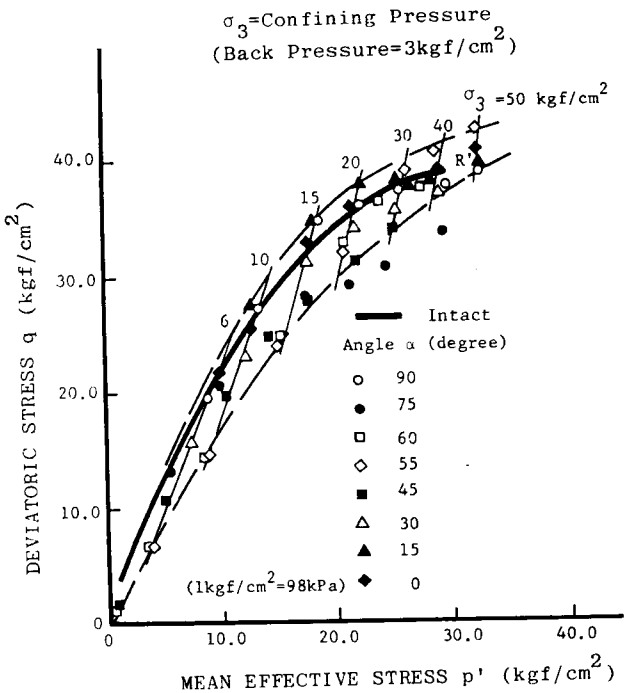

Fig. 4-4-14 Residual strength envelopes of sandy silt rock in q-p' plane

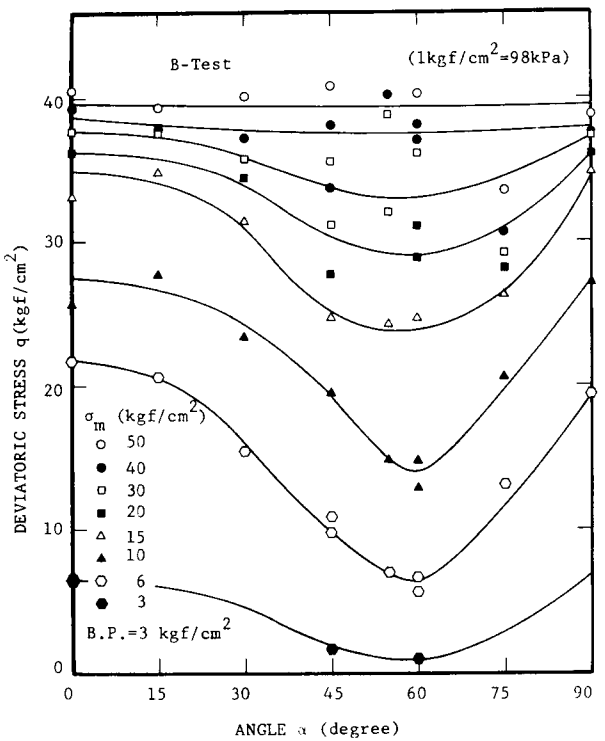

Fig. 4-4-15 The variation of $q_{residual}$ with α

Once again, the lowest residual strengths were unexceptionally produced by specimen with $\alpha = 60^0$, under low and moderate confining pressures. Moreover, for confining pressure over 50 kgf/cm^2, the influence of α on residual strength vanished naturally.

4-4-4 Conclusions

Based on the experimental results presented, the influences of an artificial discontinuity on the strengths of sandy silt rock are as follows:

(1) A discontinuity usually projects its influence on the peak strength and residual strength, especially when the inclination of discontinuity α nears to 60^0. On the contrary, the nearer for the α closes to 0^0 or 90^0, the negligible the influence is on the deviatoric stress, or may even dismiss completely.

(2) Substantially, a discontinuity is influential on peak strength than on residual strength. But, when the confining pressure is high enough, the prescribed effect can totally be neglected in both cases.

(3) According to Figs. 4-4-8 and 4-4-14, the strengths of specimen with α nears to 0^0 or 90^0, are comparable to those of intact specimen. Moreover, under high confining pressures, not only these specimens with α near 0^0 or 90^0, but also other specimens have strengths similar to those from intact specimen

(4) Upon inspecting the Mohr strength envelope of intact specimen shown in Fig. 4-4-16 it is obvious that under low confining pressure the critical plane in sandy silt rock specimen had an inclination angle θ near 60^0. Accompanying to the increasing of confining pressure, the critical plane gradually rotated into the direction with a θ near 45^0.

Therefore, according to the results in this series, it is apparent that under low confining pressure, the specimen (sample No. B60) with a 60^0 artifi-

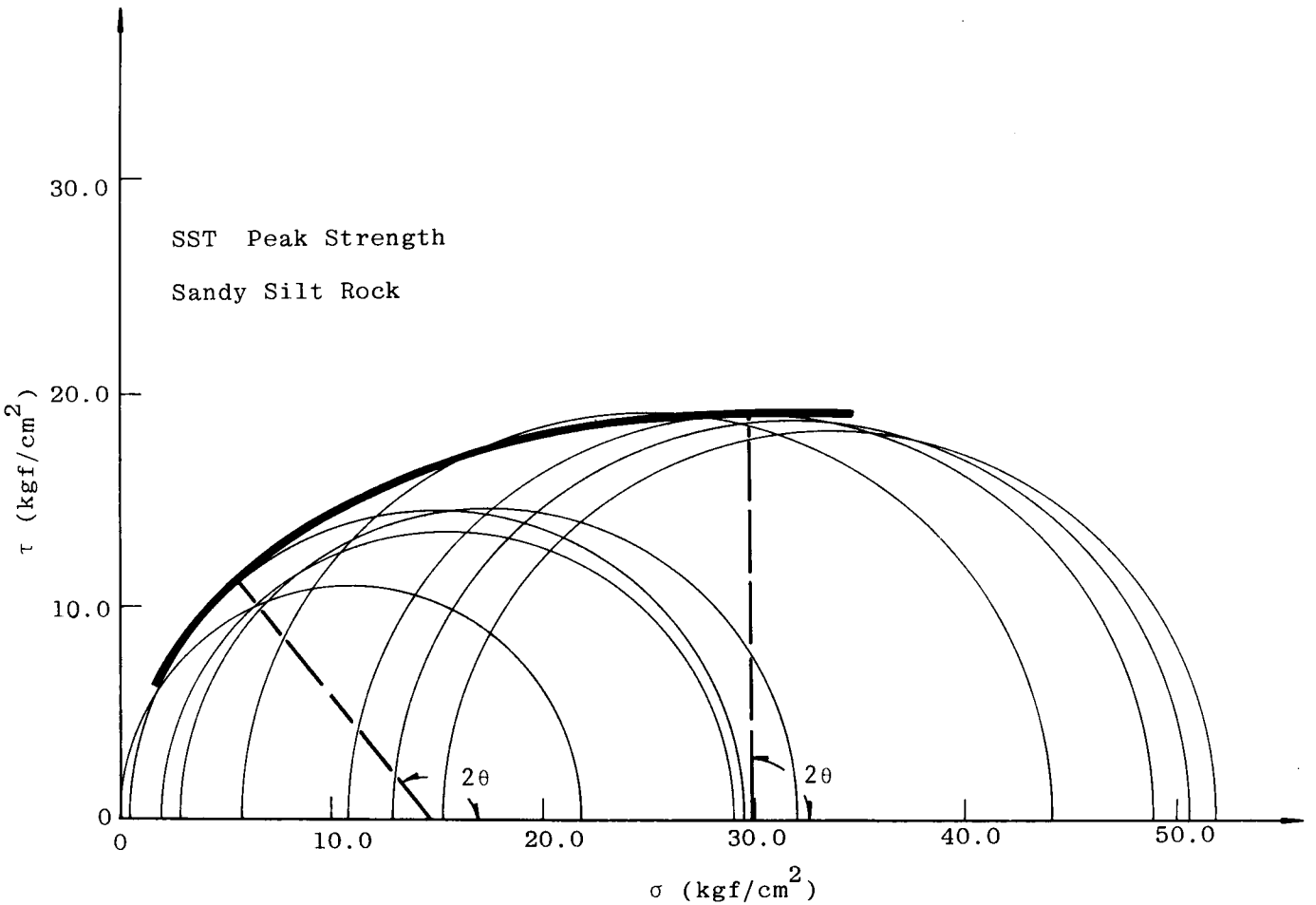

Fig. 4-4-16 Mohr strength envelope of sandy silt rock (SST)

cial discontinuity always induced the lowest strength, it was due to the discontinuity just coincided with the critical plane in low confining pressure. However, when the confining pressure increased to a high enough one, the strength of this specimen increased rapidly and was comparable to other specimens with different α. Besides the increasing of confining pressure could strengthen the frictional resistance in the discontinuity of this specimen, the critical plane had already rotated into other orientation near 45^0 was also a very important reason why the influence of discontinuity was indistinguishable when the confining pressure was high.

(5) The "residual strength" usually used in construction design is the "residual strength" of an "intact" specimen. But, from the experimental results obtained it is clear that there exist various kinds of "residual strength", with most of them lower than that of the intact specimen, especially, when $\alpha = 60^0$ and under a lower confining pressure.

Therefore, to achieve a safe and accurate construction design, it is of vital importance in able to differentiate and make good use of the differences between the residual strengths of an "intact specimen" and "specimen with a discontinuity".

4-5 Conclusions

From the work of Kovari and Tisa (1975)[1], it is apparent that the Multiple Failure State Method has been a versatile technique for obtaining the strength parameters, especially the strength envelopes, of hard rock under various kinds of confining pressure. Based on this method, MST for saturated soft rock has successfully been developed by Akai, Ohnishi, Lee and Adachi (1979)[7], with high resolution of accuracy in predicting the appearance of

peak strength point. A lateral strain gauge was introduced to monitor the lateral strain change of rock specimen, reflecting the very sensitive nature of the microstructure change of the specimen. Consequently, a modified MST method was developed with control of lateral strain rate. On the contrary, the conventional MST methods were performed under strain rate control in the axial direction.

Using the modified MST method, the abrupt rupture of specimen could be avoided under low confining pressure, thus, increasing the accuracy in predicting the peak strength.

The MST methods were applied to saturated soft rock in section 4-4 to investigate the influence of joint on strengths of rock specimen.

From the experimental results presented, the following conclusions may be arrived for the MST method and its modified version.

(1) A successful MST test method for saturated soft rock should have three essential procedures,

(a) to consolidate the specimen before shearing in each stage,

(b) to undergo unloading operation timely, just before the appearance of peak strength, and

(c) to use lower confining pressure in the earlier stage and higher values later, in each series of MST test (peak strength MST or residual strength MST).

(2) There exist some reasons that these MST methods could feasibly be employed for studying sandy silt, Funyu and Nikko rocks. Firstly, these rocks possess moderate ductility which is similar to the oil shale used in the modified MST test (Chang & Jumper (1978)[2], Chang & Bondurant (1979)[4]), and the Pierre shale, Raton shale used by Kim and Ko (1979)[3]. Therefore, within the stages of relatively low confining pressure, when stress state is near the peak strength point, the possibility of causing abrupt failure (very high in

hard rock), would be minimized.

Secondly, it would be mentioned in Chapter 5, that under intermediate confining pressure, the shear fracture plane of a soft rock was completely formed at a point within the strain-softening process (Chapter 5, permeability test results). This means that during a shear test, there has only a partial fracture plane created in rock specimen when stress state is near or at the peak strength point. Hence, if the unloading was carried out from the vicinity of the peak strength and then immediately increased the confining pressure to a higher one, the partial fracture plane would lose most of its influence in obtaining the peak strength to the new stage. These MST methods has adopted a procedure to avoid these troubles.

And finally, rock specimen under high confining pressure became more ductile than brittle, therefore inducing a more stable failure style, a "barrel" type.

(3) Lateral strain can reflect the change of microstructure within a specimen. Incorporating lateral strain control in shear test will restrict the microstructure change under an obedient way.

The MST method with lateral strain rate control is strongly recommended for test specimen of hard rock or other brittle materials.

(4) Upon combining the measurement of the lateral and axial strains as shown in Figs. 4-3-2(a) and (b), the volumetric strain change $\varepsilon_v (= \varepsilon_1 + 2\varepsilon_3)$ of the specimen could be obtained. Fig. 4-5-1(a) indicates the relationship of ε_v and ε_1 during this MST test. From Fig. 4-3-2(a) and Fig. 4-5-1(a), it is obvious that the culmination of volumetric strain curve appears before the peak strength point is reached in each stage. But, the excess pore water pressure of the same specimen reaches its maximum at a position near to that of its corresponding volumetric strain curve (Fig. 4-5-1(b)).

The SST test yields the same phenomenon discussed in section 3-2.

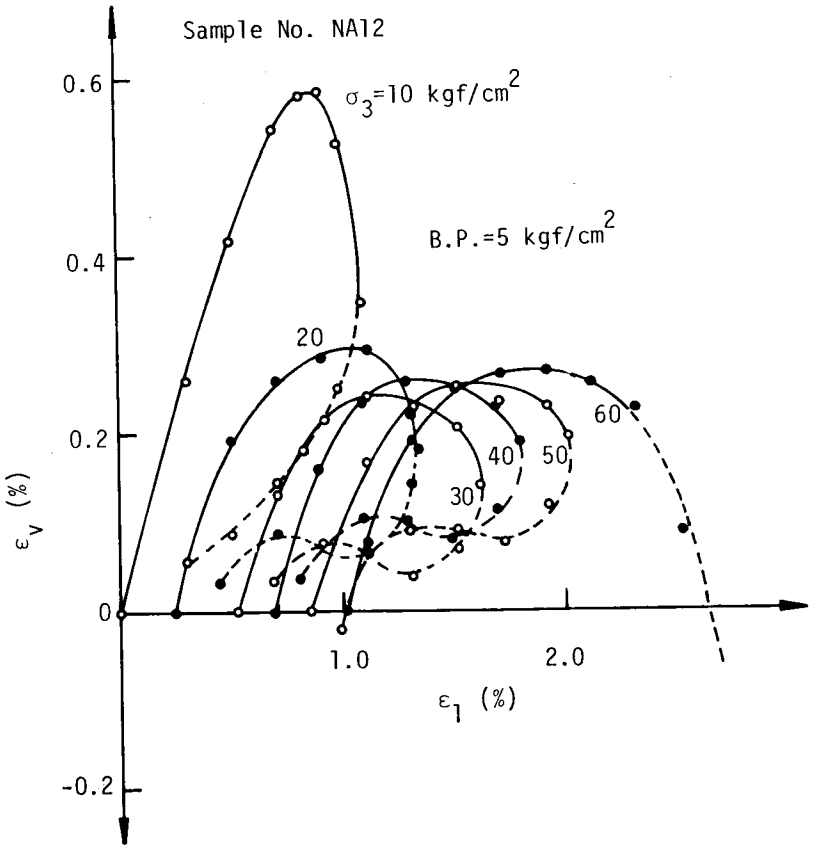

Fig.4-5-1(a) ε_v-ε_1 relationships derived by MST

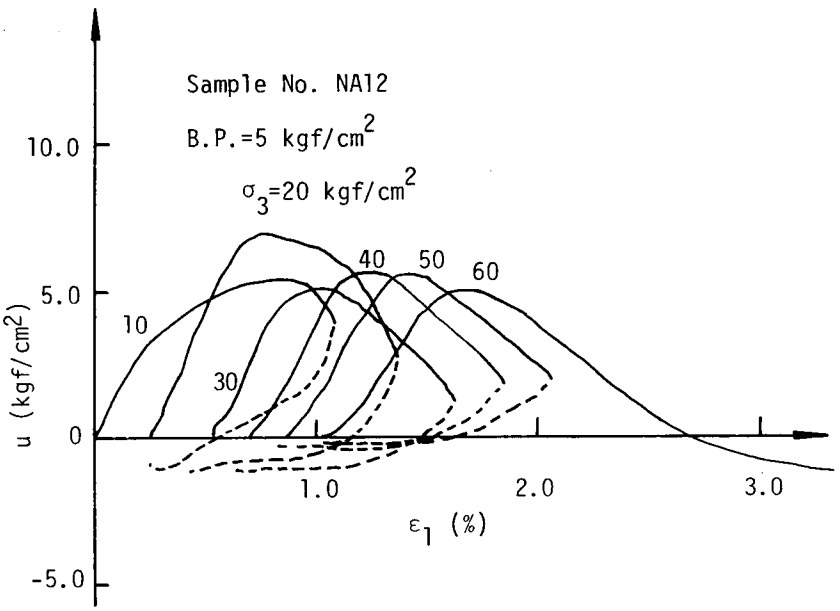

Fig.4-5-1(b) Pore water pressure created in sample No. NA12 during MST test

(5) From the effective stress paths obtained from using sample No. M24 in MST method (See Fig. 4-2-7) and the water content (or the void ratio) in each stage, a three-dimentional relationship of q-p'-w can be derived (see Fig. 4-5-2) which provides mechanical changes of this specimen.

As mentioned early in section 3-2, the specimen M24 had various degrees of "dilatancy" in the shearing process of P08, P15 and P20, i.e., the specimen behaved as a "over-consolidated" material in these stages. Moreover, the loading applied to the specimen was withdrawn before reaching the immediately due peak strength, thus, preventing the skeleton of rock from creating any apparent change. Connecting the onset of these stress paths of P08, P15, P20 and P30, the SS' line is obtained. This SS' line could be defined as one of the swelling line of the rock.

On the other hand, the vertical portion of effective stress paths perpendicular to the p'-w plane indicates that, during the initial part of shearing process, skeleton change did not happen and the specimen behaved as an elastic material. This phenomenon had also been mentioned in section 3-2.

Therefore, from connecting the upper-limits of these vertical portion of effective stress paths, an "elastic wall" could be assumed, which is similar to that of clay proposed by Roscoe and Burland (1968)[8] . The elatic wall for sandy silt rock is illustrated by the shadow area in Fig. 4-5-2.

Finally, projecting the peak strength envelope PP'and residual strength envelope RR' on the p'-w plane, P_1P_1' and R_1R_1' curves are obtained. Curves P_1P_1' , R_1R_1' and SS' intersect at point M (see Fig. 4-5-3). After checking into experimental results, it reveals that if a triaxial shear test is started at point M, neither dilatancy nor compression would occur in the specimen. Hence, point M can be designated as "critical pore ratio point".

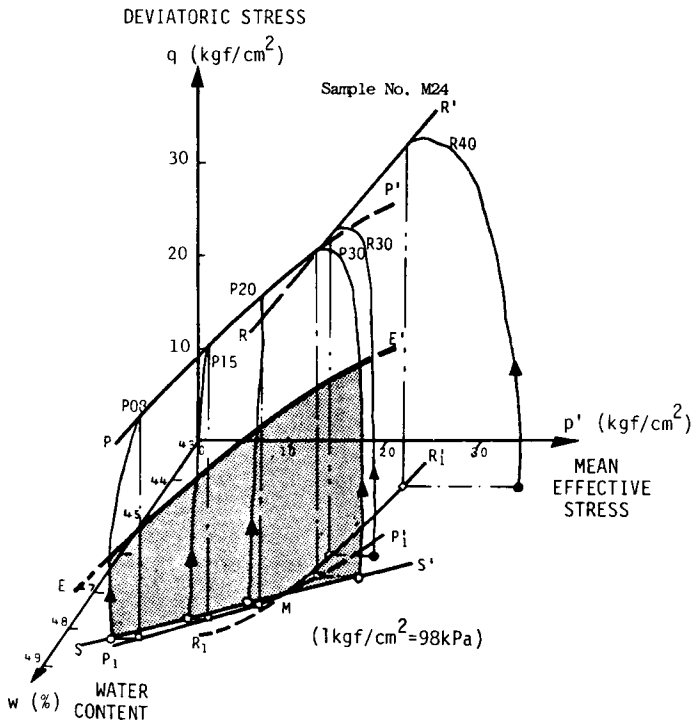

Fig. 4-5-2 Effective stress paths of Sample No. M24 in q-p'-w space. Where, pp' is the peak strength envelope, RR' is the residual strength envelope and the shadow area represents the 'elastic wall'

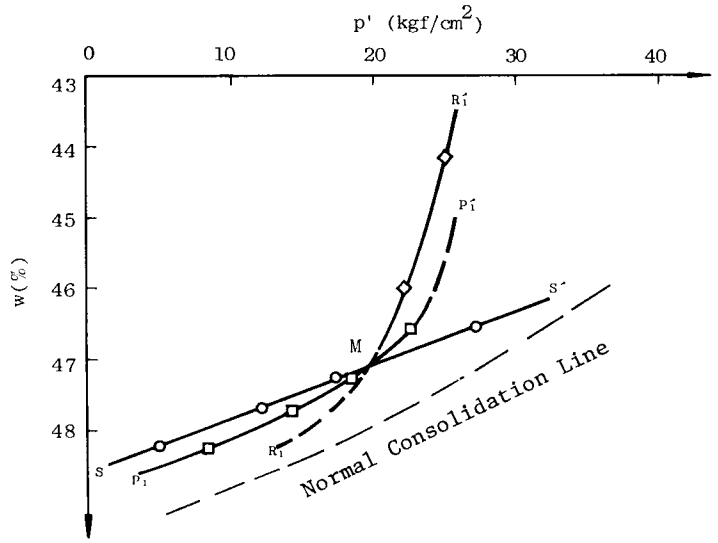

Fig. 4-5-3 The projection of peak strength and residual strength envelopes on p'-w plane

References for Chapter 4

(1) Kovari, K. and A. Tisa, "Multiple Failure State and Strain Controlled Triaxial Tests", Rock Mechanics, 7, pp. 17-33, 1975.

(2) Chang, N. Y. and A. L. Jumper, "Multiple-Stage Triaxial Test on Oil Shale" 19th U. S. Rock Mechanics Symposium, pp. 520-527, 1978.

(3) Kim, M. M. and H. Y. Ko, "Multistage Triaxial Testing of Rocks", ASTM Geotechnical Testing Journal, Vol. 2, No. 2, pp. 98-105, 1979.

(4) Chang, N. Y. and E. J. Bondurant, "Oil Shale Strength Characterization through Multiple Stage Triaxial Tests", 20th U. S. Rock Mechanics Symposium, pp. 393-401, 1979.

(5) Hudson, J. A., E. T. Brown and C. Fairhurst, "Optimizing the Control of Rock Failure in Servo-Controlled Laboratory Tests", Rock Mechanics, 3, pp. 217-224, 1971.

(6) Jaeger, J. C. and N. G. W. Cook, "Fundamentals of Rock Mechanics", Chapman and Hall Publication Co., pp. 65-68, 1979.

(7) Akai, K., Y. Ohnishi, D. H. Lee and T. Adachi, "The Multiple Stage Triaxial Test of Sandy Silt Rock with a Discontinuity", 14th JSSMFE, Ann. Meeting, pp. 1369-1372, 1979.

(8) Roscoe, K. H. and J. B. Burland, "On the Generalized Stress-Strain Behaviour of 'Wet' Clay", Engineering Plasticity, Edited by J. Heyman & F. A. Leckie, Cambridge University, pp. 535-609, 1968.

Chapter 5 THE PERMEABILITY OF SOFT ROCK IN TRIAXIAL SHEAR TEST

5-1 Introduction and Literature Review

Understanding is difficult about the mechanism of shearing failure of a rock specimen during a triaxial shear test. Nowaday, strain gauge is still the most popular instrument for measuring the deformation of a rock specimen. Yet, it can only be used to monitor the local change of strain in specimen, but not detailed information of shear failure in it.

In order to inspect the failure mechanism of a rock specimen more accurately, several methods have been proposed. Among these, Acoustic Emission method is the best. From monitoring the source locations of acoustic emission, the number of microcracks and their position can be identified. Furthermore, a uniaxial shearing test under acoustic emission counter control was developed by Terada, Yanagidani and Ehara (1981)[1]. By this method, the failure of rock specimen during shearing can stably be controlled, even with a brittle specimen.

However, the acoustic emission instrument has been very expensive, thus, it is not popular. Based on several investigations about permeability of rock, a simple substitute, proven to be economical and reliable method, has been developed to monitor the internal change of rock specimen during shear test.

From these pioneer investigations of permeability, some advanced informations has been obtained. For example, employing a special technique to measure the permeability of granite under high confining pressure, Brace, et al. (1968)[2] found that the permeability was strongly dependent upon effective pressure. Zoback and Byerlee (1975)[3], who investigated the relationship between microcracks, dilatancy and permeability, suggested that permeability

and dilatant volume changes are not functions of differential stress (deviatoric stress) alone. From the permeability measurements of intact and jointed Barre granite, Kranz and his co-workers (1979)[4] reported that the difference in permeability of jointed and unjointed rock specimens becomes indistinguishable when confining pressure reached a certain high level.

On the basis of these investigations, it is obvious that micro-structures of rock (such as microcrack, void, fault, etc.), affect directly the permeability. On the other hand, the "total" change of crack growth or shear band extension in a specimen can indirectly be perceived during shearing test from the change of permeability. Although the obtained permeability change is a "total" or "macroscopic" change in nature to the specimen, its micro-change can be smoothly and accurately estimated from inputting some reasonable judgement based on fracture mechanics.

This method can be carried out quite simply within a triaxial cell (see Fig. 2-6). It requires no special apparatus, hence, so called "economical".

5-2 Apparatus, Specimen and Testing Procedures

The main apparatus of this study had been illustrated in Fig. 2-6. Originally, it was used to perform triaxial shearing test of rock specimen with confining pressure up to 200 kgf/cm^2. A hole was especially drilled in the center of the loading rod to inject pressurized water into the rock specimen. The water which had passed through the specimen was then collected from the bottom of the specimen and calculated by a burette which connects with the cell.

A saturated Funyu rock specimen, 5 cm in diameter and 10 cm high, was used. A waterproofing layer about 0.5 mm thick, which is made from rubber

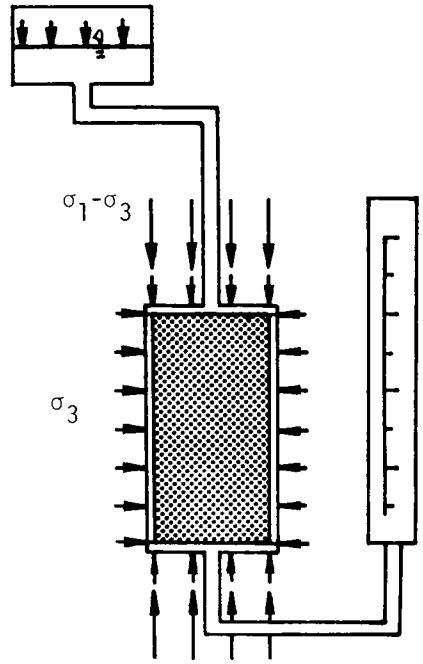

Fig.5-1 Experimental arrangement shown schematically

bond, was pasted on to the lateral side of the specimen.

After setting the specimen into the triaxial shearing cell, and loaded with an adequate confining pressure σ_3 to perform consolidation, water with pressure about 7 kgf/cm^2 was injected into the specimen from its upper surface. While the drainage gathered from the bottom of the specimen reached a stable state, an axial strain control shearing test with a rate 0.04 %/min was then carried out (see Fig. 5-1).

During the shearing process, the volume of drainage was measured from a reading in the burette at constant time intervals.

5-3 Experimental Results in Low Confining Pressure

In order to investigate the failure mechanism of the specimen more extensively, permeability measurement in relaxation test and cyclic loading test had also been conducted, besides the triaxial shearing test with constant axial strain rate.

The test results obtained under a lower confining pressure (σ_3=40 kgf/cm^2) are discussed in detail in the following sections.

5-3-1 The Behavior of a Rock Specimen during Triaxial Shear Test with Constant Axial Strain Rate

The relationship between deviatoric stress (q) and axial strain (ε_1) of a rock specimen during shearing is presented in Fig. 5-2(a). The permeability (v) versus axial strain (ε_1) of the same specimen test is depicted in Fig. 5-2(b). Here, permeability is defined as the drainage gathered from the bottom of the specimen per minute. Before inspecting these two figures, it is necessary to examine the influence of the volumetric change of specimen itself on the permeability measured during shear test.

A drained triaxial shear test was conducted under the same testing condition as that used in the permeability test of sample P46. The resultant volumetric change of the specimen per minute (v_s) and axial strain (ε_1) was obtained (see Fig. 5-3).

Comparing Fig. 5-3 with Fig. 5-2(b), it is apparent that the value of v_s was only about 10 % of the permeated water in the permeability test, and the variation of the former was about one fourth of the latter.

Therefore, it can be concluded that the influence of v_s on permeability can be neglected and the result of permeability test can be used to represent the internal change of a specimen.

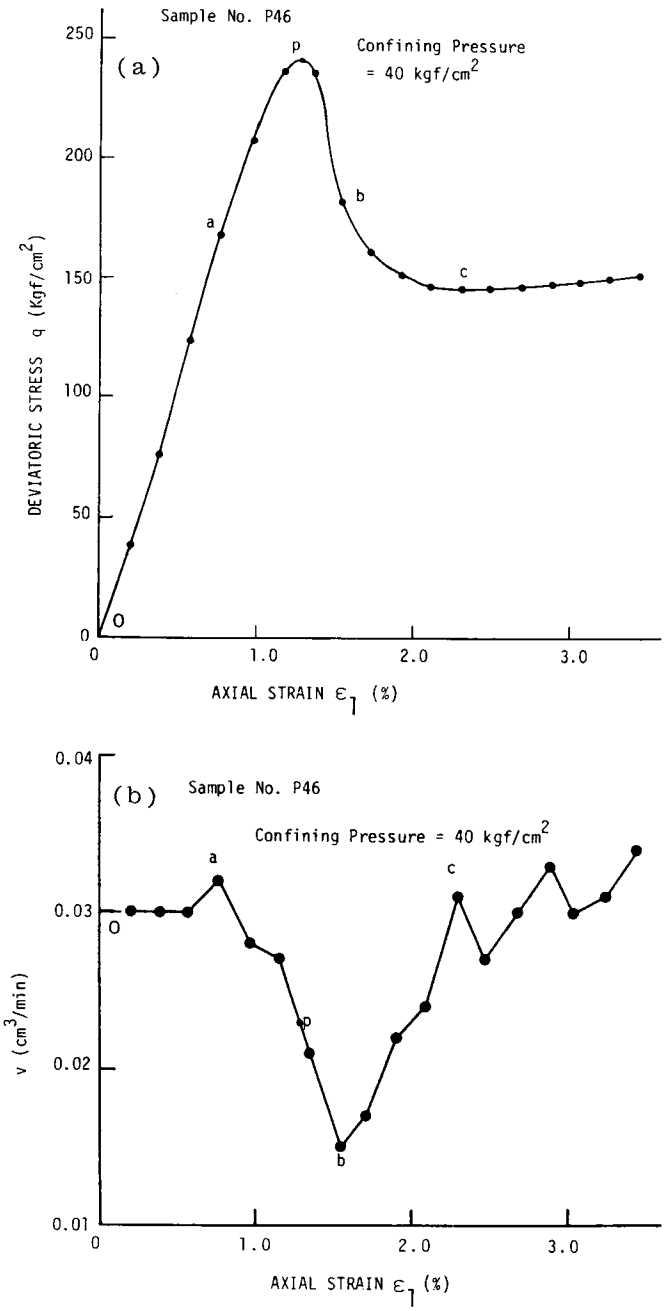

Fig.5-2 (a) Deviatoric stress-axial strain curve
(b) permeability-axial strain curve,
derived by triaxial shear test ($\dot{\varepsilon}_1$=0.04 %/min).

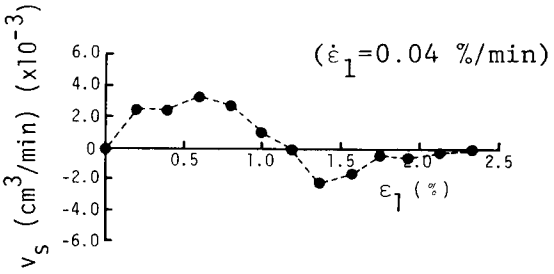

Fig.5-3 Volumetric change of Funyu rock specimen during a drained triaxial shear test

Based on Figs. 5-2(a) and (b), the micro-change of the specimen may be established based upon the knowledge of fracture mechanism. The permeability of rock specimen improved slightly during the initial part of shearing. But, beyond point a, it decreased rapidly. The decreasing trend did not stop, it passed over the peak strength point p, see Fig. 5-2(b), and finally reaching point b where v value being the minimum.

Point b was located about midway on the strain softening process. After point b, the permeability recovered swiftly, but temporarily stopped at point c. From the changing of permeability, it is clear that micro-structure within the specimen changed accordingly during shearing test. Therefore, from Fig. 5-2(b), the changes of micro-structure can also be divided into 4 stages, the first region from 'o' to 'a', followed by a-b region, b-c region and lastly region beyond point c. In order to explore the relationship between the changes of permeability and micro-structure of this specimen, it is necessary to review the reports of some pioneer investigators about crack growth.

Odè (1960)[5] suggests that the applied stress on a specimen locally modified by 'Griffith cracks', which was named by Griffith (1921)[6] and meaned the existing cracks in brittle material, may become tensile on certain points

on a crack surface, even when applied stress is wholly compressive. Furthermore, Brace and Bombolakis (1963)[7], performing a compression experiment of brittle material with an artificial crack, suggests that if the applied stress is approximately equal to the tensile strength of the material, then, the crack spreads and material fractures. They also observed an evidence that a crack growth was formed by extensing the artificial crack along a curving path which gradually became parallel with the direction of compression. But, once this direction was attained, further crack growth stopped. Similar results were also reported by Bieniawski (1967)[8] and Cotterell (1972)[9].

Therefore, under axial loading, the cracks growth in a rock specimen spread significantly in the direction parallel to the loading increment, and then stopped their growth. Simultaneously, the opening of the crack, perpendicular to the loading direction, also expanded. As a result, the permeability improved.

The characteristic of the first region o-a (see Figs. 5-2(a), (b), Figs. 5-4(a), (b) and Figs. 5-5(a), (b)) reveals that the increasing of deviatoric stress in specimen induces the increase of permeability. According to the proposition of Brace and Bombolakis (1963)[7], mentioned above, it is obvious that region o-a is a crack-growth region. And, crack-growth stopped at the point a, where all cracks reached a stable state.

As to extend these stable cracks need large amount of energy, thus, beyond point a, the increse of external loading would inadvertently avoid performing the new crack growth, but, would create other type of micro-structure changing which needed less energy.

Moreover, in the second region (a-b), permeability decreased considerably, whilst the q-ε_1 relationship became nonlinear till reaching the peak strength point at p. With the great fall of v value and the nonlinear relation of q-ε_1 curve, it seemingly predicts that a substantial change inside

the specimen was going to happen when shearing process passed point a.

The most reasonable answer to the question on "what happened in the specimen during region 2 ?" is that only the "progressive formation of shearing failure plane occurred in this region". Immediately, another question arises "why does the permeability decrease during the forming of a shearing failure plane?"

To answer this question, we must recognise the fact that the progressive completion of a failure plane was started from the penetration of some opened microcracks, might follow the manners proposed by Kranz (1979)[10] , and these cracks often located near to the center of the specimen[11] . While the penetration of crack took place, part of the surface energy originally stored in each crack, especially these cracks near the fracture plane, was released. In addition to the increasing of applied stress, microcrack and its expanded part became narrow and stable. Therefore, to permeate water through the specimen gradually became more difficult. This difficulty reversed when the shearing fracture plane stretched out big enough, so affecting the permeation of water.

On the other hand, from the macroscopic concepts, point a has its special significance. From Fig. 3-2-9 (the results of a Nikko rock specimen), point a, the onset of nonlinear part of q-ε_1 curve, located near to the point of peak pore water pressure, also served as the starting point of the appearance of dilatancy. It is the initial point of the unstable fracture propagation region, suggested by Bieniawski, et al. (1969)[12] or the onset of stable microcrack dilatancy region proposed by Tapponnier and Brace (1976)[13].

From the relation curves of v-ε_1 (Fig. 5-2(b)), u-ε_1 (Fig.3-2-9(b)) and ε_v-ε_1 (Fig. 3-2-9(c)), it can be found that continuity exists from point a to point b. In other words, the change in the specimen within this region is plainly the same style throughout, i.e., only the progressive formation of

shearing fracture plane.

Should the trend of change be correctly estimated, then, the fracture plane would be completely formed near point b, but not at the peak strength point p. However, because of the hypothesis that "the fracture plane is formed at the peak strength point p", has long been employed. This experimental evidence is consistent with the investigation of Hallbauer, Wagner and Cook (1973)[11] about quartzite specimen. In their study, they found that "at the point of the ultimate specimen strength a macroscopic fracture plane develops in the central portion of the specimen. With further shearing, this fracture plane grows towards one or both ends of the specimen by stepwise joining at existing microcracks". In other words, the fracture plane is completely formed in a point which located beyond the peak strength point.

However, more detailed investigation with soft rock is necessary in order to verify it.

Further beyond the minimum permeability point b, the shearing test entered region 3 (b-c). Point c was the end of this region and also was the onset of residual state. This region served as a transition from region 2 (progressive formation of shearing fracture plane) to region 4 (constant strength region - residual state).

Because the whole fracture surface is created at point b, any increment of axial strain would induce the relative sliding along the shearing fracture plane. According to the investigation about the friction on fracture surface of granite, Byerlee (1967)[14] suggested that there exist many asperities in the fracture surface of granite, and brittle fracture of surface asperities may be the controlling mechanism during the friction sliding. In our testing, when local shearing also took place around asperities, then, many broken-up grains would be produced and friction resistance along this fracture plane would decrease from an initially high value at point b to a constant value at

point c after about 0.07 cm of sliding has occurred. In granite, it needs 0.1 cm (Byerlee (1967))[14].

Accompanying the relative sliding and local shearing of asperities, the shearing fracture plane became a fracture "band". It contained many different sizes of grains over the whole of the surface. As the "band" was a good permeable layer and the applied stress was also decreasing in the region 3, so that the permeability of the specimen recovered rapidly in the region which is apparently shown in the Fig. 5-2(b).

In the last region 4, the strength of the specimen remained unchanged, proving that there was no new local shearing of asperities on the fracture plane. But, because permeability varied with the degree of relative sliding, so the v value fluctuated randomly.

This phenomenon can well be explained as a result of the stick-slip action which always happens in a relative sliding along shearing fracture plane of rock. Though, we can not find apparently any stick-slip phenomenon in the q-ε_1 curve of region 4 (see Fig. 5-2 (a)), it is reasonable to consider that a miniature stick-slip action might be happened in the fracture "band". Relative sliding can not put its influence on the strength of friction, but, it was able to compress the grains in the fracture band and increase the real area of contact. Therefore, it was considered as one of the processes of the stick-slip instability by Scholz and Engelder (1976)[15].

In short, the behavior of the specimen in this region 4 might be estimated as a combination of compression-sliding and its repeatness in the shearing fracture band.

5-3-2 The Behavior of a Rock Specimen during Triaxial Relaxation Test

After a rock specimen is loaded with an axial strain, a horizontal extension stress arises. If this stress is larger than the cohesive strength

between particles within the specimen, the crack growth parallel to the axial direction results. This phenomenon had been mentioned in section 5-3-1, and can be found in the Brazilian Test[16].

But, what kind of change will happen in the crack growth if the axial strain is restrictly kept constant? A triaxial shear test under the same conditions explained in section 5-3-1 above was conducted, but exercising several times of relaxation during test. The experimental results of this test are given in Figs. 5-4(a) and 5-4(b), showing the relationships of deviatoric stress (q) - axial strain (ε_1), and permeability (v) - axial strain (ε_1).

Upon observing Fig. 5-4(b), the result of changing permeability during shearing process (solid line with black dots) resembled that of the original triaxial shear test presented in Fig. 5-2(b). Therefore, it can certainly be concluded that the failure mechanism during shearing process was identical to that mentioned in section 5-3-1.

However, from the change of permeability in relaxation process (dotted lines and white circles) depicted in Fig. 5-4(b), particularly for regions 1 and 2 (i.e., for between points o-a-b), the permeability dropped down vertically to a minimal when axial strain was kept constant. Because crack growth and progressive formation of shearing fracture plane are the major change inside the specimen in regions 1 and 2, respectively, the decreasing of resisting stress and permeability can be inferred to as a result affected by the changing (narrowing) of crack width and progressive fracture plane. Comparing the drop of resisting stress in regions 1 and 2 with that in regions 3 and 4, we can found an evidence like that obtained from Tennessee marble and Arkose sandstone by Peng (1973)[17]. Namely, the "load relaxation" in the prefailure region is inappreciable.

In region 3 (b-c), permeability increased with relaxation. It can instinctively be imagined that, under constant axial strain, the concentration

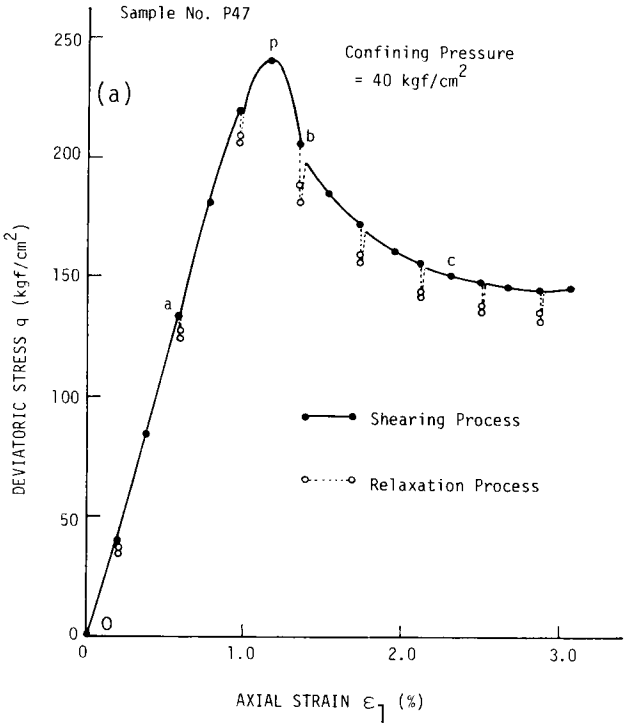

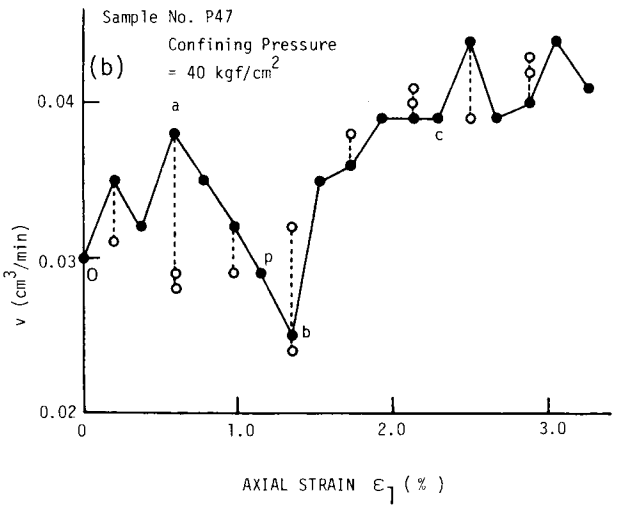

Fig. 5-4 (a) q-ε_1 curve (b) v-ε_1 curve of a Funyu rock specimen obtained from triaxial relaxation test ($\dot{\varepsilon}_1$=0.04 %/min).

of stress around the asperities in the shearing fracture plane can slightly be relaxed and allowed the voids between crashed particles in shear plane more permeable.

This consideration is also appropriate in region 4.

5-3-3 The Behavior of a Rock Specimen during Cyclic Loading Test

To investigate the change of the internal structure within a specimen due to unloading-reloading procedure is the purpose of conducting a cyclic loading test.

An example of this test is illustrated in Figs. 5-5(a) and (b). Before reaching the peak strength, three cycles of unloading-reloading were carried out, while one of them further performed in residual state. Similar to the results of relaxation test mentioned previously, the inclination of permeability curve during shearing process (solid line and black dots) is identical to that in Fig. 5-2(b), which represented the variations of permeability in original triaxial shear test.

From a various combination of shearing process and unloading-reloading cycle, according to the Fig. 5-5(b), it is obvious that at the commencing of unloading, the permeability dropped rapidly to a low level and recovered straight away after starting the reloading. They would then end up at or near the same point on the original shearing process curve from where the unloading -reloading cycle had started.

Therefore, we can confidently estimate that when the unloading procedure is adopted into a shearing test, during the initial stage of unloading process, the crack width of the most of opened cracks and shearing fractures would swiftly become narrower. At the beginning of reloading, the closed cracks or fractures should be reopened instantly. Following this, we can conclude that the close up and reopening of a crack or fracture is a kind of

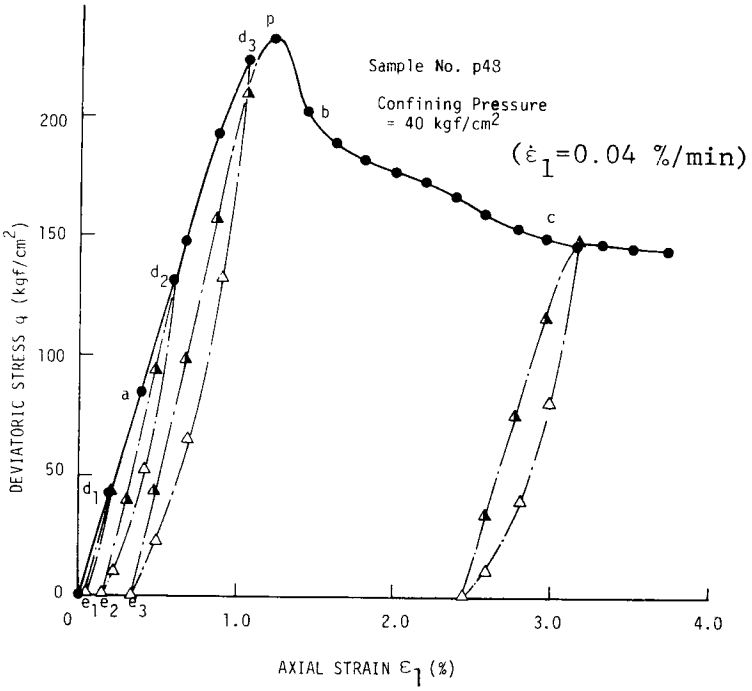

Fig.5-5(a) q-ε_1 curve drived by a cyclic loading test.

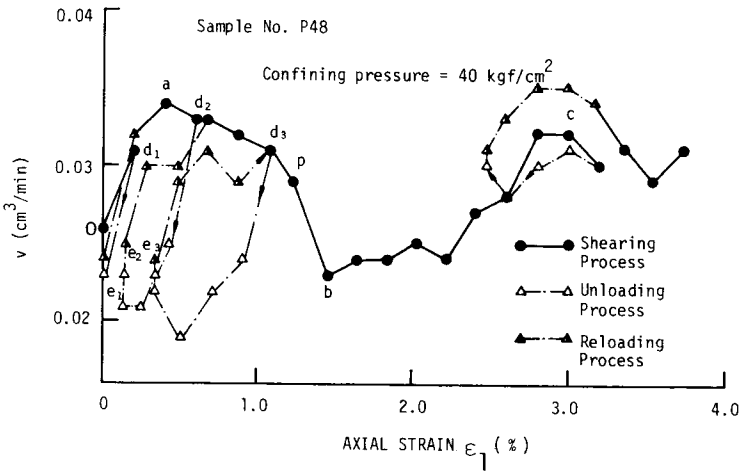

Fig.5-5(b) v-ε_1 relationship during a cylic loading test

time-independent phenomenon.

5-4 Permeability of Soft Rock under Higher Confining Pressure

In this section, permeability was measured when performing the triaxial shear test under a higher confining pressure (160 kgf/cm^2).

Employing the same experimental procedures used in section 5-3-1, test was carried out under higher confining pressure. Results are depicted in Figs. 5-6(a) and (b), showing the q-ε_1 and v-ε_1 relationship, respectively. From Fig. 5-6(a), under confining pressure at 160 kgf/cm^2, the specimen behaved as an elastic - complete plastic material. That is to say, under this confining pressure, the specimen was starting to act as a ductile material. And Orowan (1960)[18] and Maurer (1965)[19] proposed that the apparent ductility created in a brittle material may be caused by the frictional strength of the material being equal to or greater than its fracture strength, while a shearing test is being underway. Therefore, the failure style of rock specimen under 160 kgf/cm^2 is certainly different from that under lower confining pressure (40 kgf/cm^2).

Upon inspecting Fig. 5-6(b), it is obvious that the gradual increase of permeability was accompanied by the advancement of shearing test, although having irregular inclination of permeability change.

Because the change of permeability can reflect the failure style within the specimen, we can detect that the failure mechanism, similar to the change of permeability, is also a simple style.

Examining the outer appearance of the specimen after shearing test, the internal failure mode can be estimated. The failure occurred under high confining pressure was probably caused by the crack growths which were uniformly created all over the specimen and by rigorously cohesion crash between parti-

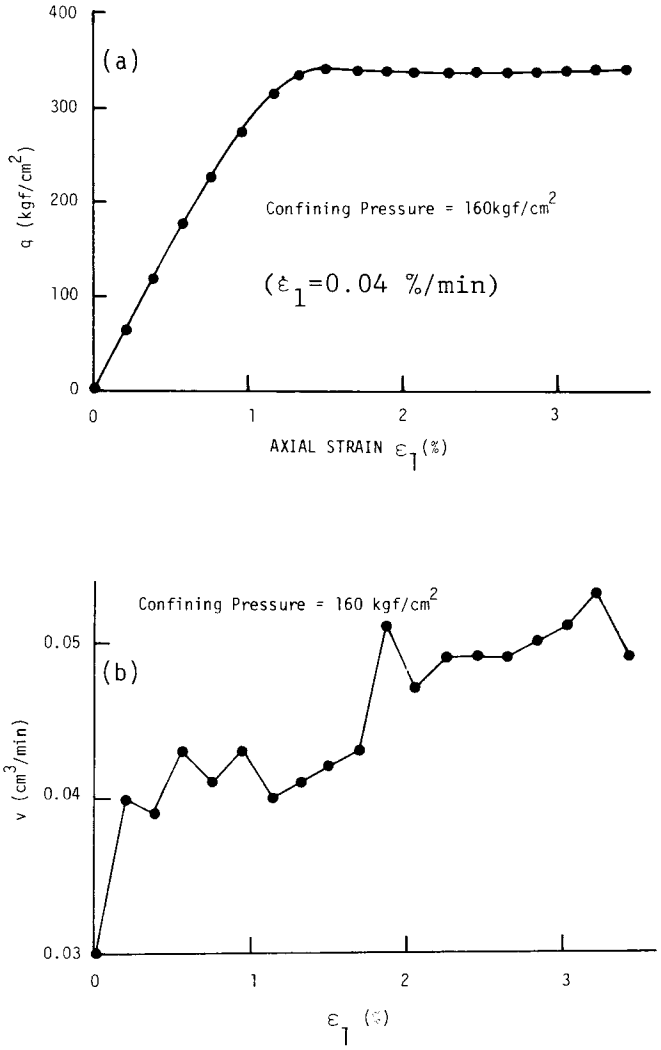

Fig.5-6 (a) $q-\varepsilon_1$ curve (b) $v-\varepsilon_1$ curve of a Funyu rock specimen drived by a triaxial shear test with higher confining pressure.

cles. These made the specimen behaved as a ductile material rather than a brittle one during the shearing process. The specimen was finally deformed into a shape like a "barrel".

5-5 Multiple Stage Permeability Test

According to the change of permeability during triaxial shear test presented in previous sections, the internal change of a soft rock specimen can indirectly be detected. Now, applying this technique in MST method, the immanent change of specimen can also be explored in each stage of MST test.

Test procedure is a combination of the MST method (mentioned in section 4-2) and the technique of permeability test. This combined procedure may be tentatively called as Multiple Stage Permeability Test (MSPT).

Test results of a Funyu rock specimen are illustrated in Figs. 5-7(a) and (b). Fig. 5-7(a) shows the relationship between q and ε_1 in the test. From this, it promises that various peak strengths could adequately be obtained even under different confining pressures, a result similar to that of MST for saturated soft rock (section 4-2).

On the contrary, Fig. 5-7(b) contains many new significations which are helpful in understanding the internal change of specimen in each stage of MST test. The main issues are as follows:

(1) Permeability v decreased while its corresponding confining pressure increased. However, with a large increment of confining pressure it was not necessary that a significant drop in permeability could be expected.

(2) Under lower confining pressure (σ_3=40 and 80 kgf/cm^2), v increased rapidly in the initial portion of shearing, becoming flatter under higher confining pressure, and near horizontally under a very high pressure (σ_3 = 160

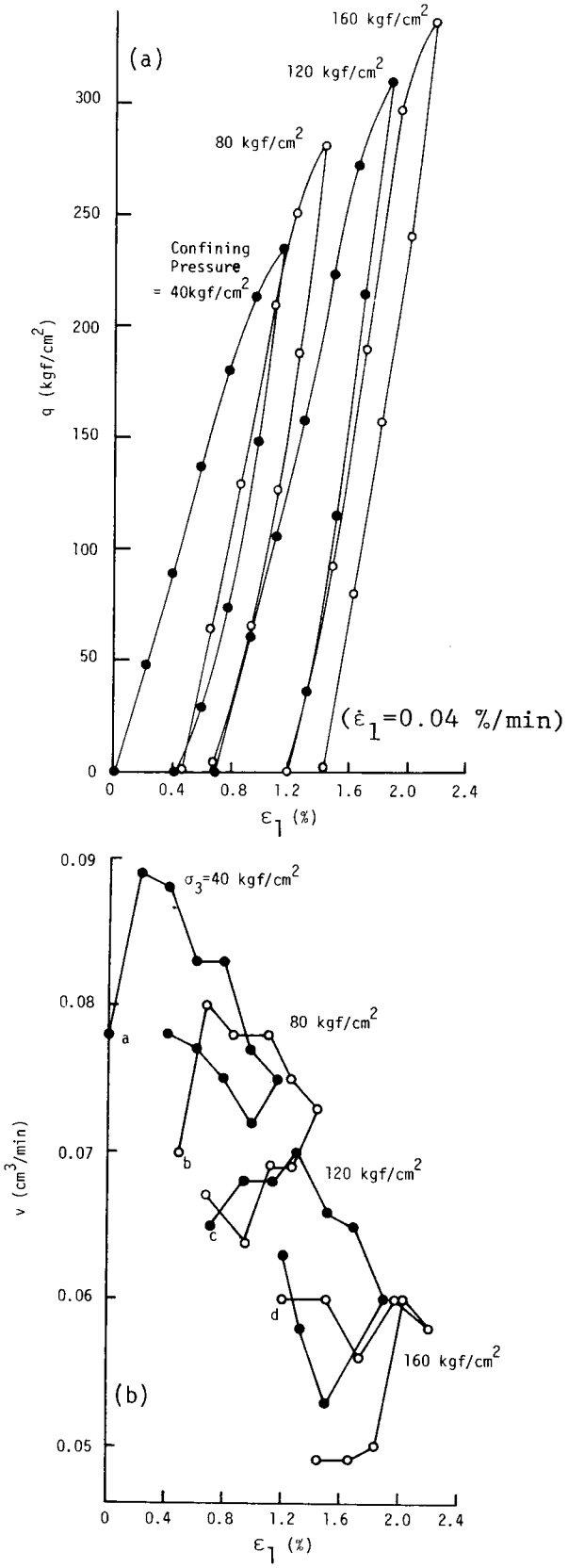

Fig.5-7 Example of multiple stage permeability test (a) q-ε_1 curve (b) v-ε_1 curve

kgf/cm^2).

As discussed in section 5-3, v value increases in the initial portion of shearing reflects the fact that crack or pore is expanding their size (crack growth) during the initial part of shearing test. Similarly, most of the crack growths in the MSTP specimen, produced in early stages (particularly when σ_3= 40 or 80 kgf/cm^2).

(3) Generally, permeability decreased after the initial portion of shearing test. Again, according to section 5-3, this fact means that a shearing failure plane was probably progressing in the specimen. Therefore, Fig. 5-7 (b) suggests that progressive shearing failure plane might have taken place in each new stage. With the increase of confining pressure used in a new stage, the starting value of v decreased accordingly when compared with the former stage. But, σ_3 must definitely be limited to a value under which it could still make the specimen behaved as a brittle material rather than ductile.

(4) Unloading process induced rapid reduction of permeability in each stage of test. Regardless the kind of confining pressure or failure style, unloading promoted and closed existing cracks.

5-6 Conclusions

The permeability change of a rock specimen can not be directly used to inspect the accurate position and number of crack growth whereas acoustic emission method can do (Byerlee and Lockner (1977),(1977)[20), 21)]). But, in addition to some reasonable judgement based on fracture mechanics, it can be used as a versatile and economical tool to estimate the micro-change within a rock specimen.

After performing a series of tests, some conclusions are obtained as

follows:

(1) Under a low confining pressure (40 kgf/cm^2), the internal change of a specimen during a triaxial shear test would be divided into 4 stages;

stage 1, the opening and growth of existing cracks,

stage 2, the formation of a progressive fracture plane,

stage 3, relative sliding along the fracture plane with local shearing of asperities, and

stage 4, the residual state (see Fig. 5-8).

(2) Under the confining pressure of 40 kgf/cm^2, the fracture plane might be completely formed at the end of stage 2, that is to say, not at the peak

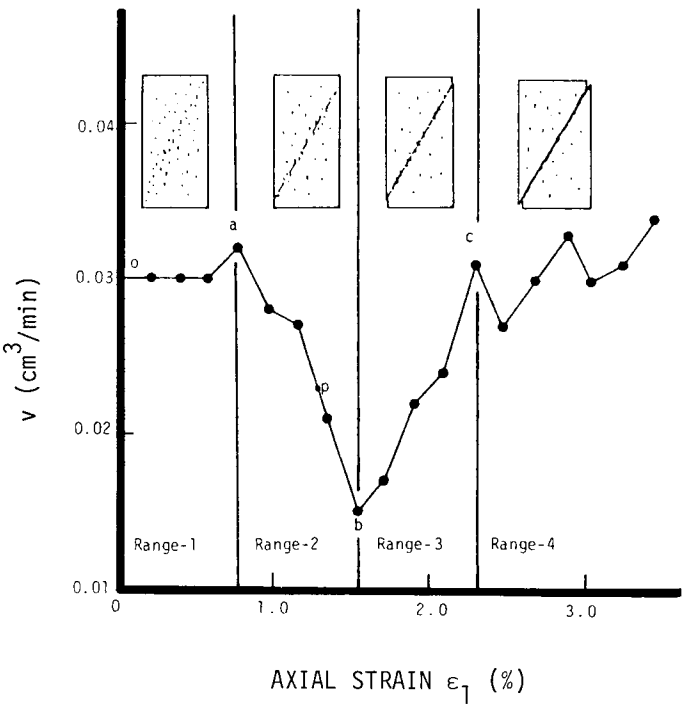

Fig. 5-8 The relationship between the internal structure change and the variation of permeability of rock specimen (σ_3 = 40 kgf/cm^2)

strength point but at a point within the strain-softening process.

(3) The close-up and reopening of a crack or a fracture, when the applied load is drawn out or reloaded, is a time-independent phenomenon.

(4) There had different patterns of permeability change when triaxial shear tests were performed under different confining pressures (40 kgf/cm^2 and 160 kgf/cm^2). It indicates that changing the confining pressure would induce different kinds of internal failure style.

(5) The permeability decreased with the increasing of confining pressure, but the decrement was not so apparent.

References for Chapter 5

(1) Terada, M., T. Yanagidani and S. Ehara, "A.E. Rate Controlled Compression Test of Rocks", Third Conference on Acoustic Emission / Microseismic Activity in Geologic Structures and Materials, Pennsylvania State University, 1981.

(2) Brace, W. F., J. B. Walsh and W. T. Frangos, "Permeability of Granite under High Pressure", J. of Geophysical Research, Vol. 73, No. 6, pp. 2225-2236, 1968.

(3) Zoback, M. D. and J. D. Byerlee, "The Effect of Microcrack Dilatancy on the Permeability of Westerly Granite", J. of Geophysical Research, Vol. 80, No. 5, pp. 752-755, 1975.

(4) Kranz, R. L., A. D. Frankel, T. Engelder and C. H. Scholz, "The Permeability of Whole and Jointed Barre Granite", Int. J. Rock Mech. Min. Sci. & Geomech. Abstr., Vol. 16, pp. 225-234, 1979.

(5) Odè , H., "Faulting as a Velocity Discontinuity in Plastic Deformation",

Geol. Soc. Am. Mem., 79, pp. 293-321, 1960.

(6) Griffith, A. A., "The Phenomenon of Rupture and Flow in Solids", Phil. Trans. Roy. Soc. London, A., 221, pp. 163-197, 1921.

(7) Brace, W. F. and E. G. Bombolakis, "A Note on Brittle Crack Growth in Compression", Journal of Geophysical Research, Vol. 68, No. 12, pp. 3709-3713, 1963.

(8) Bieniawski, Z. T., "Mechanism of Brittle Fracture of Rock, Part II . Experimental Studies", Int. J. Rock Mech. Min. Sci., Vol. 4, pp. 407-423, 1967.

(9) Cotterell, B., "Brittle Fracture in Compression", Int. J. Fracture Mechanics, Vol. 8, No. 2, pp. 195-208, 1972.

(10) Kranz, R. L., "Crack-Crack and Crack-Pore Interactions in Stressed Granite", Int. J. Rock Mech. Min. Sci. & Geomech. Abstr., Vol. 16, pp. 37-47, 1979.

(11) Hallbauer, D. K., H. Wagner and N. G. W. Cook, "Some Observations Concerning the Microscopic and Mechanical Behaviour of Quartzite Specimens in Stiff, Triaxial Compression Tests", Int. J. Rock Mech. Min. Sci. & Geomech. Abstr., Vol. 10, pp. 713-726, 1973.

(12) Bieniawski, Z. T., H. G. Denkhaus and U. W. Vogler, "Failure of Fractured Rock", Int. J. Rock Mech. Min. Sci., Vol. 6, pp. 323-341, 1969.

(13) Tapponnier, P. and W. F. Brace, "Development of Stress - Induced Microcracks in Westerly Granite", Int. J. Rock Mech. Min. Sci. & Geomech. Abstr., Vol. 13, pp. 103-112, 1976.

(14) Byerlee, J. D., "Frictional Characteristics of Granite under High Confining Pressure", J. of Geophys. Res., Vol. 72, No. 14, pp. 3639-3648, 1967.

(15) Scholz, C. H. and J. T. Engelder, "The Role of Asperity Indentation and Ploughing in Rock Friction - I. Asperity Creep and Stick-Slip", Int.

J. Rock Mech. Min. Sci. & Geomech. Abstr., Vol. 13, pp. 149-154, 1976.

(16) Jaeger, J. C. and E. R. Hoskins, "Rock Failure under the Confining Brazilian Test", J. of Geophys. Res., Vol. 71, No. 10, pp. 2651-2659, 1966.

(17) Peng, S. S., "Time-Dependent Aspects of Rock Behavior as Measured by a Servocontrolled Hydraulic Testing Machine", Int. J. Rock Mech. Min. Sci. & Geomech. Abstr., Vol. 10, pp. 235-246, 1973.

(18) Orowan, E., "Mechanism of Seismic Faulting", Geol. Soc. Am. Mem., 79, pp. 323-345, 1960.

(19) Maurer, W. C., "Shear Failure of Rock under Compression", Soc. Petrol. Engrs. J., 5, pp. 167-175, 1965.

(20) Byerlee, J. D. and D. Lockner, "Acoustic Emission during Fluid Injection into Rock", Proc. 1st Conf. A. E., Trans. Tech. Publications, pp. 87-98, 1977.

(21) Lockner, D. and J. Byerlee, "Acoustic Emission and Fault Formation in Rocks", Proc. 1st Conf. A. E., Trans. Tech. Publications, pp. 99-107, 1977.

Chapter 6 APPLICATIONS TO GEOTECHNICAL ENGINEERING

Following upon the reports of several test series of rock specimens, such as the fundamental tests in Chapter 3, multiple stage triaxial test method for saturated soft rocks in Chapter 4 and their variations in permeability in Chapter 5, two potential applications to geotechnical engineering will be envisaged.

The first application is to investigate the influence of rocking of structure induced by various forces from wind, wave and current alike on the behavior of rock mass beneath its foundation. The rock damage caused by the rocking of structure can be inspected by measuring the permeability variation of rock specimen. In addition, the response occurred in rock by different degrees of rocking will also be examined.

The other application is to simulate the behavior of the rock mass around an opening, by using experimental methods developed in the laboratory, whilst an opening excavation is being underway. It is also aimed to derive the relationship between the reaction of rock mass and deformation of opening wall, which has been used for the support design of opening.

Theoretically, the speed of opening excavation influences the rock reaction and the deformation of tunnel opening wall, in other words, a support designed for tunneling may be affected by the excavation speed. Therefore, the results generated by variable excavation speeds should be monitored by means of laboratory test methods, such as the multiple stage triaxial test method with improved testing procedures.

6-1 Application of Laboratory Test Results to Foundation Engineering

Along with the rapid increase of social activities, the need of even larger structures becomes more apparent. The construction of skyscrapers, long bridges and atomic power plants, etc. can now be found ubiquitously. Unfortunately, the bigger the structure is, the more serious damage may cause when it fails. It is also necessary to pre-investigate the influence of violent vibration induced by earthquake. Along this line, grave concerns have been focused on the interaction of structure foundation and ground during earthquake, and so far with excellent success. Yet, besides the disastrous effect from earthquake, forces induced by wind, wave or currents are also predominent to foundation design for structure, especially in a non-earthquake region.

The behaviors of rock mass under the influence of rocking of large structure, which might be caused in a strong wind blow, will be monitored qualitatively by a laboratory test method discribed previously.

6-1-1 Wind Force and Wind Breathing

On the basis of Bernoulli theory, the air pressure acts on a body in airflow satisfies the relation:

$$\frac{1}{2}\rho V^2 + p = \text{const} \quad \ldots\ldots\ldots (6\text{-}1)$$

where, ρ is air density, V the air flow speed and p the static pressure.

This equation states that at any point in the air flow (wind) it will be subjected to a static pressure p in additional to dynamic pressure $\frac{1}{2}\rho V^2$. However, the sum of static and dynamic pressures remains constant at all points.

Whenever airflow (wind) strikes perpendicularly to a structure, it would come to a rest, i.e., decreasing to zero. Consequently, an increment of static pressure Δp will be created on the surface of structure. Where,

$$\Delta p = \frac{1}{2}\rho V^2 \quad \ldots\ldots\ldots\ldots\ldots (6\text{-}2)$$

Naito[1] reported that wind speed V varies with the height of structure measuring from groundlevel, i.e.,

$$V = V_0 \sqrt[8]{\frac{h}{h_0}} \quad \text{.....(6-3)}$$

in which h_0 is the height of anemometer in a weather bureau. If h_0=15 m, then the average wind speed measured by anemometer is V_0 = 63 m/sec, and ρ = 0.125 kg·sec^2/m^4 (at 15 ^{0}c, 760 mm Hg). Hence, the wind pressure increases on the surface of structure can be repesented by:

$$\Delta p = \frac{1}{2}\rho V^2 = \frac{1}{16}\left(V_0 \sqrt[8]{\frac{h}{h_0}}\right)^2 = 127\sqrt[4]{h} \doteqdot 120\sqrt[4]{h} \quad \text{....(6-4)}$$

In order to calculate the wind force, the duration of wind gust is also important. Although there is no versatile standard to it, it is wise to consider the work of Takahashi[1], in which it is reported that the duration of wind gust (or the wind breathing) was about 60 seconds at 66 meters above the ground surface measured at Tokyo Tower.

Therefore, in spite of the actual magnitudes of wind force and wind breathing, it is apparent that any high-rised building will be pondered by strong wind now and then, resulting in low frequency rocking. Thus, the rock mass beneath the structure is subjected to a low frequency cyclic loading similar to the pattern illustrated in Fig. 6-1.

6-1-2 Simulation Tests in Laboratory

To explore the characteristic change of rock mass induced by the rocking of structure, two kinds of test was carried out in laboratory with Funyu rock specimen. Two cyclic loading tests were performed. The loading pattern is shown in Fig. 6-2, which is a modified pattern of Fig. 6-1. In addition, to establish the influence of different degrees of rocking, various upper limits of the cyclic loadings were simulated in these tests. Shear test was conducted

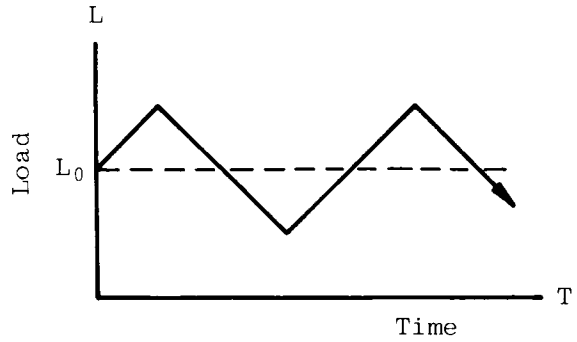

Fig. 6-1 The cyclic loading acting on foundation rock mass

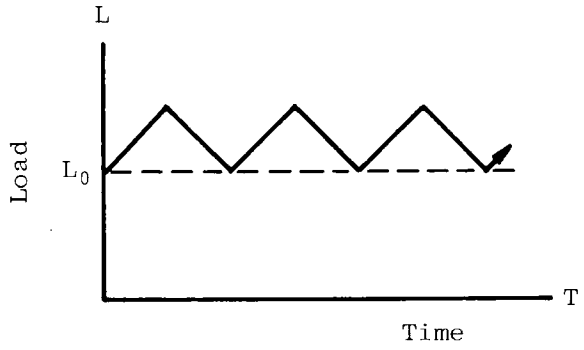

Fig. 6-2 The modified cyclic loading pattern adopted in simulation test.

in the first test (designated as Test A) for up to the peak strength of rock specimen in each cycle, whilst the other (Test C) performed tests with deviatoric stress q between 0 and 0.8 x q_{peak}. While testing, the variations of permeability of rock specimen were also measured (Chapter 5). With the procedure adopted, these two cyclic tests can be considered as multiple stage triaxial tests with constant confining pressure at different stages.

The results of cyclic loading test C are depicted in Fig. 6-3 for the relationship between the deviatoric stress-axial strain versus number of cycles, and in Fig. 6-4 for the permeability against axial strain and number of cycles. The pattern in Fig. 6-3 was used (as in Chapter 3) to discuss the characteristic of cyclic loading test from the view point of stress - strain relationship and the dissipated energy in each cycle. In addition to this, the properties change in rock specimen can now be expected by examining the permeability variation during cyclic test.

The deviatoric stress - axial strain versus number of cycles and the permeability variation of the cyclic loading Test A are shown in Fig. 6-5 and Fig. 6-6, respectively. Firstly, upon comparing Figs. 6-4 and 6-6 for the variation of permeability of tests C and A with different loading magnitudes (simulating different degrees of rocking), the change of internal structure within rock specimen can be obtained. It is clear that,

(1) Permeabilities measured at the initial stage of each cycle in Test A, (see Fig. 6-6), possesed an inclination showing the permeability of rock specimen was improved gradually with increasing number of cycles. This phenomenon indicates that the crack in rock mass propagated with proportional to the increase of rocking time of structure. However, this inclination can not clearly be found in Fig. 6-4 for cyclic loading Test C.

(2) The average slope of each initial range of these permeability - axial strain curves, i.e., $a_i s_i$ in Fig. 6-4 and Fig. 6-6, indicated that an increase

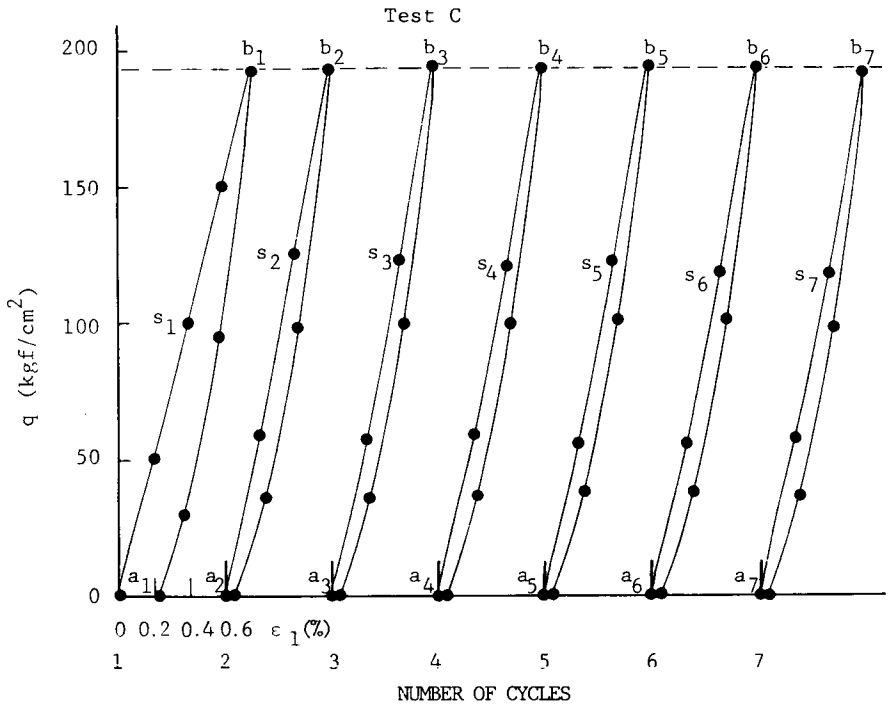

Fig. 6-3 The relationship between q-ε_1 versus number of cycles of Test C (ultimate cyclic loading = 0.8 x q_{peak}).

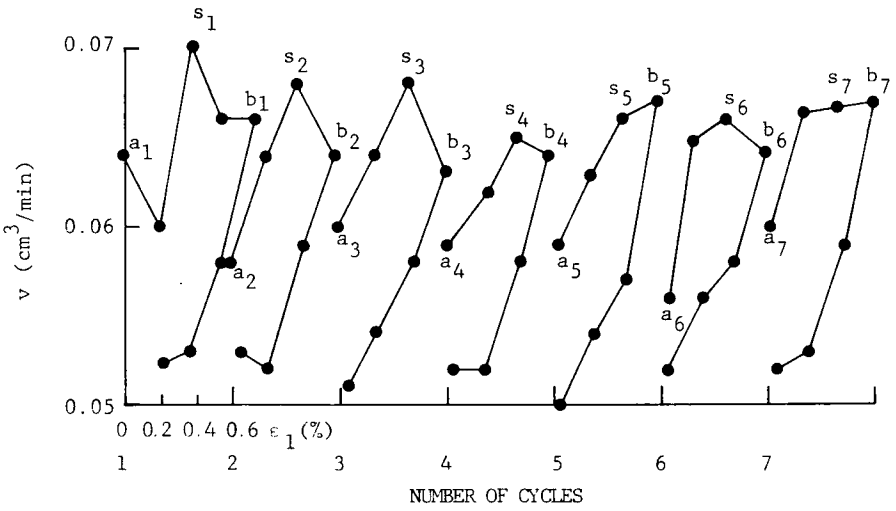

Fig. 6-4 The permeability against axial strain and number of cycles of Test C. Where, a_i: starting points; b_i: upper stress points; s_i: final points of Range I.

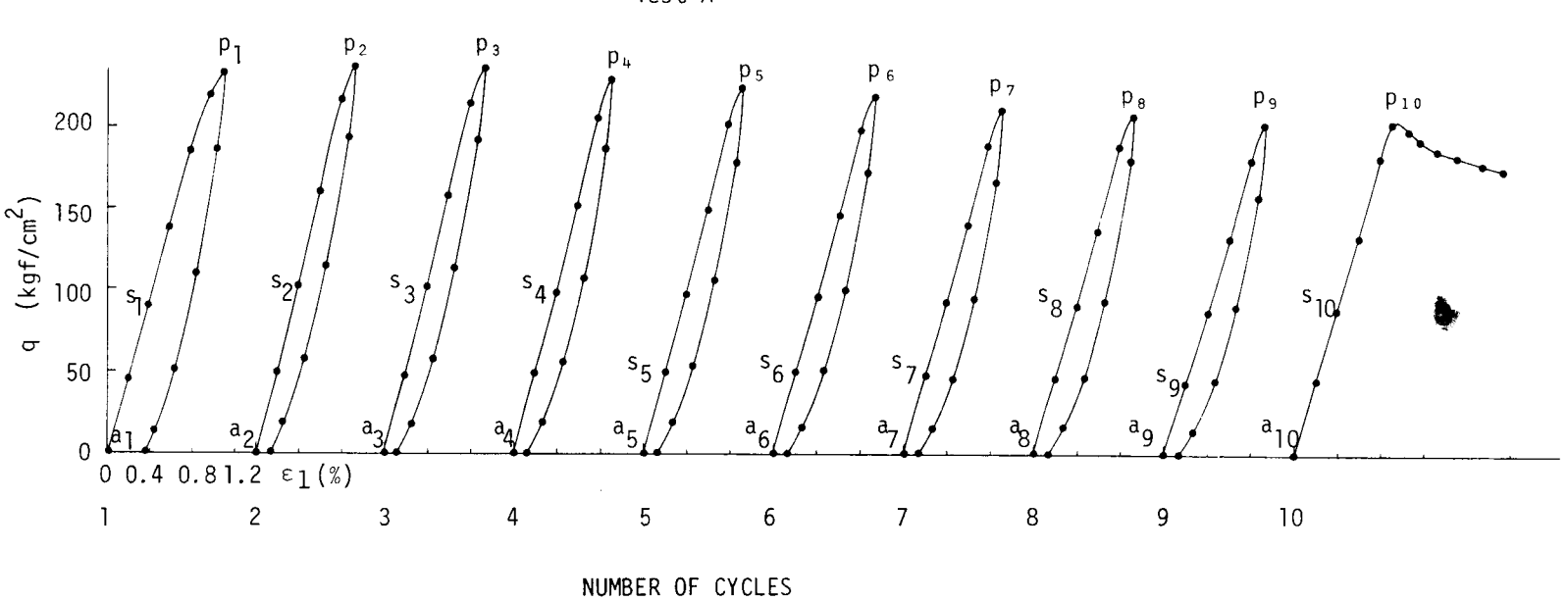

Fig. 6-5 q-ε_1 versus number of cycles of Test A (ultimate cyclic loading = q_{peak})

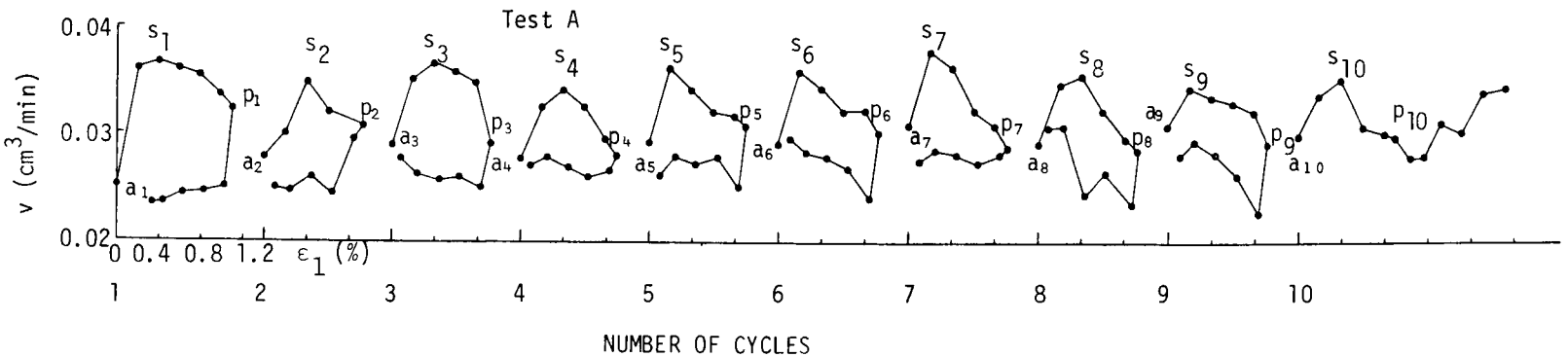

Fig. 6-6 v-ε_1 versus number of cycles of Test A

of cyclic loading tends to introduce a milder slope.

As already discussed in Chapter 5, crack growth or reopening occurs in the initial range, therefore, the slope of the $a_i s_i$ becoming milder implies that the cracks are gradually losing their elastic ability to reopen with increasing number of cycles. This phenomenon can be detected in both tests.

(3) The location of the boundary point between the initial range (crack propagation region) and the second range (the region of forming a shear failure plane) in Test A, i.e. the apex point s_i on each permeability curve, depended upon the number of loading cycles, with an early locality to higher number of loading cycles. This was resulted from the increase of cyclic loading, and gradual crack propogation, which in turns, actively promoting the formation of a shear failure plane.

The same phenomenon was not apparent in the Test C, when examining the positions of point s_i in Fig. 6-4.

(4) In Test A, after 9 cycles of shear test up to the peak strength of the specimen, a loading test was carried out beyond the peak strength in the 10th cycle and a residual state was obtained.

As the shape of a permeability-axial strain curve measured in the shearing process on the 10th cycle was similar to that of a virgin rock specimen, the one which has never been subjected to shear, presented in Fig. 5-2(b), it is likely the history of being sheared did not bear apparent effects to the basic properties of specimen in spite of that it had been sheared 9 times to the peak strength.

Other than comparing the permeability changes of these two tests, differences of mechanical behavior rendered in these tests will now be presented.

(5) Firstly, the elastic shear moduli G measured for each cycle of these tests are depicted in Fig. 6-7 (for Test A) and Fig. 6-8 (for Test C), respectively. The result of Test B, shown in Fig. 6-7, was obtained from another

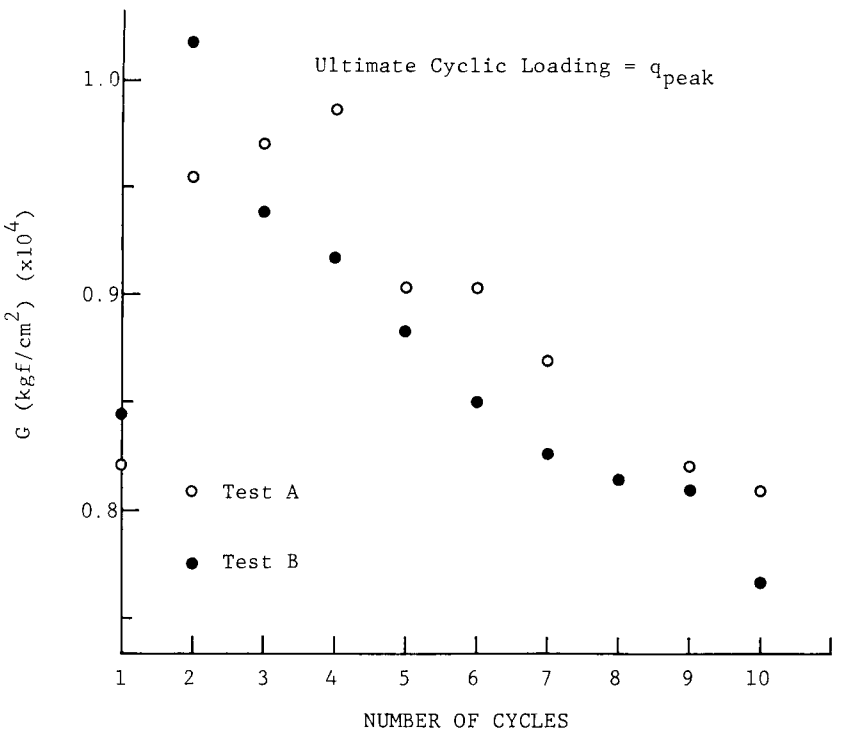

Fig. 6-7 The variation of elastic shear moduli G due to shearing history

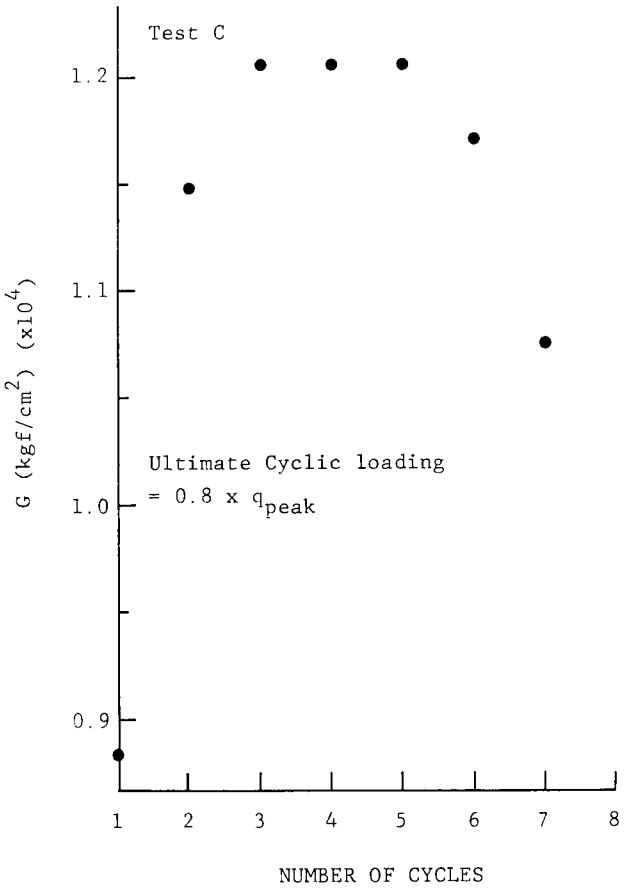

Fig. 6-8 The relationship of G and number of cycles in Test C

specimen performed by a cyclic loading test same as Test A.

Except for the result of the first cycle, the G value derived in each cycle of Test A and Test B (both with specimen sheared up to peak strength under same testing conditions) reduced progressively according to the number of times of loading-unloading process.

On the other hand, the G-values obtained in Test C did not share the same tendency. Because the decrease in elastic shear modulus can be considered as a loss of elastic capacity or a kind of damage in rock specimen, therefore, it is obvious that the internal structure damage induced by cyclic loading was significant in Test A, but not in Test C. Similar results was discussed in (2) and (3), deduced from permeability variation.

(6) In test A, shearing was performed in each cycle up to peak strength point. The magnitude of peak strength points was seen to decrease gradually with the increase of the number of cycles, as shown in Fig. 6-5 and Fig. 6-9. Undoubtedly, the reduction of peak strength which is similar to the loss of elastic shear modulus, (mentioned in (5)) was mainly attributed to the damage of internal structure of specimen.

Furthermore, plastic strain ε_p accumulated in specimen during cyclic test, may serve as an index for indicating the degree of the damage or crack growth within specimen as a result of cyclic loading.

The accumulated plastic strains developed in Test A and Test B are given in Fig. 6-10. By combining Fig. 6-7, Fig. 6-9 and Fig. 6-10, the relationship of G and ε_p as well as q_{peak} and ε_p can be acquired as illustrated in Fig. 6-11 and Fig. 6-12, respectively. From these figures, it is apparent that accompanying with the settlement of structure owing to low frequency rocking, with a pattern similar to Test A, the bearing capacity or elastic property of rock mass beneath the structure will diminish gradually.

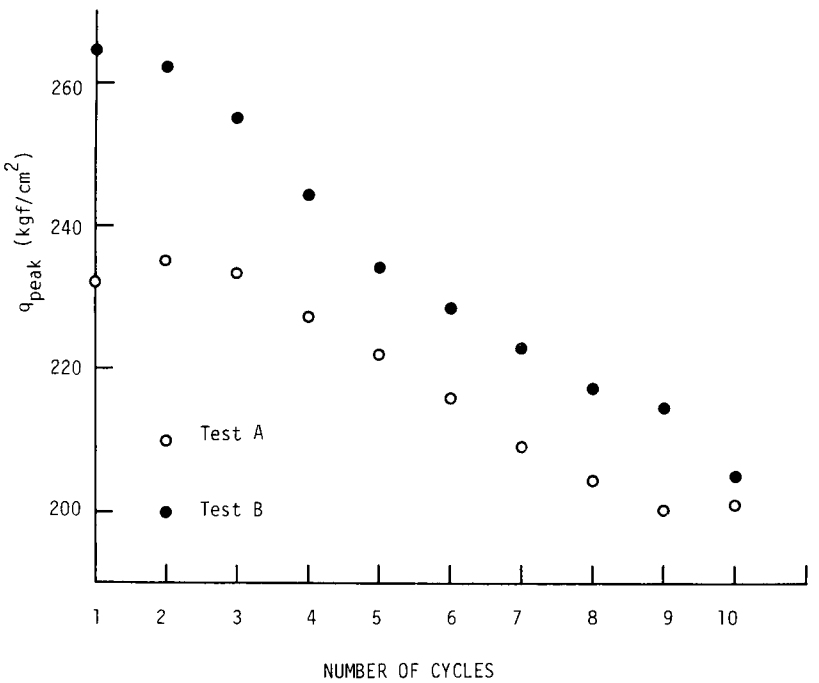

Fig. 6-9 The decrease of peak strength with the increase of the number of cycles (Test A and Test B)

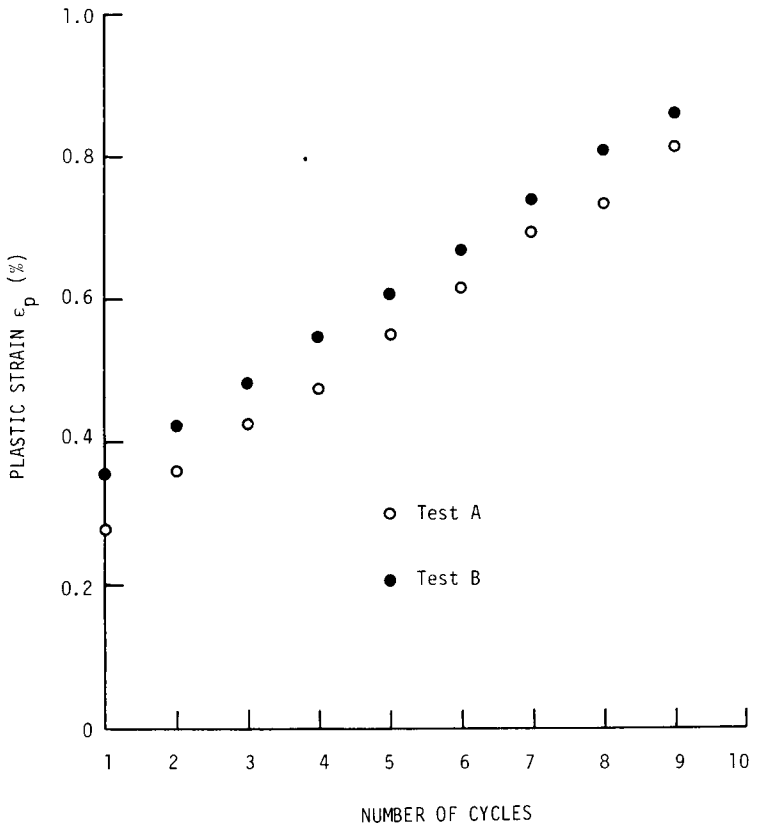

Fig. 6-10 The accumulated plastic strains created in rock specimens (Test A and Test B).

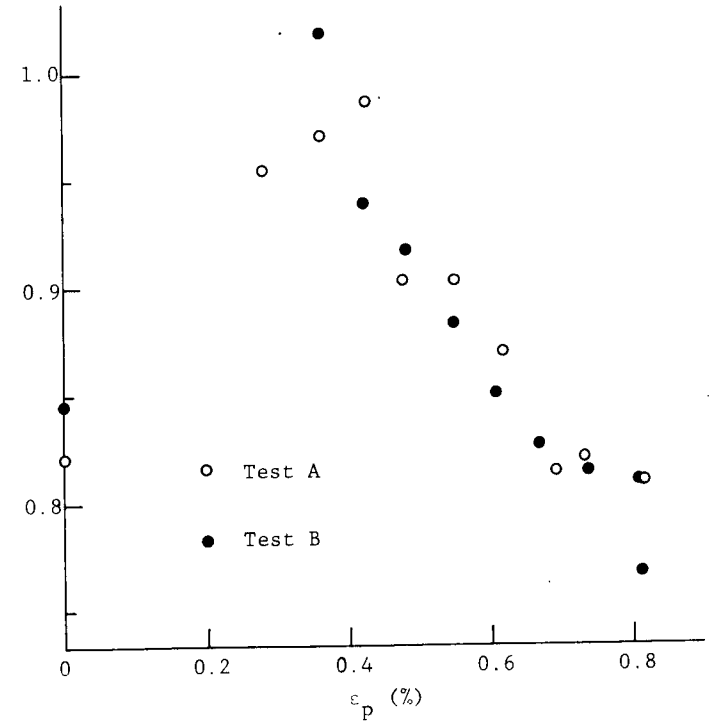

Fig. 6-11 The relation of G and ε_p in Test and Test B

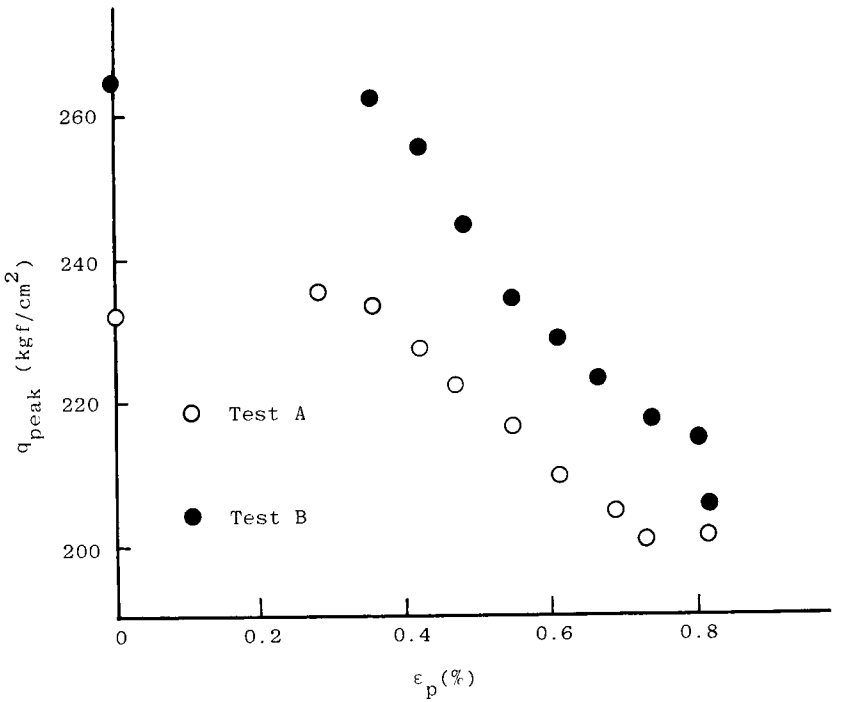

Fig. 6-12 The q_{peak}-ε_p relationship in Test A and Test B

6-1-3 Conclusions

On the basis of the result (1) mentioned in section 6-1-2, it is obvious that regardless to various amplitudes of cyclic loading illustrated in Test A and Test B, internal damage has always been developed within rock mass due to rocking of structure. Therefore, in designing a foundation, low frequency structure rocking is of paramount importance, among other factors. Of course, in active volcano or fault area, earthquake is a principal parameter for foundation design.

The rock specimen used in Test A was subjected to an ultimate cyclic loading q_{peak}, though, only slightly bigger than that of Test C at 0.8 q_{peak}, the crack propagation within specimen was very active. In addition to points (5) and (6), the loss of elastic capacity and strength was also apparently prompted by cyclic loading. Therefore, when accomplish foundation design for a tall building, the meteorological conditions especially the maximum wind speed and wind breathing in situ should be acknowledged. Moreover, preventing the weight of structure from being greater than the peak bearing capacity of rock mass during rocking is also an essential.

However, in accordance with point (4), in spite of the strength of specimen in Test A dropped down progressively as the number of loading cycle increased, no rigorous failure, such as complete shear failure plane created in it (Funyu rock) had occurred. In other words, once the weight of structure in the duration of low frequency rocking increases up to the peak strength of rock mass, no abrupt failure of rock mass may cause sudden settlement of structure will happen.

The phenomenon of rocking can also be found in ocean construction, whereas the wind force is substituted by wave force or current force. Certainly in the foundation design of ocean construction the magnitude of forces and their associated period must also be taken into account. From these, the safety of

the construction can be checked, even when wave force and current force are acting.

6-2 Application of Laboratory Test to Tunneling

6-2-1 Introduction

A brief literature review reveals that two different tunneling mechanics have been employed. The first group concerns various "loads" acting on support or lining of tunnel, i.e., the load of loosening rock around the tunnel. The other analyses stress distribution around the excavation surface of opening, with elastic theory and/or plastic theory as tool.

The former adopted basic theory derived from the concept of loosening rock load. Because a dome-shaped failure zone can always be found above the failed opening, it is logical to consider that support and lining are necessary to safeguard against the weight of failed zone around the opening. Some representative classic theories of support design were proposed by Bierbaumer (1913)[2], Kommerell (1940)[3] and Terzaghi (1946)[4], etc.. These theories were supported by many practical failure measurements and field experiences.

On the contrary, the latter did not focus their attention on supporting work, but rather on the rock mass itself which is around a tunnel opening. They analysed the stress and strain redistribution in rock mass during and after tunnel excavation.

Since analysing stress and strain redistribution was often difficult and complicate, hence, only tunnels of simple shape in simple stress environment had so far been investigated and only elastic theory was used. Representative works in this period were proposed by Yamaguti (1929)[5], Yu (1952)[6], etc..

In addition to elastic theory, Duvall and Obert[7], Egger (1973)[8] and

Kastner (1971)[9] introduced plastic analysis into their derivation of the stress-strain redistribution around opening. With the aids of analytical technique using a computer, such as finite element method, treatment of more complicated condition of stress-strain redistribution has become possible. However, the question remains that "how to accurately input a true mechanical behavior into an analytic approximation ?" Thus, more effort is required to combine practical experience and analytical technology[10].

Based upon historical background, a relatively new method of tunneling was developed in 1960's, bearing the name as the "New Austrian Tunneling Method" (NATM in short).

Constructing a tunnel with NATM, the inherent strength of rock mass can be positively availed. Therefore, a strong enough support can be achieved by the use of only rock bolts and thin layer of shotcrete, instead of using steel ribs and thick concrete as the support in conventional tunneling method. The chief advantage of NATM was contributed by accurate monitor of opening wall deformation and pressure change in rock during excavation. These informations were used as direct input for construction design in their routine calculation steps. Detailed description of NATM was reported by Rabcewicz (1964, 1965, 1969)[11),12)], one of the pioneer inventors of NATM.

Although many modifications to NATM had been proposed, no standardized support design theories have been deduced to NATM. Nevertheless, a common recognization was reached among researchers working in NATM, i.e. "NATM is a tunneling method, by which the inherent strength of rock mass can be effectively availed to keep tunnel stable".

In this chapter, the stress redistribution around opening is simulated by considering the equations of stress distribution derived from elastic and plastic theories. Furthermore, the relation between rock pressure and the swelling deformation of excavation wall, which is employed in NATM, will be

also simulated by using laboratory testing method. The influence of changing excavation speed and different overburden on support design will be investigated experimentally in a laboratory with a multiple triaxial test method for saturated soft rock (mentioned in Chapter 4) with minor modification of testing procedure.

6-2-2 Deformation of Excavation Wall and Rock Pressure

It is a common belief that the relation curve between rock pressure and opening wall deformation during excavation of tunnel can greatly assist a support design and in deciding the suitable timing to set up the support. Although, this curve can be calculated from the elastic and plastic theories, it is strongly affected by the shape of opening, initial stress state and the mechanical properties of rock mass, etc.. Hence, in order to simulate successfully the behavior of opening wall in laboratory, a most simplified case was selected, - a circular opening located in a homogeneous and isotropic rock mass with $p_v=p_h=p_0$, as shown in Fig. 6-13(a), where p_v and p_h are the initial vertical and horizontal stresses of rock mass, respectively.

To calculate the elastic stress and strain created in the area around the circular opening in this figure, few different approaches are available, these being methods proposed by Yamaguti (1929)[5] , Yu (1952)[6] and Muir Wood (1975)[13]. Besides, Tanimoto (1980)[14] suggested a unique and comprehensive method bases on the concept of superposition, by dividing the complicated problem of calculating stress and strain in Fig. 6-13(a) into two simpler parts, as depicted in Figs. 6-13 (b) and (c), respectively.

Fig. 6-13(b) represents the initial state of rock mass before excavation, being subjected to primary stress p_0 uniformly, whilst Fig. 6-13(c) designates the stress state of a rock mass during an excavation of opening, which was free from the primary stress p_0 . However, since the part of rock mass around

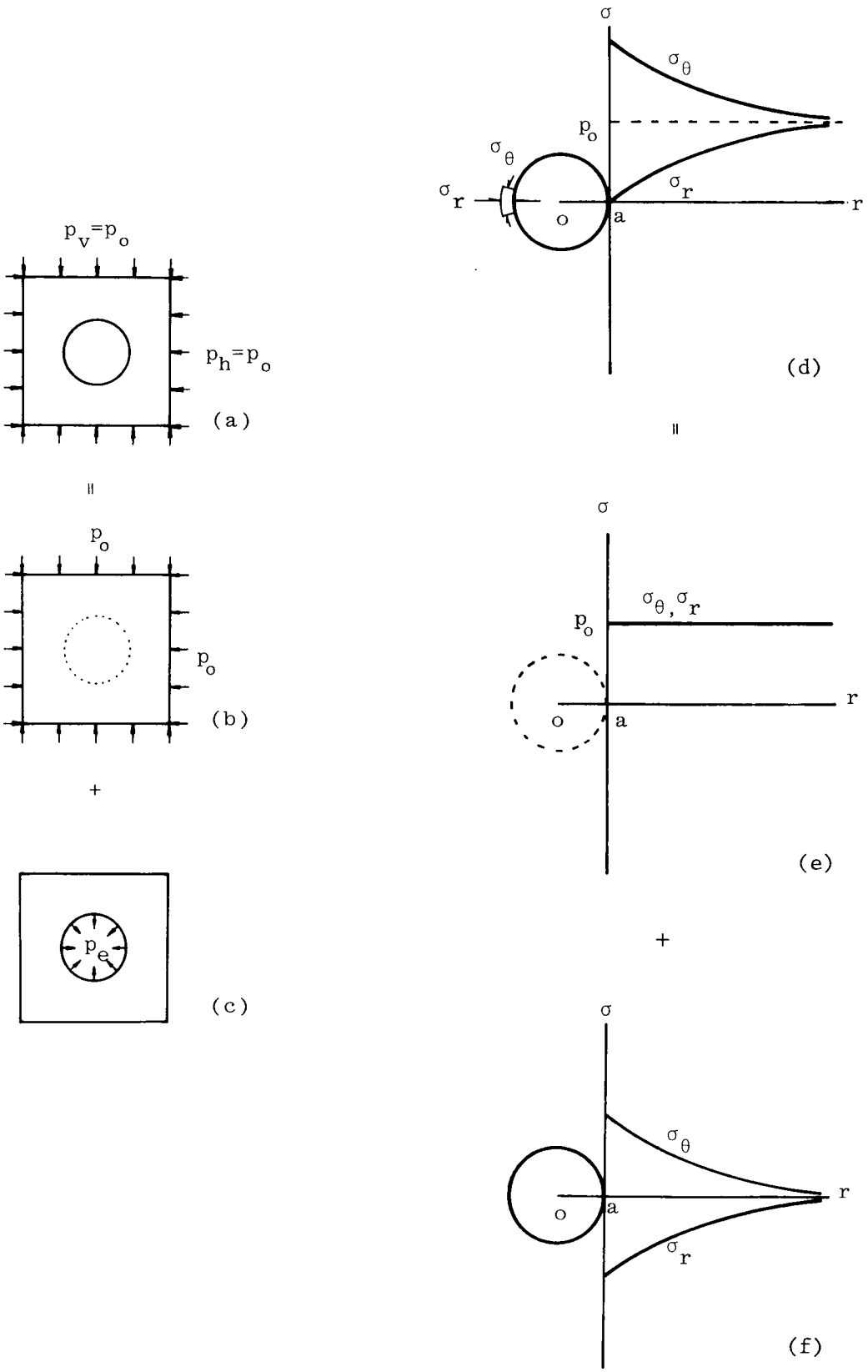

Fig. 6-13 Stresses around a circular opening (Ref. 6-14).

the opening in Fig. 6-13(c) was supported by the internal part of rock inside the opening before excavation, therefore, after excavation, a uniformly distributed excavation force p_e, a kind of extraction force, will act on the opening wall.

As to be discussed later, that the p_e is a variable, changes from 0 to p_0, depending on the advance of the face of excavation. Accordingly, the problem of calculating the stress and strain generated in the rock mass around an opening during the advance of excavation face, such as the model illustrated in Fig. 6-13(a), can be obtained by combining the results gained from Fig. 6-13(b) with that from Fig. 6-13(c).

Because the rock mass is assumed as homogeneous and isotropic, the stress acts on every element in Fig. 6-13(b) can be expressed in terms of polar coordinates, such as : $\sigma_\theta=\sigma_r=p_0$ (see Fig. 6-13(e)). In this figure, "a" represents the radius of opening and "r" is the distance measured from the center of opening, and an opening is not yet made. On the other hand, the stress and deformation distributed in the rock mass around the opening shown in Fig. 6-13 (c) can be calculated by Eqs. (6-5) and (6-6) below. This is illustrated in Fig. 6-13(f), for stress distribution, whilst the rock mass is in elastic state as follows,

$$\left.\begin{matrix}\sigma_\theta \\ \sigma_r\end{matrix}\right\} = \mp p_e \left(\frac{a}{r}\right)^2 \qquad \text{.....(6-5)}$$

$$u_\theta = f_1(r) - \int f(\theta)d\theta$$
$$u_r = \frac{1}{E}\frac{(1+\nu)}{r} p_e a^2 \qquad \text{.....(6-6)}$$

The detailed derivation of Eqs. (6-5) and (6-6) is given in appendix B, by using elastic theory and some mathematical technique.

Therefore, the stress distribution in Fig. 6-13(a) during and after an

excavation of opening can be obtained by adding the results calculated from Fig. 6-13(b) and Fig. 6-13(c), i.e.,

$$\left.\begin{matrix}\sigma_\theta \\ \sigma_r\end{matrix}\right\} = p_0 \pm p_e\left(\frac{a}{r}\right)^2 \quad \text{.....(6-7)}$$

This is depicted in Fig. 6-13(d), showing a result of superposing Fig. 6-13(e) on to Fig. 6-13(f).

It is worth noting that p_e in Eq. 6-7 is a variable influenced wholly by position of excavation face, because the rock mass near an excavation face will deform gradually due to the damage of ring action induced by the opening.

According to the practical measurement in Seikan Tunnel (1977)[15], such a deformation begins from a point at a distance (2-3) r_0 (opening radius) in front of the excavation face, and finishes at another point about (2-3) r_0 distance behind the face (see Fig. 6-14). Hence, it is reaonable to consider that the excavation force p_e will also increase stepwise from 0 (at -(2-3) r_0) to p_0 (at + (2-3) r_0) as illustrated in Fig. 6-14.

The stress change at an element on the wall of opening during excavation can be evaluated by Eq. (6-7) with r=a. It shows that p_e begins to change from 0 to p_0, the σ_θ, σ_r of wall element will depart from the p_0 with equal increment but different sign. The process of changing σ_θ and σ_r can also be displayed in τ-σ plane by Mohr's stress circles, thus, forming a family of concentric circles as shown in Fig. 6-15.

Upon examining Eq. (6-7), it is apparent that, when $p_e=p_0$ and r=a, the σ_r on wall element becomes 0, but, $\sigma_\theta=2\ p_0$. This is represented by the biggest Mohr's circle in Fig. 6-15. It exists only when p_e varied from 0 to p_0, there has not any Mohr's circle touched to the failure envelope of rock mass. Because no failure phenomenon happens in the wall elment, hence, this opening wall would still remain stable without requiring any additional support or lining. This case can often be found in a shallow opening, when p_0 is small or

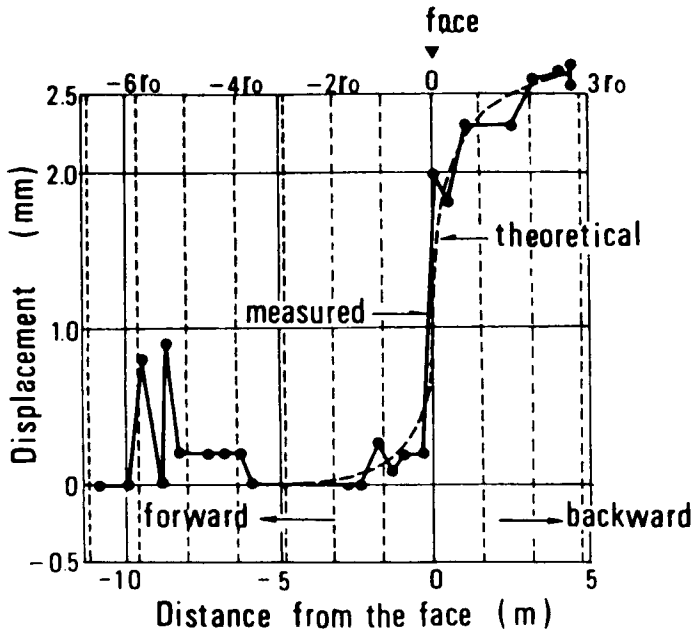

Seikan Tunnel through Andesite-Tuff

Fig. 6-14 Measured displacement curves during construction (Ref. 6-15)

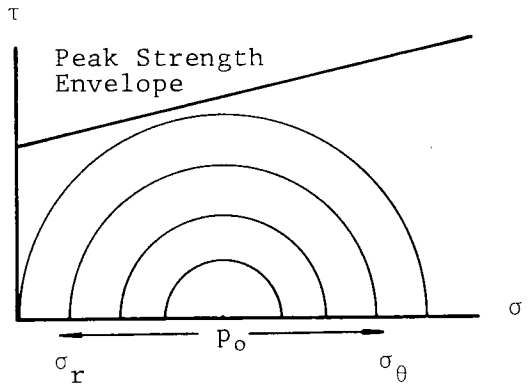

Fig. 6-15 The change of σ_r and σ_θ of opening wall during excavation (support is not necessary)

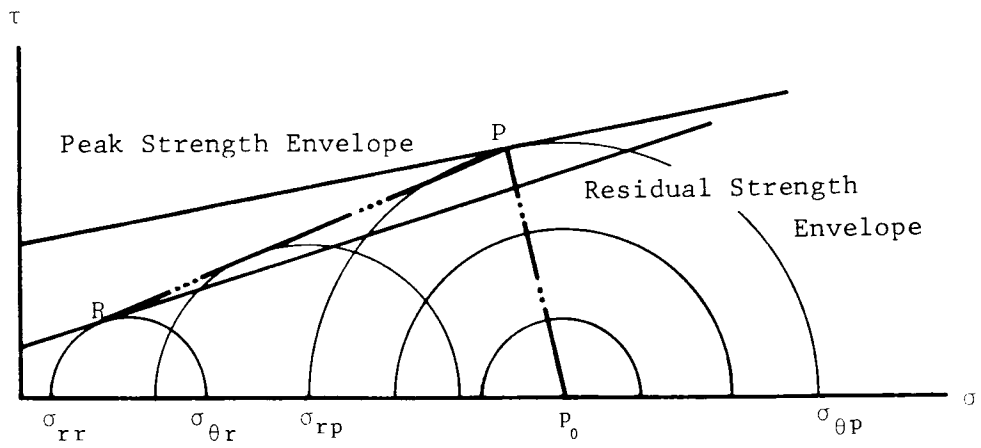

Fig. 6-16 The path of the Mohr circle of opening wall associated with the advance of the face.

the rock mass possesses a uniaxial strength stronger than twice of the initial stress ($2\ p_0$).

In common practice, however, it is very frequent to excavate an opening in a deeper place, such as for hydro-power plant, or to construct a tunnel in a mass of weak rock. Hence, before $\sigma_r \to 0$ and $\sigma_\theta \to 2\ p_0$, it is possible that a Mohr circle had already intersected with the failure envelope, this renders fracture in opening wall and rock mass around the opening. Therefore, support and lining must be constructed before rock mass reaching a complete failure.

When after reaching the peak strength envelope (failure envelope) of rock mass (i.e., in plastic state), Eq. (6-7) can not be applied any more for describing the stress state of rock mass.

Analyses of stress distribution of rock mass around an opening in plastic state had been reported. Following upon the derivation of σ_r and σ_θ in plastic state proposed by Kastner (1971)[9], the stress distribution for σ_r and σ_θ after a peak strength around an opening is given as

$$\left.\begin{aligned} \sigma_r &= (p_0 - p_e + \frac{q_u}{N_\phi - 1})(\frac{r}{a})^{N_\phi - 1} - \frac{q_u}{N_\phi - 1} \\ \sigma_\theta &= N_\phi(p_0 - p_e + \frac{q_u}{N_\phi - 1})(\frac{r}{a})^{N_\phi - 1} - \frac{q_u}{N_\phi - 1} \end{aligned}\right\} \quad \cdots\cdots\cdots \quad (6\text{-}8)$$

Where, $N_\phi = \frac{1+\sin\phi}{1-\sin\phi}$, q_u is the uniaxial strength of rock and ϕ is the internal friction angle.

From the Mohr's circles after peak strength drawn in Fig. 6-16, it is clear that when a Mohr's circle of wall element meets the peak strength envelope at point P, under the conditions that $\sigma_\theta = \sigma_{\theta p}$ and $\sigma_r = \sigma_{rp}$, $\sigma_{rp} > 0$, then, σ_r would gradually decrease as a result of the continuous increase of p_e. But σ_θ could not increase any more, on the contrary, it decreases because the element is now in a state of strain softening. Therefore, after point P, Mohr's circle will contract and move down leftward along a path PR, where R is a point of

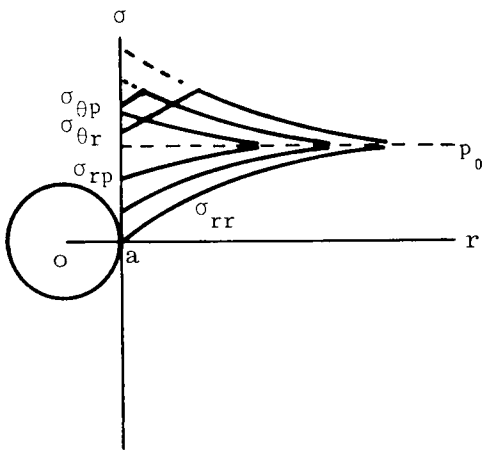

Fig. 6-17 The distribution of σ_θ and σ_r in rock mass while plastic region created around an opening

residual strength envelope of rock. Furthermore, Mohr's circle will keep sliding leftward along the residual strength envelope till σ_r=0.

Finally, the stress distribution in rock mass, while a region of it around the opening had reached plastic state can simply be illustrated as in Fig. 6-17.

6-2-3 Supporting Theory and Interaction Between Support and Rock Mass

Following upon Eq. (6-7) and Eq. (6-8) as derived from elastic and plastic theories, respectively, the variations of σ_r and σ_θ of the rock element in circular opening wall can be completely put under control during the advance of excavation face. Since the supporting work is constructed to resist against these stresses created in rock mass and subsequently to restrict the deformation of opening wall, so that the necessary strength and stiffness of support can be determined from equations of rock pressure, Eqs. (6-7) and (6-8), in addition to other equations for wall deformation (Eq. (6-6)).

Fenner (1938)[16] investigated the relationship between range of non-elastic rock zone around an opening and the rock pressure acting on support (p_i). He presumed that stress state of rock would satisfy the Mohr-Coulomb

yield criterion when it fails. Based on this assumption, the relationship between p_i and R was derived,

$$p_i = -c\cdot\cot\phi + [c\cdot\cot\phi + p_0\cdot(1-\sin\phi)]\left(\frac{a}{R}\right)^{\frac{2\sin\phi}{1-\sin\phi}}$$

where, α : radius of opening

R : distance from opening center to the boundary of elastic and plastic regions

p_0 : initial rock stress

From this equation, it is apparent that p_i decreases when the plastic zone around an opening is expanding. However, in practical excavation of a tunnel, a large enough expansion of plastic zone will render a minimum value to p_i. Any further increase in R will cause the loosening of rock mass around opening and increasing p_i. Based on this concept and after inspecting many practical failures of opening in situ, Pacher (1964)[17] proposed a curve relating p_i and u_w (the deformation of opening wall) from Fenner's equation and incorporating with modification beyond $p_{i,min}$ point. The modification displays an increase of p_i caused by rock mass loosening, resulting a new p_i-u_w curve as shown in Fig. 6-18.

This curve commonly referred as Fenner-Pacher curve, in honor of Fenner and Pacher for their great contribution on tunneling engineering, has widely been used in the support design of tunnel, especially in the NATM.

The Fenner-Pacher curve of opening wall can be considered as the lowest limiting strength of a stable support. Because the deformation of opening wall (u_w) increases with the advance of excavation face (see Fig. 6-14), on observing Fig. 6-18 there are many kinds of support can be chosen to match the increasing u_w. For example, if the deformation of opening wall is to be restricted within a small range, referring to Fig. 6-18, it needs a tremendous strong and very stiff support. Needless to say, this support is very expensive

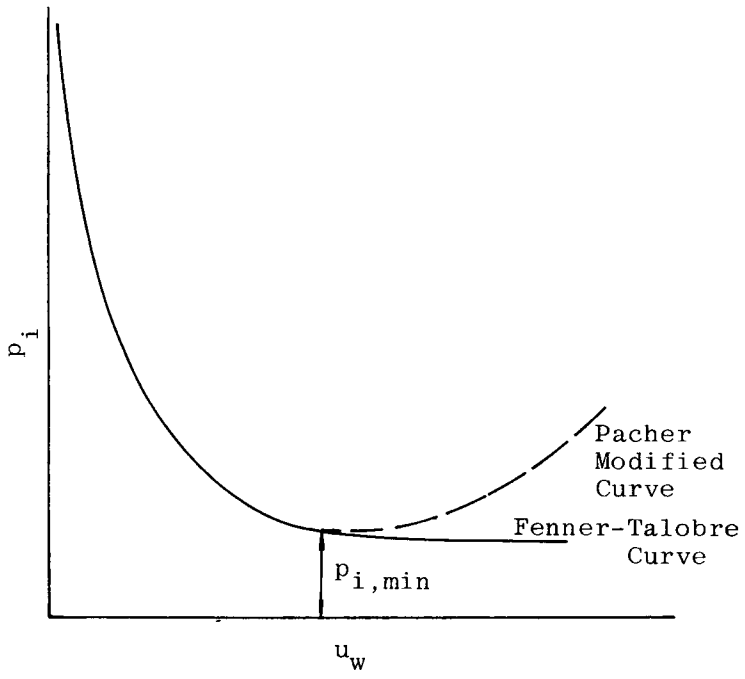

Fig.6-18 p_i-u_w curve of an opening

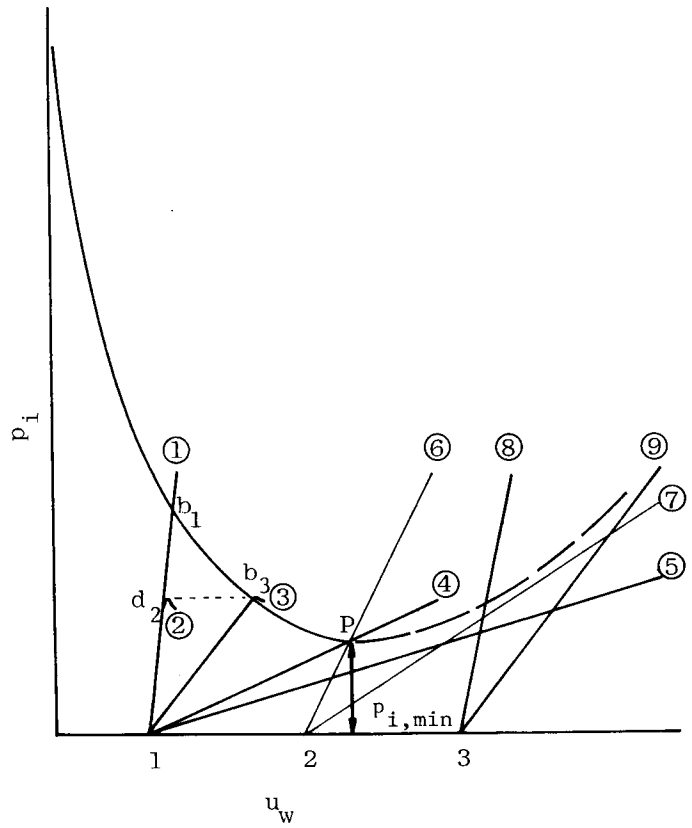

Fig.6-19 The relationship between p_i-u_w curve and several kinds of support

and must be constructed immediately after the finishing of excavation. Then, the problem of "selecting a support with suitable strength and stiffness and determining the appropriate timing to build up support" can simply be answered by using the relation curve of p_i and u_w of rock mass (Fig. 6-19)[18].

Firstly, assuming the support is to be built at Time 1, when wall deformation equals u_{w1}, and five kinds of support with different stiffnesses and various strengths can be chosen.

If the first kind of support is chosen, which has an excellent stiffness and strength, then, opening wall and support 1 shall rapid reach a balance state at point b_1, where the necessary wall deformation is very small. But, if support 2 is selected, although it possesses a stiffness same as that of support 1, but it does not have enough strength to balance with the opening wall at b_1. Hence, it will be destroyed by rock pressure at d_2, opening wall will continue to deform.

However, the wall deformation can also be restricted by using support 3, which has same strength as support 2, but behaves more flexible than the latter, a state of balance between support and opening wall will be reached point b_3.

Certainly, support 4 is the most economic one at Time 1, as its full strength can be reached just point P, where the rock pressure drops down to its minimum, $p_{i,min}$. Remarkable deformation will be generated in both the support 4 and opening wall.

However, if support 5, with a stiffness smaller than support 4, is to be adopted, no intersection can be found for this support between its σ-ε and p_i-u_w curves, accordingly to Fig. 6-19. It is apparent that either the support 5 or the opening wall will create a large deformation after constructing the support, and they would all fail completely.

Therefore, the most reasonable support to be constructed at Time 1 is

support 4, which can be called as the critical support at Time 1.

Secondly, if supports are to be constructed at Time 2, a large amount of wall deformation u_{w2} would have been occurred. Because point 2 is located just before point P, hence, the critical support of Time 2 must be a very stiff one, just like support 6. On the other hand, though having excellent strength, support 7 can not stabilize the opening wall due to weaker stiffness.

If support is to be set up at Time 3, an extensive deformation would have already been produced in the opening wall, resulting in an increase of rock pressure. It is obvious that a stiffer and stronger support (support 8) must be employed to stop the rapid increase of rock pressure. This falls within the classical consideration of support design, that is, a loosening rock pressure method.

On the basis of the discussions above, it is found that support can be constructed at suitable time when deformation of opening wall u_w had reached an allowable value, and then, the most suitable support, i.e., the critical support, can be selected from p_i-u_w curve obtained beforehand.

6-2-4 Simulating Tests in Laboratory

The geological condition in Japan and many other islands in the western Pcific Ocean is so complicated that it is not likely to meet a uniform and homogeneous rock mass during tunneling. Because different kinds of rock possess different p_i-u_w curves, even when subjected to the same stress condition, therefore, it is necessary to adopt different support design to suit each individual rock mass.

Accordingly, if we can simulate the behaviors of the rock on opening wall and derive a p_i-u_w curve for it by a simple method, it will bring much benefit to tunneling engineering. To meet this purpose Tanimoto, Hata and Kariya (19

82)[19] successfully determined the $p_{i,min}$ value of a tunnel by using triaxial shear test in laboratory.

To investigate the behavior of an opening wall in laboratory, simulation should be developed. Moreover, suitable equations for calculating stresses of rock mass around opening could also be derived by basing upon Eqs. (6-7) and (6-8).

Firstly, the elastic stress of rock mass had been given by

$$\left.\begin{matrix}\sigma_\theta \\ \sigma_r\end{matrix}\right\} = p_0 \pm p_e\left(\frac{a}{r}\right)^2 \quad \cdots\cdots\cdots \quad (6\text{-}7)$$

On the opening wall where r=a, Eq. (6-7) can be simplified to:

$$\left.\begin{matrix}\sigma_\theta \\ \sigma_r\end{matrix}\right\} = p_0 \pm p_e \quad \cdots\cdots\cdots \quad (6\text{-}9)$$

Eq. (6-9) states that σ_θ and σ_r depart from p_0 with an amount of p_e and the values of σ_θ and σ_r can be represented in the σ-axis of a τ-σ plane.

Using these (σ_θ, σ_r) values, a family of stress Mohr circles can be graphed on the τ-σ plane with the same center $\sigma = p_0$, just as the one shown in Fig. 6-15 previously.

On the other hand, in the post-failure range, the rock mass behaves as a non-elastic material, and the (σ_θ, σ_r) around opening can be evaluated from

$$\left.\begin{aligned}\sigma_r &= \left(p_0 - p_e + \frac{q_u}{N_\phi - 1}\right)\left(\frac{r}{a}\right)^{N_\phi - 1} - \frac{q_u}{N_\phi - 1} \\ \sigma_\theta &= N_\phi\left(p_0 - p_e + \frac{q_u}{N_\phi - 1}\right)\left(\frac{r}{a}\right)^{N_\phi - 1} - \frac{q_u}{N_\phi - 1}\end{aligned}\right\} \quad \cdots\cdots\cdots \quad (6\text{-}8)$$

At the opening wall r=a, it reduces to

$$\left.\begin{aligned}\sigma_r &= p_0 - p_e \\ \sigma_\theta &= N_\phi(p_0 - p_e) + q_u\end{aligned}\right\} \quad \cdots\cdots\cdots \quad (6\text{-}10)$$

where, $N_\phi = \frac{1+\sin\phi}{1-\sin\phi}$, and q_u is the uniaxial strength of rock mass.

Naturally, it is reasonable to consider that if we follow the stress formulae of an opening wall (revealed by Eqs. (6-9) and (6-10)), for carrying out a triaxial shear test with a rock specimen which was sampled from the opening wall, then it is possible to simulate in laboratory the behaviors of the opening wall. Informations about support design can thus be obtained. It is to be noted that, in this triaxial shear test, the σ_θ and σ_r are substituted by σ_1 and σ_3, respectively. In addition, N_ϕ (in Eq. (6-10)) can be calculated from the gradient of Mohr-Coulomb strength envelope which was used in deriving Eq. (6-8) and detailed in Appendix B. It then further requires a thorough understanding of the Mohr-Coulomb envelope of rock before the simulation triaxial test is implemented.

Multiple stage triaxial shear tests with different rate of shearing are needed to investigate the influence of variable rates on the strength envelope of a rock specimen.

In addition, as a higher rate of shearing is equivalent to a faster deformation rate of opening wall during excavation, therefore, the effect of excavation speed on the behaviors of opening wall should also be considered. Two kinds of rate of shearing were used in simulation triaxial shear test, 0.012 %/min and 0.24 %/min (representing a slow and rapid excavation speeds, respectively).

Whilst studying the effect of rate of shearing on strength envelope, a new application of MST test was developed. As mentioned in Chapter 4, the MST method employed only one rate of shearing to each test. However, in this new trial, an MST test will be performed with at least two different rates of shearing, thus yielding several different sets of data from using only one specimen. The total stress path of this new trial is schematically shown in Fig. 6-20(a).

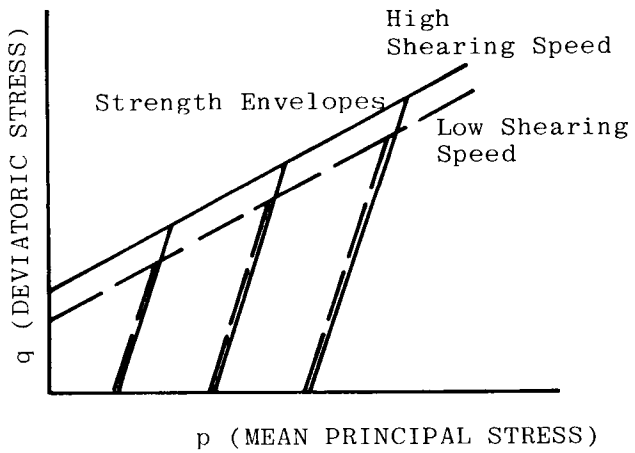

Fig. 6-20(a) The total stress paths of an MST test to study the effect of rate of shearing on strength envelope

However, from Figs. 6-20(b) and (c)[14], it is shown that besides the σ_θ and σ_r the element of opening wall is subjected to an other normal stress σ_z, where, $\sigma_z \neq \sigma_r$ during the advance of excavation face. Hence, it is difficult to simulate completely the variations of σ_r, σ_z and σ_θ by using a conventional triaxial shear cell ($\sigma_2 = \sigma_3$). But, on the basis of the two reasons which are presented below, the simulation test would be carried out by following this way , $\sigma_2 = \sigma_z = \sigma_r = \sigma_3$. These are:

(a) In accordance with the investigation of Tanimoto (1980)[14], the deformation of opening wall (u_w) is strongly dependent on σ_r, not σ_z. This means that the influence of σ_z on the behaviors of opening wall is not pronounced during the opening excavation. Moreover,

(b) Upon inspecting the Fig. 6-20(c), although σ_z begins to vary from a point at a distance about 3a (a is opening radius) in front of the face, it recovers to its initial value of p_0 at another point about 3a behind the exca-

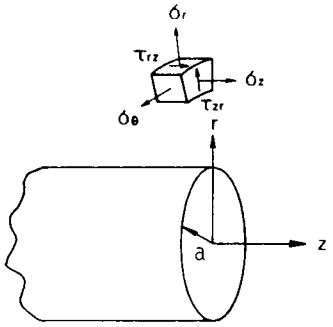

Fig. 6-20(b) State of stresses near the face (Ref. 6-14)

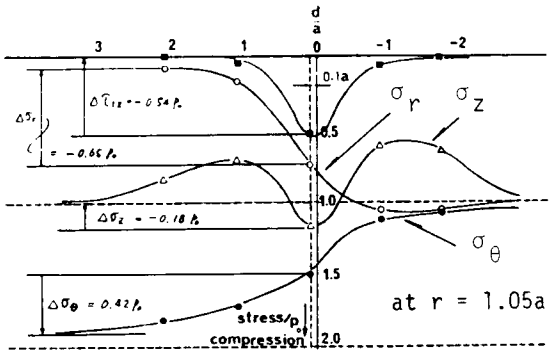

Fig. 6-20(c) Stress changes caused by the advance of the face at r=1.05a (Ref. 6-14)

vation face. On the contrary, σ_r changes from p_0 to 0, simultaneously. Therefore, it is reasonable to consider that, if the testing condition $\sigma_2=\sigma_z=\sigma_r=\sigma_3$ is adopted in the simulation test, a more vigorous result will be obtained.

Accordingly, the outline of triaxial test procedures for simulating the behaviors of opening wall can be presented as follows:

(1) As indicated in Fig. 6-21(a), the specimen was isotropically loaded with the initial stress of rock mass p_0 for consolidation process.

(2) To shear the specimen with a stress described by Eq. (6-9), that is to say, controlling the relation of σ_1 and σ_3 such that $\Delta\sigma_1 = -\Delta\sigma_3$. When the axial stress σ_1 gains an increment $\Delta\sigma_1$, a same amount of $\Delta\sigma_1$ must be released from the confining pressure σ_3, as depicted in Fig. 6-21(b). The same procedure was carried out till the stress Mohr circle of the specimen touched its peak strength envelope. Although, in practical case, before touching the peak strength envelope, a rock specimen might not behave as a complete elastic material. It was assumed, for the purpose of this study, that Eq. (6-9) are available all over the pre-peak range.

(3) After the stress Mohr circle intersected the peak strength envelope, the specimen turned into strain softening state, then, the relationship between σ_1 and σ_3 was governed by Eq. (6-10). This means that the deduction of confining pressure $\Delta\sigma_3$ (see Fig. 6-21(c)) was proportional to $\Delta\sigma_1$, where $\Delta\sigma_3 = \frac{1}{N_\phi}\Delta\sigma_1$.

This relationship was closely observed till confining pressure gradually became zero, i.e., when the specimen arrived at its residual state.

6-2-5 Results of Simulation Tests

(a) Effect of rate of shearing on rock strength

Besides the derivation of an N_ϕ value to monitor the simulation test, a new

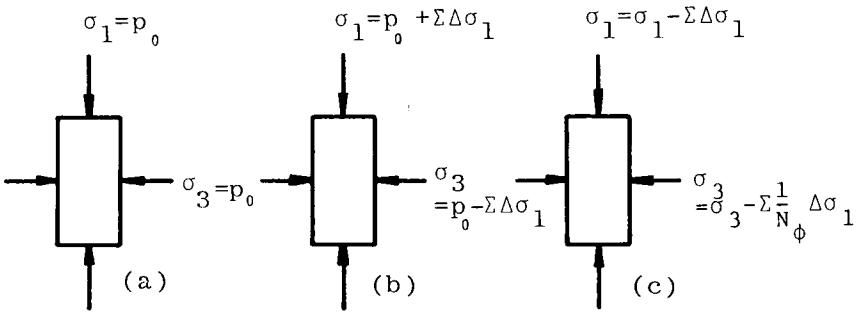

Fig.6-21 The procedures of simulation test

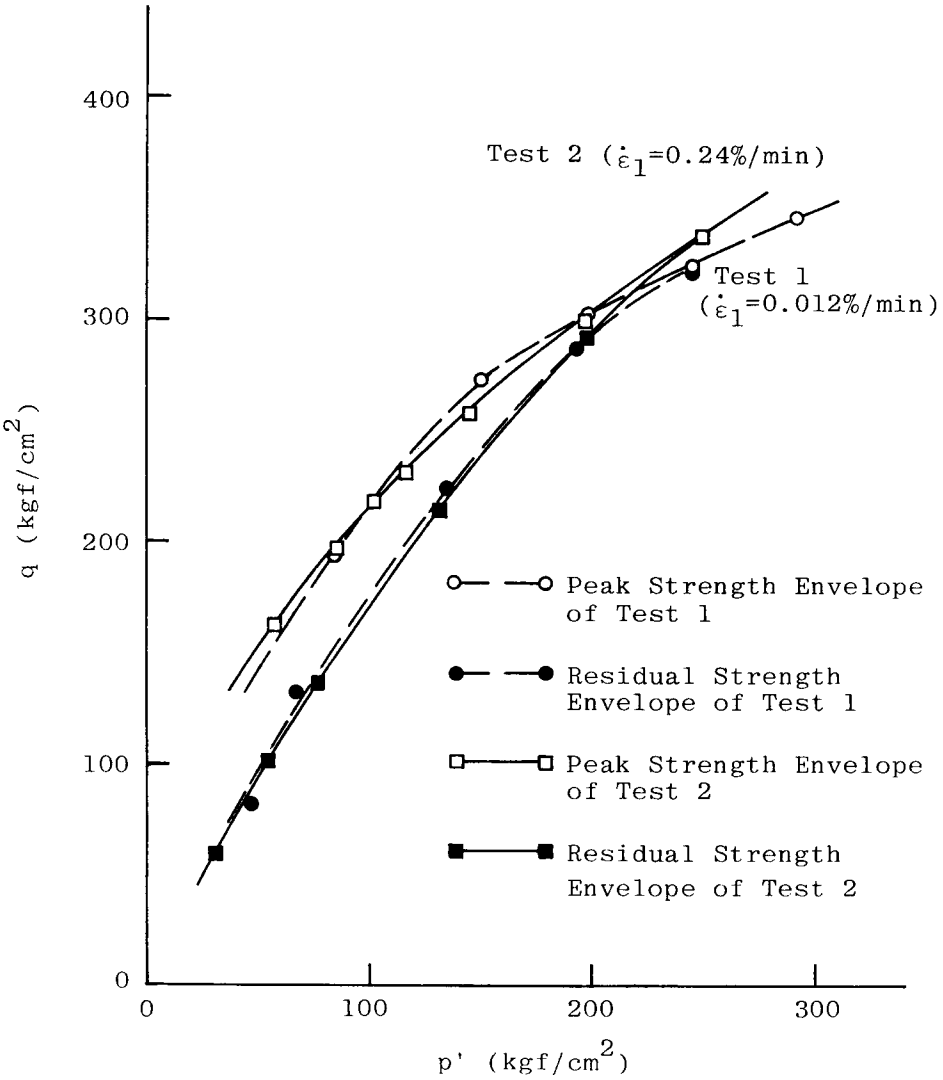

Fig.6-22(a) Strength envelopes obtained from Test 1 and Test 2

application of MST method was also attempted to explore several strength envelopes under various rate of shearing from only one specimen.

Three MST tests (tentatively designated as Test 1, Test 2 and Test 3) were conducted with two different rates of shearing. Test 1 was performed using the rate $\dot{\varepsilon}_1$ = 0.012 %/min, whilst Test 2 adopting $\dot{\varepsilon}_1$ = 0.24 %/min, both served to find out the peak and residual strength envelopes of Funyu rock. Moreover, Test 3 was a combination of Test 1 and Test 2, using alternatively the two rates of shearing mentioned above and following the total stress path as shown in Fig. 6-20.

Under various confining pressures, many peak and residual strengths were obtained in each test. All results were plotted on q-p' plane, thus constituting peak and residual strength envelopes of Test 1 and Test 2 (see Fig. 6-22 (a)). Although beyond p'=190 kgf/cm^2 the strength envelope of Test 2 showed higher values than those of Test 1, but, there was no apparent difference between them for p'<190 kgf/cm^2. Around p'=150 kgf/cm^2 Test 1 had higher peak strength than Test 2.

Upon inspecting Fig. 6-22(a), it is difficult to say that higher rate of shearing would create a stronger rock strength.

The unconformity between the rate of shearing and strength envelopes obtained from Tests 1 and 2 may be attributed to the randomness of rock properties in different rock specimens. It is therefore felt that if these two tests were performed on the same rock specimen, then the difference could be eliminated.

To meet this purpose, Test 3 was then carried out and the resultant pairs of strength envelopes derived from different rate of shearing are depicted in Fig. 6-22(b). From Fig. 6-22(b), the strengths associated with $\dot{\varepsilon}_1$ = 0.24 %/min are higher than those of $\dot{\varepsilon}_1$ = 0.012 %/min. Although the difference in strength between them was not significant, yet, it is sufficient to conclude, from Figs.

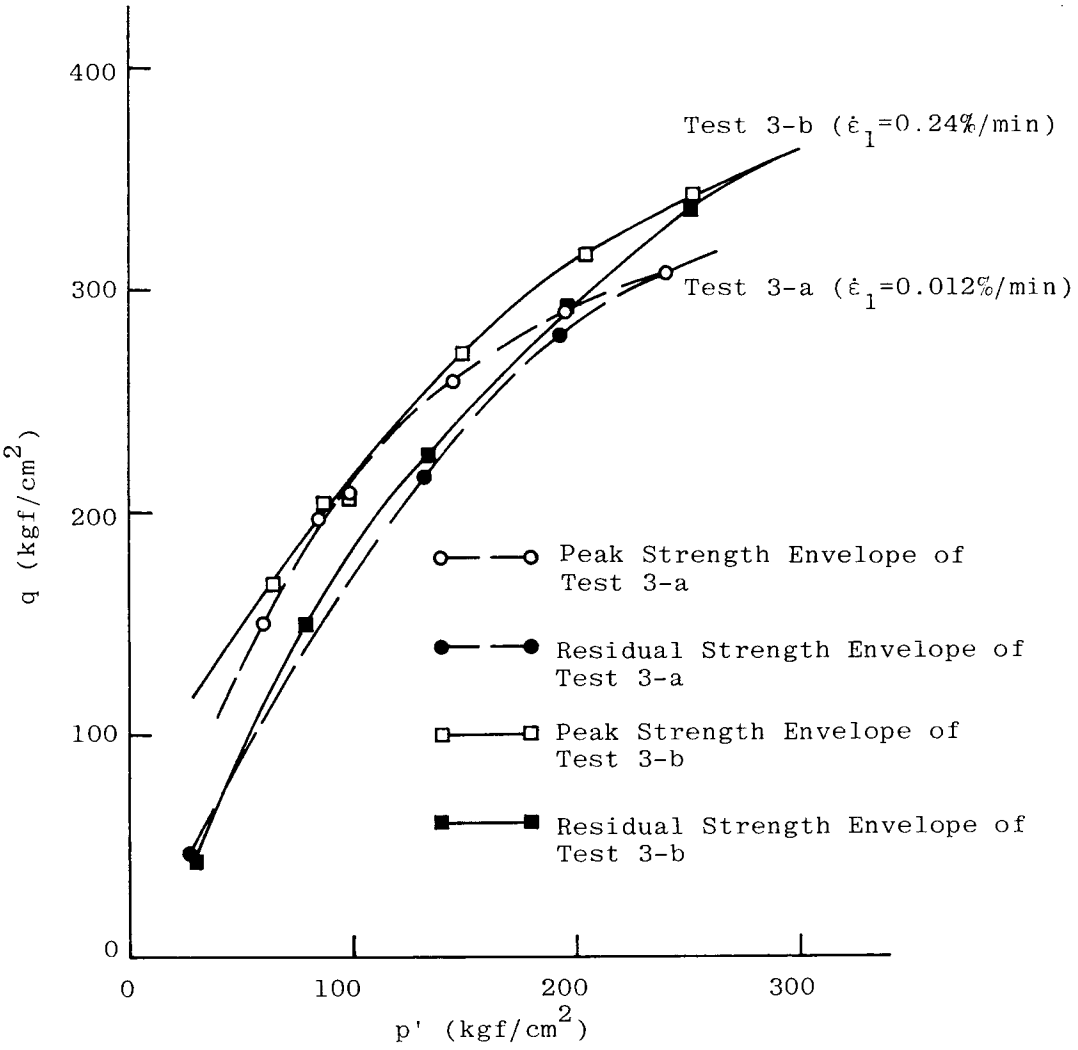

Fig.6-22(b) Strength envelopes derived by Test 3

6-22(a) and (b), that higher rate of shearing would induce higher strength in shearing test.

Comparing the strength envelopes of Test 1 (Fig. 6-22(a)) with those of Test 3-a (Fig. 6-22(b)) in Fig. 6-23, as well as Test 2 and Test 3-b on Fig. 6-24, Test 3 can be considered as an adequate substitute for the two MST tests - Test 1 and Test 2. Substantiatively, an MST test such as Test 3, performed under two or more testing conditions with only one specimen, can be regarded as a new application of MST method.

When presenting the two series of peak strengths obtained in Test 3 onto the τ - σ plane, two Mohr envelopes of peak strength can be constructed as in Fig. 6-25. Except the part of high confining pressure, no obvious difference between these two envelopes exists. Since the Mohr envelope of peak strength is assumed as the boundary of elastic and non-elastic state of rock specimen, hence, as illustrated in Fig. 6-26, a simulation test with slow rate of shearing ($\dot{\varepsilon}_1$ = 0.012 %/min) performed from the point $\sigma_1=p_0$ and followed Eq. 6-9, would have the boundary appeared earlier than that of the rapid shearing ($\dot{\varepsilon}_1$ =0.24 %/min). In other words, the biggest Mohr circle of elastic stress of slow shearing speed will reach its peak strength envelope at P_1 with ($\sigma_{1p'1}$, $\sigma_{3p'1}$) and the rapid one will contact at P_2 with ($\sigma_{1p'2}$, $\sigma_{3p'2}$), where, $\sigma_{3p'1} > \sigma_{3p'2}$ and $\sigma_{3p'1} < \sigma_{1p'2}$.

From the discrepancy between points P_1 and P_2 due to different rates of shearing, it is reasonable to predict that the behavior of an opening wall will be influenced by excavation speed.

(b) Simulation of an opening wall

To continue a simulation test, the value of N_ϕ in Eq. (6-10) is needed. It is worth noting that Eq. (6-10) was derived from assuming that strength envelope of a rock specimen in τ-σ plane is a straight line and intersects the σ

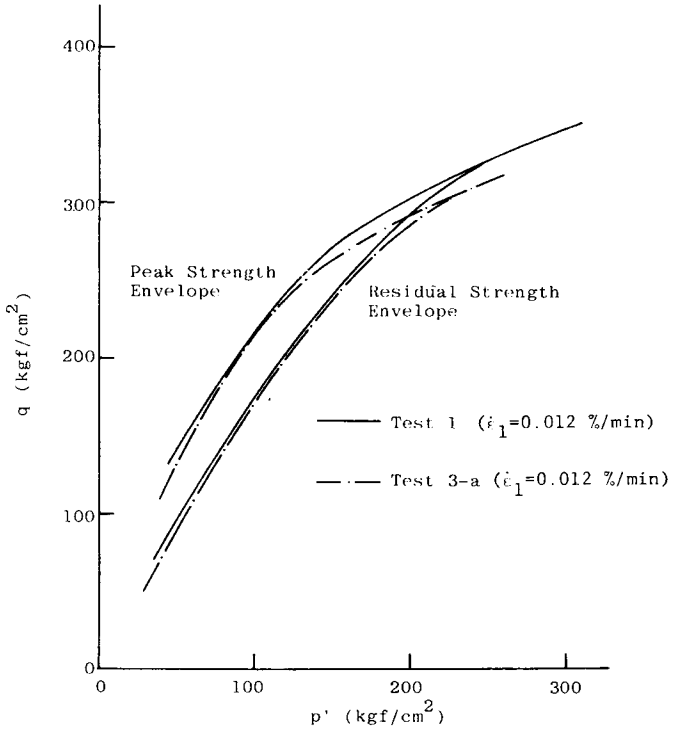

Fig. 6-23 Comparison of the results of Test 1 with those of Test 3-a

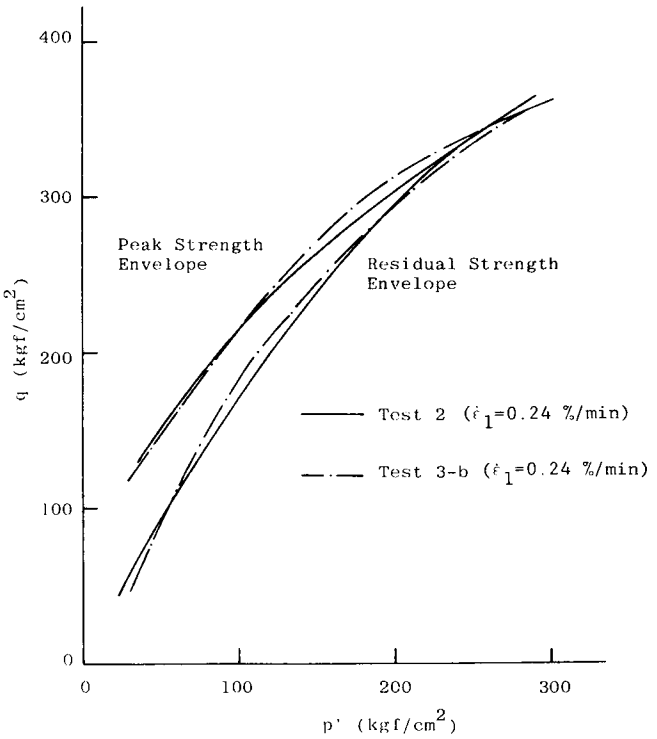

Fig. 6-24 Comparison of the strength envelopes of Test 2 with those of Test 3-b

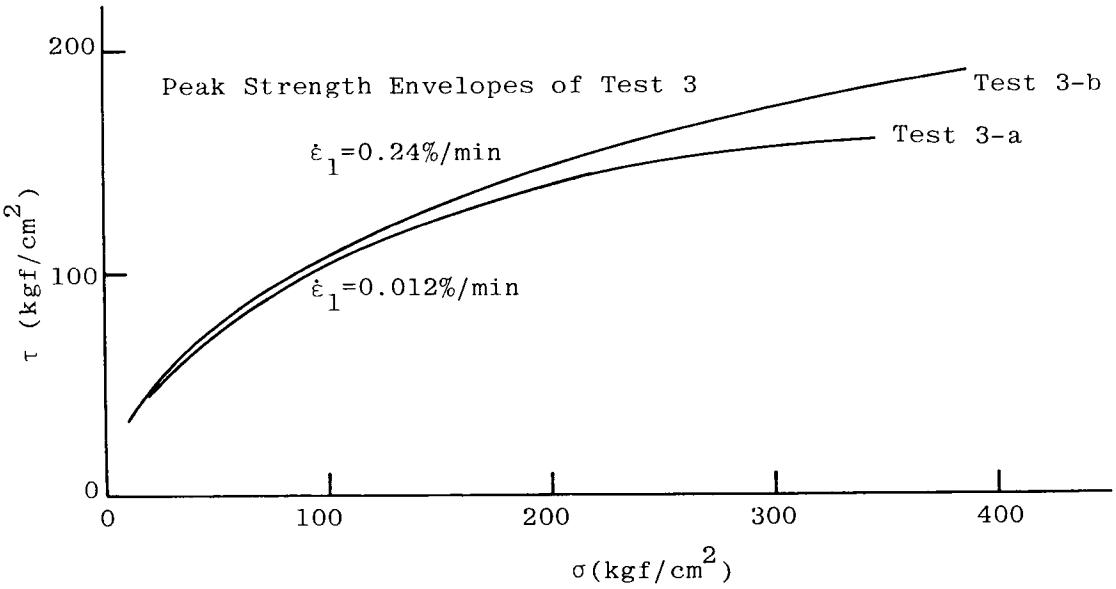

Fig.6-25. Peak strength envelopes of Test 3 in τ-σ plane

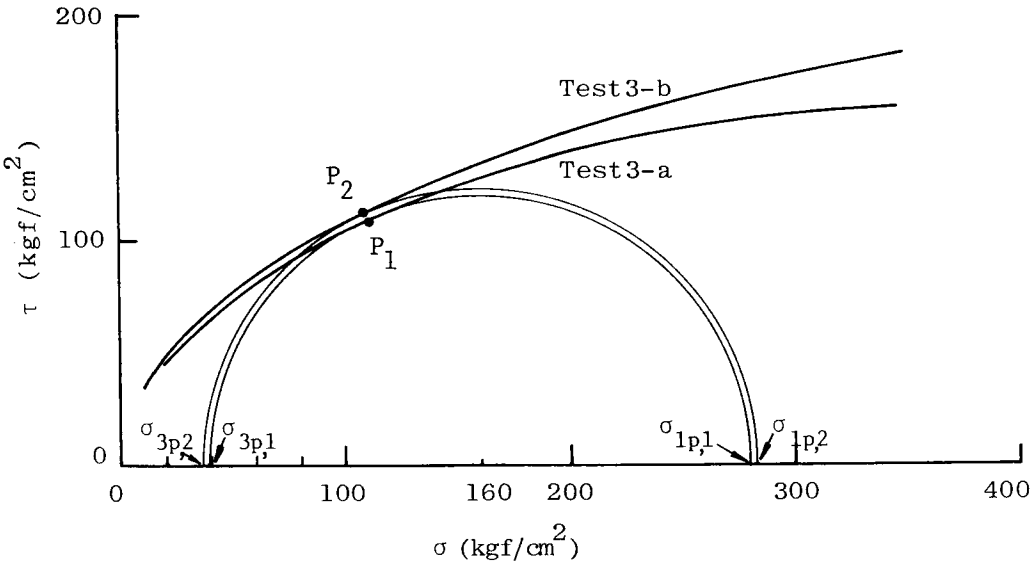

Fig. 6-26 Determination of the critical Mohr cicles of p_0 = 160 kgf/cm^2 with peak strength envelopes obtained in Test 3.

-axis with a ϕ angle. The N_ϕ value of then calculated from by $\frac{1+\sin\phi}{1-\sin\phi}$. However, upon observing Fig. 6-26, it is clear that the practical strength envelope is not straight but rather as parabolic. The determinaation of N_ϕ thus becomes very difficult. To ease the difficulty, a simplified method based on Eq. (6-10) is used in this work.

The value of N_ϕ was firstly assumed to be as a constant all over the non-elastic state.

In order to simulate the behaviors of rock element on opening wall during excavation in laboratory, three triaxial tests following the stress change described by Eqs. (6-9) and (6-10) were performed. They are tentatively referred as Test K, Test L and Test M, for inspecting the behavior of opening wall. An initial isotropic rock stress of p_0 = 60 kgf/cm^2 was used in Test K, and p_0 = 160 kgf/cm^2 in Test L and Test M. Because it was desirable to observe the influence of excavation speed on the behaviors of opening wall, different rates of shearing were employed in Test L and Test M, being $\dot{\varepsilon}_1$ = 0.012 %/min for Test L and $\dot{\varepsilon}_1$ = 0.24 %/min in Test M. In all these tests, specimens made of Funyu rock were used (see Table 2-1 for its physical properties).

Since a strain gauge was pasted on the lateral surface of every rock specimen, so that the lateral strain ε_3 of a specimen during shear simulation can be directly monitored. Informations of σ_1 and ε_1 as well as σ_3 and ε_3 were recorded in each test run. As an example, Fig. 6-27 illustrates the results obtained in Test L, being a rearranged version of all data. The first quadrant of this figure represents σ_1-ε_1 relationship and quadrant II shows the variation of σ_1 and σ_3 during test. The fourth quadrant depicts the change of ε_1 with ε_3, with the scale of ε_3 twice of that of ε_1. Finally, from the curves of σ_1-σ_3 and ε_1-ε_3 , the relationship between σ_3 and ε_3 can be calculated and plotted in the quadrant III. Close examination of these four curves in Fig. 6-27, reveals that each curve can be divided into four regions, each displaying

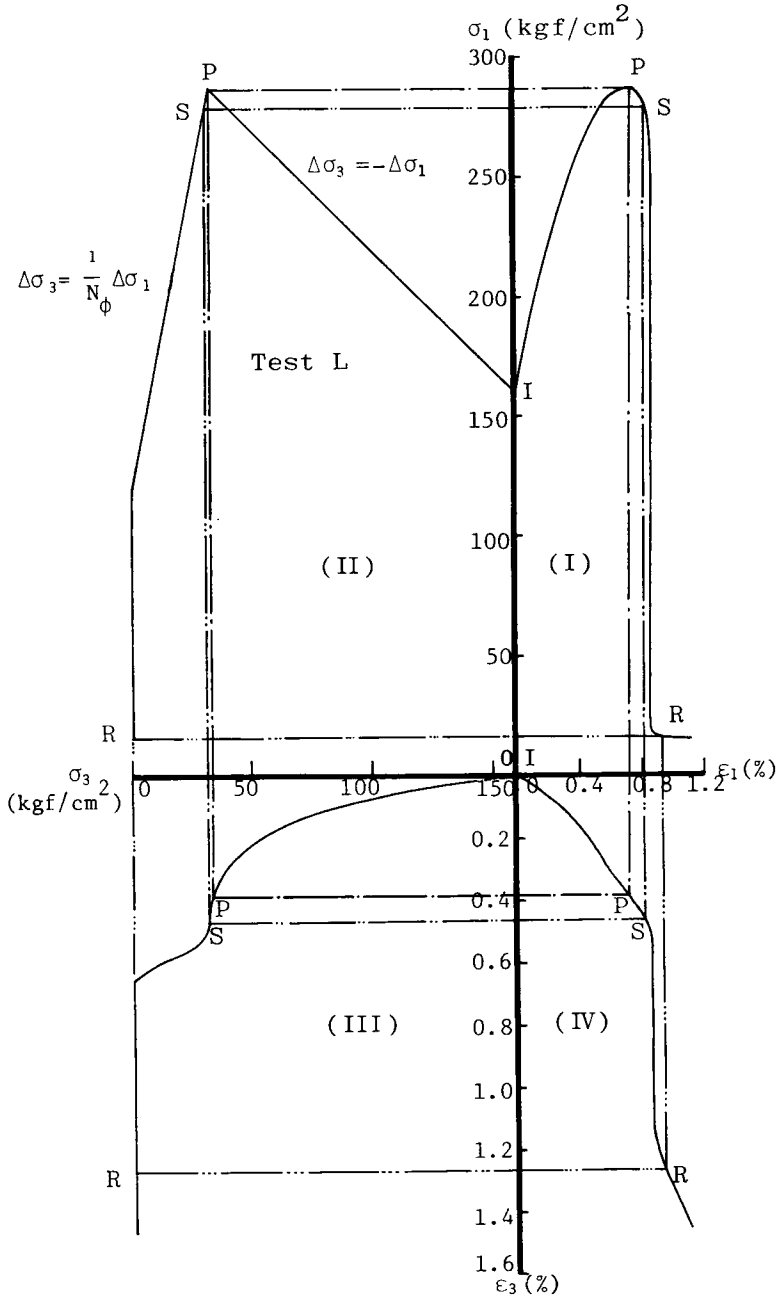

Fig. 6-27 Simulation test results of Test L ($\dot{\varepsilon}_1$=0.012%/min, p_0=160 kgf/cm^2)

quite different responses in stress and strain. Upon designating the letter 'I' as the initial point of test, 'P' for a point reaching its peak strength, 'S' for the point representing strain softening state in which a large amount of ε_3 was generated, and 'R' the initial point of residual state, then, the four regions in Fig. 6-27 can be defined as follows:

Region I : from point I to point P.

Region II : from point P to point S.

Region III : from point S to point R.

Region IV : beyond the point R.

In region I, test was carried out in following Eq. (6-9), i.e., $\Delta\sigma_3=-\Delta\sigma_1$, based upon elastic theory. Although the portion of σ_1-ε_1 curve near point P was not linear, the ε_1-ε_3 curve in quadrant IV indicates that the specimen still had elastic deformation just as that in the initial period of the test. Following the decrease of σ_3, σ_3-ε_3 curve in quadrant III gradually formed a valley and reached point P near a minimum of σ_3.

Beyond point P, rock specimen entered into strain softening state and the simulation test was then performed according to Eq. (6-10), in which $\Delta\sigma_3=\frac{1}{N_\phi}\Delta\sigma_1$.

In region II (from P to S), rock specimen was transformed from an intact state to the formation of a shear failure plane. Strength in σ_1 decreased in the portion after point P, but the inclination of deformation, ε_1-ε_3 relationship, was able to remain reasonably constant when compared with that in region I. Therefore, region II can be regarded as a temporarily stable region before a complete failure was created in the specimen.

Rock specimen lost most of its strength (σ_1) in region III over a very short time interval. Because the value of ε_1 in this region was practically unchanged, it can be said that the failure phenomenon was induced by a suddenly swelling in ε_3. At point R and beyond it, the specimen entered into the residual state.

Three main features can be found in region IV; namely,

(1) that σ_1 reached its minimum and remained at that level,

(2) that both ε_1 and ε_3 increase continuously, and

(3) that σ_3 was again perfectly constant in the σ_3-ε_3 curve.

The results of Test M, which was carried out under the same test condition as in Test L except the rate of shearing, are illustrated in Fig. 6-28. Whilst the results of Test K, which started at a point with initial rock stress p_0 = 60 kgf/cm^2 and performed with the rate of shearing 0.012 %/min (same as the one adopted in Test L), are given by Fig. 6-29.

After comparing the results presented in Figs. 6-27, 6-28 and 6-29, several significant characteristics of rock specimen can be derived as follows:

(1) There were two rather constant values of σ_3 with respect to ε_3 over a portion of σ_3-ε_3 curve in quadrant III (see Fig. 6-27). These two σ_3 values could be tentatively designated as $\sigma_{3,min}$ (minimum of σ_3), when viewed the σ_3-ε_3 curve using ε_3 as the abscissa. The first $\sigma_{3,min}$ appeared near the peak strength point P, whilst the second one was found when the specimen reaching its residual state. However, because the triaxial cell used in this investigation was not equipped to tolerate very high confining pressure during simulation tests, the actual confining pressure σ_3 might have been already decreased down to zero before reaching a residual state. Consequently, the second constant value of σ_3 in σ_3-ε_3 curve was not apparent near point R.

On the other hand, a σ_3-ε_3 curve is seen to be equivalent to a p_i-u_w curve for an opening wall. But, a p_i-u_w curve, (for example, the Fenner-Pacher curve), had only one $p_{i,min}$ near to the early stage of residual state of rock (review Fig. 6-18). In the current investigation, two $\sigma_{3,min}$ values can be clearly seen in σ_3-ε_3 curve. At the first minimum of σ_3, i.e. $\sigma_{3,min,1}$, a specimen reached its own peak strength (σ_1) and with relatively small defor-

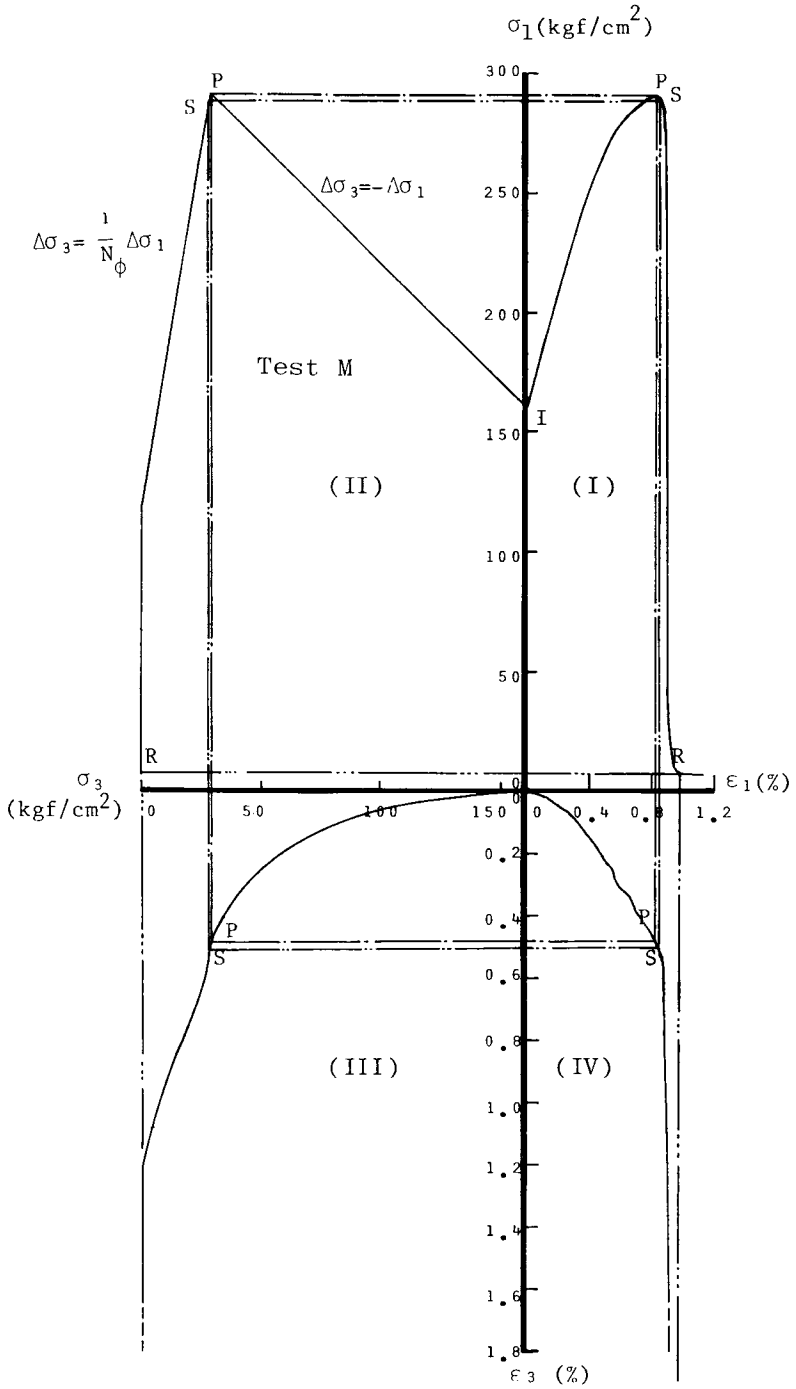

Fig. 6-28 The results of simulation Test M with $\dot{\varepsilon}_1$=0.24 %/min and p_0=160 kgf/cm^2

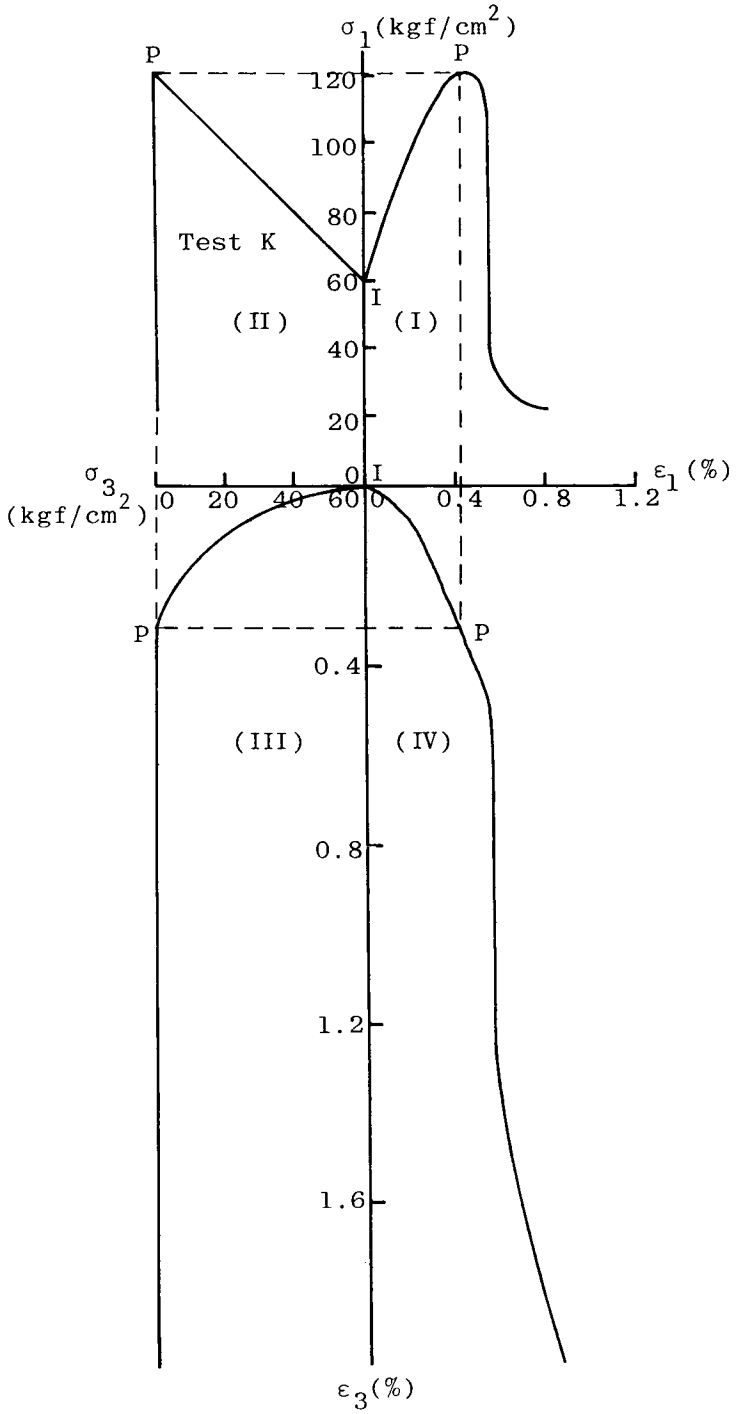

Fig. 6-29 Results of Test K (p_0=60 kgf/cm^2, $\dot{\varepsilon}_1$=0.012 %/min)

mation. On the contrary, when reaching $\sigma_{3,min,2}$, the specimen had already failed. At this second stage, not only the apparent $\varepsilon_1(\varepsilon_\theta)$ was created but also a large $\varepsilon_3(\varepsilon_r)$ was detected in the lateral direction of the specimen. Then, beyond point R, rock pressure created by failed rock would begin to act on the support as proposed by Pacher (1964)[17](see the dot line in Fig. 6-18). Unfortunately, this phenomenon could not be simulated in the present experiment.

(2) The effect of excavation speed on a p_i-u_w curve can be investigated upon comparing a σ_3-ε_3 curves obtained in Test L (rate of shearing 0.012 %/min) with that of Test M (rate of shearing 0.24 %/min). As shown in Fig. 6-30, it is apparent that before points P_1 and P_2 just within region I, there were no obvious differences between these two curves. Although in Test M a lower $\sigma_{3,min,1}$ was obtained at point P_2, together with a rather short section of temporarily stable region beyond P_2, the point P_1 of Test L had only slightly greater strength in σ_3.

From the above discussion, it is apparent that in spite of different excavation speeds were used in tunneling Funyu rock mass, the p_i-u_w curves of opening wall are similar to each other before peak strength point (P_1 and P_2). Beyond P_2 and before reaching residual state, the p_i-u_w curve of a higher excavation speed has a shape which is identical to the Fenner-Pacher curve, whereas the p_i-u_w curve of a slower excavation speed is not so.

(3) Test K simulated the behaviors of opening wall of a shallow tunnel located at a place where p_0 = 60 kgf/cm^2 . Upon inspecting Fig. 6-29, it is found that the peak strength was reached just when σ_3=0, i.e., the $\sigma_{3,min,1}$=0. Because during the excavation of opening, if $\sigma_3(p_i)$ decreases to zero at or before the appearance of peak strength point P, then no failure will be resulted in rock and the opening wall will remain stable, thus no support is required at all. In the case of Test K, since σ_3=0 appeared just at P point, it

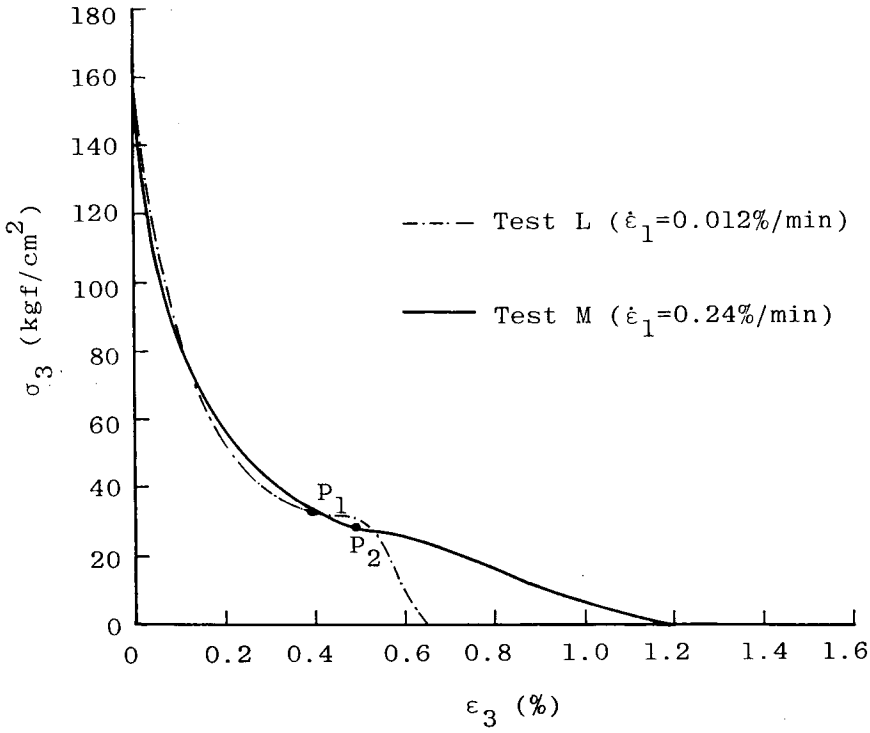

Fig. 6-30 The σ_3-ε_3 curves obtained in Test L and Test M with different rates of shearing.

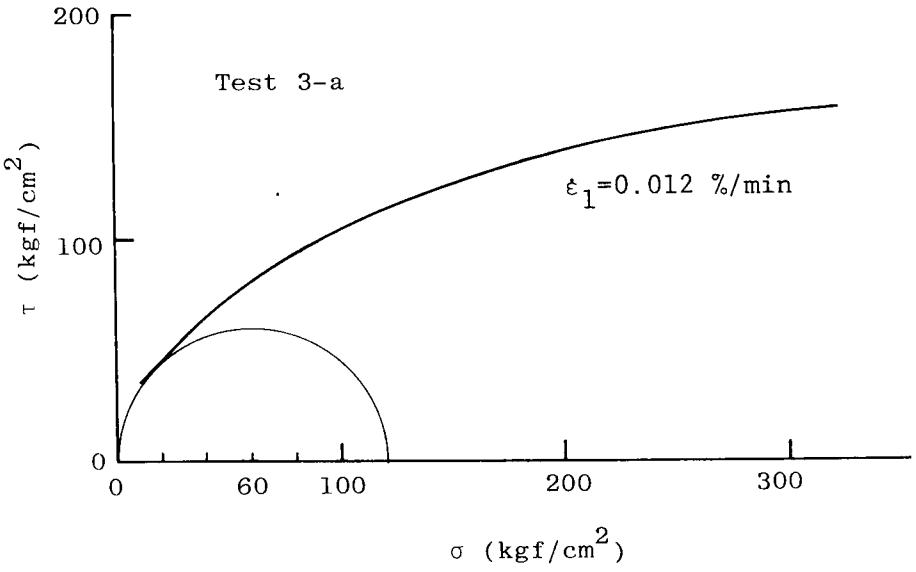

Fig. 6-31 The critical Mohr circle of p_0=60 kgf/cm^2 intersecting simultaneously the peak strength envelope and the origin of τ-σ plane. It means that no support is necessary when p_0<60 kgf/cm^2.

means that an opening wall in Funyu rock mass can stand by itself without needing reinforcement from a support under the pressure less than 60 kgf/cm^2.

In other words, the value of p_0 = 60 kgf/cm^2 is the limit in deciding whether an opening needs a support or not. This value of pressure can be tentatively called as the critical self-stable initial rock pressure of Funyu rock mass.

6-2-6 Conclusions from Simulation Tests

From the discussions made in sections 6-2-5(a) and (b) for investigating the effect of shearing speed on rock strength and the behaviors of opening wall, respectively, the following conclusions can be arrived.

(1) Incorporating with variable rates of shearing to triaxial shear test, which in turns simulate different excavation speeds, various rock strengths can be induced. From this, a new extension of MST method has been developed, in which two series of MST were performed using only one specimen but different rates of shearing. As shown in Figs. 6-23 and 6-24, it is clear that the new application of MST is an adequate and convenient substitution for analysing the effect of changing experimental condition on the strength envelope of rock.

(2) Based on Fig. 6-26, the biggest stress Mohr circle intersected with the peak strength envelope of rates of shearing 0.012 %/min and 0.24 %/min at points P_1 and P_2, respectively (where $\sigma_{3p,1}$=39 kgf/cm^2 and $\sigma_{3p,2}$=36 kgf/cm^2). On the other hand, the value of $\sigma_{3,min,1}$ was 33 kgf/cm^2 for Test L (with $\dot{\varepsilon}_1$= 0.012 %/min), and 30 kgf/cm^2 for Test M ($\dot{\varepsilon}_1$=0.24 %/min). Although discrepancy exists between $\sigma_{3p,1}$ and $\sigma_{3,min,1}$ of Test L, as well as $\sigma_{3p,2}$ and $\sigma_{3,min,1}$ of Test M, rough prediction of $\sigma_{3,min,1}$ and $\sigma_{1p,1}$ is still possible by using these peak strength envelopes on τ-σ plane. Replotting the peak strength envelope of Test 3-a ($\dot{\varepsilon}_1$= 0.012 %/min), given by Fig. 6-31, shows that the big-

gest Mohr circle centered at $\sigma = p_0 = 60$ kgf/cm^2 will intersect simultaneously the peak strength envelope and the origin of this $\tau - \sigma$ coordinate system. Hence, if a simulation test is performed under $p_0 < 60$ kgf/cm^2, no failure will be found within the specimen even when σ_3 is reduced to zero. It also indicates that no support is required for an opening on Funyu rock mass which might be located at shallower place where $p_0 < 60$ kgf/cm^2. This was mentioned in section 6-2-5.

(3) The value of $\sigma_{3,min,2}$ can be estimated from residual strength envelope using a simpler graphical method as follows,

(a) Plotting the peak and residual strength envelopes of rock obtained by MST method on τ-σ plane (see Fig. 6-32).

(b) Locating the center of Mohr circle at point C, where $\sigma=p_0$ (initial isotropic stress of rock mass), and drawing a biggest Mohr circle which just intersects the peak strength envelope at point P. Then, calculating N_ϕ value from Eq. (6-10) using $\sigma_{3,min,1}$ and σ_{1p}.

(c) By means of "trial and error" method to find a Mohr circle which just contacts the residual strength envelope at a point R and intercepts the abscissa at $\sigma_1=\sigma_{1r}$ and $\sigma_3=\sigma_{3,min,2}$, respectively, in which σ_1 and σ_3 satisfying the relation that $\sigma_{1p} - \sigma_1 = N_\phi \times (\sigma_{3,min,1} - \sigma_3)$. Thus, finally $\sigma_{3,min,2} \fallingdotseq \sigma_3$.

(4) The relationship of ε_1-ε_3 in quadrant IV of Fig. 6-27 is represented in Fig. 6-33 for ready comparison with the result measured at Seikan Tunnel. The latter was shown in Fig. 6-14. A high degree of similarity exists between the results of simulation test (Fig. 6-33) and that of practical measurement in situ (Fig. 6-14). Since most wall deformation occurs when the excavation face comes near, see Fig. 6-14, in addition to the fact that $\sigma_{3,min,1}$ often appears near the onset of region II, see Fig. 6-27 and Fig. 6-33, it can be considered that $\sigma_{3,min,1}$ ($p_{i,min,1}$) should be addressed to near the excavation

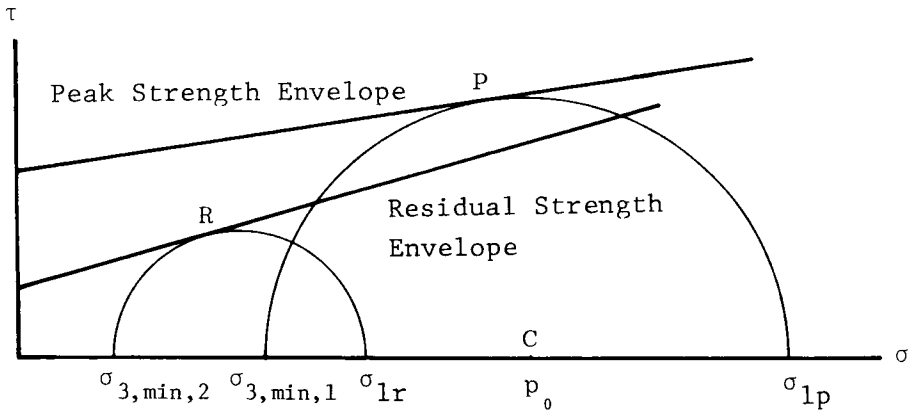

Fig.6-32 A simple graphical method for determining $\sigma_{3,min,2}$

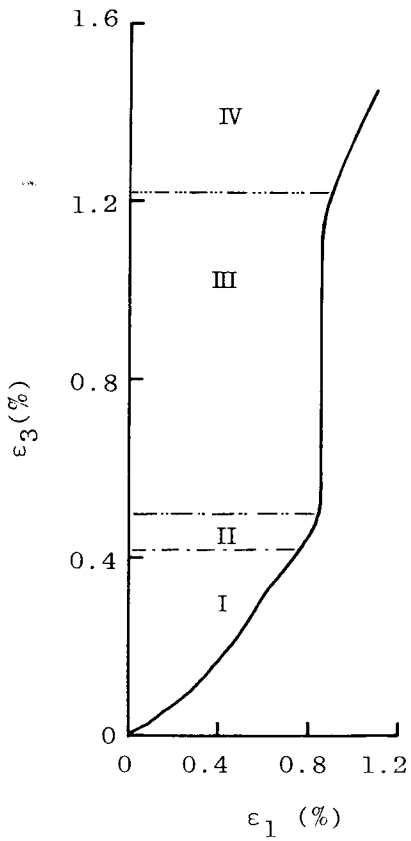

Fig.6-33 The ε_1-ε_3 relationship of Test L

face of an opening. Therefore, the use of the first minimum value of σ_3 (p_i) to construct a support is practically difficult, because the section concerned is within the immediate vicinity of the excavation face.

(5) A simulation test of the rock element on opening wall was performed till the residual state of rock was reached, i.e., when reaching the corresponding point of $p_{i,min}$ on Fenner-Pacher curve. As the portion of Fenner-Pacher curve after $p_{i,min}$ is practically not important for support design, the simulation test method mentioned in section 6-2-5(b) is an adequate and proper method for elementary support design of an opening.

6-3 Conclusions

Besides the violent vibration of rock mass itself caused by an earthquake, as discussed early in section 6-1, low frequency rocking of structure can also induce damage to the supporting rock mass beneath the structure.

Although, a sudden failure of rock mass can not be promoted by structural rocking, rock may gradually lose its elastic property according to the results of simulation tests. For example, the loss of properties includes the lowing of elastic shear modulus and a decrease of its peak strength.

Furthermore, the internal damage of a rock specimen can be monitored by the change of permeability and the augmentation of plastic strain in it during simulation test.

As a long term effect, structure rocking will stepwisely diminish the supporting strength of a rock mass, resulting in a state of residual strength only to the rock mass. Hence, the residual strength of rock mass is suggested as the rock strength to be adopted in foundation design to resist the loading of structure rocking.

On the other hand, from the results obtained in section 6-2, it is apparent that the simulation test to investigate the behaviors of an opening wall is beneficial to rock tunneling. The series of simulation tests were begin from sampling typical rock specimens beyond the excavation face using preboring technique. The peak and residual strength envelopes of rock mass were then explored by MST test method. From the results described in section 6-2-6, the position of point P together with the values of N_{ϕ} , $p_{i,min,1}$ and $p_{i,min,2}$ can be estimated. If the value of $p_{i,min,1}$ is positive, suitable support is then necessary to prevent an opening wall from failure.

Finally, from the result of σ_3-ε_3 obtained from a simulation test (see section 6-2-4), a p_i-u_w curve for opening wall can be derived by changing the scales and sequence of the co-ordinates of σ_3-ε_3. And then, a rudimentary design of support, for example, the selection of stiffness and strength of support, as well as the timing of setting up support, can be performed.

It is with confidence that this series of simulation tests proposed in section 6-2-4 can be very useful as a preliminary test for a support design of an opening, with noticeable benefit to NATM.

References for Chapter 6

(1) Naito, T., et al., "Aseismatic, Wind-Prof Structures", Kasshima Publication Co., pp. 263-267 (In Japanese).

(2) Bierbaumer, A., "Die Dimensionierung des Tunnelmauerwerkes", Leipzig / Berlin Engelmann, 1913.

(3) Kommerell, O., "Statische Berechnung von Tunnelmauerwerk", Ernst & Sohn, Berlin, 1940.

(4) Terzaghi, K., "Rock Defects and Loads on Tunnel Support", Rock Tunneling with Steel Supports, eds. R. V. Proctor and T. White, Commercial shearing Co., Youngstown, Ohio, 1946.

(5) Yamaguti, N., "On the Stress around a Horizontal Circular Hole in a Gravitating Elastic Solid", J. of the Civil Engineering Society of Japan, vol. 15, pp. 291-304, 1929.

(6) Yu, Y., "Gravitational Stresses on Deep Tunnels", J. of Appl. Mech., Dec. 1952.

(7) Duvall, I. R. and L. Obert, "Rock Mechanics and the Design of Structure in Rock", John Wiley & Sons, Inc.

(8) Egger, P., "Einfluss des Post-Failure-Verhaltens von Fels auf den Tunnelausbau unter besonderer Berucksichtigung des Ankerausbaus, Habilitationsschrift, Univ. Karlsruhe, 1973.

(9) Kastner, H., "Statik des Tunnel-und Stollenbaus", Springer-Verlag, 1971.

(10) Takayama, A. and T. Imata, "NATM (1)", Tunnels and Underground, Vol. 12, No. 1, pp. 61-69, 1981. (In Japanese)

(11) Rabcewicz, L. V., "The New Austrian Tunneling Method", Water Power, Nov. 1964, pp. 453-515., Jan. 1965, pp. 19-24.

(12) Rabcewicz, L. V., "Stability of Tunnels under Rock Load", Water Power, June 1969, pp. 225-273., August 1969, pp. 297-302.

(13) Muir Wod, A. M., "The Circular Tunnel in Elastic Ground", Geotechnique, 25, No. 1, pp.115-127, 1975.

(14) Tanimoto, C., "Tunnelling in Rock with Rockbolts and Shotcrete", Doctoral Thesis, Kyoto University, 1980.

(15) "Report on the Investigation of the Earth/Rock Pressure in Seikan Tunnel" JSCE, pp. 352, 1977 (In Japanese).

(16) Fenner, R., "Unltersuchungen zur Erkenntnis des Gebirgsdruckes", Gluckauf Ann. 74, Vol. 32, 33, Essen., 1938.

(17) Pacher, F., "Deformationsmessungen im Versuchsstollen als Mittel zur Erforschung des Gebirgsverhaltens und zur Bemessung des Ausbaues", Felsmechanik und Ingenieurgeologie, Suppl. I, 1964.

(18) Takayama, A. and T. Imada, "NATM (2)", Tunnels and Underground, Vol. 12, No. 2, pp. 149-155, 1981 (In Japanese).

(19) Tanimoto, C., S. Hata and K. Kariya, "Interpretation of Characteristic Line for Tunnel Stability", Proceedings of the 14th Symposium on Rock Mechanics, JSCE, pp. 86-90, 1982 (In Japanese).

Chapter 7 CONCLUSIONS AND RECOMMENDATION FOR FURTHER RESEARCH

With the aim to explore the behaviors of rock mass in field under construction, technical simulations were developed in laboratory. From the results obtained in these tests, many valuable information can be derived for relevant constructions on or in a rock mass. Based upon the work carried out in the preceeding chapters, the following conclusions can be drawn, with the source of each reference in the text indicated within the brackets immediately after each item.

(1) A stiff loading system can be employed to monitor the σ-ε relationship of a rock specimen before reaching its peak strength, as well as a conventional loading system (flexible system) can serve the same purpose (2-1 and Appendix A).

(2) When a shear test was performed using a flexible loading system, abrupt failure of rock specimen would occur soon after passing its peak strength. The continuous recording of σ-ε curve then becomes terminated. Based upon the incomplete σ-ε curve, the stiffness of flexible loading system can be obtained indirectly (Appendix A).

(3) A complete σ-ε curve of a rock specimen, which should included residual state as well as peak strength, can only be monitored by a stiff loading machine, whose stiffness is higher than that of the rock specimen (2-1 and Appendix A).

(4) In a triaxial test with low and mediate confining pressures, the peak strength of a rock specimen always appeared later in time than its peak pore water pressure. This phenomenon was frequently used to predict the appearance of a peak strength in each stage of MST test method (3-2-1).

(5) During a shearing test, the occurrence of dilatancy within a rock

specimen can be judged by inspecting the direction of effective stress path. In the case of a rock specimen with B = 1 (B being the pore pressure coefficient), an effective stress path toward the right-hand side of a p' = constant in q-p' plane, where $q = \sigma_1 - \sigma_3$ and $p' = \frac{1}{3}(\sigma_1' + 2\sigma_3')$, means the specimen is dilatant. For B < 1, the tendency of dilatancy is determined when the effective stress path progresses into the right-hand side of the line with a inclination of 3/(1-B) (3-2-2).

(6) Based on the σ-ε curve of each loading-unloading cycle in cyclic loading test, it is able to define the energy used to perform the shear test in terms of E_r (recoverable energy) and E_i (irrecoverable energy). The irrecoverable energy E_i can further be divided into E_{crack} and $E_{friction}$ designated the energy used to progress the crack growth in rock and to resist the friction force in cracks or pores, respectively (3-3-2).

(7) After some cycles, say 4 or 5, of loading-unloading, the value of E_i almost converges to a constant which is equal to $E_{friction}$.

Subtracting $E_{friction}$ from E_i of each cycle, the E_{crack} dissipated in each cycle can be evaluated. The E_{crack} in the first cycle is often much greater than that of other cycles, implying that most of the crack are generated in the first cycle of a cyclic loading test (3-3-2).

(8) Increasing the time of consolidation before shearing process of a cyclic loading test, E_i would be improved slightly, due to the fact that more excess water in cracks and pores are drained out by consolidation, thus, improving the frictional resistance between crack surfaces (3-3-2).

(9) To explore the strength envelopes of saturated soft rocks, the Multiple Stage Triaxial test method is a suitable and convenient substitution for the conventional triaxial test. However, consolidation process must be carried out in each stage of MST test (4-2-3).

(10) With the aid of monitoring the change of lateral strain of a satu-

rated soft rock specimen (by using a lateral strain gauge), the accuracy of predicting the appearance of peak strength in each stage can be improved. Consequently, a more exact peak strength envelope can be resulted (4-3-1).

(11) The improved MST test method is also adopted to investigate the mechanical behaviors of saturated soft rock with artificial shear plane under various confining pressures. On the basis of this study, it is clear that,

(a) Rock specimen with an artificial shear plane of 60^0, which is measured by the direction of σ_3, to the shear plane, possesses the lowest peak and residual strength. However, the angular influence of shear plane on the strengths of rock specimen becomes weaker and even vanished when a higher confining pressure is used in test (4-4-3).

(b) Under low confining pressure, the residual strength of an intact specimen is somewhat higher than that of the specimen having a 60^0 or nearly 60^0 shear plane. This indicates that under suitable confining pressure and angle of shear plane, this rock specimen shows lower residual strength when compared with the intact rock specimen, although the residual strength of intact specimen has always been considered as the lowest strength, as far as construction design is concerned (4-4-4).

(12) The behavior of rock often strongly depends on its internal structures, such as cracks, voids and joints. And, the change of internal structure can be monitored indirectly by the permeability of rock specimen.

Hence, under a lower confining pressure (40 kgf/cm^2), the process of a common triaxial shear test of Funyu rock specimen can be divided into four stages according to its permeability variation. These are:

Stage 1, a region of crack opening and growth,

Stage 2, a region of forming a shear failure plane,

Stage 3, a region of relative sliding along shear failure plane, and

Stage 4, containing residual state (5-3-1).

(13) In triaxial shear test under 40 kgf/cm^2 of confining pressure, the shear failure plane is completely formed at the final portion of stage 2, which corresponds to strain softening state but not peak strength (5-3-1).

(14) The inclination of permeability - axial strain curve of a rock specimen varies with different confining pressures in triaxial shear test, due to variable failure shapes within specimen under different confining pressures (5-5).

(15) The technique developed has been applied to geotechnical engineering. The first application is to investigate damage created in the supporting rock mass under low frequency structure rocking. Permeability variations are measured in test with different loading amplitudes. This is expected to benifit foundation design (6-1).

(16) As the second application, the behaviors of rock element located in the vicinity of an opening wall during tunneling has been simulated. A resultant σ_3-ε_3 curve corresponding to the p_i-u_w curve of opening wall has been obtained, providing useful information for support design (6-2).

(17) The influence of changing excavation speed on the shape of p_i-u_w curve has been simulated by using two different rates of shearing. Although no apparent differences in σ_3-ε_3 curves before reaching peak strength have been derived from different rates of shearing, different shape of the σ_3-ε_3 and stability have been significant beyond peak strength point (6-2-5).

(18) To explore the strength envelopes of rock under different shearing speeds, a new application of MST method is developed, in which two or more strength envelopes of different test conditions can be obtained from using only one specimen (6-2-5).

The following research should be carried out either in the short or long term:

(19) Since simulation tests reported in Chapter 6 are performed under the

assumptions that (i) p_e (loosening pressure of rock, induced by the opening excavation) increases propertionally to the deformation of opening wall, and (ii) the rate of ε_θ (ε_1) is constant during the opening excavation, these tests have been performed in a simpler way. However, a more practical simulation is desirable, in which the second assumption should be discarded. Without the axial strain rate control (i.e., $\dot{\varepsilon}_1 \neq$ constant), and directly following the variation of opening wall deformation (reviewing Fig. 6-14), tests can be carried out under lateral strain control (ε_3 changed to follow u_w in Fig. 6-14). Then, the degree of similarity between the practical behaviors of opening wall and the simulated test in laboratory can be promoted.

(20) Although the in situ measurement of Seikan Tunnel is adopted to compare with the experimental result in section 6-2-6, the likely application of these tests to tunneling has not yet been carried out. For engineering purposes, case study should be regarded as of vital importance, besides a practical theorectical consideration.

Appendix A THE RELATIVE STIFFNESS BETWEEN LOADING SYSTEM AND ROCK SPECIMEN

The influence of relative stiffness between the loading system and rock specimen on the shape of resistance - deformation curve of a rock specimen will be investigated in this appendix.

Upon inspecting a complete curve of load (resistance) - deformation relationship of a rock specimen as shown in Fig. A-1(a), it is reasonable to consider that this curve is resulted from a load L_i on the specimen from the loading frame against an induced deformation S_i in the loading direction, and simultaneously creating a resistant force R_i within the specimen which is just equal to the external load L_i . This is located at point i on the load - deformation curve. Repeating the procedure above, a series of such points will appear one after another; finally, forming a complete resistance - deformation curve of the rock specimen. However, while generating the load L_i, the loading frame might have slightly deformed, because of the insufficient stiffness.

To explore the relation between loading machine and rock specimen, Bieniawski, et al. (1969)[1] proposed a model which composed of a spring with stiffness C, representing the loading frame, in addition to a specimen loaded in series with the spring. The spring and specimen were then placed between two idealized stiff plates as sketched in Fig. A-1(b). From this figure, it is apparent that, if any loading increment ΔL_i had been created due to the contraction of spring C, the specimen would receive the same load ΔL_i. However, a different contraction would result in the specimen as it possessed different stiffness.

Consider two different loading machines, tentatively referred to as machine 1 and machine 2 with stiffness C_1 and C_2 , respectively, and a rock specimen with stiffness C_s in which $C_1 > C_s > C_2$.

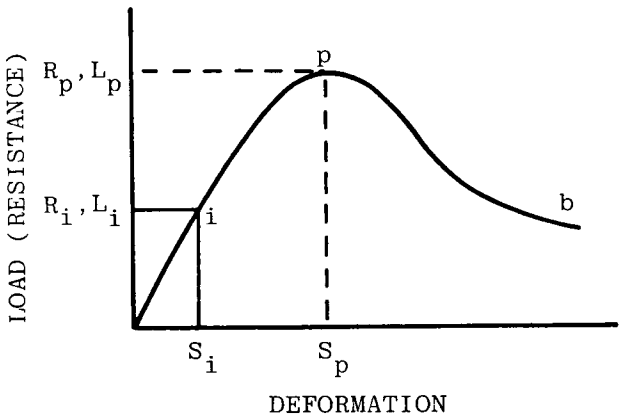

Fig. A-1(a)

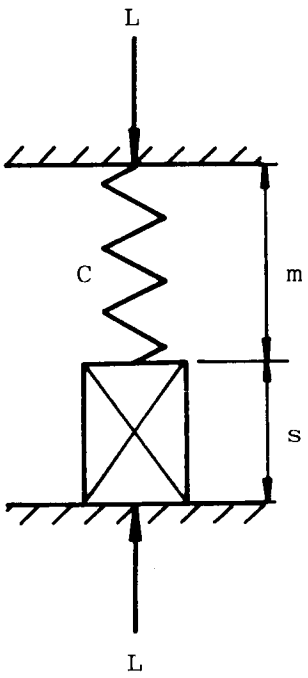

Fig. A-1(b) A model of loading machine and rock specimen (Ref. A-1)

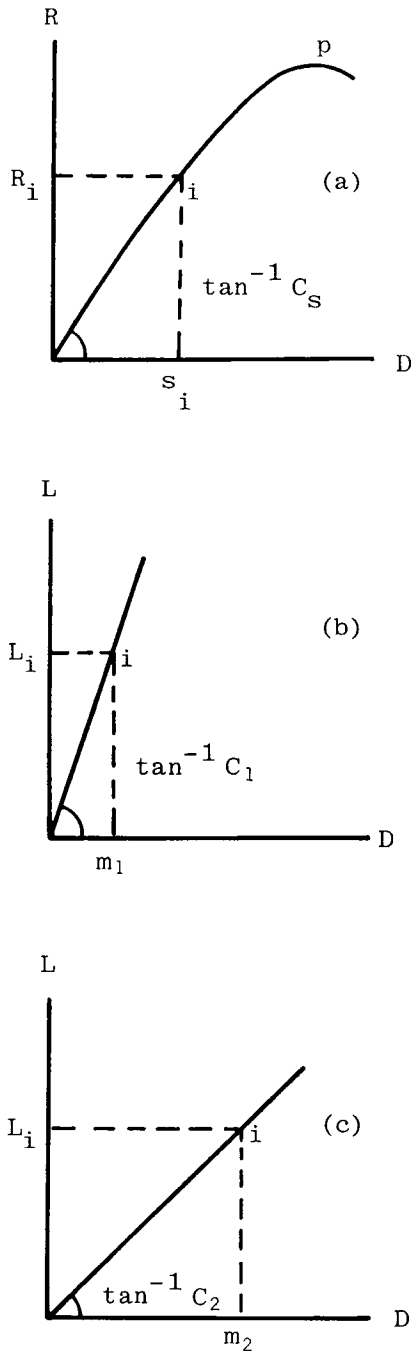

Fig.A-2 The stiffnesses of a rock specimen and two loading machines ($C_1 > C_s > C_2$)

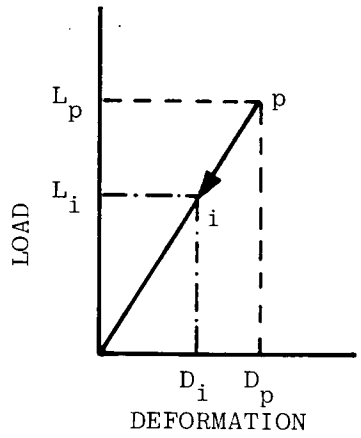

Fig. A-3

Figures A-2(a), (b) and (c) illustrate the stiffness of rock specimen, loading machine 1 and 2, respectively. Imposing a load $L_i = L_1 = L_2$, which is smaller than the peak strength, by machine 1 and machine 2, then the specimen produces a resistance $R_i = L_i$ and undergoes a deformation s_i. To maintain equilibrium to the loading system, machine 1 itself must produce a deformation m_1, whilst machine 2 with an amount m_2, in which $m_2 > s_i > m_1$.

Soon after reaching the peak strength point, the specimen will gradually lose its resistant ability with the increase of deformation, similar to the p-b portion depicted in Fig. A-1(a). This is termed as strain softening state.

With decreasing resistant force R, beyond the peak strength point, the necessary loading L to maintain the balance within this machine-specimen system will also gradually draw down (see Fig. A-3). This means that the spring shown in Fig. A-1(b) will elongate rather than in a state of being contracted, in spite of the relative distance between the two idealized stiff plates decreased continuously.

On the basis of these fundamental concepts of the interaction between loading machines and rock specimen, a thorough behavior of a rock specimen during shear test can be derived by two different loading machines.

A-1 Case 1, Shear Test with a Stiffer Loading Machine ($C_l > C_s$).

A-1-1 In the Region before Reaching the Peak Strength Point

The behaviors of loading machine and rock specimen in the region before reaching a peak strength point will be discussed. To facilitate the discussion, the model by Bieniawski, et al. (1969)[1] mentioned previously is again shown in Fig. A-4(a). Firstly, assuming the upper stiff plate displaces downward with a distance m and the displacement is temporarily and completely absorbed by spring C_l (see Fig. A-4(b)). Therefore, in accordance with Hooke's law, a load $L_a = C_l \cdot m$ is produced by the loading machine and can be displayed in load (resistant force) - deformation plane as vector $\overrightarrow{oa}$ (Fig. A-5). As a result of this loading, the specimen is compressed, thereby inducing a resistance just equal to L_a. Since the stiffness of the rock C_s is less than C_l, so that as shown in Fig. A-4(c), even when the specimen is deformed a distance m, the resistance generated in the specimen is only R_b, where $R_b = C_s \cdot m < L_a$. At this stage, the loading machine-specimen system is not in a state of equilibrium. Hence, the specimen would deform further, until its total deformation s satisfies the relation $C_s \cdot s = R_n = L_a = C_l \cdot m$. Correspondingly the total distance in which the upper stiff plate has travelled becomes m+s. The system now reaches a stable state at n, rendering the resistance (R) - deformation (D) curve of rock specimen obn.

Repeating the same procedure, the R-D curve can smoothly be achieved till reaching the peak strength point p.

A-1-2 In the Region of Post-Peak Strength

The relationship between the loading machine and specimen in the range of post-peak strength will now be considered.

As shown in Figs. A-6(a) and A-7, assume that the accumulated deformation

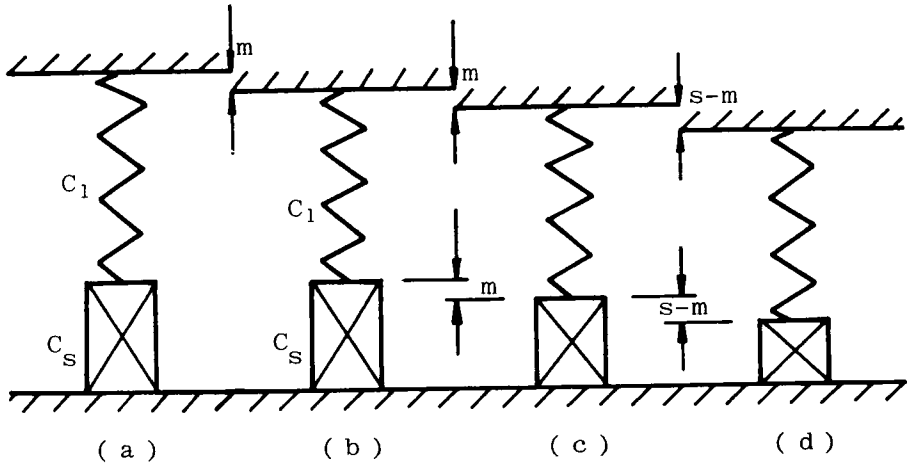

Fig.A-4

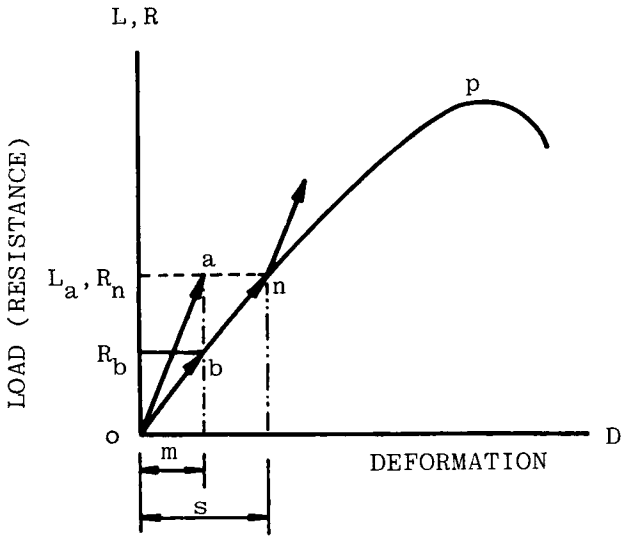

Fig.A-5 Shear test with a stiffer loading machine (before peak strength point)

of the rock specimen at peak strength point p is s_p and the loading machine C_l has already contracted for a distance m_a. Beyond the peak strength point p, the resistant force of specimen will decrease stepwise with the increasing contraction. Therefore, it is clear that even the specimen possesses a resistant force $R_p = C_s \cdot s_p$ strong enough to support the load L_a, after the point p, specimen can not resist against L_a and will be continuously subjected to L_a for a while around the vicinity of the peak strength point p.

Certainly, specimen is undergoing compression. As depicted in Fig. A-6(b) and Fig. A-7, a new deformation s created in the specimen will drop the resistant force down to R_q, resulting $R_p - R_q = c_s \cdot s$ and

$$R_q = C_s(s_p - s) = C_l m_a - C_s s \quad \text{.....(A-1)}$$

whilst the spring C_l will elongate over an amount s which is equal to the amount that the specimen is compressed. Following Fig. A-3, the load stored in spring C_l will be dropped down to a lower value L_c, see Fig. A-7, due to the elongation s, where, $L_c = c_l(m_a - s)$. Because $C_l > C_s$ and from Eq. (A-1), $R_q = C_l m_a - c_s s$, it is apparent that R_q is greater than L_c. That is to say that the resistant force of specimen is stronger than the loading force, therefore, specimen can gain a temporarily stable state at the point q. However, once the upper stiff plate continues to displace over a distance m, the spring will be recontracted (see Fig. A-6(c)), and the loading force will also recover to a higher value L_b identical to the specimen resistant force R_q. Further contraction of spring will generate a load bigger than L_b, then, compression of specimen will proceed again.

Consequently, the resistant force - deformation curve of a rock specimen beyond peak strength can be obtained step by step, upon repeating the same procedures mentioned.

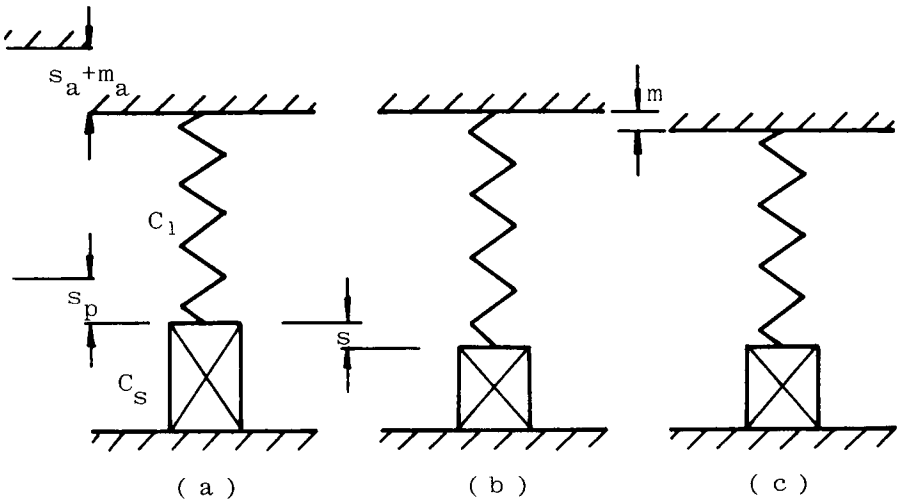

Fig.A-6

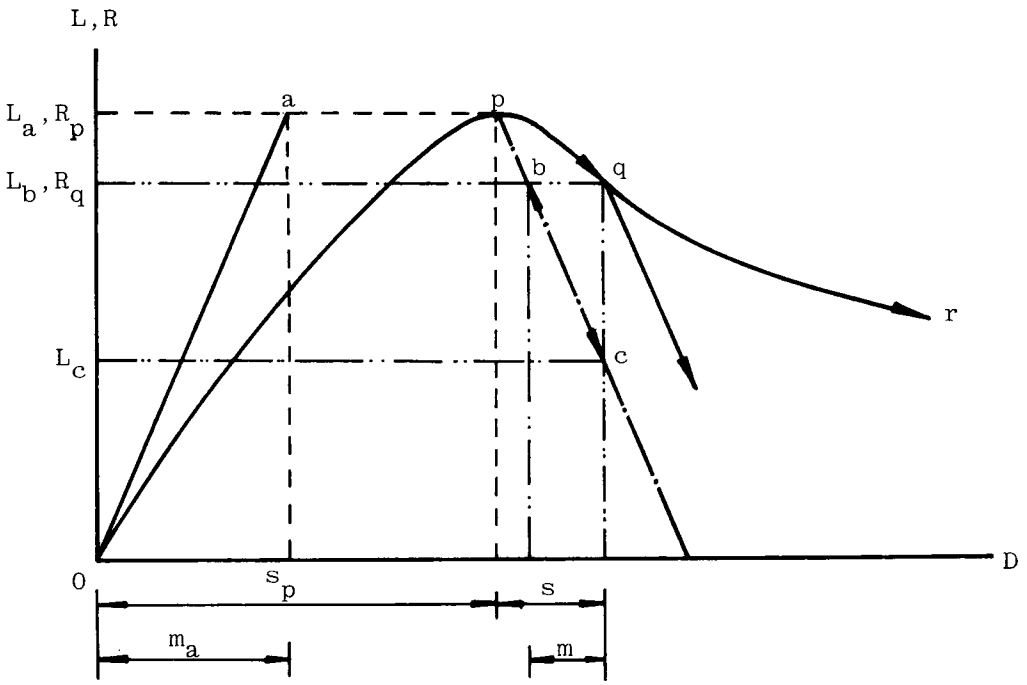

Fig.A-7 Shear test with a stiffer loading machine (beyond peak strength point)

A-2 Case 2, Shear Test Using a Less Stiff Loading Machine ($C_2<C_s$).

A-2-1 In the Region before the Peak Strength Point

With the upper stiff plate travelled over a distance m_1 which might be fully absorbed by the loading machine, a loading force L_a is generated (see Figs. A-8(a), (b) and Fig. A-9). The specimen (shown in Fig. A-8) is then compressed by an amount s_1, and a resistant force R_n equal to L_a induced. Hence, a portion of the resistant force (R) - deformation (D) curve of the specimen $\widehat{on}$ can be monitored. As $C_2<C_s$ even when $L_a=R_n$, it is very easy to find that $s_1<m_1$. However, at this stage, assuming the upper stiff plate remains fixed in position, then, the amount of contraction of s_1 to the specimen must induce an elongation s_1 to the spring. It is likely that the loading machine will decrease its loading ability from L_a to L_b, where $L_b = C_2\cdot(m_1-s_1)$. Accordingly, the resistant force R_n, then, will become bigger than loading force L_b and the specimen would maintain a stable state temporarily at point n. But, when the upper stiff plate propagates further downwards, the loading machine spring C_2 will again be compressed. When the loading force recovers to a value which is same as or even bigger than the resistance R_n, the shearing process of rock specimen will continue. A complete R-D curve of the specimen after point n, but before point p, can be obtained in a similar manner.

Following the discussions in sections A-1-1 and A-2-1, it is obvious that either the stiff loading machine C_1 or the flexible loading machine C_2 is capable to be adopted to monitor the portion of resistant force - deformation relation curve before peak strength of rock specimen, although the latter possesses a weak stiffness smaller than the C_s of the rock specimen used.

A-2-2 In the Region of the Post-Peak Strength

As exhibited in Fig. A-10, if $C_s<C_2$ can be sustained over a short period

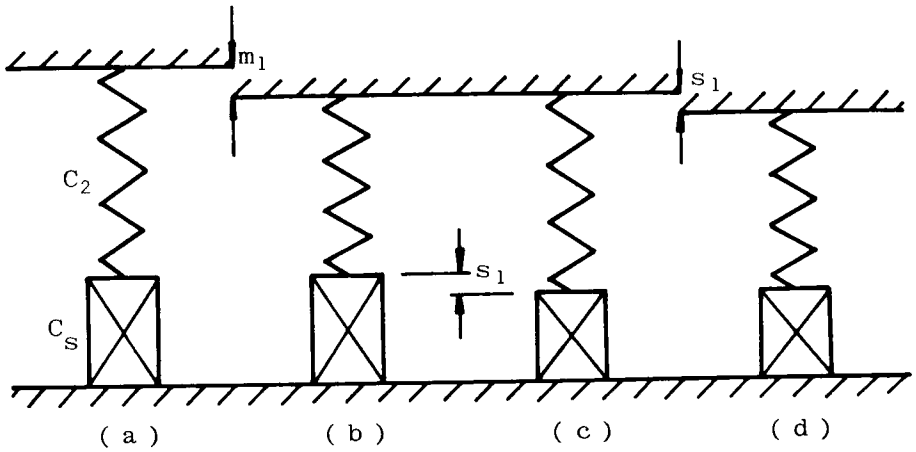

Fig.A-8

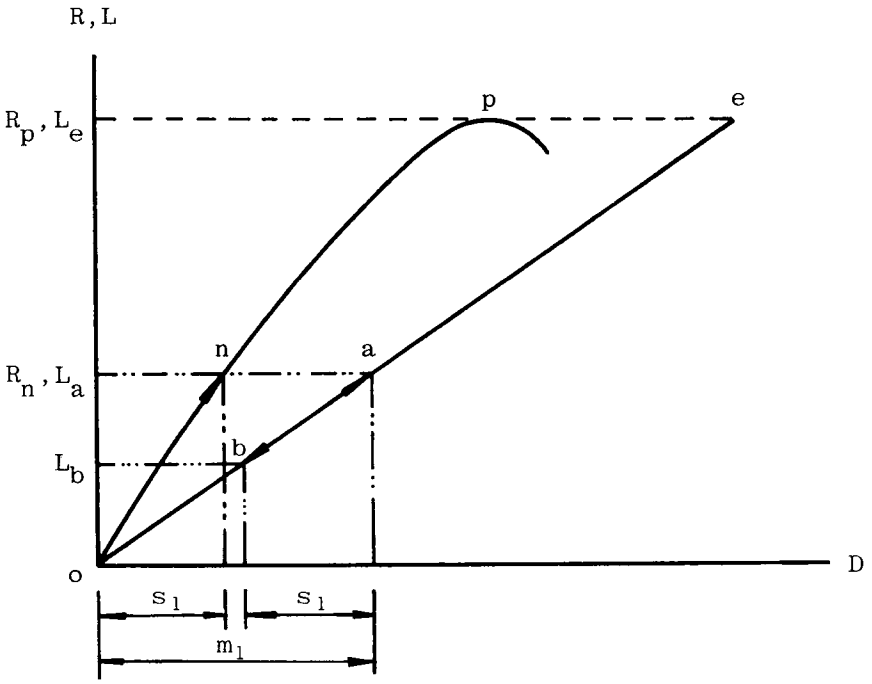

Fig.A-9 Shear test using a less stiff loading machine before peak strength point

of time beyond the peak strength point p, then, a rather smooth portion $\widehat{pq}$ of the R-D curve can be obtained as mentioned in Fig. A-7.

But, when the shear test progresses beyond point q, where $C_2 > C_s$, the rock specimen may collapse abruptly by the loading machine and loses most of its strength in a short time intervals. As this is of a highly transient phenomenon, the process is almost not possible to be monitored with a X-Y recorder.

However, the mechanism of such a sudden collapse of the specimen can be explained by the same model used above.

After point q, the specimen deforms continuously and loses its strength, as shown in Figs. A-11(a), (b). If the specimen is contracted over a distance m_1, the loading spring would extend the same distance m_1 simultaneously. Because the C_2 is smaller than C_s (Fig. A-10), the load released from the loading machine due to the elongation m_1 is equal to $\Delta L = L_q - L_h = C_2 \cdot m_1$. However, at the same time the specimen had already lost its strength from R_q to R_r, where $R_q - R_r = \Delta R = C_s \cdot m_1$ and $\Delta L < \Delta R$. That is to say, $L_h > R_r$ and yet the rock specimen still have not enough strength to support the loading force. Therefore, it will be compressed continuously by the load, till a point s where loading force L_s is just equal to the resistant force R_s (see Fig. A-10), whereas the machine-specimen system can reach a stable state.

Because the unstable process between points q and s occurs so rapidly that the true resistant force - deformation curve qrs can not be correctly pursued. However, after point s, the stiffness of specimen C_s becomes smaller than C_2, the R-D curve can again be monitored.

According to the above explanations, conclusions based on the relative stiffness of loading machine and specimen are arrived as follows:

(1) The resistant force - deformation curve of a rock specimen before peak strength point can be correctly monitored by both of stiff loading ma-

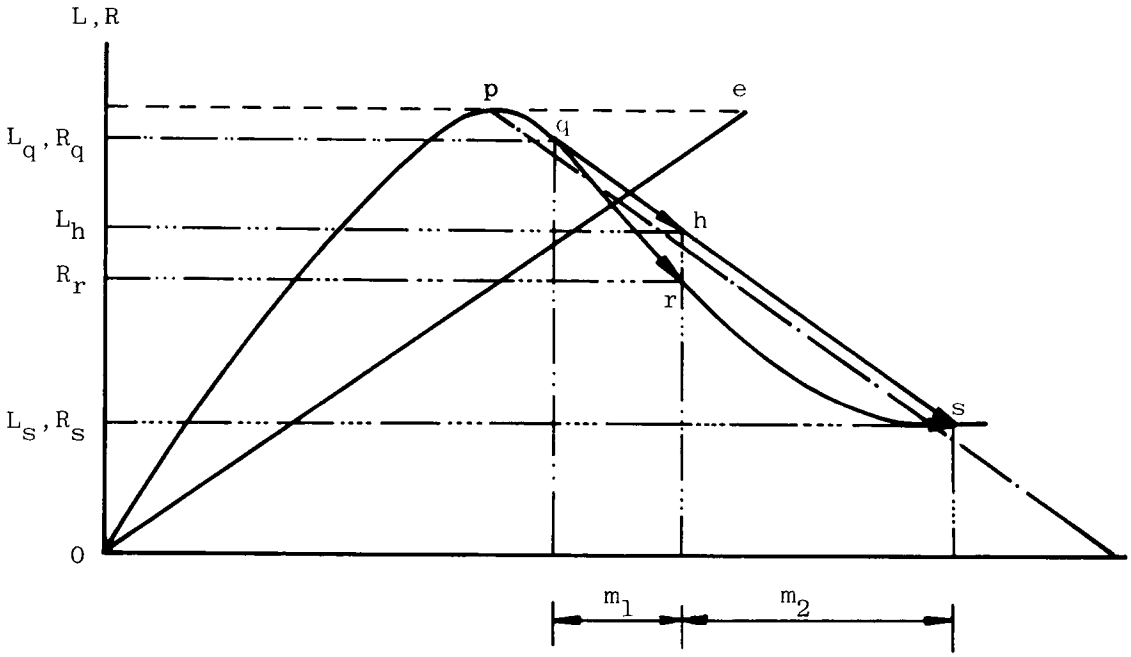

Fig.A-10. Shear test with a less stiff loading machine in the region of post-peak strength

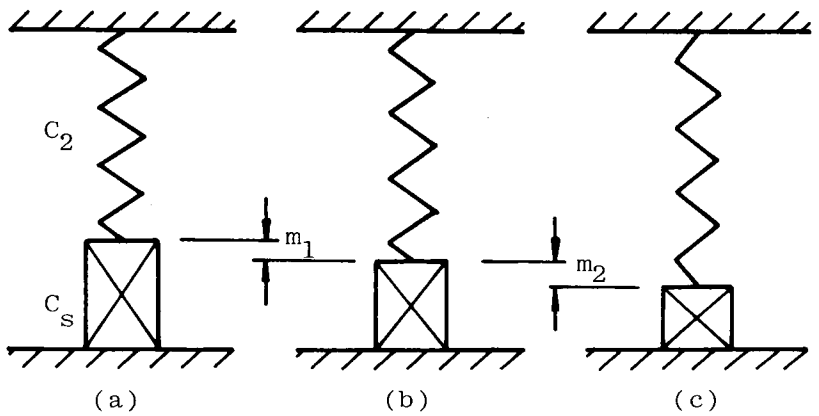

Fig. A-11

chine C_1, $C_1 > C_s$, and flexible loading machine C_2 ($C_2 < C_s$). However, in order to shear the rock specimen, a significant deformation will be produced in the loading direction with the flexible loading machine itself.

(2) The abrupt crush of rock specimen occurs at a point in region of post-peak strength, when the stiffness of the loading system is equal or just smaller than that of rock specimen. The monitoring of resistance-deformation process of a rock specimen will thus be temporarily out of control. However, after a short period of time, when rock specimen has losed most of its strength and induced an enough big strain, its stiffness may decrease and become equal or smaller than that of loading system. The desired monitoring can then be resumed.

Therefore, to explore the complete stress-strain property of a rock specimen, especially to observe the strain softening phenomenon, it is required to use a stiff loading machine with a stiffness C_1 which is greater than all the gradients (stiffness) of the stress-strain curve of this specimen.

(3) As shown in Fig. A-10, if a shear test is carried out using a flexible loading machine, an abrupt failure will be resulted in the rock specimen at some stage after the peak strength point. Therefore, part of the resistant force - deformation curve of the specimen can not be monitored. By connecting the initial and final points of this unstable state, i.e., q and s, the trace of the behavior of the loading machine during this unstable process can be evaluated. The gradient of the qs line gives the stiffness of the loading machine C_2. This conclusion can adequately be supported by test data obtained by Hinde (1964)[2] as shown in Fig. A-12.

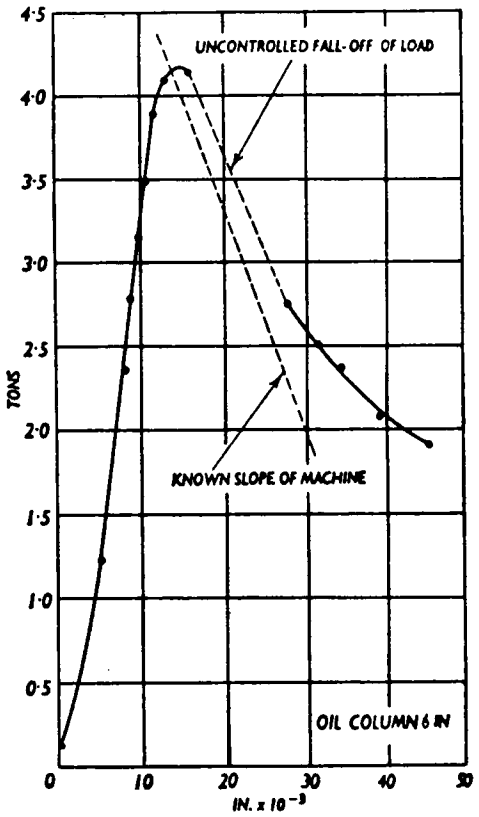

Fig. A-12 Strut test without compensator (Ref. A-2)

References for Appendix A

(1) Bieniawski, Z. T., H. G. Denkhans and U. W. Vogler, "Failure of Fractured Rock", Int. J. Rock Mech. Min. Sci., Vol. 6, pp. 323-341, 1969.

(2) Hinde, P. B., "Testing Machine Stiffness Problem", The Engineer, pp. 1124-1127, 1964.

Appendix B THE STRESS AND STRAIN AROUND A CIRCULAR OPENING SUBJECTED TO A UNIFORM RADIAL TENSILE STRESS

B-1 Airy's Stress Function[1)]

In an elastic body, when body force is the only conservative force, the potential V gives the components of body force F_x, F_y as:

$$F_x = -\frac{\partial V}{\partial x} \quad , \quad F_y = -\frac{\partial V}{\partial y} \qquad \text{..... (1)}$$

which satisfies the equilibrium equations

$$\frac{\partial \sigma_x}{\partial x} + \frac{\partial \tau_{xy}}{\partial y} + F_x = 0 \quad , \quad \frac{\partial \tau_{xy}}{\partial x} + \frac{\partial \sigma_y}{\partial y} + F_y = 0 \qquad \text{..... (2)}$$

together with stress components σ_x, σ_y and τ_{xy}.

Substituting Eq. (1) into Eq. (2), it renders

$$\frac{\partial}{\partial x}(\sigma_x - V) + \frac{\partial \tau_{xy}}{\partial y} = 0 \quad , \quad \frac{\partial \tau_{xy}}{\partial x} + \frac{\partial}{\partial y}(\sigma_y - V) = 0 \qquad \text{..... (3)}$$

Upon introducing functions ψ and χ and defining

$$\left.\begin{aligned} \sigma_x - V &= \frac{\partial \psi}{\partial y} \quad , \quad \tau_{xy} = -\frac{\partial \psi}{\partial x} \\ \tau_{xy} &= -\frac{\partial \chi}{\partial y} \quad , \quad \sigma_y - V = \frac{\partial \chi}{\partial x} \end{aligned}\right\} \qquad \text{..... (4)}$$

Equation (3) becomes

$$\left.\begin{aligned} \frac{\partial^2 \psi}{\partial x \partial y} - \frac{\partial^2 \chi}{\partial y^2} &= 0 \\ -\frac{\partial^2 \psi}{\partial x^2} + \frac{\partial^2 \chi}{\partial x \partial y} &= 0 \end{aligned}\right\} \qquad \text{..... (3)'}$$

Introducing also a function ϕ, which gives

$$\chi = \frac{\partial \phi}{\partial x} \quad , \quad \psi = \frac{\partial \phi}{\partial y} \qquad \text{..... (5)}$$

thus, $\sigma_x - V = \frac{\partial^2\phi}{\partial y^2}$, $\sigma_y - V = \frac{\partial^2\phi}{\partial x^2}$, $\tau_{xy} = \frac{\partial^2\phi}{\partial x \partial y}$ ..... (6)

for ready use to Eq. (3).

This function ϕ is called as Airy's stress function.

When body forces F_x and F_y are absent, the form of $\nabla^4\phi=0$ should be used for both cases of plane stress and plane strain, rather than $\nabla^2\phi=0$, in which,

$$\nabla^2 = \frac{\partial^2}{\partial x^2} + \frac{\partial^2}{\partial y^2} , \quad \nabla^4 = \frac{\partial^4}{\partial x^4} + 2\frac{\partial^4}{\partial x^2 \partial y^2} + \frac{\partial^4}{\partial y^4} \quad \text{..... (7)}$$

Airy's stress function can also be expressed using polar coordinates. Since

$$\left.\begin{aligned} \frac{\partial}{\partial x} &= \frac{\partial r}{\partial x}\frac{\partial}{\partial r} + \frac{\partial \theta}{\partial x}\frac{\partial}{\partial \theta} = \cos\theta \frac{\partial}{\partial r} - \frac{\sin\theta}{r}\frac{\partial}{\partial \theta} \\ \frac{\partial}{\partial y} &= \frac{\partial r}{\partial y}\frac{\partial}{\partial r} + \frac{\partial r}{\partial y}\frac{\partial}{\partial \theta} = \sin\theta \frac{\partial}{\partial r} + \frac{\cos\theta}{r}\frac{\partial}{\partial \theta} \end{aligned}\right\} \text{..... (8)}$$

and

$$\left.\begin{aligned} \sigma_r &= \sigma_x \cos^2\theta + \sigma_y \sin^2\theta + 2\tau_{xy}\sin\theta\cos\theta \\ \sigma_\theta &= \sigma_x \sin^2\theta + \sigma_y \cos^2\theta - 2\tau_{xy}\cos\theta\sin\theta \\ \tau_{r\theta} &= (\sigma_y - \sigma_x)\sin\theta\cos\theta + \tau_{xy}(\cos^2\theta - \sin^2\theta) \end{aligned}\right\} \text{..... (9)}$$

it follows that

$$\left.\begin{aligned} \frac{\partial^2}{\partial x^2} &= \left(\cos\theta\frac{\partial}{\partial r} - \frac{\sin\theta}{r}\frac{\partial}{\partial\theta}\right)^2 = \cos^2\theta\frac{\partial^2}{\partial r^2} - \frac{2\sin\theta\cos\theta}{r}\frac{\partial^2}{\partial r\partial\theta} \\ &\quad + \frac{\sin^2\theta}{r}\frac{\partial}{\partial r} + \frac{2\sin\theta\cos\theta}{r^2}\frac{\partial}{\partial\theta} + \frac{\sin^2\theta}{r^2}\frac{\partial^2}{\partial\theta^2} \\ \frac{\partial^2}{\partial y^2} &= \left(\sin\theta\frac{\partial}{\partial r} + \frac{\cos\theta}{r}\frac{\partial}{\partial\theta}\right)^2 = \sin^2\theta\frac{\partial^2}{\partial r^2} + \frac{2\sin\theta\cos\theta}{r}\frac{\partial^2}{\partial r\partial\theta} \\ &\quad + \frac{\cos^2\theta}{r}\frac{\partial}{\partial r} - \frac{2\sin\theta\cos\theta}{r^2}\frac{\partial}{\partial\theta} + \frac{\cos^2\theta}{r^2}\frac{\partial^2}{\partial\theta^2} \end{aligned}\right\} \text{..(10)}$$

and,

$$\left.\begin{aligned} \frac{\partial^2}{\partial x\partial y} &= \left(\cos\theta\frac{\partial}{\partial r} - \frac{\sin\theta}{r}\frac{\partial}{\partial\theta}\right)\left(\sin\theta\frac{\partial}{\partial r} + \frac{\cos\theta}{r}\frac{\partial}{\partial\theta}\right) \\ &= \sin\theta\cos\theta\frac{\partial^2}{\partial r^2} + \frac{\cos^2\theta - \sin^2\theta}{r}\frac{\partial^2}{\partial r\partial\theta} - \frac{\sin\theta\cos\theta}{r}\frac{\partial}{\partial r} \\ &\quad - \frac{\cos^2\theta - \sin^2\theta}{r^2}\frac{\partial}{\partial r} - \frac{\sin\theta\cos\theta}{r^2}\frac{\partial^2}{\partial\theta^2} \end{aligned}\right\}$$

Inserting Eqs. (6) and (10) into Eq. (9) yields

$$\left.\begin{aligned} \sigma_r &= \frac{1}{r}\frac{\partial\phi}{\partial r} + \frac{1}{r^2}\frac{\partial^2\phi}{\partial\theta^2} \\ \sigma_\theta &= \frac{\partial^2\phi}{\partial r^2} \\ \tau_{r\theta} &= \frac{1}{r^2}\frac{\partial\phi}{\partial\theta} - \frac{1}{r}\frac{\partial^2\phi}{\partial r\partial\theta} = -\frac{\partial}{\partial r}\left(\frac{1}{r}\frac{\partial\phi}{\partial\theta}\right) \end{aligned}\right\} \quad \ldots\ldots\ldots\ldots (11)$$

and,

$$\nabla^2 = \frac{\partial^2}{\partial x^2} + \frac{\partial^2}{\partial y^2} = \frac{\partial^2}{\partial r^2} + \frac{1}{r}\frac{\partial}{\partial r} + \frac{1}{r^2}\frac{\partial^2}{\partial\theta^2} \quad \ldots\ldots\ldots\ldots\ldots\ldots (12)$$

$$\nabla^4\phi = \left(\frac{\partial^2}{\partial r^2} + \frac{1}{r}\frac{\partial}{\partial r} + \frac{1}{r^2}\frac{\partial^2}{\partial\theta^2}\right)^2\phi = 0 \quad \ldots\ldots\ldots\ldots\ldots\ldots (13)$$

B-2 Deriving the Stress and Strain around an Opening Subjected to a Uniform Radial Tensile Stress

As shown in Fig. B-1, a uniform radial tensile stress p_e acting on the wall of opening, so that the stress distribution in the rock mass around the opening is axially symmetric, therefore, Eq. (13) can be rewritten as

$$\nabla^4\phi = \left(\frac{\partial^2}{\partial r^2} + \frac{1}{r}\frac{\partial}{\partial r}\right)^2\phi = \frac{d^4\phi}{dr^4} + \frac{2}{r}\frac{d^3\phi}{dr^3} - \frac{1}{r^2}\frac{d^2\phi}{dr^2} + \frac{1}{r^3}\frac{d\phi}{dr} = 0 \quad \ldots\ldots (14)$$

Assuming $\phi = r^m$, where r is the distance measured from the center of opening, and inserting it into Eq. (14), then

$$\nabla^4\phi = m^2\,(m-2)^2\,r^{m-4} = 0 \quad \ldots\ldots\ldots\ldots\ldots\ldots\ldots (14\text{-a})$$

where 'm' takes a value either zero or 2;

when $m=0$, $\phi=1$ or $\ln r$,

$m=2$, $\phi=r^2$ or $r^2\ln r$.

Hence, $\phi = A\ln r + B\,r^2\ln r + C\,r^2 + D$ ..... (14-b)

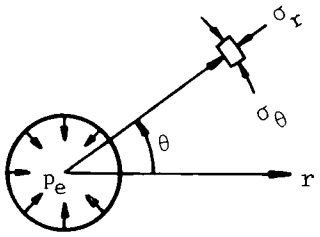

Fig. B-1 State of stresses near the opening

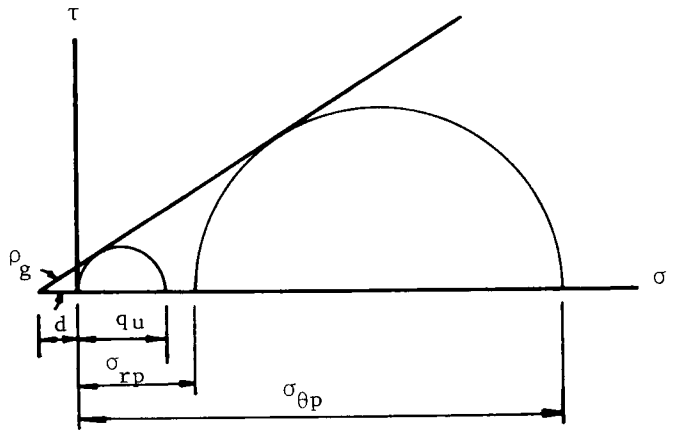

Fig. B-2 The relationship among q_u, σ_{rp} and $\sigma_{\theta p}$ illustrated schematically

Inserting Eq. (14-b) into Eq. (11), the latter becomes

$$\left.\begin{aligned} \sigma_r &= \frac{1}{r}\frac{d}{dr} = \frac{A}{r^2} + B(1 + 2\ln r) + 2C \\ \sigma_\theta &= \frac{d^2\phi}{dr^2} = -\frac{A}{r^2} + B(3 + 2\ln r) + 2C \\ \tau_{r\theta} &= 0 \end{aligned}\right\} \quad \ldots\ldots\ldots (15)$$

Under elastic plane stress condition, the strain created around the opening can be obtained from Eq. (16)

$$\left.\begin{aligned} \varepsilon_r &= \frac{1}{E}(\sigma_r - \nu\sigma_\theta) \\ \varepsilon_\theta &= \frac{1}{E}(\sigma_\theta - \nu\sigma_r) \\ \gamma_{r\theta} &= \frac{\tau_{r\theta}}{G} \end{aligned}\right\} \quad \ldots\ldots\ldots\ldots\ldots\ldots\ldots (16)$$

As

$$\varepsilon_r = \frac{\partial u_r}{\partial r}, \quad \varepsilon_\theta = \frac{1}{r}\frac{\partial u_\theta}{\partial \theta} + \frac{u_r}{r} \quad \text{and}$$

$$\frac{\partial u_r}{\partial r} = \varepsilon_r = \frac{1}{E}(\sigma_r - \nu\sigma_\theta), \quad \frac{\partial u_\theta}{\partial \theta} = r\varepsilon_\theta - u_r,$$

hence,

$$\begin{aligned} u_r &= \frac{1}{E}\left(\int \sigma_r\, dr - \int \nu\,\sigma_\theta\, dr\right) + f(\theta) \\ &= \frac{1}{E}\left[\int \left(\frac{A}{r^2} + B(1 + 2\ln r) + 2C\right) dr - \nu\int \left(-\frac{A}{r^2} + B(3 + 2\ln r) + 2C\right) dr\right] \\ &\quad + f(\theta) \\ &= \frac{1}{E}\left[-\frac{(1+\nu)}{r}A + 2(1-\nu)Br\ln r - B(1-\nu)r + 2C(1-\nu)r + 2(1-\nu)Br\ln r\right] + f(\theta) \end{aligned}$$

$$\ldots\ldots\ldots\ldots\ldots (17\text{-a})$$

and

$$\begin{aligned} \frac{\partial u_\theta}{\partial \theta} &= r\varepsilon_\theta - u_r = r\frac{1}{E}(\sigma_\theta - \nu\sigma_r) - u_r \\ &= r\frac{1}{E}\left[\left(-\frac{A}{r^2} + B(3 + 2\ln r) + 2C\right) - \nu\left(\frac{A}{r^2} + B(1 + 2\ln r) + 2C\right)\right] \\ &\quad - \frac{1}{E}\left[-\frac{(1+\nu)}{r}A + 2(1-\nu)Br\ln r - B(1-\nu)r + 2C(1-\nu)r\right] - f(\theta) \\ &= \frac{1}{E}\left[-(1+\nu)\frac{A}{r^2} + 2(1-\nu)B\ln r + B(3-\nu) + 2C(1-\nu)\right] r \\ &\quad - \frac{1}{E}\left[-(1+\nu)\frac{A}{r} + 2(1-\nu)Br\ln r - B(1-\nu)r + 2C(1-\nu)r\right] - f(\theta) \\ &= \frac{4Br}{E} - f(\theta) \end{aligned}$$

Therefore, $$u_\theta = \frac{4Br}{E}\theta - \int f(\theta)d\theta + f_1(r) \quad \text{..... (17-b)}$$

where, $f(\theta)$ and $f_1(r)$ are only functions of θ and r, respectively.

However, as the deformation u_θ is also axial symmetric, then, it is clear that the value of u_θ at $\theta=\theta_1$, $r=r_1$ in the rock mass must equal to that of $\theta=\theta_1+2\pi$, $r=r_1$. Thus, the B parameter in Eq. (17-6) must be equal to zero. Eq. (15) can be simplified as

$$\left.\begin{aligned}\sigma_r &= \frac{A}{r^2} + 2C \\ \sigma_\theta &= -\frac{A}{r^2} + 2C\end{aligned}\right\} \quad \text{..... (18)}$$

Subjected to the boundary conditions

$$(\sigma_r)_{r=a} = -p_e = \frac{A}{a^2} + 2C \qquad \text{and}$$

$$(\sigma_r)_{r=\infty} = 0 = 2C$$

thus, $A = -p_e a^2$,

and

$$\left.\begin{aligned}\sigma_\theta &= p_e \frac{a^2}{r^2} \\ \sigma_r &= -p_e \frac{a^2}{r^2}\end{aligned}\right\} \quad \text{..... (19)}$$

with

$$\left.\begin{aligned}u_r &= \frac{1}{E}\left[\frac{1+\nu}{r} p_e a^2\right] \\ u_\theta &= -\int f(\theta)d\theta + f_1(r)\end{aligned}\right\} \quad \text{..... (20)}$$

On the other hand, once a plastic zone is created in rock mass around an opening, Kastner (1971)[2] has derived the stress distribution around the opening as follows:

Since the equilibrium equations of elastic state given by Eq. (11) is equally applicable to plastic state, these then become

$$\left.\begin{aligned} \sigma_r &= \frac{1}{r}\frac{\partial \phi}{\partial r} \\ \sigma_\theta &= \frac{\partial^2 \phi}{\partial r^2} \\ \tau_{r\theta} &= 0 \end{aligned}\right\} \quad \cdots\cdots\cdots\cdots\cdots (21)$$

If the stress function ϕ in plastic state can be defined, the stresses σ_r and σ_θ can then be solved. On this account, Kastner (1971)[2] has assumed that a rock mass will enter into plastic state if its stress state meets the critical line connecting Mohr's circles, which is a straight line on τ-σ plane, as shown in Fig. B-2.

From Fig. B-2, the rock mass to reach into plastic state can be indicated by Eq. (22).

$$\sin \rho_g = \frac{\sigma_{\theta p} - \sigma_{rp}}{\sigma_{\theta p} + \sigma_{rp} + 2d} \quad \cdots\cdots\cdots\cdots\cdots (22)$$

Because

$$\sin \rho_g = \frac{\frac{q_u}{2}}{\frac{q_u}{2} + d} \quad \cdots\cdots\cdots\cdots\cdots (23)$$

$$\text{then,} \quad d = \frac{q_u}{2}\frac{1 - \sin \rho_g}{\sin \rho_g} \quad \cdots\cdots\cdots\cdots\cdots (24)$$

Substituting Eq. (24) into Eq. (22) results in

$$\sigma_{\theta p}(1 - \sin \rho_g) - \sigma_{rp}(1 + \sin \rho_g) - q_u(1 - \sin \rho_g) = 0 \qquad \text{or}$$

$$\sigma_{\theta p} - \frac{1 + \sin \rho_g}{1 - \sin \rho_g}\sigma_{rp} - q_u = 0 \quad \cdots\cdots\cdots\cdots\cdots (25)$$

$$\text{Designating} \quad N_\phi = \frac{1 + \sin \rho_g}{1 - \sin \rho_g} \quad \cdots\cdots\cdots\cdots\cdots (26)$$

then, the condition of entering into plastic state takes a simpler form as

$$\sigma_{\theta p} - N_\phi \sigma_{rp} - q_u = 0 \quad \cdots\cdots\cdots\cdots\cdots (27)$$

Upon substituting Eq. (27) into Eq. (21), a partial differential equation can be obtained to determine the stress function ϕ

$$\frac{\partial^2\phi}{\partial r^2} - N_\phi \frac{1}{r}\frac{\partial\phi}{\partial r} - q_u = 0 \quad \cdots\cdots (28)$$

Integrating Eq. (28), the solution is

$$\left.\begin{aligned} \phi &= c_1 \frac{r^{N_\phi+1}}{N_\phi+1} - \frac{q_u}{N_\phi-1}\frac{r^2}{2} + c_2 \qquad \text{and} \\ \frac{d\phi}{dr} &= c_1 r^{N_\phi} - \frac{q_u}{N_\phi-1} r \\ \frac{d^2\phi}{dr^2} &= c_1 N_\phi r^{N_\phi-1} - \frac{q_u}{N_\phi-1} \end{aligned}\right\} \cdots\cdots (29)$$

The boundary condition at the opening wall is $\sigma_{rp}=-p_e$ at r=a, from Eqs. (21), (26) and (29), constant c_1 is given as

$$c_1 = \frac{1}{a^{N_\phi-1}}\left(-p_e + \frac{q_u}{N_\phi-1}\right) \quad \cdots\cdots (30)$$

Therefore, the stresses in the plastic zone around a circular opening, which is subjected to a uniform radial tensile force p_e, can be expressed as follows:

$$\left.\begin{aligned} \sigma_{rp} &= \frac{1}{r}\left[\frac{1}{a^{N_\phi-1}}\left(-p_e + \frac{q_u}{N_\phi-1}\right) r^{N_\phi}\right] - \frac{1}{r}\frac{q_u}{N_\phi-1} r \\ &= \left(-p_e + \frac{q_u}{N_\phi-1}\right)\left(\frac{r}{a}\right)^{N_\phi-1} - \frac{q_u}{N_\phi-1} \\ \sigma_{\theta p} &= \frac{1}{a^{N_\phi-1}}\left(-p_e + \frac{q_u}{N_\phi-1}\right) N_\phi r^{N_\phi-1} - \frac{q_u}{N_\phi-1} \\ &= N_\phi \left(\frac{r}{a}\right)^{N_\phi-1}\left(-p_e + \frac{q_u}{N_\phi-1}\right) - \frac{q_u}{N_\phi-1} \\ \tau_{r\theta p} &= 0 \end{aligned}\right\} \cdots (31)$$

References for Appendix B

(1) Inoue, T., "Fundamentals of Elasticity Mechanics", Nikkan Kougyo Sinbun

publication Co. Inc., 1979 (In Japanese).

(2) Kastner, H., "Statik des Tunnel- und Stollenbaues", Springer-Verlag, 1971.